Deep Burn Strategy for the Optimized Incineration of Reactor Waste Plutonium in Pebble Bed High Temperature Gas-Cooled Reactors

Dawid Eduard Serfontein,

MSc in physics

10119582

Thesis for the degree Doctor of Philosophy in Nuclear Engineering at the Potchefstroom Campus of the North-West University

Promoter: **Prof. E. J. Mulder,**
Postgraduate School of Nuclear Science and Engineering

Co-promoter: **Mr. F. Reitsma,**
PBMR (Pty.) Ltd.

Date: November 2011

Potchefstroom

Acknowledgements

I give thanks to my God and Father who saved me for eternal life through the blood of His Son, Jesus Christ. During a very dark time in my career, He also miraculously led me to this study, through which He supported me and my family financially and gave me new hope, opportunities and vision.

Prof. Eben J. Mulder for professional guidance and personal friendship and for having taught me so much of what I know about nuclear engineering. Also for allowing me to use his VSOP-A reactor simulation codes and the associated input models.

Mr. Frederik Reitsma, without whose detailed and expert advice, support and feedback this study would not have been possible.

Research Centre Jülich and the Pebble Bed Modular Reactor (Pty) Ltd for allowing me to freely use their VSOP 99/05 simulation code and the associated input models for the PBMR DPP-400 reactor.

The personnel of the School of Mechanical Engineering, and other support-personnel, at the North-West University for support, advice and friendship.

THRIP for financial support by means of a bursary.

My wife, Retha, and daughter, Marié for their prayers, love, support and long-suffering through all the ups and downs associated with this study.

My friends and family for their encouragement and prayers.

Abstract

Title: Deep Burn Strategy for the Optimized Incineration of Reactor Waste Plutonium in Pebble Bed High Temperature Gas-Cooled Reactors

Author: D. E. Serfontein

Promoter: Prof. E. J. Mulder

Co-promotor: Mr. Frederik Reitsma

In this thesis advanced fuel cycles for the incineration, i.e. deep-burn, of weapons-grade plutonium, reactor-grade plutonium from pressurised light water reactors and reactor-grade plutonium + the associated Minor Actinides in the 400 MW_{th} Pebble Bed Modular Reactor Demonstration Power Plant was simulated with the VSOP 99/05 diffusion code. These results were also compared to the standard 9 g/fuel sphere U/Pu 9.6% enriched uranium fuel cycle. The addition of the Minor Actinides to the reactor-grade plutonium caused an unacceptable decrease in the burn-up and thus an unacceptable increase in the heavy metal (HM) content in the spent fuel, which is intended for direct disposal in a deep geological repository, without chemical reprocessing. All the Pu fuel cycles failed the adopted safety limits in that either the maximum fuel temperature of 1130°C, during normal operation, or the maximum power of 4.5 kW/sphere was exceeded. All the Pu cycles also produced positive Uniform Temperature Reactivity Coefficients, i.e. the coefficient where the temperature of the fuel and the graphite moderator in the fuel spheres are varied together. these positive temperature coefficients were experienced at low temperatures, typically below 700°C. This was due to the influence of the thermal fission resonance of ^{241}Pu. The safety performance of the weapons-grade plutonium was the worst. The safety performance of the reactor-grade plutonium also deteriorated when the heavy metal loading was reduced from 3 g/sphere to 2 g or 1 g.

In view of these safety problems, these Pu fuel cycles were judged to be not licensable in the PBMR DPP-400 reactor. Therefore a redesign of the fuel cycle for reactor-grade plutonium, the power conversion system and the reactor geometry was proposed in order to solve these problems. The main elements of these proposals are:

1. The use of 3 g reactor-grade plutonium fuel spheres should be the point of departure. ^{232}Th will then be added in order to restore negative Uniform Temperature Reactivity Coefficients.

2. The introduction of neutron poisons into the reflectors, in order to suppress the power density peaks and thus the temperature peaks.

3. In order to counter the reduction in burn-up by this introduction of neutron poisons, a thinning of the central reflector was proposed.

Keywords:

High Temperature Gas-Cooled Reactor, simulation with VSOP-A, VSOP 99/05, reactor-grade plutonium fuel cycle with minor actinides, incineration of plutonium, deep burn, high burn-up, positive Uniform Temperature reactivity Coefficient (UTC)

Uittreksel

Titel: Diepbrandstrategie vir die geoptimiseerde verbranding van reaktorgraad afvalplutonium in Korrelbed Hoë-Temperatuur Gasverkoelde Reaktore

Outeur: D. E. Serfontein

Promotor: Prof. E. J. Mulder

Medepromotor: Mnr. F. Reitsma

Gevorderde brandstofsiklusse vir die diepverbranding van reaktorgraad plutonium, wapengraad plutonium en ’n mengsel van reaktorgraad plutonium en die geassosieerde trans-plutoniese aktiniede in die 400 MW PBMR DPP reaktor is met die VSOP 99/05 kode gesimuleer. Die resultate is ook vergelyk met die standaard 9.6% verrykte uraan brandstofsiklus vir hierdie reaktor.

Die resultate was teleurstellend aangesien nie een van die plutonium brandstofsiklusse aan die gestelde veiligheidsvereistes voldoen het nie: Die limiet vir die maksimum brandstoftemperatuur tydens normale bedryf is oorskry en positiewe temperatuurreaktiwiteitskoeffisiënte is verkry. Hierdie brandstofsiklusse is dus nie lisensieerbaar in die genoemde reaktor nie. Daarom is verskeie veranderinge aan die brandstofsiklus en reaktorontwerp voorgestel, ten einde hierdie probleme te probeer oplos.

Table of contents

Acknowledgements iii

Abstract iv

1 Introduction 1

1.1 Definition of terms 1

1.2 Problem statement 2

1.3 Structure of the thesis 4

1.4 Literature study 5

1.4.1 Context of the study 5

1.4.1.1 Opportunities created by the nuclear renaissance 5

1.4.1.2 Sustainability of nuclear fuel supplies 6

1.4.1.3 Radiation protection and nuclear waste management 9

1.4.1.4 Risk of nuclear weapons proliferation 10

1.4.2 Technical basis of plutonium management 14

1.4.2.1 Nuclear proliferation risk of waste plutonium 16

1.4.2.2 Proliferation resistance of ^{240}Pu 16

1.4.2.3 Destruction potential of fizzle-yield nuclear weapons 18

1.4.2.4 Proliferation resistance of ^{238}Pu and proliferation risk of ^{237}Np 19

1.4.2.5 Proliferation resistance of ^{232}U in Th / ^{233}U fuel cycles 23

1.4.2.6 Conclusion 26

1.4.3 Plutonium dispositioning strategies 27

1.4.3.1 Storage without recycling 27

1.4.3.2 Isotopic degradation through recycling and subsequent storage 28

1.4.3.3 GNEP: Recycling in fast reactors until practically all heavy metals have been incinerated 28

1.4.3.4 The status quo of plutonium recycling 30

1.4.4 Plutonium incineration potential of Pebble Bed Reactors 33

1.4.4.1 Potential role for PBRs in GNEP reactor waste incineration 34

1.4.4.1.1 PBRs compared to fast burner reactors 34

1.4.4.1.2 PBMRs compared to MOX fuelled PWR reactors 34

1.4.5 Technical information for the simulations 36

1.4.5.1 Near total incineration of ^{239}Pu 36

1.4.5.2 Plutonium incineration potential of the PBMR DPP-400 design 37

1.4.5.3 Influence of the neutron spectrum on reactor safety and conversion ratio in PWRs 40

1.4.5.4 Pebble Bed Reactor spectra 42

1.4.5.5 Positive temperature reactivity coefficients for Pu in HTRs 44

1.4.5.6 Investigation of shell-type fuel pebbles 44

1.4.6 Towards a thorium/^{233}U breeder 45

1.4.6.1 Thorium/uranium in light water reactors 45

1.4.6.2 The fast fission potential of ^{232}Th, compared to ^{238}U 45

1.4.6.3 HEU driven thorium pebble bed reactors 50

1.4.6.4 Pu driven thermal thorium fuel cycles 51

1.4.6.4.1 Light water reactor (LWR) plutonium fuel 52

1.4.6.4.2 Minimisation of the residual plutonium in the spent fuel 52

1.4.6.4.3 Weapons-grade plutonium fuel 52

1.4.6.4.4 Conversion ratios 53

1.4.7 Conclusion on the role of thorium 54

1.5 Research aims and objectives 56

1.5.1 General aims 56

1.5.2 Specific objectives 56

1.5.3 Originality of the research aims 57

1.5.4 Demarcation of the field of study 59

2 Simulation methods 61

2.1 Incineration of pure plutonium 61

2.2 Translation of PBMR-400 VSOP-A models to VSOP 99/05 and verification of translation 61

2.2.1 Rationale for translation and verification 61

2.2.1.1 Strategy for using the LEU model to verify the translation process 62

2.2.1.2 Acceptable range for k_{eff} for the verification of the translation of the LEU model: 63

2.2.1.3 Method for translation and verification of LEU model 63

2.2.1.4 Verification of the VSOP-A code for Pu(PWR) fuel cycles 65

2.2.2 Translation challenges 65

2.2.3 Results for verification of translation of VSOP-A LEU model to VSOP 99/05 66

2.2.3.1 Modifications to the VSOP-A LEU model, before translation 66

2.2.3.2 Results for VSOP-A LEU model, translated to VSOP 99/05, without temperature recalculation 67

2.2.3.2.1 Verification k_{eff} for translated model 67

2.2.3.2.2 Verification of THERMIX temperature calculations 67

2.2.3.2.3 Verification of translated burn-up 68

2.2.3.3 Discussion of the differences between VSOP-A and VSOP 99/05 LEU results. 69

2.2.4 Results for verification and validation of VSOP-A for the simulation of Pu(PWR) fuel cycles 69

2.2.4.1 Verification of VSOP-A for the simulation of fresh Pu(PWR) fuel 70

2.2.4.1.1 Global parameters 70

2.2.4.1.2 Regional absorption 72

2.2.4.1.3 Thermal spectra 74

2.2.4.1.4 Global scattering 76

2.2.4.1.5 Leakage feedback 78

2.2.4.1.6 Conclusion 80

2.2.4.2 Verification of VSOP-A for the simulation of the Pu(PWR) equilibrium cycle 80

2.2.5 Conclusion on the verification and validation of the Pu(PWR) VSOP models 82

2.3 Resonance and coated-particle structure treatment in VSOP 84

2.3.1 Epithermal resonances 85

2.3.2 Thermal resonances 86

2.4 Geometry of the reactor 90

2.5 Simulation of control rods 90

2.5.1 Introduction 91

2.5.2 Method 92

2.5.2.1 3-D MECS simulations in VSOP-A 92

2.5.2.2 2-D MEB simulations in VSOP-A. 94

2.5.2.3 2-D control rod xenon transient override margin calculations in VSOP 99/05 94

2.5.2.4 2-D control rod shut-down balance in VSOP 99/05 95

2.5.3 Results for control rod calculations 97

2.5.3.1 3-D MECS control rod worths and 2-D MEB in VSOP-A 97

2.5.3.2 2-D control rod xenon transient override margin calculations in VSOP 99/05 98

2.5.3.3 2-D 12 control rod shut-down balance in VSOP 99/05 101

2.5.4 Discussion of the control rod performance 103

2.5.4.1 Uncertainties in the results 103

2.5.4.2 Safety analysis 103

2.5.5 Verification and validation of control rod calculations 104

2.5.6 Conclusions 105

3 Results 106

3.1 Comparison of calculation speed of VSOP-A and VSOP 99/05 106

3.2 k_{eff} as a function of burn-up 107

3.2.1 VSOP-A results from the pilot study 107

3.2.2 Simulation parameters for VSOP 99/05 109

3.2.3 VSOP 99/05 results for k_{eff} for U/Pu(LEU), Pu(PWR) and Pu(WGR) 110

3.2.4 Discussion of results for k_{eff} 112

3.3 Burn-up calculations for the incineration of U/Pu(LEU) Pu(PWR), Pu(WGR) and Pu(PWR)+MA 113

3.3.1 Simulation parameters and fuel compositions 113

3.3.2 VSOP-A results from the pilot study..... 118

3.3.3 Summary of VSOP99/05 results 121

3.3.3.1 Burn-up and fuel cycle characteristics 121

3.3.3.2 Fuel materials balance..... 123

3.3.4 Discussion of summary of VSOP 99/05 results 125

3.3.4.1 Limits of TRISO fuel..... 125

3.3.4.2 Burn-up 126

3.3.4.3 Maximum temperatures during normal operation 128

3.3.4.4 Maximum power per fuel sphere..... 129

3.3.4.5 Maximum fluence in spent fuel..... 132

3.3.4.6 Proliferation resistance..... 133

3.4 Optimisation of fuel cycle 133

3.4.1 Temperature reactivity coefficients 133

3.4.1.1 Calculation methods for temperature reactivity coefficients in VSOP 99/05. 133

3.4.1.2 Results for temperature reactivity coefficients 136

3.4.1.2.1 Verification 136

3.4.1.2.2 Conclusion on verification 138

3.4.1.2.3 Comparison of Pu(PWR) to U/Pu(LEU) 138

3.4.1.3 Discussion of temperature reactivity coefficients 139

3.4.1.4 Comparison of uniform temperature reactivity coefficient to results by Boer and Ougouag (2010a and 2010b)..... 140

3.4.1.4.1 Methods and results..... 140

3.4.1.4.2 Discussion 143
3.4.1.4.3 Conclusion 147
3.4.2 Optimisation of the uniform temperature reactivity coefficient 148
3.4.2.1 Theoretical considerations 148
3.4.2.2 Simulation parameters and fuel compositions 151
3.4.2.2.1 Standard cases 151
3.4.2.2.2 Decay of ^{241}Pu to ^{241}Am 151
3.4.2.2.3 Low density kernels 152
3.4.2.2.4 Results 153
3.4.2.2.5 Discussion 153
3.4.2.3 Investigation into mechanism of the positive uniform temperature reactivity coefficient 155
3.4.2.3.1 Method 155
3.4.2.3.2 Results 156
3.4.2.3.3 Discussion and conclusion 157
3.4.2.4 Conclusion on optimisation of the uniform temperature reactivity coefficient 158
3.4.3 Power and temperature peaks 159
3.4.3.1 Method 159
3.4.3.2 Results 159
3.4.3.3 Discussion 163
3.4.3.3.1 Maximum fuel temperatures 163
3.4.3.3.2 Temperature peak in spent fuel outlet chute 164
3.4.3.3.3 Maximum power densities 165

3.4.3.4 Conclusions on maximum fuel temperature and power density 166

3.4.4 Maximising proliferation resistance 166

3.4.4.1 Simulation parameters 167

3.4.4.2 Results 167

3.4.4.3 Discussion and conclusions 168

4 Discussions of study and conclusions 169

4.1 Assessment of the originality of the results 169

4.2 Implications of the results 170

4.2.1 Development of a computer code for the translation of VSOP-A input models to VSOP 99/05 170

4.2.2 Comparison of VSOP-A and VSOP 99/05 171

4.2.3 Burn-up simulations for the different Pu fuel mixtures 171

4.2.3.1 Burn-up 171

4.2.3.2 Safety 172

4.2.3.3 Nuclear weapons proliferation resistance 172

4.3 Suggestions for future studies 173

4.3.1 Verification of VSOP-A vs. VSOP 99/05 with MCNP 173

4.3.2 Reconciliation with the results of Boer and Ougouag 173

4.3.3 Simulation of DLOFC temperatures, using the Multi-group TINTE code. 173

4.3.4 Verification of the MEB for Pu fuel against MCNPX 173

4.3.5 Simulation of the reactivity of fresh Pu(PWR) fuel in the fuel exit cones 173

4.4 Proposal for the redesign of the PBMR DPP-400 for Pu(PWR) 174

4.4.1 Pu fuel composition 174

4.4.1.1 Deep-burn pure Pu(PWR) fuel cycle 174

4.4.1.2 Pu-driven ^{232}Th fuel cycles 175

4.4.2 Power conversion system 175

4.4.3 Neutron poisons in the reflectors 175

4.4.4 Thinning of the central reflector 177

4.5 Final conclusions 178

5 References 179

6 APPENDIX: Automatic translation of VSOP-A input models to VSOP 99/05 191

6.1 Discrepancies between the VSOP-A and VSOP 99/05 input models 191

6.2 C++ translation code for VSOP-A models to VSOP 99/05 193

6.3 Manual corrections to automatically translated VSOP 99/05 models 196

6.3.1 Concatenation of IN-VOLMA, IN-DA2 and IN-HL 196

6.3.2 Translation of definitions of reactor geometry 196

6.3.3 THERMIX calculations in the VSOP 99/05 model 203

6.3.4 Translation of GAM-I- and VSOP-identification numbers 203

6.3.5 Translation of ^{238}Pu definitions 205

6.3.5.1 Removal of ^{238}Pu definitions from LEU fuel cycles 205

6.3.5.2 Translation of ^{238}Pu in Pu fuel cycles 206

6.3.6 Addition of new VSOP 99/05 card R14A 207

6.3.7 Automatic admixture of graphite (“dummy”) spheres 208

6.4 Replacement of Dummy Poison in graphite with natural Boron 208

6.5 Corrections to the VSOP-A input model 211

6.5.1 Fission spectrum 211

6.5.2 Specification of x and y in Pu-O_x-C_y in VSOP-A 211

6.5.3 Specification of the fissile enrichment for Pu 212

6.5.4 Specification of FUTYP on card T6 212

6.5.5 Discrepancies between the interpretation of the heavy metal densities between VSOP-A and VSOP 99/05 213

6.5.5.1 Differences in coated particle packing fraction and homogenised heavy metal density 213

6.5.5.2 Analysis 214

6.5.5.2.1 Correction to the VSOP-A packing fraction calculations 214

6.5.5.2.2 Results 214

6.5.5.3 Discrepancies between the interpretations of input and burn-up heavy metal densities in VSOP 99/05 215

6.5.5.3.1 Input heavy metal densities 215

6.5.5.3.2 Heavy metal densities in burn-up results 215

6.5.5.4 Conclusion on heavy metal nomenclature 216

6.5.6 Modifications to SUBROUTINE ZUT for the PuO_2-case 216

6.5.7 Differences in treatment of ^{234}U 217

6.5.8 Batch and storage box volume fluctuations during fuel shuffling 217

6.5.8.1 Method 217

6.5.8.2 Results 228

6.5.8.3 Conclusion 228

7 Appendix: Miscellaneous methods and data 229

7.1 Discussion of the differences between VSOP-A and VSOP 99/05 LEU results. 229

7.2 Simulation of control rods 234

7.2.1 Introduction 234

7.2.2 Method 235

7.2.2.1 3-D MECS simulations in VSOP-A. 235

7.2.2.2 2-D MEB simulations in VSOP-A. 238

7.2.2.3 2-D control rod xenon transient override margin calculations in VSOP 99/05 239

7.2.2.4 2-D control rod shut-down balance in VSOP 99/05 241

7.2.3 Results for control rod calculations 243

7.2.3.1 Simulation of diffusion coefficients with TOTMOS 243

7.2.3.2 3-D MECS control rod worths and 2-D MEB in VSOP-A 246

7.2.3.3 2-D control rod xenon transient override margin calculations in VSOP 99/05 248

7.2.3.4 2-D 12 control rod shut-down balance in VSOP 99/05 251

7.2.4 Discussion of the control rod performance 253

7.2.4.1 Uncertainties in the results 253

7.2.4.2 Safety analysis 253

7.2.5 Verification and validation of control rod calculations 255

7.2.6 Proposal for control rod follow-up study 257

7.2.7 Conclusions 259

List of figures

Figure 1: Nuclear weapons yield limitation due to pre-detonation. 17

Figure 2**:** The most important actinide nuclides and their relations via α-decay, β-decay and neutron capture reactions. (Cross-sections for capture, σ_c, and fission, σ_f , are given for thermal neutron energies.) 21

Figure 3: Accumulation of Pu with different incineration options 36

Figure 4: Breeding potential of ^{238}U and ^{232}Th. 49

Figure 5: Comparison of the thermal neutron spectrum of VSOP-A to VSOP 99/05. 75

Figure 6: Comparison of the thermal self-shielding factors for VSOP-A to VSOP 99/05. 75

Figure 7: Comparison of axial thermal flux profile in Channel(1) for VSOP-A to VSOP 99/05. 77

Figure 8: Comparison of axial thermal flux profile in Channel(3) for VSOP-A to VSOP 99/05. 78

Figure 9: Theoretical normalised Maxwellian flux distribution for thermalised neutrons at 1000°C. 88

Figure 10: Neutron spectra of the PWR and VHTR fuels at beginning of life. 89

Figure 11: Physical layout of the PBMR-400 reactor, as modelled in VSOP 99/05. 90

Figure 12: Decrease of K_∞ during burn-up. ($K_\infty = \nu\Sigma_f/\Sigma_a$.) Target burn-up: U/Pu Cycle 95 MWd/kg$_{HM}$, Pu Cycle 692 MWd/kg$_{HM}$. 108

Figure 13: Pu-Cycle - Burn-up history of Pu-isotopes with target burn-up of 692 MWd/kg$_{HM}$. 109

Figure 14: Comparison of evolution of k_{eff} with core residence time for different fuel cycles. 111

Figure 15: Evolution of k_{eff} as a function of the core residence time, normalised to the time it takes for k_{eff} to decrease to 1.00. 112

Figure 16: Release rate of radioactive ^{110m}Ag out of the coated fuel particles, as a function of temperature. 129

Figure 17: Maximum uniform temperature reactivity coefficient (UTC) and power/coated particle (CP) for different heavy metal loadings for Pu(PWR). 131

Figure 18: Trade-off between the maximum uniform temperature reactivity coefficient (UTC) and the fast fluence on the spent fuel, as a function of the Pu(PWR) heavy metal loading/sphere. 132

Figure 19: Comparison of the finite resonance integrals for the standard 9 g LEU and 3 g Pu(PWR) fuel spheres. 135

Figure 20: Temperature reactivity coefficient for the standard U/Pu(LEU) case, for verification against Figure 21. 136

Figure 21: Published temperature reactivity coefficients for the standard U/Pu(LEU) fuel in the PBMR-400. 137

Figure 22: Comparison of temperature reactivity coefficients for 3 g Pu(PWR) to 9 g U/Pu(LEU). 139

Figure 23: Temperature reactivity coefficients for fuel spheres of different burn-ups, in an infinite cylinder. 141

Figure 24: Uniform Temperature Coefficients (UTC_∞) of reactivity in the deep-burn Pu(PWR)-fuelled PBMR DPP-400, as a function of the axial core position and temperature; for the reference case without addition of Er. The core has a positive UTC_∞ at low temperatures, except near the top of the core. 142

Figure 25: Thermal (0.25 to 1.0 eV) fission resonances for ^{239}Pu and ^{241}Pu and σ_γ for the neutron capturers with thermal capture resonances. (ENDFB 7.0 from JANIS.) 148

Figure 26: Uniform temperature reactivity coefficient (UTC) for all the Pu fuel compositions, as function of temperature. 153

Figure 27: The relevant components of the neutron balance for the analysis of the mechanism of the variations in the moderator temperature reactivity coefficient for the 1 g Pu(PWR) case, with the moderator temperature reactivity coefficient displayed as reference on the separate axis on the right. 156

Figure 28: Axial profiles for the maximum fuel temperatures and power densities for 3 g Pu(PWR) and the reference 9 g U/Pu(LEU) at two radial positions. 160

Figure 29: Axial profiles for the maximum fuel temperature, He coolant temperature and power densities for 3 g Pu(PWR) and the reference maximum fuel temperature for the 9 g U/Pu(LEU) at R = 102.3 cm, next to the central reflector. 161

Figure 30: Axial power profiles at the radius at maximum power density (R = 102.3 cm) next to the central reflector and the minimum power densities (R = 145.9 cm for 3 g Pu(PWR) and R = 156.9 cm for 9 g U/Pu(LEU)), near the centre of the fuel annulus. 162

Figure 31: Radial power profiles at the maximum axial power density (Z = 277.0 cm) and in the lower half of the core (Z = 659.0 cm) for 3 g Pu(PWR) and the reference 9 g U/Pu(LEU)). 163

List of tables

Table 1: List of acronyms..... 1

Table 2: Nuclear proliferation classification of plutonium grades..... 16

Table 3: OECD benchmark isotopic composition for simulations with reactor-grade plutonium (41.2 GWd/t burn-up + 3 years cooling). 31

Table 4: Reference MOX composition (excluding the ^{238}U) at the beginning of multiple recycles in a standard PWR 32

Table 5: Stockpiles of extracted reactor-grade plutonium. 33

Table 6: Summary of factors responsible for the difference in k_{eff} between VSOP 99/05 and VSOP-A for fresh fuel 71

Table 7: Whole core fractional absorptions per one lost neutron. 72

Table 8: Microscopic absorption cross-sections in Region (48) 73

Table 9: Neutron balance per one lost neutron. 76

Table 10: Comparison of k_{eff} for fresh Pu(PWR) core with and without leakage feedback.... 79

Table 11: Summary of factors responsible for the difference in k_{eff} between VSOP 99/05 and VSOP-A for the equilibrium fuel cycle 81

Table 12: 3-D MECS control rod worths and 2-D MEB in VSOP-A for the equilibrium cores, without control rods and after ^{135}Xe decay. 97

Table 13: 2-D control rod worths in VSOP 99/05 equilibrium cores, with equilibrium temperatures, after ^{135}Xe decay and for 12 control rods completely out versus completely in..... 98

Table 14: 2-D control rod xenon override margins in VSOP 99/05 for partial insertion of 24 control rods into equilibrium cores. 98

Table 15: ^{135}Xe atom density variations responsible for override requirement. 99

Table 16 2-D 12 control rod shut-down balance in VSOP 99/05. 102

Table 17: Lay-out of the reference fuel elements 114

Table 18: Radial mesh intervals in fuel spheres for THERMIX..... 115

Table 19: Design of PBMR DPP-400 reactor core 116

Table 20: Isotopic composition for simulations with reactor-grade plutonium (41.2 GWd/t burn-up + 3 years cooling) from the OECD benchmark (from Organisation for Economic Co-Operation and Development, 2003b: Figure 6). 117

Table 21: Atom fractions for Pu(PWR) + MA. 118

Table 22: Characteristics of the U/Pu-cycle vs. the Pu(PWR)-cycle from the VSOP-A calculations of the pilot study..... 119

Table 23: Fuel materials balance for the U/Pu-cycle vs. the Pu(PWR)-cycle from the VSOP-A calculations of the pilot study..... 120

Table 24: Characteristics of the U/Pu vs. Pu-fuel cycles for VSOP 99/05. 122

Table 25: Materials balance for Pu(PWR) vs. U/Pu(LEU) fuel for the PBMR-400 MW_{th} 123

Table 26: Materials balance for Pu(PWR)+MA vs. Pu(PWR) fuel. 124

Table 27: Temperatures for resonance integral calculations for VSOP 99/05..... 135

Table 28: Materials balance for Pu(PWR)+ ^{237}Np vs. Pu(PWR) fuel 167

Table 29: Important new variables in VSOP 99/05..... 193

Table 30: k_{eff} as a function of GAM-I-150 concentration..... 209

Table 31: k_{eff} as a function of B-Nat concentration 210

Table 32: Shuffling of fresh fuel into the batches of the central flow channels (Ch(2), Ch(3) and Ch(4)), flowing down into the storage boxes (STB()) and recirculation to top of channels, for a standard 3-pass fuel cycle. 220

Table 33: Shuffling of fresh fuel into the batches of the inner flow channel next to the central reflector, Ch(1), flowing down and out into the spent fuel tank, for the modified 3-pass Pu-fuel cycle. 224

Table 34: Shuffling of fresh fuel into the batches of the flow channel next to the external reflector, Ch(5), flowing down into the spent fuel tank and into the STB(2), with recirculation to top of channels, for the modified 3-pass Pu-fuel cycle..... 224

Table 35: Shuffling of fresh fuel into the batches of the central flow channels (Ch(2), Ch(3) and Ch(4)), flowing down into the storage boxes (STB()) and recirculation to top of channels, for a the replacement of the start-up fuel core in the modified 3-pass Pu fuel cycle. 227

Table 36: Shuffling of fresh fuel into the batches of the inner flow channel next to the central reflector, Ch(1), flowing down and out into the spent fuel tank, for a the replacement of the start-up fuel core in the modified 3-pass Pu fuel cycle. 227

Table 37: Shuffling of fresh fuel into the batches of the flow channel next to the external reflector, Ch(5), flowing down into the spent fuel tank and into the STB(2), with recirculation to top of channels, for a the replacement of the start-up fuel core in the modified 3-pass Pu fuel cycle..... 227

Table 38: Input data for the 1-D cylindrical cell transport simulation of the control rod in TOTMOS. 244

Table 39: Energy groups for TOTMOS simulation 245

Table 40: Diffusion constants produced by 1-D transport calculations in TOTMOS for VSOP-A card C7-6. 246

Table 41: 3-D MECS control rod worths and 2-D MEB in VSOP-A, based upon the start-up or equilibrium cores, without control rods and after ^{135}Xe decay. 247

Table 42: 2-D control rod worths in VSOP 99/05 equilibrium cores, with equilibrium temperatures, after ^{135}Xe decay and for 12 CRs completely out versus completely in. 247

Table 43: 2-D control rod xenon override margins in VSOP 99/05 for partial insertion of 24 control rods into equilibrium cores..... 248

Table 44: ^{135}Xe atom density variations responsible for override requirement..... 248

Table 45 2-D 12 control rod shut-down balance in VSOP 99/05..... 252

1 Introduction

1.1 Definition of terms

Unless stated otherwise, the definitions from Lamarsh and Baratta (2001) will be used throughout this thesis. Therefore definitions will only be given when the author wants to highlight specific aspects from these definitions, or when new concepts are defined.

Definition of the reactor:

Unless stated otherwise, the reactor configuration that will be studied is be the PBMR DPP-400, which refers to the 400 MW_{th} Pebble Bed Modular Reactor Demonstration Power Plant, which was the original standard design for the PBMR (Pty.) Ltd. This reactor must be distinguished from the 200 MW_{th} PBMR reactor, based on the HTR MEDUL, which, shortly before the downsizing of the company, was accepted as new demonstration plant and was therefore also called the PBMR DPP.

Two distinct simulation input models were used for this PBMR DPP-400 reactor, i.e. the official model of the PBMR (Pty.) Ltd. for the VSOP 99/05 simulation code, which will here be referred to as the PBMR DPP-400 model, and the model developed by E.J. Mulder for the VSOP-A code, independently developed for review purposes, which will be referred to as the PBMR-400 model.

The most frequently used acronyms and symbols are summarised in Table 1.

Table 1: List of acronyms

1-D/ 2-D or 3-D	One/ two or three dimensional
α	Capture-to-fission ratio
Am	Americium
AVR	Arbeitsgemeinschaftsversuchsreaktor
Cm	Curium
CP	Coated particle
CR	Control rod
DLOFC	Depressurised Loss of Forced Cooling
η	Number of fission neutrons produced per neutron absorbed in the fissile fuel nuclides.
ENDFB	Nuclear library name: Evaluated Nuclear Data File/B
FTC	Fuel temperature reactivity coefficient, i.e. Doppler coefficient, calculated over a finite core.
FTC_{∞}	Fuel temperature reactivity coefficient, calculated over an infinite cylinder.
FZJ	Research Centre Jülich
GNEP	Global Nuclear Energy Partnership

GWd	Gigawatt days
GWd/t_{HM}	Gigawatt days/ton heavy metal
HM	Heavy metal
IAEA	International Atomic Energy Agency
k_{eff} / K_{eff}	Neutron multiplication factor of a finite reactor core, also called the eigenvalue.
k_∞ / K_∞	Infinite neutron multiplication factor of a reactor fuel and moderator mixture
LFR	Lead-Cooled Fast Reactors
LWR	Light water reactor
MA	Minor Actinides
MTC	Moderator temperature reactivity coefficient, calculated over a finite core.
MTC_∞	Moderator temperature reactivity coefficient, calculated over an infinite cylinder.
MOX	Mixed oxide fuel (Pu + ^{238}U)
Np	Neptunium
NWU	North-West University
OECD	Organisation for Economic Co-operation and Development
PBR	Pebble Bed Reactor
PHWR	Pressurised Heavy Water Reactor
Pu	Plutonium
Pu_{HM}	Sum of all Pu isotopes, excluding ^{238}Pu, as defined by the VSOP heavy metal accounting. (See note with Table 25.)
Pu(MOX)	MOX-grade Pu from the spent fuel of MOX-fuelled PWRs
Pu(PWR)	Reactor-grade plutonium from the spent fuel of LEU-fuelled PWRs
Pu(PWR)+MA	Reactor-grade plutonium + Minor Actinides from the spent fuel of LEU-fuelled PWRs
Pu(WGR)	Weapons grade Pu
PUREX	Plutonium extraction process
PWR	Pressurised (light) water reactor
RCS	Reactivity control system, i.e. the system of control rods
RPV	Reactor pressure vessel
SFR	Sodium-Cooled Fast Reactors
TRISO	Tri-structural Isotropic
UTC	Uniform temperature reactivity coefficient i.e. moderator and fuel temperatures are varied by the same ΔT.
UTC_∞	Uniform temperature reactivity coefficient, i.e. moderator and fuel temperatures are varied by the same ΔT, calculated over an infinite cylinder.
TW	Terra watt
U	Uranium
VSOP	Very Superior Old Programs
VSOP 99/05	VSOP 99, version 5 – Developed by FZJ
VSOP-A	VSOP-Advanced

1.2 Problem statement

The world is facing potentially serious plutonium management challenges: hundreds of tons of reactor-grade plutonium have been separated from spent fuel from nuclear reactors in

several reprocessing plants in different countries. According to the US' original Global Nuclear Energy Partnership (GNEP) Strategic Plan, the US also intended to reprocess all its existing and future spent fuel and burn the separated plutonium and Minor Actinide mixture in fast reactors. However, the technology for safe fast reactors is not yet fully developed. Public perception simply leaves this technology in the lurch, though a significant drive to promote the technology has been demonstrated by vendor industries. Light water MOX-fuelled reactors, of which 37 reactors are currently operating satisfactorily in Europe, also cannot incinerate these plutonium mixtures safely to a high extent. By this is meant that because these reactors breed substantial amounts of ^{238}U to ^{239}Pu, the incineration of the ^{239}Pu loaded in its fresh fuel is partly offset by the production of fresh ^{239}Pu. Therefore the net rate of incineration of ^{239}Pu is low and thus substantial quantities of Pu remain in the spent fuel (Mulder *et al*, 2008). Therefore there exists a risk that the world's growing stockpiles of reactor-grade Pu may never be incinerated completely. This plutonium may then pose an ever growing proliferation risk since it can potentially be stolen by terrorists in order to build low yield nuclear bombs. However, during the pilot study (Mulder *et al*, 2008) for the present study, simulations with the VSOP-A code of the PBMR DPP-400 reactor fuelled with pure Pu(PWR) showed that about 99% of the ^{239}Pu in this mixture was safely incinerated. However, VSOP-A excludes the transmutation of the minor actinides (MA) above ^{242}Pu. It also excludes the resonance integrals for ^{240}Pu and ^{242}Pu. The exclusion of these resonance integrals was compensated for by including self-shielding factors for the resonances of ^{242}Pu in the VSOP-A input model, as will be explained in more detail below. For all these reasons, it was uncertain how applicable the VSOP-A code is for simulating Pu(PWR) based fuel cycles. Therefore the VSOP-A input models from the pilot study were translated to VSOP 99/05 for the present study, in order to:

1. include the transmutation of the MA when pure Pu(PWR) is used as fresh fuel,
2. repeat the same calculations with those MA, normally present in spent PWR fuel, included in the fresh fuel,
3. include the resonance integrals for ^{240}Pu and ^{242}Pu fuel, and
4. investigate ways to maximise the nuclear weapons proliferation resistance of the Pu(PWR) fuel cycle.

Thus, the problem to be solved is the simulation and evaluation of the incineration of reactor-grade Pu, with and without the addition of Minor Actinides, in an optimised fuel cycle for Pebble Bed Reactors. The main criterion for the evaluation of these fuel cycles will be the

maximisation of nuclear proliferation resistance of the spent fuel mixture by means of optimising the denaturisation of ^{239}Pu by ^{238}Pu and ^{240}Pu. Secondary criteria will be:

- a negative temperature reactivity coefficient,
- a sufficient shut-down reactivity margin,
- an acceptable maximum fuel temperature, and
- an acceptable maximum power per fuel sphere and per coated fuel particle.

1.3 Structure of the thesis

The thesis will consist of the following chapters:

1. **Introduction** which will include the literature study. From the literature study the research aims and objectives will be determined and their originality will be demonstrated.
2. **Simulation methods**.
3. **Results.**
4. **Discussions** of study and conclusions, which will include the demonstration of the originality of the author's contribution and suggestions for future studies.
5. **Reference list.**
6. **Appendix: Automatic translation of VSOP-A input models to VSOP 99/05**
7. **Appendix: Miscellaneous methods and data**

1.4 Literature study

The objectives of this literature study are:

1) To provide a sketch of the technical, economical and societal context of this study.

2) To mine the relevant literature for technical information that will enhance the simulations for this study.

3) To provide evidence for the originality of the research aims and objectives of this study.

1.4.1 Context of the study

1.4.1.1 Opportunities created by the nuclear renaissance

Today many governments of the world, led by the scientific community, realise that air pollution from coal fired power stations with its associated health risks, acid rain and potential contribution to global warming poses a threat to the global climate, economy and the wellbeing of society in general. These disadvantages must of course be weighed against the benefits supplied to society by the electricity produced by these plants. Even if the advantages of coal power outweighs the disadvantages, it would still be beneficial to reduce the disadvantages. The ExternE commission estimated the external cost of nuclear power in Europe, i.e. the probable costs, due mainly to cancers and subsequent deaths that could be caused by accidental releases of radioactivity, as happened at Chernobyl and Fukushima, at more than a factor 10 lower than for coal fired power stations (European Commission, 2003: 13). Therefore nuclear power could play a substantial role in supplying base-load electricity at lower external cost than coal.

Fossil fuel reserves are also finite. The World Energy Outlook 2009 report (International Energy Agency, 2009) has based its estimates of the available fuel resources and reserves on the German report *Reserves, Resources and Availability of Energy Resources 2009* (BGR, 2009): "Peak oil" is estimated to occur between 2020 and 2025. Hard coal, which will last the longest of all the fossil fuels, is sufficient for only about 125 years of production at the current level.

These problems with fossil fuels led to massive subsidies for renewable energies like wind and solar power (Borenstein, 2008) and consequently significant rollouts of these technologies occurred. Impressive cost reductions, especially for solar power (Fthenakis, 2009), have also been achieved. However, despite massive investment and ongoing research, large–scale economic viability of renewable energy sources like wind and solar

electricity remains challenging, mainly due to low availability and high variability of wind and solar power. After the Fukushima nuclear accident Germany decided to phase out nuclear power and to invest substantial amounts of research and development funding in order to try and overcome these challenges. Power produced by load following power plants is in many cases more expensive than base load power, mainly due to high fuel costs. Power storage systems, of which pumped storage is the most economical large scale option currently available, remain expensive and often cause a significant loss of energy due to conversion inefficiencies. Whilst these losses can be eliminated when the pumped storage scheme is combined with a tidal lagoon, the economics of such a scheme depend on large tidal variation and shallow seas so that large tidal lagoons with low dam walls can be built (MacKay, 2007).

The challenges posed with renewable energies, combined with recent sharp increases, and large fluctuations in fossil fuel prices, led to the hope of a strong *nuclear renaissance* in which expanding nuclear power production would be seen as an essential component of the fight against pollution and global warming. John Ritch, Director General of the World Nuclear Association, projects that in order to mitigate economic, health and environmental disaster, the world needs to expand its current fleet of around 443 nuclear power reactors by a factor of twenty (Ritch, 2007) with a view to supplying the twenty first century with clean energy. However, high capital cost of nuclear power plants, delays in their construction and questions regarding the safe and economical disposal of nuclear waste, combined with a recent sharp declined in the price of natural gas, due to amongst others cheap exploitation of shale gas in the USA, as well as a sharp deterioration of the public's perception of the safety of nuclear power plants, due to the Fukushima nuclear accident, are currently threatening the nuclear *renaissance*. Therefore the nuclear industry may have to improve its performance even further if the expected nuclear *renaissance* is to be accomplished.

1.4.1.2 Sustainability of nuclear fuel supplies

An expansion of the nuclear reactor fleet will cause a huge increase in the demand for nuclear fuels. Recent surveys published by the OECD Nuclear Energy Agency (NEA) and the International Atomic Energy Agency (IAEA) on uranium *Resources, Production and Demand* (World Nuclear News, 2010), commonly known as the Red Book, estimated the known current reserves of high grade natural uranium ore, which can be economically mined at conservative prices (< 260 $/kgU), at 6.3 million tonnes. (By kgU is meant kg U_3O_8.) At the current consumption rate of 66,500 tonnes per year, in the current fleet of Light Water Reactors, which burn mainly the 0.7% fissile uranium-235 in natural uranium, this will last about 95 years. As will now be shown, this assumption of "conservative prices" may cause a

significant under-estimation of the potential long term uranium reserves for a sustainable nuclear reactor industry:

Since the cost of the natural uranium in the fuel comprises a small fraction of the generation cost of nuclear power, the operating margins of nuclear reactors are extremely insensitive to increases in the uranium price. At a uranium price of 110 $/kg (i.e. 50 $/lb), which is reasonably representative of recent uranium prices, uranium would contribute about 0.5 $cent/kWh to generation cost (World Nuclear Association, 2005: 49). The generation cost of newly built nuclear reactors is estimated at about 5.0 $cent/kWh, excluding uranium costs, which is competitive compared to the other power options (World Nuclear Association, 2005: 56). Uranium, at 110 $/kg would thus contribute less than 10% of the total new build nuclear electricity generation cost. This means that if the uranium price were to increase with a factor 2.36 to the current upper limit of the Red Book data, i.e. 260 $/kg, the generation price of new build nuclear power will increase by only 12%. The magnitude of the economically extractable uranium reserves, on the other hand, may be more sensitive to price. Because the selling price of uranium comprises 100% of the income of a mine which only mines uranium, the same factor 2.36 increase in the uranium price will cause a 136% increase in the income of such a mine. It is thus to be expected that price increases will aggressively incentivise marginal mines to increase their production, thereby increasing the available resources. From the Red Book data (IAEA, 2010: 10) it is, however, clear that while sharp increases in resources did indeed occur between 40 $/kgU and 80 $/kgU, the expected increase in resources did not occur in the upper part of the price range that the Red Book covered. A 100% price increase from 130 $/kgU to 260 $/kgU only increased the total global resource by 17% from 5.4 million tonnes to 6.3 million tonnes. However, Fetter and Bun (2006) point out that other geologic data indicate that the total amount of uranium increases exponentially with decreasing ore grade. It must further be noted that during the long slump in uranium prices which followed the demise of the nuclear power industry after the Chernobyl disaster, prices were usually below 40 $/kgU and thus very little uranium exploration was undertaken, especially regarding the lower grade uranium ores with production costs above 40 $/kgU. It can be assumed that our current knowledge of the low grade uranium reserves is very limited. This suggests that new exploration, and recovery from the non-conventional sources, which are not covered by the Red Book, might well replace the current plateau in resources at the higher end of the price range with the expected exponential increase. If such resources were, however, not to be discovered, the upper limit of the uranium price will probably be determined by uranium extraction from sea water. Tamada *et al* (2006) reported extraction costs as low as 250 $/kgU. With about 4 billion tons of uranium dissolved in the seas, this resource dwarfs the mineable resources in

the earth's crust and will probably be more than enough to supply any conceivable demand for thousands of years.

After performing exhaustive sensitivity calculations on the break-even uranium price in order for fast breeder reactors to become economic viability, Bunn, Fetter *et al* (2003: 94-95) concluded that a chemical reprocessing price of 1,000 $/kg_{HM}$ (in 2003 dollars), and on condition that the capital costs of fast breeder reactors could be reduced to the same levels as PWRs, breeder reactors would become economical when the uranium price rose above 140 $/kgU. However, if the capital cost of the breeder reactors exceeded that of the PWRs by 200 $/kW_e$ installed, the breakeven price would go up to 340 $/kgU. It is thus clear that if the economics of chemical reprocessing and of breeder reactors cannot be improved, the 250 $/kgU sea water ceiling in the uranium price may prevent the anticipated large scale introduction of breeder reactors by keeping PWRs economical over very long time scales. If, however, the anticipated large scale extraction of uranium from sea water does not materialise, it is comforting to know that breeder reactors can take over the task of supplying the world's energy needs at as low a uranium price as 340 $/kg. It is further comforting to know that even this price increase will increase the generation costs of the new build PWRs by only about 31%, which should not threaten their long-term exploitation.

^{238}U is 141.9 times as abundant as ^{235}U in natural uranium, i.e. the total mass of natural uranium is 142.9 times the mass of ^{235}U. It would thus appear that the replacement of the utilisation of mainly ^{235}U in PWRs by full utilisation of both ^{235}U and ^{238}U in fast breeder reactors, would increase the total amount of energy that can be extracted from natural uranium by a factor of 142.9. However, PWRs convert small, but significant, fractions of the ^{238}U in their LEU fuel to fissile ^{239}Pu and fission a large fraction of this ^{239}Pu. They further fast-fission a small fraction of the fissionable ^{238}U directly. Therefore PWRs, as well as other thermal reactors, are more efficient than where they would only have fissioned the ^{235}U. Furthermore, with continuous recycling in fast breeder reactors, some of the ^{238}U would be lost through inefficiency in the chemical reprocessing. Some of the MA will also be transmuted to isotopes that cannot easily be fissioned. Therefore fast breeder reactors cannot fission 100% of the available natural uranium. It is thus generally accepted that fast breeder reactors can potentially increase the amount of energy that can be extracted from natural uranium by about a factor fifty. Recent successes with the designs of Molten Lead-Cooled, as well as Molten Sodium-cooled, Fast Breeder Reactors (FBRs) promise commercialisation of these reactors in about 25 years' time (see detailed discussion below). This means that the above mentioned 100 years' worth of uranium resources will then last in the order of 5,000 years in such reactors. Due to the 50-fold increase in fuel efficiency of FBRs, uranium fuel costs would then comprise only about 0.2% of their power costs. This

means that even a 100-fold increase in the uranium price to 11,000 $/kgU will cause only about a 20% increase in their power costs. While it is not easy to estimate the available resources at such extravagant prices, it is clear from the discussion above that either extraction from seawater or the mining of low grade ores and non-conventional resources will make massive uranium resources available at such prices. Combining this analysis with the fact that thorium-232 is three to four times more abundant in the earth's crust than uranium, it becomes clear that the earth most probably has enough combined uranium and thorium reserves to fuel extravagant energy demands for millions of years with breeder reactors.

1.4.1.3 Radiation protection and nuclear waste management

Despite the factors described above, the nuclear renaissance did not get off to a smooth start. The global panic after the Three Mile Island and Chernobyl accidents caused governments to create irrational, and thus unreasonably strict, regulations for new nuclear reactors (Hoegberg, 1998). By irrational is meant that in spite of the fact that the external cost of nuclear power, i.e. the probable costs, due mainly to cancers and subsequent deaths that could be caused by accidental releases of radioactivity, as happened at Chernobyl, is more than a factor 10 lower for nuclear power plants than for coal fired power stations (European Commission, 2003: 13), license applications for nuclear power plants are often refused or delayed, while a licence for a coal fired plant to replace this nuclear plant is, at least in South Africa, granted without a problem. In fact, with the exception of wind power, which cannot provide base load power, nuclear has lower external costs than even hydro and solar power. However the regulatory burden imposed on nuclear technology is far greater than that faced by other sources of power, especially in relation to external cost.

These fears have recently increased strongly after the Fukushima nuclear accident in March 2011, leading to the German Government's latest decision to phase out all nuclear power plants in Germany (World Nuclear News, 2011). Similar fears led to recent scrapping of the Yucca Mountain high level nuclear waste repository in the United States of America (World Nuclear News, 2009). These political and regulatory challenges caused many nuclear building projects to end up over budget and behind schedule (Cooper, 2009), thereby damaging the economics of nuclear power plants to the point that globally private firms are not willing to build nuclear power plants without government subsidies and/or guarantees.

Furthermore, the *World Energy Outlook 2009* report found that the financial crisis of 2008 led to a global reduction in energy consumption, which caused sharp reductions in fossil fuel prices and strong cutbacks in spending on research and development of all energy technologies and in investment in all types of new energy projects (International Energy Agency, 2009). These cutbacks, together with the above mentioned regulatory and cost

challenges, led to several nuclear building projects being cancelled (or put on hold), including the PBMR-DPP in South Africa. Therefore the nuclear renaissance kicked off much slower than originally anticipated.

It should, however, be noted that none of these problems are inherent to nuclear power. By this is meant that the current fleet of nuclear reactors, even when the Three Mile Island and Fukushima nuclear accidents and the Chernobyl nuclear disaster are included, has an excellent safety record. After the Chernobyl disaster the designs of all susceptible reactors in the remaining fleet of mainly Generation II reactors have been corrected in order to make a Chernobyl-style explosion impossible in all currently operating commercial reactors. Furthermore new nuclear reactors, i.e. Generations III, III+ (Schulz, 2006) and IV (DOE, 2002), are several orders of magnitude safer than these remaining Generation II reactors. Several safe techniques for high level waste disposal in deep geological repositories have also been developed and plans for final spent fuel repositories are in advanced stages in several countries (Lidskog and Andersson, 2002). Research has shown that the probabilities that the radioactive waste will escape from these repositories and pose a significant threat to human health are negligible. Therefore the constant refrain in public debate that no safe solution for the final disposal of high level nuclear waste has yet been found, is not supported by the scientific evidence. Rather, it seems to be a remnant from fears instilled in the public mind by the horrors of the atomic bomb explosions at Hiroshima and Nagasaki. The prospects for safe and affordable disposal of nuclear waste thus seem bright, provided that the public can be convinced of the validity of the scientific basis for these disposal techniques.

1.4.1.4 Risk of nuclear weapons proliferation

The main, serious and unresolved problems for the nuclear power industry are:

1. The perception amongst the general public that nuclear reactors are not safe, i.e. they are prone to exploding like the Chernobyl reactor did.

2. The public perception that nuclear waste cannot be disposed of safely.

3. Nuclear weapons proliferation.

As has been shown above the problem of reactor safety has already been solved on a technical level, to the extent that the real risk to the public is very small, compared to, for instance, the risk that the public normally accepts from coal-fired power stations. This was recently demonstrated by the Fukushima Daiichi nuclear reactor accidents. Although this was the second worst nuclear accident in known history, and although it has been classified in the

same category as the Chernobyl accident, there have thus far been no fatalities due to the radiation that was released. The expected number of long term cancer deaths due to this radiation is also very small. While there is broad consensus amongst the nuclear community that this accident showed that nuclear safety measures need to be improved even further, it also demonstrated the excellent safety standards of current reactor designs. Therefore the problem of exaggerated safety fears needs to be addressed mainly on a political and public relations level. It has also been shown that, while no firm decision has been made on which waste disposal technique will be best, several options exist that will limit the real risk to the public to very small levels. While research should obviously continue to optimise these techniques, the waste problem should also be addressed mainly in the political and public relations arenas. However, since the total amount of radiotoxicity of nuclear waste remains a concern, this study will also continue the investigation into the optimised incineration of pure Pu(PWR) in the PBMR DPP-400, started in the pilot study (Mulder *et al*, 2008), by investigating the possibility of including MA from spent nuclear fuel in this fuel mixture.

Unfortunately the risks of nuclear weapons proliferation and of nuclear war and/or nuclear terrorism do not exist in the public imagination only, but constitute a very real threat to the peaceful existence of humanity. Therefore, a main aim of this study will be the reduction of the proliferation risk associated with nuclear fuels in nuclear waste, by developing an optimised fuel cycle for the incineration of pure Pu(PWR).

As can be seen from their respective critical masses (European Nuclear Society, 2010 and Ezoubtchenko *et al*, 2005), almost all of the isotopes in the transmutation chains of U and Pu can theoretically be used to build a bare critical assembly, i.e. a nuclear weapon and thus pose some hypothetical proliferation risk. Fortunately many of these isotopes have properties that cause their utilisation as nuclear weapons fuel to be impractical. Therefore, several fuel cycles that have high resistance to proliferation have been developed (Ezoubtchenko *et al*, 2005). The build-up of ^{240}Pu in the waste of high burn-up U/Pu fuel cycles denatures the ^{239}Pu, making it impossible to build high yield nuclear weapons from this waste (see detailed discussion below). Similarly the build-up of ^{232}U, due to a (n,2n) reaction with ^{233}U, produces highly radioactive daughter products in high burn-up ^{232}Th/^{233}U fuel cycles, which makes it very dangerous to work with the material and therefore acts as a deterrent against nuclear proliferation (Herring *et al*, 2001). The spent fuel from Pebble Bed reactors are also highly proliferation resistant because of the very high burn-ups that produce very high radioactivity of the waste and extreme denaturisation of the ^{239}Pu with ^{240}Pu and of the ^{233}U with ^{232}U (Teuchert *et al*, 1979: 23). Furthermore it would be challenging, but not impossible, to extract the fissile isotopes from the millions of coated particles in the spent fuel spheres.

The sad reality, however, is that all fissile isotopes can be fissioned in the fast spectra of nuclear weapons and that, therefore, there is no nuclear reactor fuel cycle which caries absolutely no proliferation risk:

- The deterrent value of radioactive isotopes in the waste can be reduced by shielding materials or by modifying the fuel cycle in order to produce low burn-up waste which will be less denatured (Kang and Von Hippel, 2001). It is also regularly pointed out in the public debate regarding the nuclear proliferation resistance of $^{232}Th/^{233}U$ fuel cycles that the higher ^{235}U enriched (20%) LEU, normally proposed as a driver material for these fuel cycles, can potentially be diverted before entering the reactor. It would then be easier to enrich this fuel to weapons grade (> 90%) HEU, compared to the lower enriched (about 3%) LEU used in traditional PWR fuel cycles (Makhijani and Boyd, 2009). Therefore the driver material in thorium fuel cycles does carry some proliferation risk. In the case of radical terrorists who are more than willing to sacrifice their lives during the construction or deployment of such a nuclear weapon, the deterrent value of high levels of radioactivity, due to high concentrations of ^{232}U in high burn-up ^{233}U, will probably not be enough to prevent them from building nuclear weapons from these materials.

  As for the ^{233}U in the spent fuel of Th-cycles, it should be noted that ^{233}U has a lower critical mass than ^{235}U, also when it is doped to ^{238}U. Doping to ^{238}U to a level of 20% ^{235}U makes the mixture proliferation resistant by increasing the critical mass of a bare metallic sphere to 803 kg. However, when this ^{235}U is replaced with ^{233}U, the critical mass decreases and therefore the doping must be reduced to 11.5% ^{233}U in order to regain the same critical mass (Ezoubtchenko *et al*, 2005: Fig. 2).

  Furthermore, as will be pointed out below in more detail, the denaturisation of ^{239}Pu with ^{240}Pu only gives proliferation resistance against the manufacture of high yield nuclear weapons, but not against low yield nuclear weapons, which may still be suitable weapons for the purposes of terrorists. This realistic view about the inability of proliferation resistant fuel cycles to completely eradicate proliferation is echoed by the modest way in which the Technology Roadmap for Generation IV Nuclear Energy Systems (DOE, 2002: 6), which represent the high road in proliferation resistant fuel cycles, summarises its proliferation resistance goal: “Generation IV nuclear energy systems will increase the assurance that they are a very unattractive and the least desirable route for diversion or theft of weapons-usable materials, and provide increased physical protection against acts of terrorism.”

- It is thus clear that where governments harbour the ambition to develop nuclear weapons, the proliferation resistance of some fuel cycles will not be sufficient to stop them. While some fuel cycles do possess high levels of proliferation resistance, other fuel cycles with low proliferation resistance always remain available for such countries. Starting a civil nuclear power programme and signing the nuclear Non-Proliferation Treaty (NPT), will offer a useful cover to such governments for acquiring the necessary skills and materials for the production of nuclear weapons, with the help of the international nuclear establishment. Meanwhile such governments can then, under this cover, start to implement other fuel cycle options that are proliferation friendly, such as producing low burn-up plutonium in a research reactor, as North-Korea did, or developing a uranium enrichment programme, as Iran is currently doing. Once all these skills and materials are in place, it will be easy to cancel the NPT, expel the IAEA's inspectors and simply go ahead and build nuclear weapons, as North-Korea recently did.

  It is thus clear that allowing the start of a civilian nuclear power programme in a country which harbours the ambition to develop nuclear weapons, significantly increases the proliferation risk, regardless of the proliferation resistance of the specific fuel cycle of that nuclear power programme. It thus seems inescapable that, at least on a technical level, there is currently no viable solution for the proliferation problem and that ongoing proliferation will, for the foreseeable future, remain a fact of life, just as the increasing risk of nuclear war.

Environmental groups often use similar arguments to call for the total global abolition of nuclear power as the best way to stop nuclear proliferation. However, the following analysis will show that this call is not supported by the above set of arguments.

- While it is clear that the envisioned expansion of nuclear power programmes to many new countries will increase the proliferation risk, the opposite is not true, i.e. shutting down all existing civilian nuclear power programs, or refusing the start of any new ones, will not stop global nuclear proliferation: It should be remembered that many of the countries who developed nuclear weapons, did so before introducing civilian nuclear power programmes, for instance the USA and Israel. Furthermore, no such country has yet used the fissile isotopes from the waste of a civil nuclear power plant to develop its arsenals of nuclear weapons. It should further be remembered that AQ Khan's nuclear weapons technology smuggling network has recently spread the necessary skills and technology for nuclear weapons production far and wide. Forcing all civilian nuclear power programs to close down, or preventing the start of new

ones, will not make these skills and technologies go away.
Therefore, denying a country a civil nuclear power programme will not be an effective means of preventing it from developing nuclear weapons.

- It should further be noted that it would be virtually impossible to circumvent the IAEA's proliferation safeguards, which are connected with any legal civil nuclear power programme, in a country where the government is strongly opposed to proliferation. In fact, in all recent examples of nuclear proliferation, it is well known that the support of the governments of the countries that developed these nuclear weapons was the key driving force behind the successes of these projects, for instance the USA, Russia, China, Israel, South Africa, India, Pakistan and North-Korea. This underscores the point that in the analysis of the proliferation risk of civil nuclear power programmes, a fundamental distinction should be made between countries where the government harbours nuclear weapons ambitions and those that are opposed to all proliferation.

It is thus clear that the central risk factor regarding nuclear weapons proliferation is a political one, i.e. the nuclear weapons ambitions of the respective countries. Therefore the solution to the problem should also be mainly political. Since politics fall outside the scope of this study, it will suffice to say that the central strategy for the prevention of nuclear weapons proliferation should not be to discourage countries from starting or expanding civil nuclear power programs, but rather to discourage governments from seeking to developing nuclear weapons.

1.4.2 Technical basis of plutonium management

The anticipated massive and widespread increase in nuclear power production will seriously increase global plutonium stockpiles. In line with the distinction that was made between the technical and political strategies to prevent nuclear proliferation, there are also two opposing ways to view these plutonium stockpiles:

- Since ^{239}Pu is a prime fuel for nuclear weapons, many view **all Pu as so inherently dangerous that it should either be disposed of in irretrievably deep geological nuclear waste repositories, or be extracted from the waste through chemical reprocessing and then incinerated as completely as possible**. In this view the prevention of nuclear proliferation is viewed as more important than conserving the planet's nuclear fuel supplies. Within this one view, the following two opposing views on reprocessing coexist:

- The traditional view of, for instance, the USA that reprocessing opens up new avenues for proliferation and that all nuclear waste should therefore rather be stored in geological repositories without reprocessing.

- The view of, for instance, those countries that operate MOX-fuelled PWRs, that proliferation can be combated effectively by extracting the Pu from the waste and by subsequent incineration in thermal reactors with low conversion ratios. This will then reduce the total mass of Pu on the planet and, more importantly, denature the Pu to the extent that it will become highly proliferation resistant. The subject of this study, i.e. incinerating reactor-grade Pu in a PBMR DPP-400, falls in this category.

- The **nuclear fuel conservation view**: ^{239}Pu and the other Pu isotopes, used in combination with depleted uranium, are viewed as the best fuels we have for fast breeder reactors (Stacey, 2001: 204-206), since they give the highest conversion ratios and thus the highest levels of conservation of nuclear fuel supplies. Therefore, in the case that the earth's uranium reserves may get depleted, these Pu stockpiles and the stockpiles of depleted U could form the basis of a virtually unlimited nuclear power supply, based on FBRs. Therefore all waste Pu stock piles are viewed as a most valuable resource for the future that should be conserved. Our Pu stockpiles should only be burned in fast breeder reactors so that these stockpiles will be increased, rather than be incinerated.

  Accordingly, the proliferation risk of the Pu stockpiles is something that should be dealt with on a political level and, on a technical level, by increasing the proliferation resistance of the fuel cycles involved, rather than by incineration of our Pu stockpiles.

Which one of these views eventually will prevail will depend to a large extent on whether the earth's nuclear fuel reserves will prove to be sufficient to eliminate the need for fuel conservation through fast breeder reactors and on the outcome of the present political attempts to stem nuclear weapons proliferation. At this stage it does not seem possible to predict with reasonable certainty the outcomes of these two scenarios and therefore, in this study, no choice will be made between these two opposing views on plutonium. Since the topic of this study is incineration of reactor-grade Pu in a PBMR DPP-400, this option will be studied through detailed simulations, while the technical feasibility of the option of using these Pu stockpiles as fuel for fast breeder reactors will only be illuminated from the literature. By presenting both options and indicating their advantages and disadvantages, future decision makers will be empowered to make better choices.

In order to understand to what extent the plutonium should be incinerated in order to give it a high proliferation resistance, it is necessary to investigate the proliferation potential of different Pu mixtures.

1.4.2.1 Nuclear proliferation risk of waste plutonium

The proliferation potential of waste Pu depends sensitively on the presence of ^{240}Pu and ^{238}Pu, which denature the ^{239}Pu and ^{241}Pu.

1.4.2.2 Proliferation resistance of ^{240}Pu

As is well known, ^{239}Pu is a prime fuel for modern nuclear weapons, due to its high values for η and σ_f, when irradiated with high energy neutrons, as is the case in nuclear weapons. However, as can be seen from the current generally accepted classification of the proliferation potential of the different Pu mixtures in Table 2 (Pellaud, 2002: Table 1), the presence of more than 7 percent of ^{240}Pu reduces the weapons usability of the plutonium mixture in reactor waste.

Table 2: Nuclear proliferation classification of plutonium grades.

Grades	^{240}Pu	Usability
Super-grade (SG)	<3 percent	Best quality
Weapon-grade (WG)	3–7 percent	Standard material
Fuel-grade (FG)	7–18 percent	Practically usable
Reactor-grade (RG)	18–30 percent	Conceivably usable
MOX-grade	>30 percent	Practically unusable

This reduction is due to the ^{240}Pu having a relatively high spontaneous fission rate, which increases the spontaneous neutron flux within the fuel at all times. When the nuclear weapon is triggered and the high explosives around the plutonium shell start to implode the fuel, these neutrons cause the nuclear chain reaction to accelerate prematurely. This blows the imploding fuel outward before the designed level of compression could be attained and could be maintained for the designed duration. The fuel assembly thus becomes subcritical before the designed number of about 45 multiplication generations could occur. This process, called pre-detonation, greatly reduces the average energy yield of such weapons, so that these are often referred to as fizzle bombs, producing fizzle yields. This is a stochastic effect which depends on the statistical probability that a few more or a few less spontaneous fission neutrons will be floating around in the fuel at the moment of the implosion, which may cause

a large variation in the magnitude of the premature explosion and therefore in the energy yield. Herring *et al* (2001) used a simplified equation, based on zero-dimensional models of an implosion by Von Hippel and Edwin Lyman, cited in Mark (1992), to calculate the probability of different minimum energy yields, as a function of the ^{240}Pu content, as shown in Figure **1** (Herring *et al*, 2001: Fig. 13).

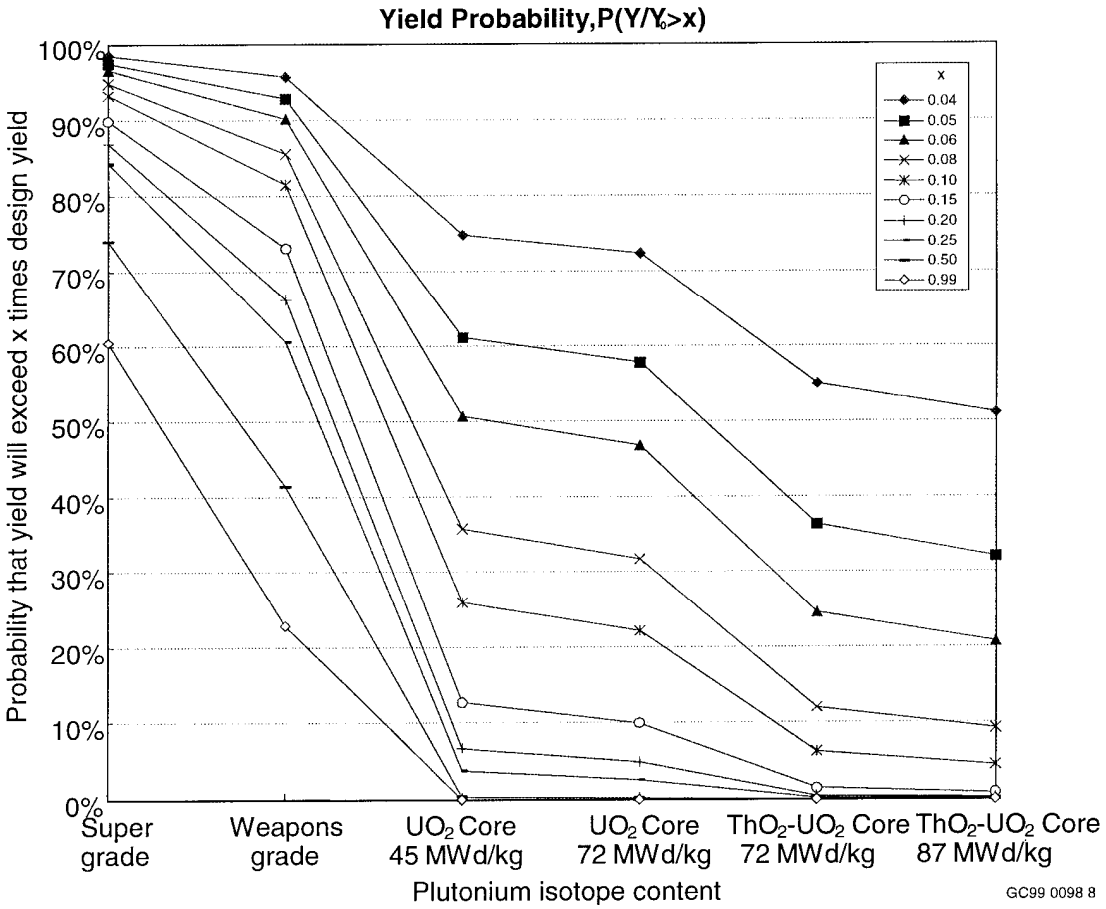

Figure 1: Nuclear weapons yield limitation due to pre-detonation.

From the 50% probability line (X = 0.5 in legend) in this chart it is clear that, while the probable yield of super-grade plutonium exceeds 99% of the designed yield, this quickly drops off to about 6% for standard reactor-grade plutonium, i.e. waste plutonium from a UO_2 core with a 45 MWd/kg burn-up. When it is taken into account that the yield of the Nagasaki plutonium bomb was about 20 kt TNT equivalent, this means that 6% of such a designed yield would amount to 1.2 kt of TNT. Kessler *et al* (2008a) performed much more detailed calculations and arrived at much lower fizzle yields, i.e. 0.1 kt to 0.35 kt TNT. In a related article Kessler *et al* (2008b) performed detailed calculations for the temperature increases in the high explosive lenses surrounding the plutonium core, due mainly to the heat produced by $\alpha-$ decay in the ^{238}Pu. They found that reactor-grade Pu contains enough ^{238}Pu to melt

these explosives or even to cause it to explode, unless some cooling system is implemented, which is deemed to be unfeasible for low-technology proliferators like terrorists groups. They also analysed several fuel cycle options that would produce waste with such high fractions of ^{238}Pu that even medium technology cooling systems would make these weapons unfeasible. They conclude that above 9% ^{238}Pu, only very high technology cooling systems, which only nuclear weapon states would be able to build, would be able to make such a weapon feasible. There is thus a principle difference between the effects of ^{240}Pu and ^{238}Pu in the Pu mixture: while ^{240}Pu does not prevent the nuclear explosion, but only reduces the yield, ^{238}Pu can actually make the construction of an implosion-type weapon impossible, leaving would be proliferators with only the option of gun-type weapons, which would produce even lower yields.

In spite of these reassurances the US government still felt the need to raise awareness about the prospect of reactor-grade Pu being used for proliferation and thus in 1962 actually built and exploded a so-called “dirty bomb”, fuelled with reactor-grade plutonium, in order to demonstrate the possibility (Pellaud, 2002: 31 and Australian Safeguards and Non-Proliferation Office, 1997: Par. 3).

1.4.2.3 Destruction potential of fizzle-yield nuclear weapons

Before a conclusion regarding the danger of nuclear weapons fuelled with reactor-grade Pu can be reached, the effects of fizzle yield bombs should first be investigated. Bell and Dallas (2007) published detailed simulation results for the destruction that the explosion of a 20 kt TNT or a very large 500 kt TNT nuclear bomb would respectively cause in four large American cities. The effects of nuclear weapons depend on many factors such as the height at which the bomb explodes, whether there is snow on the ground, the extent of cloud cover, the wind direction and speed, the type of buildings in the area etc. Since the detailed dynamics of a nuclear explosion fall outside the scope of this study, only the following very limited analysis will be given, in order to obtain a rough estimate of the levels of damage a fizzle bomb might cause.

Blasts decay as the inverse cube of the distance. Therefore the destruction radius of a blast increases as the $yield^{\frac{1}{3}}$, i.e. a 1000-fold reduction in the yield will only cause a 10-fold reduction in the destruction radius. Where, for instance, a 20 kt TNT bomb will break windows with enough force to injure people, due to pieces of flying glass, up to a radius of 6 km (Bell and Dallas, 2007: 5), the same radius for the smallest fizzle yield reported above, i.e. 0.1 kt TNT, will still be 1 km. Since the number of people affected varies with the area, i.e. with the square of the destruction radius, the number of people affected will be directly

proportional to the $yield^{\frac{2}{3}}$, i.e. this smallest fizzle bomb will injure only about 2.9% of number of people that the 20 kt bomb would. Fortunately the thermal radiation decays as the inverse square of the distance from the detonation (Bell and Dallas, 2007: 6) and thus the number of people affected by burn wounds or fires will be directly proportional to the yield. Thus the 0.1 kt fizzle bomb will burn only 0.5% of the number people that the 20 kt bomb would, which would make fizzle bombs very ineffective at creating firestorms in cities. Therefore the main physical effects of fizzle bombs would be destruction by their blasts and radiation injuries.

Conclusion

It is clear from this analysis that the fizzle yields, produced by nuclear weapons fuelled with reactor-grade Pu, are reduced to such an extent that governments will probably consider it not be worth the risk and effort of employing these weapons for military purposes or to arm missiles with them. Therefore the proliferation risk of reactor-grade Pu, in respect of the military arsenals of countries, can be regarded as insignificant.

However, in view of the significant blast damage, combined with the high levels of fear that the associated release of radioactivity will cause in a city, these weapons may be considered sufficiently effective psychological weapons for the purposes of terrorists (which are to terrorise the public), and therefore fizzle bombs might still be attractive to terrorists.

Therefore the ability of the increased levels of ^{240}Pu to reduce the yield of fizzle bombs may not, in itself, be a sufficient deterrent to proliferation by terrorists.

1.4.2.4 Proliferation resistance of ^{238}Pu and proliferation risk of ^{237}Np

Since increased levels of ^{240}Pu alone may not offer sufficient protection against proliferation by terrorists, more emphasis should thus be placed on the ^{238}Pu content, since this has the potential to actually make the construction of an implosion type weapon technically unfeasible, due to melting or exploding of the high explosives by its decay heat. This conclusion will guide the evaluation of the proliferation resistance of various fuel cycles in this study. One important production route for ^{238}Pu (Kang and Von Hippel, 2001: Fig. 6) is:

$$^{235}U \xrightarrow{n,\gamma} {}^{236}U \xrightarrow{n,\gamma} {}^{237}U \xrightarrow{\beta^-} {}^{237}Np \xrightarrow{n,\gamma} {}^{238}Np \xrightarrow{\beta^-} {}^{238}Pu$$

Obviously this production route is cut off if a reactor is fuelled with pure reactor-grade Pu, or is seriously limited in MOX-fuelled reactors where the depleted uranium contains very little

^{235}U. This implies that effective ways to increase the proliferation resistance of reactor fuel cycles even further may be to:

- Add the ^{237}Np from the reprocessed spent fuel of U/Pu cycles to Pu-mixtures, either for pure Pu or MOX fuel cycles. While americium and curium are proliferation resistant due to the high spontaneous fission neutron rates of the different Am isotopes and of ^{244}Cm and the high heat production rate due to alpha-decay of ^{241}Am and the different Cm isotopes, ^{237}NP does pose a significant proliferation risk because it has very low spontaneous fission and heat production rates and because there is no other suitable Np isotope available with which it can be denatured (Rineiski and Kessler, 2010: 501 and 503). Therefore, adding the ^{237}Np to the Pu would improve the proliferation resistance both by destroying ^{237}Np and by producing ^{238}Pu.

  It should also be noted that ^{241}Am alpha-decays slowly ($t_{1/2}$ = 433 y) to ^{237}Np, which is responsible for the small fractions of ^{237}Np in Rineiski and Kessler's (2010: 505) proliferation resistant Pu cycles. This production is limited by both the slow rate of decay of ^{241}Am and the low fractions of ^{241}Am during burn-up, due to its continuous transmutation to ^{242}Am through radiative neutron capture. However, once the spent fuel has been discharged, most of the ^{241}Pu will decay to ^{241}Am within about two decades, as can be seen from the transmutation chain in Figure 2 (Westlén, 2007: 4, Fig. 1.1). Due to the absence of the normal depletion of ^{241}Am by neutron captures, this will lead to sharp increases in ^{241}Am fractions and thus small, but significant, decay rates of ^{241}Am to ^{237}Np. Over many decades this may cause a large enough build-up of ^{237}Np to pose some proliferation risk. Furthermore, ^{237}Np is easily transported to the biosphere, without much absorption in the underground, if it were to escape from a spent fuel repository (Kloosterman and Li, 1995). This means that one of the proliferation resistance aims should be to incinerate large fractions of the ^{241}Pu before permanent discharge or else to keep recycling the spent fuel continuously, in which case both the ^{241}Am and the ^{237}Np will keep being depleted by radiative capture.

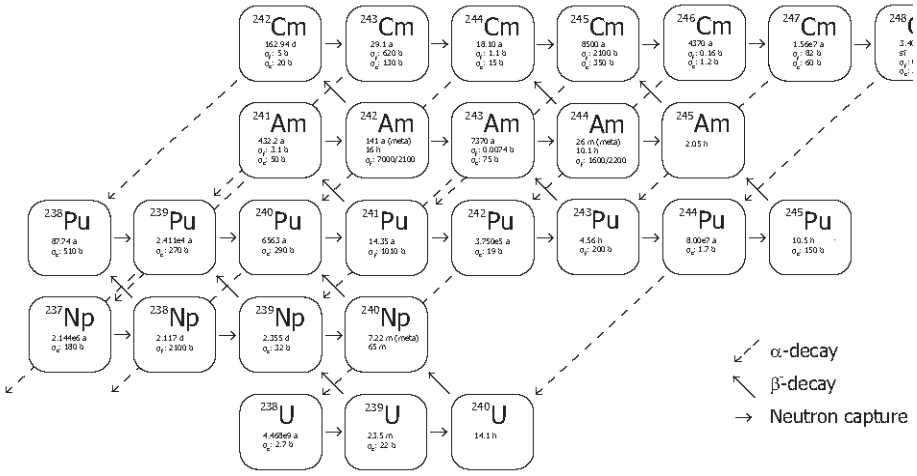

Figure 2**:** The most important actinide nuclides and their relations via α-decay, β-decay and neutron capture reactions. (Cross-sections for capture, σ_c, and fission, σ_f, are given for thermal neutron energies.)

- To replace the normal enriched uranium in U/Pu cycles with re-enriched uranium from reprocessed spent fuel or to replace depleted uranium in MOX with non-re-enriched uranium from spent fuel, since the uranium from spent fuel contains significant concentrations of ^{236}U, which will feed the production route of ^{238}Pu. Unfortunately this will also produce ^{237}Np, thereby increasing the proliferation risk. Therefore this is not a desirable route (Rineiski and Kessler, 2010: 500-501).

- Another way to increase the ^{238}Pu fraction in the waste of U/Pu fuel cycles is to increase the burn-up, since the fraction of ^{238}Pu increases approximately with the square of the burn-up (Herring *et al*, 2001: 68).

The other production route, which is automatically calculated by VSOP 99/05, in Pu-containing fuel cycles is (Rineiski and Kessler, 2010: Fig. 1):

$$^{241}Pu \xrightarrow{\beta^-(t_{1/2}=14y)} {}^{241}Am \xrightarrow{n,\gamma} {}^{242}Am \xrightarrow{\beta^-} {}^{242}Cm \xrightarrow{\alpha(t_{1/2}=163d)} {}^{238}Pu$$

It is clear from this transmutation chain that, apart from increasing the burn-up, which will increase the build-up of ^{241}Pu, other ways to increase the production of ^{238}Pu may be to:

- After chemical separation of the Pu, delay the onset of irradiation in a reactor in order to allow a significant fraction of the ^{241}Pu to decay through its 14 year half-life to ^{241}Am. This option will be simulated in this study.

- Once significant concentrations of ^{241}Pu have built up during burn-up in a reactor, delay the final burn-up phase by temporarily removing the fuel from the reactor. When the fuel is then re-inserted into the reactor, this enhanced concentration of ^{241}Am will act as a source for the radiative capture route to ^{238}Pu. This can possibly be implemented in multi-pass pebble bed reactors by delaying the last pass. This option will not be simulated in this study.

- Add MA, or Am, from reprocessed spent fuel to the Pu mixture, for the sake of the ^{241}Am it contains (Rineiski and Kessler, 2010: 501). This, however, will not be an effective production route, because the Ma mixture in spent fuel consists almost exclusively of ^{243}Am. This is because ^{241}Am has high capture cross-sections, both in the thermal and epithermal energy ranges, and therefore is quickly transmuted via ^{242}Cm to ^{238}Pu during irradiation, thereby preventing significant build-up of ^{241}Am in the mixture. Therefore its build-up only becomes significant once the spent fuel is removed from the reactor.

- Add some ^{233}U and Th to the MOX PWR fuel cycles (Rineiski and Kessler, 2010). This is done in such a way that the ^{233}U is always denatured by the ^{238}U and ^{232}U. While a too high Pu content leads to positive void reactivity coefficients, the addition of the ^{233}U/Th restores a negative void reactivity coefficient. It also leads to a reduction in ^{239}Pu inventory and to higher burn-ups, which result in higher build-ups of ^{238}Pu.

- Recycle the Pu and other selected isotopes continually in fast breeder reactors (Rineiski and Kessler, 2010: Par. 7). In this way the ^{238}Pu builds up to even higher levels and maximal utilisation of uranium resources is assured.

Conclusion

Several highly proliferation resistant Pu fuel cycles for PWRs and fast breeder reactors have been reported from the literature. They are based on:

- removing ^{235}U and ^{236}U from the fuel cycle in order to sharply reduce the production of ^{237}Np,

- adding Am to the Pu fuel in order to stimulate the production of ^{238}U (to levels of 6 – 9 wt% of the Pu spent fuel mixtures) and, in some cases, on

- adding a ^{233}U/Th component to the MOX.

1.4.2.5 Proliferation resistance of ^{232}U in Th / ^{233}U fuel cycles

The most important way to increase the proliferation resistance of ^{232}Th/^{233}U fuel cycles is to increase the denaturisation of the ^{233}U in the spent fuel with ^{232}U. Near the end of the $\alpha-$ decay chain of ^{232}U (Kang and Von Hippel, 2001: Fig. 4), ^{208}Tl builds up which is highly radioactive and produces a 2.6 MeV $\gamma-$ ray when it decays, which potentially poses a large radiation as well as a detection risk to would-be proliferators during the construction and deployment of a ^{233}U fuelled nuclear weapon. For realistic burn-ups in PWRs with a Th-cycle, ^{232}U would build up to about 0.3% (Kang and Von Hippel, 2001: Fig. 10), compared to ^{233}U. ^{232}U $\alpha-$ decays with a half-life similar to ^{238}Pu and will thus also produce some decay heat. Unfortunately this 0.3% ^{232}U fraction is more than a factor ten less than the target of 6 – 9% ^{238}Pu for proliferation resistance in Pu due to decay heat that would melt or explode the high explosives around an implosion type nuclear weapon. Therefore decay heat does not add significantly to the proliferation resistance offered by ^{232}U. Furthermore, due to the very low rate of spontaneous fission neutron emissions in ^{233}U/^{232}U mixtures, these mixtures are suitable for the construction of simple high-yield gun-type nuclear weapons (Kang and Von Hippel, 2001: 23). This deprives this mixture of the proliferation resistance offered by the fizzle-yield limitations which spontaneous fission neutrons from ^{240}Pu offer to, for instance, reactor-grade Pu.

Therefore the only significant source of proliferation resistance in chemically separated ^{233}U/^{232}U mixtures is the radiation threat from ^{208}Tl, which is proportional to the ^{232}U fraction. Apart from the obvious ^{233}U(n,2n)^{232}U reaction, the other production route for ^{232}U is:

$$^{231}Th \xrightarrow{\beta^-} {}^{231}Pa \xrightarrow{n,\gamma} {}^{232}Pa \xrightarrow{\beta^-} {}^{232}U$$

The two source reactions for this ^{231}Th are ^{232}Th(n,2n)^{231}Th and ^{230}Th(n,γ)^{231}Th. Since two of the three mother isotopes for ^{232}U, i.e. ^{233}U and ^{232}Th, are a standard presence in Th/^{233}U fuel cycles, the remaining means to increase the production of ^{232}U are to:

- Use a spectrum with more neutrons with energies above the 6 MeV threshold for the (n,2n) reactions, for instance to use PWRs instead of Pressurised Heavy Water Reactors (PHWRs) (Kang and Von Hippel, 2001: 14-19).

- Increase the fraction of ^{230}Th in the Th-mixture in the fresh fuel, possibly by standard isotope enrichment processes or by using Th from mines with a higher fraction of ^{230}Th. Since ^{230}Th is a by-product of natural uranium decay chains, this will probably be mines that contain both uranium and thorium, or else the ^{230}Th can probably be extracted from the tailings of uranium mines.

- Increase the burn-up. Since all the production routes described above require two subsequent neutron captures, the production rate of ^{232}U is low at the beginning of the burn cycle and increases with burn-up as the intermediate isotopes in these transmutation chains build up.

Build-up of radiation dose through ^{208}Tl:

Since all the other half-lives in the decay chain from ^{232}U to ^{208}Tl are short, the bottleneck for the production of ^{208}Tl is the in-growth of ^{228}Th, which has a half-life of 1.9 years (Kang and Von Hippel, 2001: 7). This means that chemical separation of the ^{233}U/^{232}U mixture reduces the concentrations of ^{228}Th and ^{208}Tl to virtually zero and therefore the radiation threat becomes negligible. The build-up of the dose rate then restarts and reaches about 30% of its maximum level one year after chemical separation (Kang and Von Hippel, 2001: Fig. 5a).

Conclusion

Several means have been shown for maximising the fractions of ^{232}U in the spent fuel and thereby the proliferation resistance from the radiation dose from ^{208}Tl. Unfortunately, reversing these procedures would offer countries with proliferation ambitions the means for minimising this proliferation resistance:

- Using reactors with low fractions of fast (> 6MeV) neutrons, such as PHWRs, will minimise the build-up of ^{232}U.

- Using short burn-up cycles or using Th-mixtures that are low in ^{230}Th will do the same.

- As has been shown above, ^{233}U and ^{232}U are formed in two, chemically similar, nuclear reactions:
  ^{232}Th(n,γ)^{233}Pa, which β^--decays ($t_{½}$=26.97 d) to ^{233}U and
  ^{231}Th, which β^--decays to ^{231}Pa(n,γ)^{232}Pa, which β^--decays ($t_{½}$=1.31 d) to ^{232}U.
  This means that when, in a Molten Salt Breeder, the Pa isotope mixture is chemically

separated from the circulating fluoride salt mixture (Lamarsh and Baratta, 2001: 178), the ^{233}Pa and ^{232}Pa will be separated together. However, the fact that the half-life of ^{232}Pa is much shorter than that of ^{233}Pa means that if the would-be proliferators would wait 3 days, most of the ^{232}Pa will have decayed to the denaturing ^{232}U. This can then be chemically separated and discarded. During the next two months, most of the ^{233}Pa will then decay to pure ^{233}U, which will be only minimally denatured by ^{232}U and will thus make excellent high-yield nuclear weapons fuel.

- Using reactor-grade Pu, instead of reprocessed ^{233}U, as driver material for the Th fuel cycle, will reduce the number of (n,2n) reactions in ^{233}U in the fresh fuel and thereby the build-up of ^{232}U. By eliminating the need to use LEU as driver material, Pu will also eliminate the denaturing of ^{233}U by ^{238}U.

- Repeating chemical separation of the ^{233}U/^{232}U will once again reset the concentrations of ^{228}Th and ^{208}Tl and thus reduce the radiation threat to virtually zero and provide would-be proliferators with a window of opportunity of several months with a sharply reduced radiation risk to the construction workers of the nuclear weapon (Kang and Von Hippel, 2001: Fig. 5a).

- The suitability of ^{233}U/^{232}U mixtures for the construction of simple high-yield gun-type weapons by unsophisticated groups/countries, significantly reduces the proliferation resistance of these mixtures.

  This option also reduces the proliferation resistance offered by the radiation dose: Once the ^{233}U/^{232}U "pits" for a gun-type weapon have been manufactured, these can be stored and shielded separately and can then be inserted into the weapon minutes before detonation (Kang and Von Hippel, 2001: 21-22). Since these pits are very small, small portable lead shields could be used for shielding, compared to the much larger and heavier lead shields that would be required around the outer shell of the high-explosives of a plutonium implosion-type weapon.

These arguments imply that a sharp distinction should be made between the proliferation resistance of a Th-cycle in the hands of countries that are genuinely opposed to nuclear weapons proliferation, such as South Africa, and countries with proliferation ambitions.

By sticking to the principles above, a country that is opposed to nuclear proliferation can operate a Th/^{233}U fuelled reactor in such a way that the ^{233}U is highly radioactive due to a large fraction of ^{232}U. It would then be easy to use radiation monitors to detect and prevent

diversion of the ^{233}U. Extra security measures can also be put in place to safeguard the separated ^{233}U mixture more carefully in the first year after chemical separation, while the concentration of ^{228}Th is still building up. Such a country could consequently rest assured that the way in which it operates its Th-fuel cycle, will make it virtually impossible for another country or terrorist group to steal the ^{233}U from its spent fuel and use it for proliferation purposes. There is thus no reason for such a country to refrain from building such reactors out of concerns about the proliferation risk.

However, countries with proliferation ambitions could easily modify these fuel cycles in such a way that the fraction of the contaminating ^{232}U in the produced ^{233}U will be very low. Such a country could also give the U-mixture to a terrorist group directly after chemical separation. Since the middle part of the decay chain that leads to build-up of the $\gamma-$radioactive ^{208}Tl, will have been removed during chemical separation, the $\gamma-$radiation from the mixture will be reduced sharply for several months, which will reduce the probability of detection while smuggling it into other countries.

These arguments point to the same conclusion that was made earlier, i.e. nuclear weapons proliferation is a political problem which cannot be stopped by proliferation resistant fuel cycles alone and thus also requires political solutions.

1.4.2.6 Conclusion

Several fuel cycles for PWRs and fast breeder reactors, which produce highly proliferation resistant waste Pu, have been demonstrated. They are based on sharply reducing the production of ^{237}Np, increasing the production of ^{238}Pu and, in some cases, on denaturing ^{233}U with ^{232}U. A full section below will also be devoted to the literature on incineration of Pu in PBRs.

An important aspect of these results is, that by emphasising the serious proliferation potential of ^{237}Np, which is produced in significant quantities in all ^{235}U driven fuel cycles, the quoted studies refuted the standard view, described above, that once-through LEU fuel cycles represent the most proliferation resistant option. Since reprocessing and recycling of Pu- and/or ^{233}U- driven spent fuels are obviously the only ways to replace ^{235}U based fuel cycles, it is now clear that recycling, if executed with the right aims, will actually increase proliferation resistance. This does not mean that ^{235}U cannot be incinerated in a proliferation resistant way, but rather that recycling of its waste Pu and, more importantly, its waste ^{237}Np is necessary in order to achieve the highest levels of proliferation resistance.

Once the recycled Pu-mixture has been denatured sufficiently, it should be viable to even export these fuels to countries with proliferation ambitions without significantly increasing the proliferation risk (Rineiski and Kessler, 2010). However, since the $^{233}U/^{232}U$-mixtures can be temporarily decontaminated from ^{228}Th, and thus from the highly radioactive ^{208}Tl, by chemically re-separating the U, it would present a serious proliferation risk to supply ^{233}U-dominated mixtures to countries with proliferation ambitions, even if the ^{233}U is highly contaminated with ^{232}U.

Since the proliferation resistance of pebble bed fuel cycles will be studied in detail throughout the simulations in this study, and since a full section will be devoted to it, the literature on the incineration of Pu in PBRs was excluded from this introductory discussion.

1.4.3 Plutonium dispositioning strategies

The three dominant philosophies regarding the prevention of proliferation, which have been mentioned above, are now described in more detail.

1.4.3.1 Storage without recycling

After having cooled for several years in water in a spent fuel tank, the spent fuel assemblies are entombed in concrete, with a view to subsequent final disposal in a deep geological repository. For about the first 40 years it is stored in a safeguarded repository. Over the medium term, the spent fuel is lethally radioactive, the concrete casks very heavy and bulky and the chemical reprocessing required for the extraction of plutonium very expensive. Therefore, the clandestine diversion and extraction of the Pu or ^{237}Np will be very difficult. This interim storage was meant to be followed by permanent deep geological disposal in the Yucca Mountain repository (Wikipedia, 2007). Due to the stability of this site, the fuel was expected to become chemically exposed only after about a million years (Herring *et al*, 2001: 81-83), while its radioactivity would already have become comparable to the natural U from which it was produced between about 20,000 and 30,000 years (Lamarsh and Baratta, 2001: Fig. 4.56).

However, the future of the nuclear waste management in the USA is currently uncertain. After longstanding opposition by the Democratic Party (Lando, 2006), the Yucca Mountain repository project, which was 20 years behind schedule, was effectively scrapped by pres. Barack Obama (World Nuclear News, 2009, 27 February), shortly after he took office. This decision is currently being challenged in court cases and the outcome is currently uncertain. In the same announcement Pres. Obama mentioned that his administration is busy devising a new strategy toward nuclear waste disposal. Unless such an effective and affordable solution is found, waste management may become a major bottle neck for the US nuclear

renaissance. Even if Yucca Mountain would have succeeded, its capacity was limited and the US has no approved plan to develop other waste repositories. Therefore, without waste reprocessing, Yucca Mountain's capacity would have been exceeded within a few decades. This was probably a principle reason why chemical reprocessing became a corner stone of the new GNEP Strategic Plan. Since only the much condensed volume of long lived fission products, which also produces much less heat, would have been disposed permanently in Yucca Mountain, the waste capacity of the repository would be extended by up to a factor 100. The radiotoxicity of the fission products also become comparable to the natural uranium from which it was mined more than 10 times quicker than for the un-reprocessed once-through PWR spent fuel and thus the time span for which the integrity of a repository must be guaranteed is reduced to about a 1000 years. This is a great advantage since the modelling and prediction of future geological stability become more and more difficult as time spans for these predictions grow to extremely long periods.

1.4.3.2 Isotopic degradation through recycling and subsequent storage

The proliferation resistance is increased by a single recycle of the reactor-grade Pu as MOX in a thermal reactor, normally as MOX in a PWR, in order to reduce the ^{239}Pu inventory somewhat, but much more importantly to heavily denature it by strongly increasing the fractions of ^{240}Pu and ^{238}Pu. This spent fuel is then destined for permanent storage in a deep geological repository, without chemical reprocessing. The most serious problems with this approach are the high volumes as well as the high levels of radiotoxicity of the spent fuel over at least ten thousand years, due to the decay chains of Pu and minor actinides that remain in the spent fuel. Also the fact that the valuable fissile and fertile fuel isotopes in the spent fuel are discarded, thereby potentially reducing the long term sustainability of the global nuclear fuel supply. This approach is therefore regarded as insufficient by the GNEP criteria (DOE, 2007: 4).

1.4.3.3 GNEP: Recycling in fast reactors until practically all heavy metals have been incinerated

The United States' original Global Nuclear Energy Partnership (GNEP) (DOE, 2006a) included an announcement that the US would resume the reprocessing of its massive and growing stockpiles of spent fuel. Since the GNEP embodies important scientific and technical developments, it will still be described here, in spite of its uncertain future. The reprocessing was planned to take place in an advanced facility, scheduled to start operating in 2025 (DOE, 2007). The process was designed to improve the proliferation resistance of reprocessing. Current PUREX reprocessing plants separate the plutonium into a separate stream, thereby increasing the proliferation risk. The GNEP process would purposely produce a mixture of

plutonium, certain very long-lived minor actinides, like Np, Am and Cm and some depleted uranium. These isotopes would then be recycled continuously in fast reactors, until practically all of it has been fissioned. The Technology Roadmap for Generation IV Nuclear Energy Systems (DOE, 2002: 15-16) estimated that, due to research and development needs, Lead-Cooled Fast Reactors (LFRs) will be deployable only from 2025, while Sodium-Cooled Fast Reactors (SFRs) will already be deployable from 2015. GNEP's fuel cycle aims were spelled out in more detail in the objectives of the Advanced Fuel Cycle Initiative (AFCI) (DOE, 2006b).

A major problem with SFRs and LFRs is lack of inherent safety features, because of positive void reactivity coefficients. The mechanism is similar to that in high Pu content MOX-fuelled PWRs, as is explained in detail in Par. 1.4.5.3 below. An anticipated transient without scram (ATWS) would thus increase the power dramatically, so that the fuel would melt within seconds. Tuˇcek *et al* (2006) published simulations that indicated that careful design could improve the inherent safety features of these reactors:

1. In the case of the loss of the circulation pumps for the molten sodium, the sodium would boil within seconds. This would cause a power excursion that would melt parts of the fuel. The molten fuel will then flow out of the core with the sodium. This loss of fuel will cause the reactor to become subcritical so that the fission chain reaction will die down.

   In reality this mechanism does provide some measure of inherent passive safety, since it will prevent a Chernobyl-type explosion of the core. However, this level of inherent safety is much less that the standard that has become customary in HTR safety analysis, i.e. the first level of containment should never be breached no fuel should melt.

2. For LFRs the situation is more favourable. The magnitude of the positive void reactivity coefficient in fast reactors increases with the volume fraction of the coolant, which also moderates the neutrons to a certain extent, during normal operating conditions. Since the sodium atoms are much lighter that lead atoms, they moderate the neutrons more efficiently and thus the positive void reactivity coefficient is larger for SFRs than for LFRs. This problem is countered by using extremely tight lattices in SFR cores. This restricts the coolant flow due to natural convection during a loss of the circulation pumps, which, together with the low boiling point of sodium, induces boiling and thus dangerous void creation within seconds, followed by the power excursion and melting of the fuel described above. However, since lead moderates

the neutrons to a much lesser extent, the lattices can be made much less tight and thus significant natural convection would occur during pump failures. Together with the higher boiling point of lead, this will prevent boiling and void formation and thus will prevent a power excursion. The lead also has a high heat capacity which will enable passive removal of the decay heat, which will prevent fuel melting. While these simulation results still need to be proofed in practice, they provide hope for reasonable passive inherent safety features in LFRs, provided that the core always remains flooded with lead.

An important objective of the GNEP was to extract about 50 times the normal amount of energy from a given mass of natural uranium by fissioning the fertile isotopes too, either directly through fast fission or through first transmutating it to fissile isotopes.

Another aim of the GNEP was to limit uranium enrichment as well as plutonium reprocessing facilities to the countries that already possess well developed fuel cycle capabilities. These "fuel cycle states" would then manufacture and "lease" enriched nuclear fuels to the "reactor states" at a lower cost than what the reactor states could manufacture these by doing their own enrichment or reprocessing (DOE, 2006b: 5-6). The reactor states would then eventually return their spent fuel to the fuel cycle states for reprocessing.

The extreme proliferation resistance of Pu mixtures that have been highly denatured by ^{240}Pu and especially ^{238}Pu, as has been shown above, means that these mixtures can even be safely supplied to countries with proliferation ambitions. The case for plutonium recycling is further enhanced by the fact that the start of the nuclear renaissance caused a spike in the price of natural uranium.

1.4.3.4 The status quo of plutonium recycling

Reactor-grade plutonium is obtained by chemical separation from first generation light water reactor spent fuel with a burn-up of between 45 and 60 GWdays/t_{HM}. A typical isotope vector is shown in **Table 3** (Organisation for Economic Co-Operation and Development, 2003b: Figure 6).

Table 3: OECD benchmark isotopic composition for simulations with reactor-grade plutonium (41.2 GWd/t burn-up + 3 years cooling).

Isotope	Fraction (wt%)
^{238}Pu	2.59
^{239}Pu	53.85
^{240}Pu	23.66
^{241}Pu	13.13
^{242}Pu	6.77

For the purpose of recycling in PWRs, this reactor-grade plutonium is normally mixed with a high percentage of depleted uranium to produce MOX fuel. In order to compensate for the neutronic differences between the usual LEU and this MOX, the fuel loading pattern is normally modified by placing the MOX assemblies in the centre and the LEU assemblies around the periphery of the core. The recycling of reactor-grade Pu in PWRs is already well established on a commercial basis with 37 reactors in Europe currently fuelled in this way (Organisation for Economic Co-Operation and Development: 2003a: 11). While some ^{239}Pu is burned, fresh ^{239}Pu is also produced. Therefore the net consumption of plutonium is limited (Organisation for Economic Co-Operation and Development, 2003a: 14, 17-18). The Pu-mixture, resulting from the recycling of reactor-grade plutonium in the form of MOX, is called MOX-grade Pu and is highly proliferation resistant, due to the increased fractions of ^{240}Pu and ^{238}Pu, as has been showed above.

The OECD created a benchmark for the simulation of repeated plutonium recycling in PWRs. Their reference isotopic composition of the MOX fuel at the beginning of each recycle generation is shown in Table 3 (Organisation for Economic Co-Operation and Development, 2002: 23 (Table 2.4)). The Pu in which this benchmark calls “generation 1” MOX, is what is called reactor-grade plutonium (Pu(PWR)) in the present study. Therefore the Pu in the benchmark’s “generation 2” MOX corresponds to MOX-grade plutonium (Pu(MOX)) in the present study.

Table 4: Reference MOX composition (excluding the ^{238}U) at the beginning of multiple recycles in a standard PWR

Pu generation	**1 Pu(PWR)**	**2 Pu(MOX)**	**3 Pu(MOX2)**	**4 Pu(MOX3)**	**5 Pu(MOX4)**
Total Pu content (wt%)	10.15	13.63	15.98	17.78	19.23
^{238}PU (wt%)	4.00	4.83	5.29	5.54	5.66
^{239}Pu (wt%)	50.40	42.62	39.19	37.12	35.68
^{240}Pu (wt%)	23.00	26.93	28.28	28.93	29.29
^{241}Pu (wt%)	13.50	13.41	12.86	12.31	11.85
^{242}Pu (wt%)	9.10	12.22	14.39	16.10	17.52
^{235}U in depleted U (wt%)	0.25	0.25	0.25	0.25	0.25

Note: Values rounded off to two decimal places.

As can be seen from the first row of these simulated values, the fraction of total plutonium in the fresh MOX fuel starts at 10% and is increases by about 3% with each recycle. The reason is that the fissile quality of the plutonium decreases with every recycle due to increasing contamination with the fertile isotopes ^{238}Pu, ^{240}Pu and ^{242}Pu, which strongly absorb epithermal neutrons through radiative capture, thereby decreasing the reactivity of the reactor. The total plutonium content of the MOX must therefore be increased in order to maintain the reactivity. However, this increased plutonium content causes a serious problem in light water reactors, When the total plutonium content of the MOX goes above about 10 - 14%, the void reactivity coefficient becomes positive (Organisation for Economic Co-Operation and Development, 1995: 17 and Takano *et al*, 1990: Table 6), thereby creating a very dangerous safety problem. Therefore light water reactors are by law prohibited from using MOX fuel with a high total plutonium content. However, since gas-cooled reactors do not suffer from void conditions, this limitation does not apply to Pebble Bed Reactors. As will be shown in this study, these reactors can safely burn even pure reactor or MOX-grade plutonium.

Many environmental groups protested that, since it is much easier to divert the separated plutonium than the raw spent fuel, reprocessing creates a serious proliferation risk. Therefore they called for an end to all reprocessing (Burnie *et al*, 1999). However, the fact remains that past reprocessing already produced massive stockpiles of reactor-grade plutonium, as can be seen in Table 5 (International Panel on Fissile Materials, 2006: Table 2.A.2.).

Table 5: Stockpiles of extracted reactor-grade plutonium.

	Civilian stocks (end of 2004) (metric tons)
France	79 (30 foreign owned)
Japan	5 (+37 in France & U.K.)
Russia	41 (2005)
U.K.	103 (26 foreign owned, plus 1 abroad)
Global total	240

On top of this, the IAEA (2005: Table A20) estimates the amount of plutonium in the spent fuel under its supervision is at about 10 times the extracted amount. The United States and Russia also dismantled a substantial number of their nuclear bombs and consequently declared an excess of a total of approximately 100 tons of weapons-grade plutonium (Oi, 1998). Both countries decided to burn a major portion of this plutonium in nuclear reactors, but have not commenced yet. Therefore it is too late to prevent the proliferation risk by refusing to reprocess spent fuel. Rather, the obvious way to permanently destroy its proliferation threat is to recycle it in reactors until it has been thoroughly denatured, as has been showed above.

1.4.4 Plutonium incineration potential of Pebble Bed Reactors

The PBMR DPP-400 is a high temperature, thermal neutron spectrum, graphite moderated, helium-cooled nuclear reactor (Reitsma, 2004). Together with its specified geometry and low core power density, the PBMR design provides unsurpassed inherent safety features, making a core meltdown practically impossible and major radioactivity release extremely unlikely. Other advantages over standard reactors include improved economics, shorter construction times, distributed power generation, high temperature availability for process heat applications such as hydrogen production, and the possibility of deploying advanced fuel cycles in the existing design.

Gintner (2010) demonstrated the versatility of PBRs in that driver fuel and breeding fuel can be inserted in different fuel sphere types. These fuel sphere types can then be mixed in the core in appropriate ratios. This allows for the possibility of discarding the different types of fuel spheres at different burn-ups, thereby optimising the reactor physics parameters.

1.4.4.1 Potential role for PBRs in GNEP reactor waste incineration

1.4.4.1.1 PBRs compared to fast burner reactors

It has been shown above that the ultimate long term goal of GNEP is to extract practically all of the energy in nuclear fuel, also from the fertile isotopes and the minor actinides. Due to their predominantly thermal and epithermal neutron spectra, low fuel to moderator ratios and tiny fuel kernels, thermal PBRs will not be able to significantly employ fast fissions as a tool to incinerate large amounts of non-fissile transuranic isotopes or the stockpiles of depleted uranium, as is envisaged for GNEP fast burner reactors. Therefore, PBRs will not be able to completely replace fast burner reactors in the GNEP vision. However, as will also be shown in this study, PBMRs can efficiently fission large fractions of the fissile Pu isotopes in light water reactor spent fuel and can transmutate most of the fertile ^{240}Pu to fissile ^{241}Pu and fission it. Although PBRs cannot efficiently incinerate the minor actinides in reactor spent fuel, they could potentially replace fast reactors for the task of Pu incineration. Therefore, until fast reactors can be commercialised safely and cost effectively, PBRs may realise a significant portion of the GNEP waste incineration goals.

1.4.4.1.2 PBMRs compared to MOX fuelled PWR reactors

Burning Pu(PWR) in MOX fuel assemblies in PWRs is the main Pu transmutation strategy currently employed commercially. Unfortunately this strategy is not very efficient, since significant amounts of fresh ^{239}Pu is bred from ^{238}U, limiting the net consumption of plutonium (all isotopes included) to about 15 kg/Terra Watt hour electrical energy (kg/TWh_e) (Organisation for Economic Co-Operation and Development, 2003a: 14). Building dedicated MOX light water reactors may boost the net plutonium consumption to approximately to 60 kg/TWh_e (= 0.5256 Ton Pu/GW_eY) (Organisation for Economic Co-Operation and Development, 2003a: 17-18). Furthermore, the 10 - 14% ceiling for the total plutonium fraction in fresh MOX means that in practice recycling stops after the first recycle, which still leaves large amounts of MOX-grade plutonium, that will ultimately have to be incinerated by fast burner reactors.

Mulder *et al* (2008) employed the following simplified model to estimate the Pu(PWR) incineration potential of PBMRs: assuming an efficiency of 41% and a target burn-up of 692.6 MW_td/kg_{HM} for Reactor-grade Pu (Mulder *et al,* 2008: Table 24), a PBMR will load 1.285 Ton Pu/GW_eY and unload 0.1759 Ton Pu/GW_eY (Mulder *et al,* 2008: Table 25) in its spent fuel, giving a net Pu consumption of 1.109 Ton Pu/GW_eY. For illustrative purposes a simplified mass balance model for the global Pu production and incineration was developed, based on the following assumptions:

1. The current global light water nuclear generation capacity remains fixed at about 370 GW_e.

2. All nuclear new-built is aimed at waste Pu incineration. In the first scenario, all is MOX fuelled PWRs and in the second scenario all is PBMRs fuelled with pure Reactor-grade Pu.

3. This new-built takes place at a compounded rate of 4% per year.

4. Production of waste by the light water fleet starts in 2007 at a rate of 0.328 Ton Pu/GW_eY (Lamarsh and Baratta, 2001: 185-188 and Fig. 4.37).

5. Incineration of the waste Pu by the new-built reactors start in 2008, at the net consumptions described above. No previously produced waste is taken into account.

Figure 3 shows the accumulated mass of waste Pu for the two incineration scenarios, compared to no incineration. The PBMR fleet dramatically outperformed the MOX PWRs. The net incineration of Pu by the PBMRs surpasses the production by the current light water fleet by 2012. By 2018 the backlog of waste will have been cleared and the PBMRs can start to incinerate the stockpiles of Pu produced before 2007.

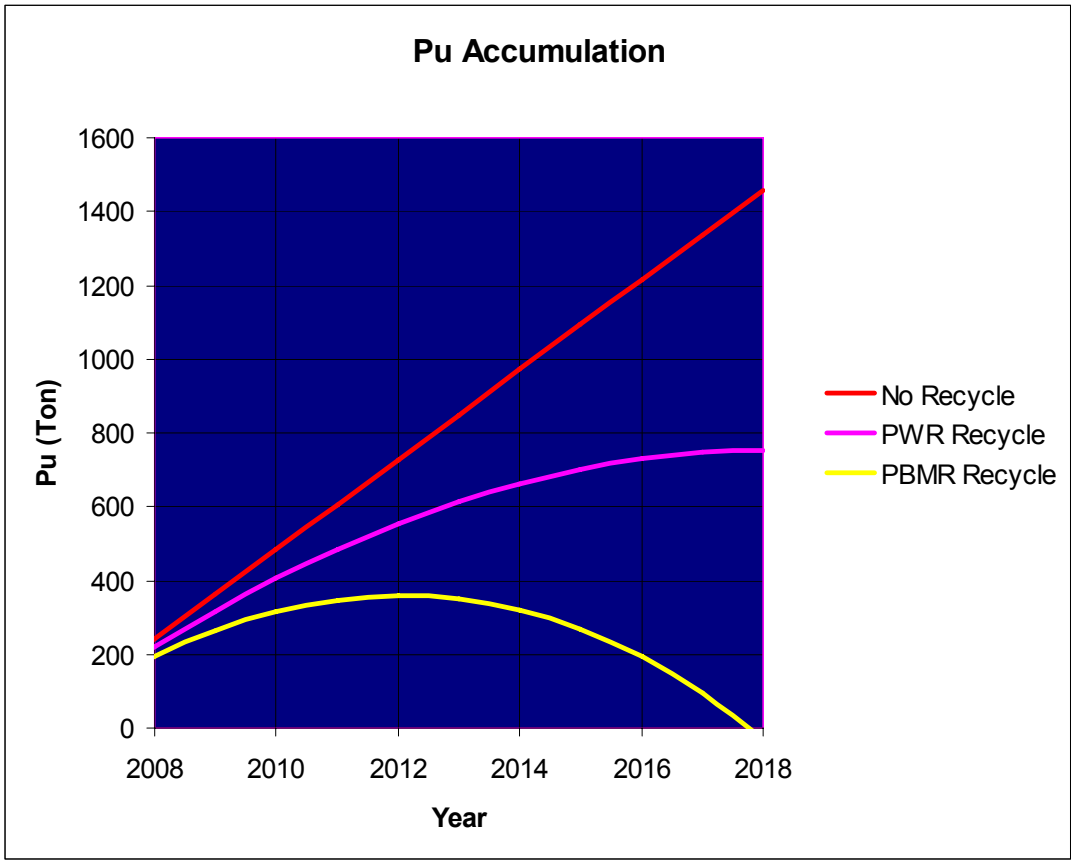

Figure 3: Accumulation of Pu with different incineration options

1.4.5 Technical information for the simulations

1.4.5.1 Near total incineration of ^{239}Pu

In this study a new proliferation prevention strategy will be tested, namely the near total incineration of waste plutonium in Pebble Bed Reactors, specifically optimised to maximise the levels of denaturisation of ^{239}Pu by ^{240}Pu and ^{238}Pu. Due to the high *in-situ* utilisation of the Pu that is produced using the normal LEU fuel cycle in pebble bed reactors (PBRs), a commercially viable Pu reprocessing plant for PBR spent fuel has not yet been developed. Deploying PBRs for proliferation control would thus currently make the most sense if the desired level of proliferation resistance can be achieved in a single burn-up cycle. Fortunately, gas-cooled reactors do not suffer from the above noted positive void reactivity problems, and therefore can safely burn mixtures with a high content of Pu. Rodriguez *et al* (2003) gave an overview of the benefits of deep-burning pure reactor-grade plutonium in a block-fuel type Modular Helium Reactor (MHR), with special reference to the use of Minor Actinides for the purpose of incinerating them on the one hand and using them to supply a negative fuel temperature reactivity coefficient on the other hand. Plukienë (2003) published

Monte Carlo simulations for the incineration of weapons-grade plutonium in the block fuel type Gas Turbine Modular Helium Reactor (GT-MHR). Very high net Pu(LWR) consumption rates for block fuelled Modular Helium-cooled Reactors in closed cycles have also been simulated (Takano *et al,* 1990 and Salvatores *et al*, 2004)).

Mulder *et al* (2008) introduced a new multi-pass fuel cycle for the incineration of pure reactor-grade plutonium in the PBMR DPP-400 which achieved incineration of more than 99% of the ^{239}Pu in a single burn-up cycle of 693 MWd/kg$_{HM}$. That study, which was simulated with VSOP-A, will serve as the pilot study for this PhD study, which will be simulated with VSOP 99/05 (see below for a discussion of the differences between VSOP-A and VSOP 99/05).

The burn-up in the pilot study was enhanced by the multiple recirculation capacity of PBRs which means that highly depleted pebbles will be recirculated together with fresh fuel pebbles. In this way, even the most depleted pebbles will still be irradiated strongly with neutrons and will therefore continue to burn significantly up to the point where very little of the fuel is left. Therefore this reactor achieved an order of magnitude higher burn-up than light water reactors. Since no ^{238}U was added to its fuel, no fresh ^{239}Pu was produced. The very high (66.7%) fissile content of the fuel enabled it to convert practically all the ^{240}Pu isotopes to ^{241}Pu and incinerate it. The total plutonium destruction rate, including transmutation to the MA, was therefore 86.3%. Due to the very high burn-up, the Pu-mixture in the spent fuel was highly denatured by the presence of 4.1% ^{240}Pu, 9.1% ^{238}Pu and 64.4% ^{242}Pu.

1.4.5.2 Plutonium incineration potential of the PBMR DPP-400 design

Talamo *et al* (2004) simulated the incineration of reactor-grade plutonium in a block fuelled Modular Helium-cooled Reactor (MHR) in a closed cycle. They found that an increase in fuel kernel size improved the moderation and therefore slightly reduced the capture-to-fission ratio for ^{239}Pu and strongly increased k_{eff}. This is due to improved lumping, provided by the larger fuel kernels. Improved moderation can also be achieved by using shell-fuel in PBRs and a correspondingly higher volume fraction for the coated particles in the fuel shell. However, it should be borne in mind that increasing the volume fraction too much may lead to increased fractions of crushed fuel particles, as more individual coated particles start to touch each other.

The fuel cycle for the 400 MW$_{th}$ PBMR Demonstration Power Plant (PBMR DPP-400) was designed for a burn-up of 90 GWd/t$_{HM}$. This could possibly be extended to the limit of the German fuel integrity experience, i.e. about 200 GWd/t$_{HM}$ (Kugeler, 2007: Chapter 4). This is much lower than the 693 GWd/t$_{HM}$ target burn-up achieved in the simulations of the pilot

study (Mulder *et al*, 2008: Table 8). Increasing the burn-up to these levels could potentially stress the miniature pressure vessels of the TRISO-coated particles beyond the limits of its integrity, due to disintegration of its structure by excessive radiation damage. At low burn-ups (e.g. 10% FIMA) the fission products are partly retained inside the fuel matrix of the fuel kernels, due to the largely intact fuel matrix. However, at these massive burn-ups, this matrix will be largely destroyed, leaving the coating layers as the only containment mechanism.

Tests at Peach Bottom-1 showed that although plutonium oxide TRISO fuel with an O/Pu atom ratio of 1.68 performed well for extremely high burn-ups of approximately 747 MWd/kg_{HM}, coating failure by kernel migration was seen in particles with O/Pu=1.85, indicating that optimal kernel composition is essential for good performance. The TRISO coated oxide kernels containing 3Th/1Pu performed well under conditions in which almost all fissionable plutonium was fissioned. However, coating integrity of the fuel was not measured on-line in the Peach Bottom-1 experiments, and post-irradiation examinations were cursory, and thus the coating integrity of these samples could not be determined quantitatively. Data on the response of the coatings in high burn-up plutonium fuel during accidents are also not available. (IAEA, 2009: 8-9.)

It should, however, be noted that kernel migration in prismatic block fuelled HTRs, the amoeba effect (Slabber, 2004), is caused by the large temperature gradients inside the blocks, caused by the highly heterogeneous composition of the blocks, i.e. fuel pins containing high packing fractions of coated particles embedded in fuel free graphite blocks. As a result of the varying equilibrium between CO and CO_2 at different temperatures, the oxygen in the PuO_x fuel kernel burns away carbon at its high temperature front and deposits it at the opposing colder front. It is because of this role of oxygen that the amoeba effect can be limited by reducing the oxygen content of the PuO_x mixture. The net effect of this carbon transport is to gradually push the kernel in the direction of increasing temperature, so that the kernel moves toward the SiC layer and it may, when it eventually touches the SiC coating, damage it so that the fission product gasses will leak out of the coated particle and into the He coolant. This problem is aggravated by the fact that the blocks remain stationary for long periods of time. Therefore the temperature gradient through a given coated particle also remains constantly in the same direction for long periods of time. However, the coated particle distribution in pebble fuel is much more homogeneous and therefore the temperature gradient in the radial direction from the centre of the fuel sphere will be much smaller than in the prismatic blocks. Furthermore, while significant temperature gradients do occur, both in the axial and radial directions of the fuel cores of PBRs, the effects of these can be expected to be mitigated by rotation of the fuel spheres, due to friction between the fuel spheres and reflectors and between neighbouring fuel spheres, as they move down the core. Such

rotation will thus cause the fuel kernels to successively migrate towards the coating layers and then back towards the centre of the coated particle, i.e. these migrations will tend to cancel each other out, thereby reducing the probability of the fuel kernel ever reaching and thus breaching the SiC coating.

Jonnet, Kloosterman and Boer (2010) simulated the incineration of Pu and MA in a PBMR DPP-400, with a focus on the failure of the coated particles, due to the build-up of extremely high pressures of fission product gasses, including He produced by $\alpha-$ decay in ^{238}Pu and some of the MA (IAEA, 2009: 6), and the possibility of cracks on the SiC coatings, induced by cracks in the pyrolytic carbon (PyC) layers. While they obtained good results for the incineration of Pu in inert fuel matrices, their simulations suggested probable significant coated particle failure rates for pure $PuO_{1.7}$ at very high burn-ups. Therefore they suggested further development of the TRISO-coated particles in order to achieve such high burn-ups. Simulations indicated that yttria stabilised zirconia coated particle fuel is an optimal choice (PUMA, 2010: 58).

Since it is the interaction between O and C which causes the amoeba effect, it seems logical to attempt to replace the $PuO_{1.7}$ kernels with PuC. However, this is not an option because PuC has a significant vapour pressure which causes unacceptable losses during manufacturing (PUMA, 2010: 43).

Large (500 µm) kernels, diluted with C, outperformed small undiluted PuO_2 kernels, because the larger kernels increased the buffer volume, without increasing its thickness (PUMA, 2010: 43-44). This lowered the gas pressure during irradiation and reduced the diffusion of Pu through the buffer. Good performance was obtained up to normal operating temperatures of 1300 °C; above this the kernels started to leak.

If an affordable reprocessing process for the spent fuel pebbles could be developed, PBRs would then easily be able to achieve almost total incineration of all plutonium by means of multiple recycles. However, within the envelope of the current technology, it would be safer to avoid the destruction of the fuel matrix of the kernel by mixing the Pu with an inert material or with Th (IAEA, 2003), which will reduce the burn-up to safe levels. This Th will breed some ^{233}U, which always improves the conversion ratio and thus the fuel conservation of the cycle. As long as sufficient steps are taken to denature this ^{233}U with ^{232}U and ^{238}U, such a fuel cycle will be highly proliferation resistant, as has been shown above.

1.4.5.3 Influence of the neutron spectrum on reactor safety and conversion ratio in PWRs

Two opposing avenues have been explored for burning MOX in thermal light water reactors, namely very high moderation and very low moderation:

Over-moderation in light water reactors has been simulated successfully (Organisation for Economic Co-Operation and Development, 2003a). This was achieved by increasing the lattice pitch for the fuel rods so that the volume ratio of water to fuel increased from 2.0 to about 4.0 (Organisation for Economic Co-Operation and Development, 2002). Large fractions of the energies of these well-thermalised neutron spectra lay below the epithermal capture resonances of ^{238}U and ^{240}Pu and therefore their resonance escape probabilities are relatively high. The fissile ^{235}U and ^{239}Pu also have very high fission cross-sections (σ_f) for these well-thermalised neutrons, making these spectra very effective at fissioning the fissile isotopes (Stacey, 2001: 7-8 (Fig. 1.4 and 1.5) and 36), which means that lower enrichment fuels can be used. However, the significant radiative capture cross-section (σ_γ) in hydrogen and the greater distances that these neutrons had to travel through the water, due to the increased lattice pitches, significantly increased the neutron leakage and reduced the fractions of fast fissions. Therefore the overall neutron economy and η were reduced, causing these reactors to suffer from a low conversion ratio, which reduces its efficiency in terms of the GNEP objective of extracting maximum energy from the fertile isotopes. Due to the low enrichment of the fresh fuel and due to the fact that the low conversion ratios caused the fuel's reactivity to decrease rapidly with burn-up, the fuel also had to be discarded after only a low burn-up.

By reducing neutron leakage and using a tight pitch, the US was also able to produce a light water breeder reactor that runs on a ^{232}Th/^{233}U fuel cycle (Lamarsh, 2001: 178-181).

Under-moderated light water reactors with U/Pu fuel cycles have also been simulated (Organisation for Economic Co-Operation and Development, 2003a). This was achieved by employing tight pitch configurations, which decreased the water-to-fuel volume ratios, thereby decreasing neutron leakage in the water and increasing the fraction of fast fissions. While breeding is not possible in traditional thermal U/Pu fuel cycles, the decreased water-to-fuel ratio shifted the mainly thermal spectrum of such PWRs up to a mainly epithermal and fast spectrum. In this way the very high conversion ratio of 1.2 has been achieved (Organisation for Economic Co-Operation and Development, 2002), which means that this actually is a light water breeder reactor. However, the reduced moderation exacerbated the

positive void coefficient problem in high Pu content MOX-fuelled reactors (Organisation for Economic Co-Operation and Development, 1995):

^{238}U acts as a net neutron absorber. However, in a well-thermalised neutron spectra, a large part of the spectrum lies below the epithermal capture resonances of ^{238}U (Mulder, 2006: 4, Fig. 3) and therefore the resonance escape probability is high. The moment that the water starts to boil, the steam bubbles form a void that pushes the moderating water away from the fuel rods. Because the moderation level decreases, the thermal energy spectrum immediately shifts up into the epithermal capture resonances of ^{238}U and is therefore strongly absorbed, which immediately reduces the reactivity quite dramatically (Organisation for Economic Co-Operation and Development, 1995: 20 (Table 5)) and therefore the potential runaway condition is brought under control automatically. This creates the desired negative void reactivity coefficient provided by well-thermalised spectra and a high fraction of ^{238}U, as is found in MOX with low total plutonium content.

However, in highly under-moderated spectra, this inherent safety feature disappears:
As has been pointed out above, less moderated spectra require higher enrichment fuels. In MOX fuelled cores, this is achieved by adding higher fractions of total plutonium, thereby reducing the fraction of ^{238}U. Since the spectrum is under-moderated, thermal neutrons are much less abundant. As the void develops, the small thermal part of the spectrum moves up into the epithermal resonances of the fertile isotopes and many are captured. However, the relatively abundant epithermal part of the spectrum shifts up into the high energy region, which firstly means that they are no longer captured by the fertile isotopes and secondly that they will cause more fast fissions (Lamarsh and Baratta, 2001:76-77 and 81: Fig. 3.11). Since the fast fission cross-sections for ^{240}Pu are higher than for ^{238}U and start to increase at lower energies, the fraction of fast fissions will increase dramatically due to both the higher plutonium content and the harder initial spectra (Organisation for Economic Co-Operation and Development, 1995: 14-15). Furthermore, the values for ν and η for fast fissioned ^{239}Pu are much higher than for thermally fissioned ^{239}Pu. This increase in neutron economy with increasing neutron energy is also much stronger for ^{239}Pu than for ^{235}U (Stacey, 2001: 35; 216, Fig. 6.8 and Lamarsh and Baratta, 2001: 80 (fig. 3.10d and 3.10e)). All these factors will sharply increase the reactivity for this high plutonium content core, as the void grows (Organisation for Economic Co-Operation and Development, 1995: 20 (Table 5)).

This is the much feared positive void reactivity coefficient, which was partly responsible for the Chernobyl accident. If the added reactivity is large enough to make the reactor prompt critical and is not countered by a sufficiently strong negative temperature reactivity coefficient, the chain reaction will run uncontrollably and will cause a core meltdown and

possibly a core explosion in seconds. This could happen so quickly that there may not be enough time to insert the control rods. Therefore high plutonium concentrations in light water reactors are prohibited by law. However, since the moderator in HTRs is solid graphite which cannot melt or boil at conceivable temperatures, this void problem does not apply to them.

Salvatores *et al* (2004) calculated the net number of neutrons consumed/fission for most of the important actinides from ^{238}U upwards. Takano *et al* (1990) simulated the recycling of plutonium and the other minor actinides in different types of reactors. Firstly they found that the addition of the minor actinides worked well in the sense that at the beginning of a burn cycle the fertile minor actinides, such as ^{237}Np, Am and Cm, acted as fertile poisons, countering the excess reactivity of the fresh fissile fuel. As the initial fissile fuel burned away, the reduction in reactivity is countered by the fact that some of the minor actinides are transmutated into fissile isotopes (Takano *et al*, 1990: 353). Westlén (2007: 13-20), however, reported that the inclusion of 10% Am in MOX in fast reactors dramatically reduced the magnitude of the Doppler Fuel temperature coefficient and the fraction of delayed neutrons, causing major safety concerns. Therefore the viability of the addition of Am will have to be investigated by means of detailed simulations over the whole energy region. Takano *et al* (1990: Table 6) further reported that the positive void reactivity problem worsened as the fractions of plutonium and minor actinides in their under-moderated PWR increased. Therefore they proposed that the concept of low moderation, high conversion ratio, thermal, trans-uranic burning, light water-cooled cores be abandoned in favour of well moderated spectra. However, Rineiski and Kessler (2010) solved this problem by adding some ^{233}U/Th to the MOX, thereby restoring the negative void reactivity coefficients, provided that sufficiently large fractions were used.

1.4.5.4 Pebble Bed Reactor spectra

The key mechanisms for raising the conversion ratio for light-water reactors, do not apply to pebble bed reactors. In light water reactors, reducing the lattice pitch increases fast fissions and reduces neutron capture in the water. However, the lack of lumping, due to the tiny fuel particles, reduces the fraction of fast fissions in Pebble Bed Reactors to insignificant levels, irrespective of the moderation ratio. Typically only 0.4% of the neutrons produced in LEU fuelled PBMR DPP-400 simulations were from fast fissions of ^{238}U, compared to about 10% in PWRs. Since the capture cross-section for graphite is much smaller than that for light water, capture in the moderator inside the graphite in the pebbles is insignificant and therefore reducing the moderation ratio will not significantly reduce the leakage in the fuel. The conversion ratio in the PBMR DPP-400 is also strongly reduced by the high level of neutron leakage into the reflectors, due to the high surface-to-volume ratio, caused by the

tall, slender core geometry. Consequently the conversion ratio of the PBMR DPP-400 of about 0.45 is much lower than the 0.61 that Takano *et al* (1990: Table 5)) simulated for standard uranium fuelled pressurised light water reactors (PWRs) and much lower than the approximately 0.8 for CANDU heavy water reactors fuelled with natural uranium.

Gas-cooled fast breeder reactors have been designed (La Marsh, 2001: 175-176). However, they use metal-clad fuel rods instead of fuel pebbles and therefore do not possess sound inherent safety features. Development of a pebble fuelled fast breeder reactor is currently underway (Taiwo *et al*, 2002) where simulated conversion ratios greater than 1.2. by drastically reducing the moderation were achieved. However, the practicality of such reactors remains to be seen.

A possible key towards improving the conversion ratio for the PBRs is the reduction of neutron leakage. The high 10-15% leakage for the PBMR DPP-400 occurs mainly in the reflectors and in the control rods. The current PBMR DPP-400 design loses large numbers of neutrons both in the central and outer reflectors: The 2 metre diameter graphite cylinder of the central reflector is so thick that many neutrons cannot migrate through it. As the fast and epithermal neutrons enter the reflector, they quickly get moderated down to thermal energies and therefore the fast and epithermal fluxes approach zero somewhere between 20 to 50 cm into the central reflector (Reitsma, 2004: Fig. 4). At this depth the task of thermalising the neutrons is essentially completed and the rest of the reflector does not contribute to the moderation. This is reflected in the fact that the thermal spectrum peaks at a depth of about 33 cm into the reflector for the Pu-cycle and at about 26 cm for the U-Pu-cycle (Mulder *et al,* 2008: Fig. 4). These neutron flux profiles inside the reflectors are affected by all aspects of the fuel cycles, such as the number of passes through the core and the fuel composition, since these affect both the spectra of the neutron flux that enter the reflector and the absorption rates of thermalised neutrons that leak back from the reflectors into the fuel. Neutrons that are thermalised at a depth of e.g. 50 cm then have to traverse the remaining 150 cm of the reflector to emerge on the other side or have to turn around and migrate the 50 cm back to the edge from which they had entered the reflector. Since the σ_γ increases strongly with decreasing energy, these well-thermalised neutrons have a significant probability of being captured on their way back to the fuel. These losses can be reduced by reducing the thickness of the central reflector to the point where most neutrons will exit the reflector just after they have been properly moderated.

The strong positive temperature reactivity coefficient of the central reflector (Reitsma, 2004: Table 3), is caused by the capture of thermal neutrons in the reflector. Increasing the

reflector temperature shifts the thermal spectrum up, which reduces σ_γ in the graphite, which again reduces the leakage in the reflector and thus increases the reactivity of the core. Thinning the central reflector sufficiently will essentially eliminate this phenomenon in the central reflector. The positive temperature coefficient of the central reflector will thus be replaced by a normal negative moderator temperature coefficient (Reitsma, 2004: Table 3). This may contribute towards countering the observed positive temperature reactivity coefficient for Pu in HTRs, which will be discussed below. The shut-down margin of the reactivity control system will, however, be impaired by such a thinning of the central reflector. This is because the additional fuel, which will fill the space created by the thinning of the central reflector, will be far away from the control rods in the external reflectors. This will reduce the ability of the control rods to suppress the neutron flux in these areas. Therefore care has to be exercised in a holistic, multi-physics design approach. Such a thinning of the central reflector may thus require the introduction of fixed neutron poisons in the central reflector, in order to restore the shut-down margins.

1.4.5.5 Positive temperature reactivity coefficients for Pu in HTRs

During the pilot study for the present work, Mulder *et al* (2008: Table 8) found an increase in k_{eff} of +0.0232 when the temperature of the reactor-grade Pu-fuelled PBMR DPP-400 was increased from 50°C to the full power equilibrium temperature distribution which has an average of just over 800°C. These positive temperature reactivity coefficients for reactor grade Pu, which are caused by large positive moderator temperature coefficients, and which were also reported for block-fuelled HTRs, pose a potentially serious licensing problem since positive temperature coefficients are generally forbidden by nuclear regulations. The source of this problem and possible solutions will be discussed in more detail in the discussion of the results of the present study.

1.4.5.6 Investigation of shell-type fuel pebbles

INEEL (2003: 92) increased the moderation and fuel utilisation of PBR fuel pebbles, simulated for use in the NGNP, by reducing the radius of the inner fuel zone of the pebble and thereby increasing the thickness of the pure graphite shell that surrounds it. However, the heat from the fuel must then pass through a thicker layer of graphite in order to reach the coolant, thereby increasing the fuel temperature. This would lead to a potential relicensing of the fuel. It would therefore be easier to rather add moderator balls statistically.

In the present study the Pu fuel pebbles will be of the shell type, consisting of a pure graphite moderator sphere in the centre, surrounded by a graphite matrix shell containing the fuel particles, which is again surrounded by the normal 0.5 cm thick graphite shell. While this

configuration will also improve the moderation of the neutrons, the hot fuel will now be closer to the cooled surface of the pebble, thereby decreasing the fuel temperature, which will reduce the capture to fission ratio and will therefore increase η for ^{239}Pu (Lamarsh and Baratta, 2001: 287 (Table 6.3)). The cooler fuel will also reduce ^{110m}Ag leakage.

1.4.6 Towards a thorium/^{233}U breeder

1.4.6.1 Thorium/uranium in light water reactors

It is well known that the inherent safety features of thermal reactors are generally better than those of fast reactors, especially in the sense that the combination of temperature and void reactivity coefficients of thermal reactors are normally strongly negative, while they are typically positive for fast breeder reactors. This implies that a thermal breeder or converter reactor will be ideal from a safety perspective. ^{233}U is the only readily obtainable fissile nucleus with a large enough thermal value of η to allow for a thermal breeder. Since thorium is also much more abundant than natural uranium, ^{232}Th/^{233}U fuel cycles have been studied for a long time and for different kinds of reactors, including light water reactors. (Kazimi *et al*, 1999.) Unfortunately these experimental reactors and simulations revealed that due to a variety of factors these Th/U fuel cycles did not produce the anticipated commercial benefits over U/Pu fuel cycles and therefore, apart from India which is poor in natural uranium and has an abundance of thorium, no other country has yet made a serious effort to commercialise Th/U reactors. The problem lies not with the ^{233}U, but with the ^{232}Th, as will be shown in the following analysis.

1.4.6.2 The fast fission potential of ^{232}Th, compared to ^{238}U

Most reactors with high conversion ratios combine the reasonably high values of η than can be obtained for the fissile nuclides in the thermal neutron energy region with the excellent values of η from fast fissions (above about 100 keV) (Kazimi *et al*, 1999: Fig. 1). Since σ_f in this fast region has values in the order of only a few barns, compared to hundreds of barns in the thermal region, significant numbers of these fast fissions can only be achieved by using high fuel/moderator volume ratios and/or relatively thick fuel rods with diameters mostly > 5 mm. Secondly the number of fast fissions is increased significantly by the fact that, for some fertile isotopes like ^{238}U and ^{240}Pu, σ_f in the fast region has similar values to those of fissile isotopes. Since the ^{238}U in LEU is much more abundant that the accompanying fissile ^{235}U or ^{239}Pu, fast fissions in ^{238}U contribute significantly to the reasonable conversion ratios of LEU fuelled light water reactors.

The number of fissions in a given energy region is determined by the resonance integral for σ_f for this isotope and moderator over this region.

Consider a group of neutrons slowing down through an energy interval (E + dE, E) by means of collisions with the moderator in an infinite medium, in the absence of absorptions. By definition, the number of collisions required to slow down through this energy interval

$$= \frac{d(Ln(E))}{\xi} = \frac{1}{\xi}\frac{dE}{E} \quad ,$$

where $\xi = \overline{\Delta u}$, the average change in lethargy in an elastic collision (Lamarsh and Baratta, 2001: 70-71).

This means that at high energies less collisions are required to cross an interval (E + dE, E) and therefore, all other factors being equal, collisions in high energy intervals play a lesser role than in intervals at lower energies.

It is well known that when absorptions are taken into account in a homogeneous reactor in which the absorbing material is "infinitely diluted", i.e. $\Sigma_a << \Sigma_s$:

$$p = \exp(-\frac{N_a I_{12}}{\xi \Sigma_s}),$$

where *p* is the probability of not being absorbed while slowing down through the interval (E_2, E_1), i.e. the resonance escape probability (Lamarsh and Baratta, 2001: 287),

N_a is the number density of the absorbing isotope and

$I_{12} = \int_{E_1}^{E_2} \sigma_a \frac{dE}{E}$ = the absorption resonance integral over this energy interval.

Above the epithermal capture resonances σ_γ < 1 barn for both ^{232}Th and ^{238}U. Therefore the influence of captures on the neutron population in this interval will be very small and will thus be neglected in the following analysis of fast fissions. The above can then be adapted as follows:

The probability for a neutron to cause a fast fission while slowing down through (E_2, E_1)

$= 1 - p_f$

$= 1 - \exp(\frac{-N_f I_{f12}}{\xi \Sigma_s})$, with

p_f the fission escape probability,

N_f the number density of the fuel isotope and

$I_{f12} = \int_{E_1}^{E_2} \frac{\sigma_f}{E} dE$ the fission resonance integral, with this provision that there are no resonances in the fast fission energy region.

In the case of the fissioning of a fissile nuclide, the number of fission neutrons being made available for breeding $= \eta - 2$, since the neutron that was absorbed to cause the fission, as well as an extra neutron required to breed one fissile nuclide to replace the one that was fissioned, must first be replaced before any remaining neutrons can be made available for breeding. (Lamarsh and Baratta, 2001: 122). In this analysis the absorption of neutrons in non-fuel nuclides, such as the control rods, fission products or the pressure vessel is neglected. Therefore, in a real reactor, η typically needs to be above 2.2 in order to allow breeding. The reason why $(\eta - 2)$, rather than $(\nu - 2)$, is used, is explained as follows:

The neutrons that are captured in the fissile nuclide performs no useful function, instead they transmutate a fissile nuclide to a fertile one, which is counter-productive. Therefore these captures are viewed as a pure waste of neutrons. Therefore, in the neutron economy, these are allocated to the neutron cost of producing the ν fission neutrons. Therefore the ratio of fission neutrons produced to neutrons absorbed in order to produce this fission = $\nu/(1 + \sigma_\gamma/\sigma_f) = \nu/(1 + \alpha) = \eta$ (Lamarsh and Baratta, 2001: 85).

Fast fissioning of fertile nuclides:

However, during fast fissioning of a fertile nuclide, the associated captures in this nuclide perform a useful function, i.e. each capture breeds a fertile into a fissile nuclide. Therefore these captures should be allocated to the cost of breeding, rather than to the cost of producing fission neutrons. Therefore, in the analogy to the case above, η will be replaced with ν. Secondly, no fissile nuclide is destroyed by this fission and thus the additional neutron for breeding the replacement fissile nuclide is not required. Therefore the number of neutrons made available for breeding, per fertile fission, $= \nu - 1$. Therefore the average

number of fission neutrons being made available for breeding (N_b) by fast fissioning of the fertile nuclides, by a neutron slowing down through the energy region (E_2, E_1) can be defined as:

$N_b(E_1, E_2)$ = Probability of causing a fast fission while slowing down * $(\bar{\nu} - 1)$

$$= [1 - p_f](\bar{\nu} - 1)$$

$$= [1 - \exp(\frac{-N_f I_{f12}}{\xi \Sigma_s})](\bar{\nu} - 1)$$

$$= [1 - \exp(\frac{-N_f \int_{E_1}^{E_2} \frac{\sigma_f}{E} dE}{\xi \Sigma_s})](\bar{\nu} - 1),$$

with $\bar{\nu}$ the average value of ν for all the fissions in this energy interval.

The energy differential, i.e. $n_b = dN_b/dE$, can be obtained by replacing (E1, E2) with the infinitesimal interval (E, E+dE):

$n_b(E) = N_b(E, E+dE)/dE$

$$= [1 - \exp(\frac{\frac{-N_f \sigma_f(E) dE}{E}}{\xi \Sigma_s})](\nu(E) - 1)/dE$$

A first order Taylor expansion of the exponential around the point (0 + dE) yields:

$$n_b(E) = [1 - (1 - dE \frac{N_f \sigma_f(E)}{E \xi \Sigma_s})](\nu(E) - 1)/dE$$

$$= [dE \frac{N_f \sigma_f(E)}{E \xi \Sigma_s})](\nu(E) - 1)/dE$$

$$= (\frac{N_f}{\xi \Sigma_s})(\frac{\sigma_f(E)}{E})(\nu(E) - 1)$$

While the first parenthesis is independent of the type of fertile nuclide and depends only on the type of moderator and the fuel/moderator geometry, the last two terms are independent of both the moderator and the geometry and depend solely on the choice of the fertile nuclide. From this the breeding potential of any fertile nuclide, for fast fissioning by a neutron

at energy E, which are slowing down by moderation, can now be defined uniquely, independent of the choice of moderator or reactor geometry, as:

$$\text{Breeding potential(E)} = \frac{\sigma_f(E)}{E}(\nu(E)-1)$$

The breeding potential, in barn.neutrons/MeV, of ^{232}Th is compared to that of ^{238}U in Figure 4 below .

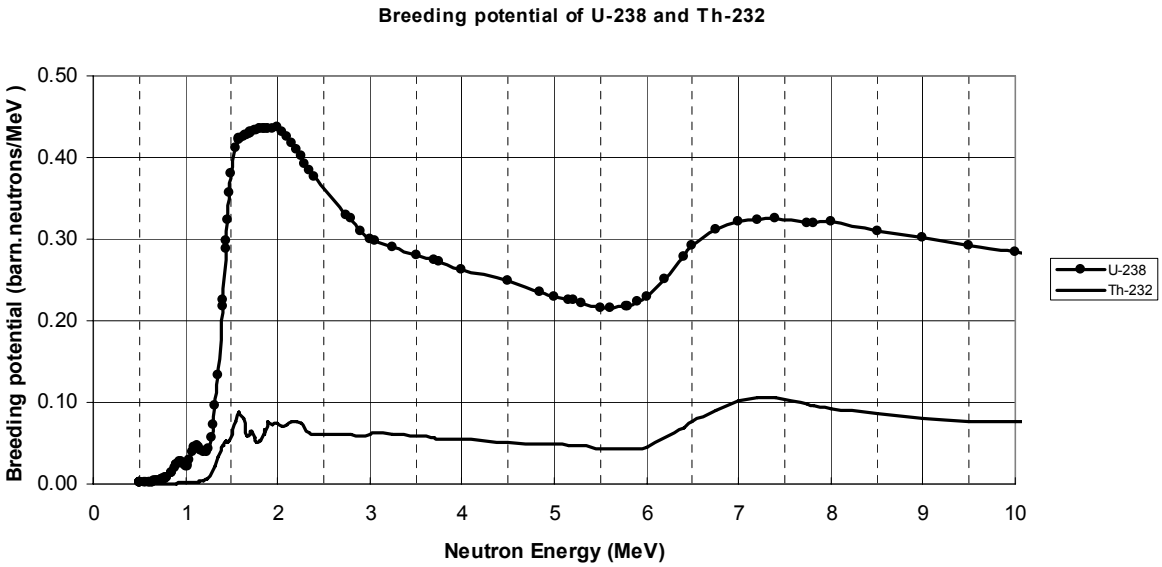

Figure 4: Breeding potential of ^{238}U and ^{232}Th.

It is clear from this chart that the breeding potential of ^{232}Th is almost an order of magnitude smaller than that of ^{238}U. This analysis is, however, over simplified. It takes into account only the slowing down process, without specifying the initial energy spectrum of the fission neutrons, which is known to peak at about 1 MeV and has an average energy of about 2 MeV (Lamarsh and Baratta, 2001: 87). Since the high energy tail of this fission neutron spectrum falls of quickly and becomes negligible above about 4 MeV, only the lower part of the breeding potential chart will be applicable in fission reactors. Since the breeding potential of ^{232}Th is much smaller than that of ^{238}U for all energies, the specific shape of the initial fission neutron spectrum will not influence the main conclusion of the analysis, namely that, in fast reactors, ^{232}Th is a much poorer breeding fuel than ^{238}U. Therefore the influence of the fission spectrum will not be investigated further.

1.4.6.3 HEU driven thorium pebble bed reactors

Another key towards higher breeding ratios is the use of a breeder blanket around the core, as has been implemented in the thorium Pebble Bed converter reactor. Teuchert *et al* (1979) simulated average conversion ratios over a 30 year period ranging from 0.751 for a pre-breeder which used HEU as driver material to breed ^{233}U, which was then fed as $^{233}U/^{232}Th$ into a net breeder which achieved a conversion ratio of 1.000 in a closed fuel cycle (Teuchert *et al,* 1979: Table IV). This net breeder had a very high core volume of 600 m^3 and performed optimally at low burn-ups of about 20 MWd/kg_{HM}. It is clear that, once equilibrium has been achieved, this net breeder requires virtually no natural uranium and thus uses only ^{232}Th as feed material. The only significant consumption of natural uranium occurs in the start-up process where the pre-breeder is used to produce the start-up fuel for the net breeder. Therefore, depending on the details of the sequence in which pre-breeders are used to start up net breeders, very large natural uranium savings can be obtained. It should, however, be taken into account that the chemical reprocessing plants for PBR spent fuel, which are essential to establishing the closed fuel cycle with its high conversion ratios, have not yet been demonstrated on a commercial scale.

The principle techniques used to achieve this excellent conversion ratio in the net breeder was to reduce the neutron leakage by increasing the heavy metal content of the fuel as well as the volume of the core. Since fractional neutron losses increase with the ratio of the leakage area, i.e. the area of the boundary surfaces between the fuel core and the reflectors, to the volume of the fuel core, increasing the core volume reduces this ratio and therefore reduces the leakage. Unfortunately, the leakage of the decay heat during a DLOFC depends similarly on this ratio. Therefore increasing the core volume reduces the reactor's ability to passively leak its decay heat and thus increases the maximum temperature during a DLOFC over the critical safety limit of 1600°C. This problem is normally solved by using much smaller PBRs, typically the PBMR DPP-400 or smaller. Therefore Mulder *et al* (2010) simulated similar HEU driven Th fuel cycles in a 200 MW_{th} PBR, a variant of the HTR-MODUL, and thus managed to limit this maximum temperature to 1607°C (Mulder *et al*, 2010: Table V). Unfortunately this reduced the conversion ratio to 0.547, which reduced the savings in natural uranium requirements to only 5.5%, compared to a simple LEU cycle in the same reactor. In a combined cycle where some pre-breeders use HEU as driver material to breed ^{233}U for a breeder reactor, the conversion ratio was increased to 0.610 for this breeder reactor and the natural uranium savings for this combination of reactors was 31% in a closed fuel cycle. It is thus clear that a heavy price is paid in terms of reduced natural uranium savings when small PBRs are used in order to obtain the desired inherent safety features.

The HEU used as driver material in these fuel cycles raises some proliferation concerns regarding the diversion of this HEU for the production of high yield nuclear weapons. If the HEU is replaced with 20% enriched uranium, this proliferation concern will be taken care of. Such a proliferation resistant fuel cycle was indeed simulated by Teuchert *et al* (1979: 21-23). Unfortunately this lower enrichment introduced significant quantities of ^{238}U into the fuel. Since the resonance integral of ^{238}U is about three times that of ^{232}Th (Teuchert *et al*, 1979: Table VIII), even the introduction of a relatively small fraction of ^{238}U will lead to the breeding of significant quantities of ^{239}Pu. Since the thermal fission cross-section of ^{239}Pu is about twice that of ^{233}U (Mulder *et al*, 2010: Table II), the fissioning of ^{239}Pu will compete significantly with the fissioning of the ^{233}U bred from the ^{232}Th. Because η = 1.82 for ^{239}Pu, averaged over the whole energy spectrum in the reactor, which is significantly lower than the 2.01 for ^{235}U and much lower than the 2.25 for ^{233}U (Teuchert *et al*, 1979: Table VIII), this fissioning of ^{239}Pu strongly reduced the conversion ratio to 0.645 (Teuchert *et al*, 1979: Table IV), which also strongly decreased the savings of natural uranium (Teuchert *et al*, 1979: Fig. 5).

The ^{239}Pu produced from the LEU (20%) will also increase global stockpiles of Pu. Fortunately this Pu will have experienced relatively high burn-ups and will contain relatively high fractions of ^{240}Pu and ^{238}Pu, which will make it highly proliferation resistant (Teuchert *et al*, 1979: 23).

1.4.6.4 Pu driven thermal thorium fuel cycles

This production of ^{239}Pu can be eliminated by replacing some or all of the U driver material with pure Pu. The IAEA (2003) published results of such a co-ordinated research project (CRP). The most important aim of this research (IAEA, 2003: 14) was to find fuelling strategies, which, on the basis of proven reactor technology, are suitable to:

- maximise the incineration rate (= reduction in Pu mass per unit electrical energy produced (kg/GW_{el}a) of LWR-plutonium and weapons grade plutonium (i.e. 94% ^{239}Pu + 6% ^{240}Pu) and to
- minimise the amount of residual plutonium to be disposed of in the spent fuel, i.e. to maximise Pu-burned/Pu-discharged.

Each participating country simulated its preferred fuel cycles in its preferred reactor. Only thermal reactors were simulated, i.e. PWRs, HTRs and a Pressurised Heavy Water Reactor (PHWR). The main results were (IAEA, 2003: 15-18) as described below.

1.4.6.4.1 Light water reactor (LWR) plutonium fuel

In any specific reactor concept, the LWR plutonium incineration rate decreases with increasing heavy metal burn-up. Therefore the maximum incineration rate of 1000 kg/GW_{el}a was achieved by the Republic of Korea's PWR (IAEA, 2003: Table 2.7).
This result was to be expected since, as the burn-up increased, the concentration of the fissile Pu isotopes (^{239}Pu and ^{241}Pu) decreased, while the concentration of the bred ^{233}U increased. Thus the relative Pu to ^{233}U fission rate decreased. By the same logic, as the conversion ratio increases, the Pu incineration rate decreases.

Germany increased the average heavy metal burn-up in their 200 MW_{th} HTR-MODUL by adding HEU driver material to the fuel. Therefore this reactor achieved the highest burn-up of 192 MWd/kg_{HM}. Because of this high burn-up, together with the fact that the fissioning of ^{235}U competed with the fissioning of the fissile Pu isotopes, this reactor achieved the lowest LWR Pu incineration rate of only 496 kg/GW_{el}a (except for a Russian LWR for which only part of the core was fuelled with Pu).

China, on the other hand, used only LWR Pu as driver material in their HTR Module. Since the neutron economy (η and k_∞) of LWR Pu in thermal reactors is much worse than that of HEU, this reactor achieved a lower burn-up of only 100 MWd/kg_{HM} (IAEA, 2003: Table 3.1.5) and consequently a very high LWR Pu incineration rate of 945 kg/GW_{el}a.

1.4.6.4.2 Minimisation of the residual plutonium in the spent fuel

It is obvious that, for a given reactor concept, Pu-burned/Pu-discharged increases with increasing burn-up. Therefore the German HTR-MODUL achieved the highest ratio of 4.2, while the Chinese HTR-Module achieved the lowest ratio of 0.6. It is thus clear that maximisation of the Pu incineration rate, on the one hand, and minimisation of the residual Pu to be disposed of, on the other hand, are opposing goals and that a trade-off will have to be made between these two.

1.4.6.4.3 Weapons-grade plutonium fuel

Incinerating weapons-grade plutonium (IAEA, 2003: Table 2.8) was generally much more effective, compared to reactor-grade Pu. The Pu incineration rate for the German HTR-MODUL increased strongly from 496 kg/GW_{el}a to 702 kg/GW_{el}a and Pu-burned/Pu-discharged for the Chinese HTR-Module increased strongly from 0.6 to 4.2.

The obvious explanation is that the absence of plutonium isotopes above ^{240}Pu in the fresh fuel, strongly delayed the build-up of the MA and, therefore, the parasitic capture of neutrons

in ^{242}Pu and the MA. Therefore k_∞ remained high up to much higher burn-ups, which allowed for much deeper burning of the Pu before the fuel elements had to be discarded. This allowed for a sharp reduction in the loading of HEU in the German HTR and consequently a much higher consumption of Pu. It also caused a sharp reduction in the Pu discharged in the spent fuel from the Chinese HTR and thus a sharp increase in the efficiency of Pu incineration.

These higher burn-ups also produced much stronger denaturisation of the residual Pu by the fertile isotopes, for instance the spent fuel contained 17.6% ^{240}Pu + 46.9% ^{242}Pu for the 7 g/ball case in the Chinese HTR (IAEA, 2003: Table 3.1.4) and 13% ^{240}Pu + 41% ^{242}Pu for the German HTR (IAEA, 2003: Table 3.2.5). Unfortunately the Chinese component of this study neglected the ^{238}Pu in the input data for both the reactor-grade and weapons-grade Pu for the fresh fuel (IAEA, 2003: Table 3.1.1). Since the ^{238}Pu in the fresh fuel is the main source of ^{238}Pu in the spent fuel in a Pu fuel cycle, the results of the Chinese study cannot predict the ^{238}Pu content of the spent fuel, which is the most important measure of proliferation in the present study. The German study assumed ^{238}Pu content of only 1% (IAEA, 2003: Table 3.2.1) in fresh reactor-grade Pu, which is much lower than the 2.6 – 4.0% assumed in Table 3 of the present study, and therefore the ^{238}Pu in the spent fuel for these studies cannot be compared on an equal basis to the present study.

While the quantity of reactor-grade Pu that potentially needs to be incinerated is much higher than for weapons-grade Pu, the proliferation risk associated with the weapons-grade Pu is obviously much higher than for reactor-grade Pu. Therefore the ability of these reactors, as well as the PHWR, to achieve such high incineration rates of the weapons-grade Pu and such low levels of residual Pu, which is so highly denatured, is a very good result from a proliferation resistance point of view.

1.4.6.4.4 Conversion ratios

Because of the very low value which η has for ^{239}Pu in thermal, and even worse in epithermal, neutron spectra, low conversion ratios are to be expected in all thermal reactors with a high ^{239}Pu incineration rate, except in those which aggressively employ lumping to increase the number of fast fissions in the fuel rods, such as PHWRs or tight pitched PWRs. The conversion ratios of these PBRs were even further reduced by the high neutron leakage rates of the small HTR Module reactors and by the fact that the tiny fuel particles severely limited fast fissions. Therefore it is not surprising that the maximum average conversion ratio achieved in the Chinese HTR-Module was 0.599 (IAEA, 2003: Table 3.1.5.). The conversion ratios for the other reactors were not listed, but can be expected to be similarly low.

It is thus clear that the aims of maximising both the Pu incineration rate and the fissile conversion ratio are not compatible and that a trade-off will have to be made between maximising Pu incineration and maximising nuclear fuel resource savings. Fortunately it is not necessary to maximise the Pu incineration rate in order to achieve good proliferation resistance. As has been shown above, Pu mixtures that are highly denatured with ^{240}Pu and, especially ^{238}Pu, are extremely proliferation resistant and can thus be viewed as a valuable nuclear fuel that should be conserved, rather than as a dangerous substance that should be incinerated.

1.4.7 Conclusion on the role of thorium

The analysis above has only shown that ^{238}U is a much better fast fission fuel than ^{232}Th. However, regarding the fuels that are bred from these fertile isotopes, it is also well known that ^{239}Pu has a higher fast fission breeding potential than ^{233}U, due to the fact that η is higher for ^{239}Pu. The higher Pu isotopes, i.e. ^{240}Pu, ^{241}Pu and ^{242}Pu also have excellent fast fission breeding potential. These factors explain why Pu + depleted uranium-based fuel cycles in molten sodium cooled fast breeder reactors gives conversion ratios of up to 1.421, while the highest for ^{233}U/^{232}Th cycles is only 1.044 (Lamarsh and Baratta, 2001: 174, Table 4.3).

While these conversion ratios for ^{233}U/^{232}Th fast breeders are high enough to enable the use of Th-based fast converter reactors, they are too low to provide meaningful options for fast breeders. Therefore, as long as ^{238}U remains plentiful, it is unlikely that ^{232}Th will replace ^{238}U as fertile fuel for fast breeders, or, by similar reasoning, in MOX-fuelled PWRs.

However, as has been shown in the literature study above, the addition of optimised concentrations of ^{232}Th to Pu/depleted U fuel mixtures for fast reactors will improve the proliferation resistance and will reduce the problem with positive void reactivity coefficients. Therefore it is to be expected that future fast reactor Pu + depleted U fuel cycles will utilise significant concentrations of ^{232}Th.

However, for thermal fissions, the situation is the opposite, i.e. it is much higher for ^{233}U than for ^{239}Pu. Therefore ^{233}U/^{232}Th-based fuel cycles provide the only realistic possibility for thermal converter reactors. The main candidates are large PBRs, molten salt and CANDU-type reactors, which are all currently being researched actively, with India being the closest to commercialising Th-based fuel cycles in CANDU-type reactors.

Converting/breeding in both the Pu/depleted U in fast reactors and the ^{233}U/^{232}Th in thermal reactor options is currently hampered by the fact that this requires chemical reprocessing in

order to provide significant savings of natural uranium. ^{233}U-based cycles face an additional challenge: while large stockpiles of Pu(PWR) are available for start-up fuel for fast reactors, ^{233}U is not freely available. Therefore the start-up of a ^{233}U-based reactor might require the breeding of the start-up ^{233}U as an intermediate step, using ^{235}U or Pu(PWR) as driver material. Depending on how it is implemented, this intermediate step may significantly increase the start-up cost and may increase the lead time. Due to the fact that natural uranium is currently relatively cheap and that chemical reprocessing is currently very expensive, both these options are currently not economically attractive and are mainly pursued by governments with a view to a future where natural uranium can be expected to become scarce.

Based on this analysis, the most probable fuel cycle utilisation patterns, for the medium term future, i.e. the period in which natural uranium is expected to still be sufficiently available, but at increasing prices as it starts to become scarce, are:

1. In reactors that do not have significant converting possibilities, such as the current generations of PWRs and small PBRs, LEU will remain the fuel of choice.

2. For thermal converters, i.e. large PBRs, CANDU-type reactors and molten salt reactors, ^{233}U/^{232}Th will be the only option.

3. For fast converters/breeders Pu + natural U fuel, with optimised concentrations of ^{232}Th, will dominate.

4. The rate at which the converter/breeder options will be phased in, will depend mainly on the rate at which the price of natural U will increase and the rate at which the cost of chemical reprocessing may decrease, due to possible future innovations and increases in economies of scale. The rate at which the price of natural U will increase will be determined mainly by the extent to which the nuclear renaissance may increase the demand for it, possible large scale discoveries of mineable resources and the economic viability of extracting uranium from sea water, as has been discussed in detail in the literature study above.

   All these factors are only now starting to unfold and their final outcomes are still largely uncertain. Therefore it is difficult to predict the medium and long term nuclear utilisation patterns with a high degree of certainty.

1.5 Research aims and objectives

1.5.1 General aims

- To simulate and evaluate a fuel cycle for the PBMR DPP-400 reactor for the advanced incineration of reactor-grade plutonium and the associated Minor Actinides. This will entail the investigation of the technical viability of the fuel cycles.

- To investigate possibilities for optimising the nuclear weapons proliferation resistance of the waste mixture from this fuel cycle.

- To create guidelines for a follow-up study to address challenges identified in this study.

1.5.2 Specific objectives

The scope of work will include:

1. Development of a computer code for the semi-automatic translation of the current VSOP-A simulation input models to the format for VSOP 99/05 code. VSOP 99/05 is required due to its ability to simulate the transmutation of the MA.

2. Verification and validation of the translation of these input models.

3. Calculation of the necessary resonance integrals for VSOP.

4. Investigation of the evolution of k_{eff} with burn-up for the different fuel mixtures, in order to establish appropriate multi-pass fuel cycles.

5. Investigation of the composition of plutonium fuel to be employed in this study.

6. Investigation of the core neutronics distribution in the PBMR DPP-400 due to the new fuel cycle layout, in comparison to the reference layout, for the following fuel cycles:

    - LEU(9.6%)

    - Pure Pu(PWR);

    - Pu(PWR+ MA)

7. Evaluation of the control rod worths and cold shut-down reactivity margins and control characteristics of the reactor with the different fuel mixtures.

8. Calculation and evaluation of the maximum temperatures and the temperature reactivity coefficients for the different fuel cycles;

9. Calculation and evaluation of the material balances for the various fuel mixtures.

10. Calculation of the reduction in MA mass in the spent fuel, due to incineration of MA in the PU(PWR)+MA fuel cycle, compared to Pu(PWR).

11. Evaluation and optimisation of the proliferation resistance of the spent fuel mixtures.

12. Recommendations for follow-up studies.

1.5.3 Originality of the research aims

Based on the literature study above and on the following additional arguments, the originality of these research aims is claimed:

1. This is the first time that the results for the VSOP-A and VSOP 99/05 codes are compared for the same PBR and for pure Pu(PWR) and Pu(PWR)+MA. Several relevant simulation results for the incineration of similar Pu-mixtures in prismatic block type HTRs have been published, both for deterministic codes, such as MCNP and MCNPX, and for diffusion codes. VSOP 99 simulations for Pu/Th fuel cycles in Pebble Bed Reactors (PBRs) have also been published, as was discussed above. However, the present VSOP 99/05 simulations for the incineration of pure Pu(PWR) and Pu(PWR)+MA in PBRs in the PBMR DPP-400, are original.

2. The performance of Pebble Bed fuel spheres has also been simulated with MCNP for many relevant Pu fuel mixtures, for instance, Bende (2000) did a parametric simulation study on the incineration of pure reactor-grade plutonium in a Pebble-Bed Reactor. However, he employed assumptions that are not necessarily fully relevant to realistic reactors:

    - He based his optimisation of the fuel spheres on single-cell calculations, i.e. an infinite reactor.

    - Once the most promising fuel spheres were selected, their performances were simulated in a very low power output reactor with no recirculation of the pebbles (Bende, 2000: 14). He also tested only one specific reactor geometry and specific fuel cycles and made no attempt to optimise this design.

Since the results for such simplified geometries markedly differ from those for fully realistic reactor geometries and fully realistic fuel cycles, these studies do not compete with the present study.

3. The VSOP-A simulation results for the pilot study for this project (Mulder *et al*, 2008) have been published for the incineration of pure Pu(PWR) in a PBMR DPP-400. These simulations were performed by E.J. Mulder and therefore are not claimed by the author of the present study as part of his original contribution. However, Mulder's simulations excluded the minor actinides from the fresh fuel, thus rendering the **minor actinide containing fuel mixtures** of the present study original.

   Furthermore, the simulations of the pilot study were performed with the VSOP-A system of codes only, which does not have the capability to simulate the build-up and transmutation of the minor actinides above ^{242}Pu during burn-up. By translating those input models to VSOP 99/05, the author added the simulation of the transmutation and burn-up of the minor actinides in the present study. As will be shown in the results, the inclusion of the minor actinides made a significant difference to the results, even when pure Pu(PWR) was used in the fresh fuel. Therefore the results of the present study are original.

4. Jonnet, Kloosterman and Boer (2010) simulated the incineration of Pu and MA in a PBMR DPP-400 core with a diffusion code. However, the combination of codes and modules they used, such as SCALE-5 and THERMIX, differs significantly from VSOP 99/05 used in the present study. Also their study focused on the failure of the coated particles, rather than on the performance and optimisation of the fuel cycle, which is the focus of the present study.

5. Boer and Ougouag (2010a and 2010b) simulated deep-burn of PU(PWR) and Pu(PWR+MA in a PBMR DPP-400, using a combination of the SCALE-6 and PEBBED, which includes THERMIX, codes (Gougar *et al*, 2010). The broad subject of their studies is therefore identical to the present study and thus comes close to threatening the uniqueness of the present study. It should, however, be noted that these studies were only published in May and June of 2010, while the research proposal for the present study was already formally accepted by the North-West University on the 16-th of May 2007. The author thus claims that the present study was originally conceived and conducted completely independent of, and without any knowledge of the studies by Boer and Ougouag. In fact, the author only became aware of these studies during December 2010, i.e. only six months before the

submission of the present study for examination.

It should further be noted that there are several differences between the present study, and the studies by Boer and Ougouag. These differences will be discussed in detail below where their results will be compared to those of the present study.

6. From the literature survey the author established the importance of high fractions of ^{238}Pu in the spent fuel Pu-mixture, as well as the importance of transmutation of ^{237}Np to ^{238}Pu for the maximisation of proliferation resistance. In previous Pu incineration studies, the proliferation resistance was mainly assessed in terms of the reduction of the total mass of Pu and the maximisation of the ^{240}Pu content of the spent fuel Pu-mixture. Therefore, optimising the fuel cycle regarding ^{238}Pu and ^{237}Np will be an original contribution.

7. The development of a computer code as a tool for the semi-automatic translation of VSOP-A input models to VSOP 99/05 input models is also an original aim.

1.5.4 Demarcation of the field of study

The aspects that will be included in the study has been stated above. However, the following will be excluded from this study:

1. The verification and validation will be limited to the input models. It will be assumed that the VSOP-A and VSOP 99/05 codes have been verified sufficiently over the years. It will also be assumed that the original VSOP-A input model for the PBMR DPP-400, developed by E.J. Mulder, is already sufficiently verified. Therefore it is only the translation of this model to VSOP 99/05 that will be verified. This choice will be explained in more detail during the actual verification process.

2. The verification and validation of the results will be limited to the neutronic aspects of the VSOP 99/05 input models. The parts of these models which define the thermo-hydraulic calculations, that is the input for the THERMIX module, will be excluded from this verification and validation process. The reason for this is that extending this study to include the thermo-hydraulic calculations would increase the scope of the study to unreasonable limits and would thus distract focus from the main scope of the study, namely the neutronic calculations. Since these THERMIX input cards come from the model developments of the PBMR (Pty.) Ltd., which have been verified and validated internally by the PBMR Pty Ltd, it is reasonable to assume that they are already sufficiently verified.

3. Similarly the input models for the TOTMOS code and for the VSOP-A code that were used for the control rod simulations, according to the Method of Equivalent Boronation, will be excluded from the verification and validation process: These models and this method had been developed and verified earlier by E.J. Mulder. The development of input models for the TOTMOS code is a study in its own right, which will not be attempted here. Therefore the models developed by Mulder will be used unaltered and based on the assumption that they are already sufficiently verified. Since the author did not make a contribution to the development of these methods for the simulation of the control rods, these are excluded from the claims for the original contribution of this study. For this reason the details of these calculations were also moved out to the appendix (Par. 7.2).

4. During the pilot study (Mulder *et al*, 2008), the temperatures during a Depressurised Loss of Forced Cooling (DLOFC) were calculated using VSOP-A. The author discovered that the details of the required input cards for these calculations in VSOP 99/05 differed substantially from those in VSOP-A, to such an extent that it was not viable to simply translate the VSOP-A input model to VSOP 99/05. Since the PBMR (Pty) Ltd used the TINTE code to simulate DLOFCs, its researchers did not have a working VSOP 99/05 input model for DLOFC calculations. On the other hand the author did not have access to the TINTE code. Therefore the author judged that a switch to TINTE would detract from the proper focus of this study and, therefore, the DLOFC calculations were excluded from this study and rather deferred to the list of follow-up studies (Par. 4.3).

2 Simulation methods

2.1 Incineration of pure plutonium

Recycling of reactor-grade plutonium in reactors suffers from the following two issues:

(1) The plutonium isotopic mixture contains a relatively high proportion of ^{240}Pu. Mulder and Teuchert (2006b) observed very strong neutron absorption in the capture resonances of the ^{240}Pu in the fresh Pu-fuel in a VSOP-A simulation of very deep burning of a mixture of 70% ^{239}Pu and 30% ^{240}Pu, using a Pu/U/Th fuel cycle in the current PBMR DPP-400 design. Therefore fissile driver material, such as ^{235}U, is often added to, for instance, Pu-Th fuel cycles, as was discussed above, in order to increase k_∞ and thus improve the burn-up.

(2) A negative Doppler temperature coefficient in thermal reactors is normally supplied by the capture resonances of the high fractions of fertile materials, such as ^{238}U, in the fuel. Unfortunately, this then breeds new ^{239}Pu, thereby reducing the anti-proliferation value of the incineration strategy.

In the present study pure reactor-grade or MOX-grade plutonium will be used, without the addition of other fertile fuels like ^{232}Th or ^{238}U. The rationale behind this is that, since the concentration of ^{240}Pu is reasonably low, and since there are no other important resonance absorbers, such as ^{238}U or ^{232}Th, the ^{240}Pu will decrease sufficiently with burn-up to maintain k_∞ and thus ensure a high burn-up.

2.2 Translation of PBMR-400 VSOP-A models to VSOP 99/05 and verification of translation

2.2.1 Rationale for translation and verification

Unfortunately VSOP 99/05 does not have downwards compatibility with the input models from VSOP-A. It would therefore have been much easier to take an existing PBMR DPP-400 VSOP 99/05 input model for the LEU fuel cycle and to only modify the fuel cycle in order to create the desired Pu(PWR) fuel cycle, rather than to translate the entire VSOP-A input model to the VSOP 99/05 format. However, the PBMR Company's PBMR DPP-400 LEU model differs significantly from E.J. Mulder's PBMR-400 VSOP-A LEU model, which was used in the pilot study (Mulder *et al*, 2008). In order to be able to directly compare the VSOP 99/05 results of the present study to the VSOP-A results from the pilot study, it was decided

to translate both the pilot study's LEU and Pu(PWR) VSOP-A models for the PBMR-400 to the VSOP 99/05 format.

2.2.1.1 Strategy for using the LEU model to verify the translation process

It was expected that, due to the large conceptual differences in the ways that VSOP-A and VSOP 99/05 calculate Pu fuel cycles, even an accurate translation of the VSOP-A Pu(PWR) model to VSOP 99/05 could possibly produce large differences in results for k_{eff} and for the other burn-up parameters. These inherent differences could thus possibly hide translation errors. Therefore it was decided against using a comparison of the results of the translated VSOP 99/05 Pu(PWR) fuel cycle to those obtained with VSOP-A, as a means of verifying this translation. The translation was thus rather verified by comparing the results for the translated LEU model, as is described below. The reasons for the expected differences in results for Pu fuel cycles in between VSOP-A and VSOP 99/05, are:

1. VSOP 99/05 includes the MA, except for ^{245}Cm and above, in the standard calculation of its transmutation chain, while VSOP-A excludes these. The part of the MA transmutation, included by VSOP 99/05, produces mostly neutron captures and thus its net effect is to significantly decrease k_{eff}.

2. Furthermore VSOP 99/05 takes the resonance integrals for ^{240}Pu and ^{242}Pu in the epithermal energy region into account, while VSOP-A excludes it. This exclusion was partly compensated for by explicitly specifying epithermal self-shielding factors for ^{242}Pu in the VSOP-A Pu(PWR) input model, derived from the ^{242}Pu resonance integral calculations from the ZUT module of VSOP 99. It should, however, be noted that these self-shielding factors are fixed for the specific temperature and ^{242}Pu concentration used for their derivation and thus cannot compensate for the variations in temperature and ^{242}Pu concentration between the various Spectrum Zones.

3. The massive 115 kilo barn thermal capture resonance of ^{240}Pu at 1.05 eV is its most important capture resonance by far. Since this was included in the thermal energy window, both in the VSOP-A and VSOP 99/05 models, capture in this resonance was explicitly calculated and thus the manual specification of its self-shielding factor was deemed unnecessary. Since capture in the epithermal resonances of ^{240}Pu is much less than in this thermal resonance, it was also deemed unnecessary to manually specify epithermal self-shielding factors for ^{240}Pu in VSOP-A. It was thus assumed that both VSOP-A and VSOP 99/05 would treat the thermal resonance of ^{240}Pu similarly and sufficiently.

The validity of this assumption of similarity will be tested by comparing the capture by ^{240}Pu in the thermal energy window by VSOP-A and VSOP 99/05, during the verification process below.

On the other hand, VSOP-A and VSOP 99/05 were expected to yield similar results for the LEU fuel cycle in the PBMR-400 model, for the following reasons:

1. Experience over the years has shown that VSOP-A and VSOP 99/05 yielded similar results for LEU fuel cycles which were simulated in other reactor geometries.

2. In spite of the many small differences between the input formats and calculation algorithms of VSOP-A and VSOP 99/05, which will be discussed in detail below, these two codes employs similar calculation strategies for LEU fuel cycles and can thus be expected to give similar results.

2.2.1.2 Acceptable range for k_{eff} for the verification of the translation of the LEU model:

Brockmann *et al* (2004: Table 4) reported the variations in simulated k_{eff} for a LEU fuel cycle between VSOP 99/03 and VSOP 99/04, due to the replacement of B^2 for the leakage term with DB^2. This increased k_{eff} by 1.3 Nile, which would increase the average burn-up by about 5 MWd/kg_{HM}.

Since the evolution of VSOP 99 was not synchronised with developments within VSOP-A, it would be difficult to establish which version of VSOP 99 is the most similar to VSOP-A. It is, however, clear that, just as VSOP 99/03, VSOP-A uses B^2 for the leakage term, instead of DB^2 used by VSOP 99/04 and VSOP 99/05. This factor would predict that VSOP 99/05 would calculate k_{eff} about 1.3% higher than VSOP-A. Since it would be very difficult to explicitly quantify the effect of all the other small differences between VSOP-A and VSOP 99/05, a relatively broad range for the acceptable value for k_{eff} for the translated model in VSOP 99/05, compared to VSOP-A, was chosen, i.e. Δk_{eff} = (+1.3 ± 1.0)%, which is equivalent to k_{eff} = 1.003 to 1.023.

2.2.1.3 Method for translation and verification of LEU model

The standard LEU PBMR-400 VSOP-A model by E.J. Mulder was translated to VSOP 99/05, using the semi-automatic translation algorithm, as described in more detail in the next sections and in the Appendix. The results of the translated VSOP 99/05 LEU model were

thus used to verify the translation process: For this verification, the results of the VSOP-A LEU model were used as the norm, i.e. the translation of the models to VSOP 99/05 were deemed to be accurate if the VSOP 99/05 results were too similar to the VSOP-A results, i.e. k_{eff} fell within the acceptable range defined above.

Once the translation process was then verified for the LEU fuel cycle, an identical procedure was used to translate the Pu(PWR) VSOP-A models to VSOP 99/05. Since the translation procedure was identical, the translated Pu(PWR) model was then assumed to be automatically verified. This assumption would, however, not hold if the translation processes for the two fuel cycles contained significant differences. Because of the large volume of data that had to be translated and the complexity of the translation procedure, it would be virtually impossible to guarantee that the translation was identical if it were to be carried out manually. Therefore it was decided to write an automatic translation code, which would then be applied to both the LEU and Pu(PWR) models.

The creation of this automatic translation code, together with the translation of the models and the verification of the full process consumed the bulk of the energy and time that was expended on the present study. Therefore, and because the creation of this translation method is claimed as one of the original contributions of this study, this procedure is described in detail.

Initially the comparison of the VSOP-A results to VSOP 99/05 for all facets of the Pu cycle studies was intended as one of the important focuses of the present study. Therefore the ability to automatically and accurately translate all VSOP-A models from VSOP-A to VSOP 99/05 was considered essential. As will be shown in the verification section below, the differences between the Pu(PWR) results for these codes were found to be so large that it was preliminarily concluded that VSOP-A is not appropriate for the simulation of these Pu fuel cycles. Therefore the choice was made to abandon the VSOP-A Pu simulations and to continue only with VSOP 99/05. Therefore the bulk of the expected benefit from the effort invested in the creation of the automatic translation algorithm was not realised in the present study. The fact that the translation of the VSOP-A Pu models added little value, could only be discovered through the actual translation, by which time the effort was already made and thus had to be regarded as water under the bridge.

A secondary aim of creating an automatic translation code was to have this tool available for the efficient translation to VSOP 99/05 of the large number of VSOP-A legacy input models for LEU and thorium fuel cycles, for various reactor geometries that currently exist. In that

this translation tool is now available, the effort spent in creating it may well be recovered in future by translating these models.

2.2.1.4 Verification of the VSOP-A code for Pu(PWR) fuel cycles

Strictly speaking, verification of the VSOP-A code for Pu(PWR) by means of comparison with the VSOP 99/05 would require that (a) this comparison was used to prove that VSOP-A solved the same equations and obtained identical results and (b) that VSOP 99/05 solves these equations correctly. For the purpose of this study, it was assumed that FZ Jülich verified the solution of the equations in VSOP 99/05 sufficiently that these could be trusted. However, as has been pointed out, these two codes do not solve the same equations: the calculation strategy of VSOP 99/05, i.e. the inclusion of the resonance integrals for ^{240}Pu and ^{242}Pu and of the MA in the transmutation chain, was deemed to be theoretically more appropriate for Pu fuel cycles than the approach of VSOP-A, as was discussed in more detail in Par. 2.2.1.1 above. Therefore the VSOP 99/05 results for the translated Pu(PWR) fuel cycle models were chosen as the standard for the verification of the corresponding VSOP-A results. If these results were to be found to be compatible, it would be interpreted as confirmations that the VSOP-A code is appropriate for the calculation of these Pu fuel cycles and *vice versa*.

This is, however, only a preliminary verification. In spite of the fact that VSOP 99/05 is theoretically more appropriate for Pu simulation, this code could possibly contain Pu-specific coding errors which might actually render it less accurate than VSOP-A. Therefore this preliminary assumption, i.e. the VSOP 99/05 results are more accurate and can thus be used as the standard for the verification of the VSOP-A results, will have to be tested further in a follow-up study by means of comparison to, for instance, MCNPX simulations.

2.2.2 Translation challenges

Unfortunately VSOP 99/05 does not have downwards compatibility with the input models from VSOP-A: the collection of VSOP-A input cards contain many variables that were omitted from, or never existed in, the VSOP 99/05 input cards. By the collection of input cards are not meant the specific set of input cards in a specific reactor model, but rather the full set of possible input cards, as described in the respective input manuals of these codes (Mulder and Teuchert, 2006a; Rütten *et al*, 2007). Sometimes the specific functionality in VSOP-A was perhaps viewed as too general and was therefore dropped in VSOP 99/05. At other occasions the functionality was retained but the variable that described the functionality was either hardwired to a specific option in VSOP 99/05 or it was integrated into an extra option of an existing variable in VSOP 99/05. The VSOP 99/05 input cards also contain many

new variables. Sometimes one variable with, for instance, four options in VSOP-A was split into a variable with the same name in VSOP 99/05, but with only two options, and a new variable which caries the remaining two options. In some cases a VSOP-A variable retained its name in VSOP 99/05, but its function changed and in other instances the name changed, but the function remained the same. Seeing that VSOP-A had branched off from the line of codes which produced VSOP 99/05 since 1994, their manuals do not refer to each other and therefore do not document these differences. The author thus had to discover them by means of a detailed variable-by-variable comparison of the two manuals. In the cases where the new variables in VSOP 99/05 were in this way derived from existing variables in VSOP-A, the translation statements that were added to the VSOP-A code were designed by the author to automatically transform the old variables into the new ones. In the cases where completely new variables with new functions were introduced in VSOP 99/05, the author selected the option that corresponded the closest to the approach which was used in the VSOP-A input model and hardwired these values into the translation statements in the VSOP-A code.

The details of the Fortran and C++ codes, which the author wrote for the semi-automatic translation of these models and thus claims as an original contribution, are described in detail in the **Appendix**.

2.2.3 Results for verification of translation of VSOP-A LEU model to VSOP 99/05

2.2.3.1 Modifications to the VSOP-A LEU model, before translation

Before translation to VSOP 99/05, various small changes were made to the VSOP-A input model, in order to obtain compatibility with the input options available in VSOP 99/05, as described in the Appendix.

- The most important of these was the removal of the neutron poison from the fuel: In the standard PBMR-400 VSOP-A input models, which E.J. Mulder used in the pilot study, “Dummy Poison in C” (GAM Id. = 150) was used to simulate the capture cross sections of a number of impurities in the graphite matrices of the fuel pebbles. However, this poison is not available in VSOP 99/05. Being of the view that, due to burn-up, these poisons in the fresh fuel would, in a real reactor, play a relatively minor role in the equilibrium core, the author decided to simply remove all the poisons from the fresh fuel spheres. This caused a slight increase in k_{eff} for the equilibrium core. After increasing the burn-up cycle length via DELDAY, in order to regain criticality, a slight increase in the average burn-up in the equilibrium core was obtained.

- Efforts to optimise the burn-in procedure towards the equilibrium core, as described in the Appendix, revealed that the equilibrium core, which was originally defined at burn-up cycle nr. 150, had not yet reached sufficient equilibrium, i.e. k_{eff} still increased significantly when burn-in cycles were increased tot 342 cycles. Restoring criticality by increasing the burn-up cycle length, increased the average burn-up.

The net effect of these, as well as the other smaller modifications described in the Appendix, was to increase the average burn-up in the LEU fuelled (U/Pu) VSOP-A equilibrium core of the PBMR-400 input model from 95.3 MWd/kg_{HM} to 96.2 MWd/kg_{HM},, which was accompanied by a slight increase in the maximum power/fuel sphere from 2.77 kW in the pilot study to 2.81 kW.

2.2.3.2 Results for VSOP-A LEU model, translated to VSOP 99/05, without temperature recalculation

2.2.3.2.1 Verification k_{eff} for translated model

The VSOP-A input model was translated to a VSOP 99/05 input model, using the semi-automatic translation algorithm described above and in the Appendix. The VSOP-A temperature field was thus automatically copied to the VSOP 99/05 input model. When this translated model was run in VSOP 99/05, without recalculation of the equilibrium temperatures, k_{eff} increased from 1.0000 for VSOP-A to 1.0061 for VSOP 99/05.

This value of k_{eff} = 1.0061 for the translated LEU model in VSOP 99/05 falls within the acceptable verification range of 1.003 to 1.023, defined above. This means that the translation process has been successfully verified, in terms of the norm described above.

2.2.3.2.2 Verification of THERMIX temperature calculations

E.J. Mulder informed the present author in private discussions that he had developed a version of the THERMIX code for VSOP-A, which differs significantly from the version of THERMIX in VSOP 99/05. There thus was a possibility that the temperature calculations with these different versions of THERMIX might have introduced significant differences in k_{eff}. However, when the equilibrium temperatures were subsequently recalculated with THERMIX in VSOP 99/05, k_{eff} decreased only slightly from 1.0061 to 1.0052. It is thus clear that there was a marked, but small, difference in the reactivity of the core when the equilibrium temperature field was calculated with the version of THERMIX in VSOP 99/05, compared to the one in VSOP-A. The change in reactivity, due to these differences in the temperatures, was about a factor five smaller than the change in reactivity due to the other differences between these codes.

In the VSOP-A input model, groups of two or more regions were fused together into single Spectrum Zones, in order to save calculation time. In VSOP 99/05, this option has been omitted, i.e. each region is assigned to its own spectrum zone. In the translation from VSOP-A, the fusion into single Spectrum Zones was retained, in the sense that the initial temperatures of all the different regions that belonged to one Spectrum Zone in VSOP-A, were assigned the same value in VSOP 99/05. However, during recalculation of the temperatures, this grouping was automatically lost, since unique temperatures were calculated for every region. This had only the reported small effect on $k_{eff.}$ This suggests that, at as far as k_{eff} was concerned, the combination of the different version of THERMIX in VSOP-A and the decision to fuse different regions together into single Spectrum Zones, did not produce large differences, compared to the methods used in VSOP 99/05.

2.2.3.2.3 Verification of translated burn-up

When criticality of the translated VSOP 99/05 LEU model was restored to k_{eff} = 1.0001 by increasing the burn-up cycle length from 8.4842 to 8.6344 days, the average burn-up increased from 96.17 to 97.87 MWd/kg_{HM}. The maximum power/fuel sphere increased from 2.92 to 2.96 kW and consequently the maximum fuel temperature also increased slightly from 1047 to 1050°C.

Mulder (1998) have shown that remarkable flattening of the axial power profile can be achieved in PBRs by adding substantial amounts of ^{10}B to the fresh fuel. This will also reduce the power and temperature peaks. In the case of the present study the small amounts of "Dummy Poison in C" was removed from the fuel. Logically this could be expected to produce the opposite effect, i.e. a slight increase in the power and temperature peaks, which was in fact observed.

In summary, the net effect of the changes for the LEU case, from the VSOP-A simulations for the pilot study to the present VSOP 99/05 simulations, was an increase in the average burn-up from 95.3 MWd/kg_{HM} to 97.87 MWd/kg_{HM}, an increase in the maximum power/fuel sphere from 2.77 kW to 2.96 kW and a decrease in the maximum fuel temperature from 1069 to 1050°C. This differs similarly from the VSOP 99/05 results for PBMR (Pty.) Ltd's PBMR DPP-400 model: 94.77 MWd/kg_{HM} burn-up, 2.98 kW maximum power/fuel sphere and a maximum fuel temperature of 1100°C, which were achieved with a He inlet temperature of 500°C and outlet of 926°C. This outlet temperature of 926°C, rather than the expected 900°C, was caused by the bypass flow, as is explained below.

2.2.3.3 Discussion of the differences between VSOP-A and VSOP 99/05 LEU results.

At the beginning of the study, an attempt was made to reconcile the LEU results for the VSOP-A and VSOP 99/05 codes. A long list of differences between both the two codes and the modelling approaches followed by E.J. Mulder and by the PBMR (Pty) Ltd was then discovered, as spelled out in Par. 7.1 in the Appendix. A key reason for many of these differences is that many of the generalities in VSOP-A, which are deemed desirable for research purposes, were removed from VSOP 99/05 in order to "hardwire" the code towards easier modelling of PBRs for the purpose of facilitating the design and licensing of the PBMR DPP reactor.

It soon became clear that, for the reasons explained in the Appendix, that reconciling these differences would be very complicated at best, and impossible at worst. The goal for the verification of the present input models was therefore not to reconcile these differences, in order to get identical results, but rather to serve as a quality control procedure in the verification of the translation of Mulder's input models from VSOP-A to VSOP 99/05, as has been explained in the rationale for the translation and verification in Par. 2.2.1 above.

Due to these inherent differences, the assumption from the outset was that the translation of the LEU models would lead to small, but significant, changes in the results, and the differences that were indeed found are therefore not viewed as a matter of concern. On the contrary, these differences can be viewed as welcome evidence of significant independence between Mulder's VSOP-A code and the VSOP 99/05 code, which would be necessary if the one code were to be used by the National Nuclear Regulator (NNR) to review results obtained with the other. Therefore the reconciliation of these differences was excluded in the demarcation section of this study.

2.2.4 Results for verification and validation of VSOP-A for the simulation of Pu(PWR) fuel cycles

The same translation algorithm was then used to translate the VSOP-A model for Pu(PWR) to VSOP 99/05, without recalculation of the temperatures. This caused a large drop in k_{eff} from 0.9994 to 0.9591. However, the translation algorithm had already been verified during the translation of the LEU model, as described above. Therefore the preliminary assumption was that this large drop in k_{eff} was due to the inherent differences in the ways in which the two codes treat Pu fuels, rather than to translation errors. However, the following series of tests were performed, in order to verify the validity of this assumption.

2.2.4.1 Verification of VSOP-A for the simulation of fresh Pu(PWR) fuel

The k_{eff} results of VSOP 99/05 and VSOP-A for the Pu(PWR) equilibrium cycle cannot be compared on an equal basis, since the simulated atom densities evolve differently for the two codes. The atom densities in their respective equilibrium cycles thus differ significantly. Therefore the start-up operating cycles for the fresh fuel, which by definition have very similar atom densities, were used as a starting point for investigating the discrepancies between the two codes.

The VSOP-A input model, as well as its translated VSOP 99/05 version, was used to fully load the respective cores identically with fresh Pu(PWR) fuel. It should, however, be noted that, due to small differences in how VSOP-A and VSOP 99/05 define the heavy metal content of the fuel, these identical fuel input specifications do lead to slightly different concentrations, as has been explained in detail in the rest of this thesis, especially in the Appendix. Fourteen full power operating cycles, during which both the Spectrum and Diffusion calculations were repeated, were then used to stabilise the calculations for the start-up core, which was then stored and used by a restart run to print the detailed results. Full power (400 MW_{th}) was used in order to obtain realistic ^{135}Xe poisoning. In this stabilisation sequence the operating cycle length for the first five burn-up cycles was set to two days, in order to allow for enough time for the ^{135}Xe concentration to reach a stable equilibrium value. Since the goal was to keep the fuel as fresh as possible, the cycle length was then reduced sharply to 0.02 days, in order to limit further burn-up. Seven additional cycles were then used to stabilise k_{eff}.

VSOP-A calculated k_{eff} = 1.0016, compared to k_{eff} = 1.1384 for VSOP 99/05.

2.2.4.1.1 Global parameters

The main global core parameters that produced this very large difference are summarised in Table 6.

Table 6: Summary of factors responsible for the difference in k_{eff} between VSOP 99/05 and VSOP-A for fresh fuel

Whole core parameters	VSOP 99/05	VSOP-A
k_{eff}	1.1384	1.0016
Avg. thermal flux (E+14/(cm2*sec))	**0.11**	**0.13**
Avg. total flux (E+14/(cm2*sec))	1.02	1.19
Fractional (%) neutron productions by:		
Pu-239	78.22	78.33
Pu-241	21.31	21.28
Neutron losses in heavy metals (%)	89.75	89.42
Esp. in fissile isotopes	**61.48**	**54.28**
Pu-238	0.43	-*
Pu-239	**50.40**	**44.54**
Pu-240	**24.78**	**31.41**
Pu-241	**11.08**	**9.74**
Pu-242	**3.03**	**3.72**
in Fission products	0.48	0.82*
Xe-135	0.39	0.36
Core-leakage	9.31	9.32

Note: * It should be noted that in its bookkeeping VSOP-A, as opposed to VSOP 99/05, defines ^{238}Pu as a fission product, instead of as a heavy metal. Therefore it does not list ^{238}Pu in the results for the neutron losses in the heavy metals. For this reason VSOP-A then calculates the neutron losses in the fission products significantly higher than VSOP 99/05. However, when the absorption in ^{238}Pu and in the fission products are summed, the result = 0.91% for VSOP 99/05, which is similar to the 0.82% for VSOP-A. These tabulated differences are thus only artefacts due to different methods of bookkeeping.

It is clear from this table that the main differences between these results are the large increase in neutron captures in ^{240}Pu, i.e. 31.41% in VSOP-A, vs. only 24.78% in VSOP 99/05, and a small increase in absorption in ^{242}Pu. This then reduces the number of neutrons available for absorption in the fissile fuels, which explains the lower neutron losses in ^{239}Pu and ^{241}Pu in VSOP-A, and thus less fissions. The increased capture and decreased fission rates explain the lower k_{eff} for VSOP-A.

In order to explain the increased absorptions in ^{240}Pu and ^{242}Pu further, these absorptions are compared for the broad energy groups in Table 7.

Table 7: Whole core fractional absorptions per one lost neutron.

Nuclide	Code	Energy Group 1 (Fast)	Energy Group 2	Energy Group 3	Energy Group 4 (Thermal)
Pu-240	VSOP 99/05	0.0009	0.0181	0.0041	**0.2247**
	VSOP-A	0.0009	0.0181	0.0040	**0.2911**
Pu-242	VSOP 99/05	0.0002	0.0019	**0.0276**	0.0006
	VSOP-A	0.0002	0.0020	**0.0344**	0.0007

It is clear from this table that there is a slight increase in the VSOP-A absorptions in ^{242}Pu in the epithermal Group 3 and a large increase in absorptions in ^{240}Pu in the thermal Group 4, from only 22.5% for VSOP-99/05 to 29.1% for VSOP-A., compared to. The other absorptions are virtually identical for the two codes. These are very surprising results:

- One of the assumptions of this verification study was that the fact that VSOP-A excluded the resonance integrals for ^{240}Pu, might have produced significant errors in the captures of ^{240}Pu. Since VSOP 99/05 applied these resonance integrals in the epithermal and fast groups only, and since the capture resonances occur in groups 2 and 3 only, this whole effect should have played out in these two groups. However, the ^{240}Pu absorptions in these two groups are virtually identical. This implies that differences in the treatment of these resonance integrals was not a significant source of the observed differences in reactivity.

- ^{240}Pu captures in the thermal group was, however, expected to be similar for the two codes: the massive capture resonance at 1.05 eV is included in the thermal groups and is thus explicitly calculated by the THERMOS subroutine in both codes. Since the differences in the use of resonance integrals applies only to the epithermal groups, these differences could not play a role in the thermal groups. Therefore the large difference in thermal capture was unexpected.

2.2.4.1.2 Regional absorption

The interpretation of these global neutron balances is not simple, because increased absorption in one part of the core might be masked by decreased absorption in other parts. Therefore a more detailed study was performed in core Region(48). Region(48) is the 6th Layer of 18 in the central fuel flow channel, i.e. Channel(3). The purpose was to see whether the differences in reactivity can be explained by differences in the average broad group

microscopic cross-sections, calculated by VSOP 99/05 and VSOP-A for a single Spectrum Zone. The central channel was selected in order to minimise the influence of the influx from already thermalised neutrons from the reflectors, in order to gain improved focus on the mechanism of the slowing down of the neutrons through, and thus their absorption in the resonances. The 6-th Layer from the top of the channel was selected since it is known that the power profile often peaks about a third from the top of the fuel core. Region(48) corresponds to Spectrum Zone(48) in VSOP 99/05. However, since several Regions are grouped together in single Spectrum Zones in VSOP-A, Region(48) forms part of Spectrum Zone(14) in VSOP-A. The microscopic absorption cross-sections in these two Spectrum Zones for ^{240}Pu (from the JEF-1 data library) and ^{242}Pu (from ENDFB-5) are compared in Table 8, as was used by VSOP 99/05 and VSOP-A.

Table 8: Microscopic absorption cross-sections in Region (48)

Nuclide	Code	Absorption cross-section (barn)			
		Energy Group 1 (Fast)	Energy Group 2	Energy Group 3	Energy Group 4 (Thermal)
Pu-240	VSOP 99/05	1.05	14.28	12.55	**951.70**
	VSOP-A	1.06	13.81	12.56	**938.10**
Pu-242	VSOP 99/05	0.84	5.13	**303.00**	7.97
	VSOP-A	0.84	5.22	**380.80**	7.94

From this table it can be seen that, while the other absorption cross sections for ^{242}Pu were virtually identical, the cross-section for VSOP-A of 380 barn in the epithermal Group 3 was substantially higher than the 303 barn for VSOP 99/05. This might explain the slightly higher global absorption in VSOP-A. For ^{240}Pu the cross-sections in the fast and epithermal groups are virtually identical. However, the thermal absorption cross-section (Group 4) of 938.1 barn for VSOP-A is significantly lower than the 951.7 barn for VSOP 99/05. This is very surprising, since the lower cross section for VSOP-A for this Region stands in sharp contrast with its much higher global absorption in the thermal group. It is thus clear that the differences in the microscopic cross-sections in this Region cannot explain the observed differences in reactivity.

2.2.4.1.3 Thermal spectra

Investigating this surprising result with the MCNPX code is deferred to a follow-up study. In order to further investigate it in the present study, the neutron spectrum for the 30 energy groups inside the thermal broad group in Region(48), as well as the associated self-shielding factors, are compared in Figure 5 and Figure 6. The purpose was to determine whether the distribution between the 30 thermal groups in THERMOS (Honek, 1961) of the source neutrons in the thermal energy group, i.e. the neutrons that are scattered down from the epithermal groups, was set up identically for VSOP 99/05 and VSOP-A.

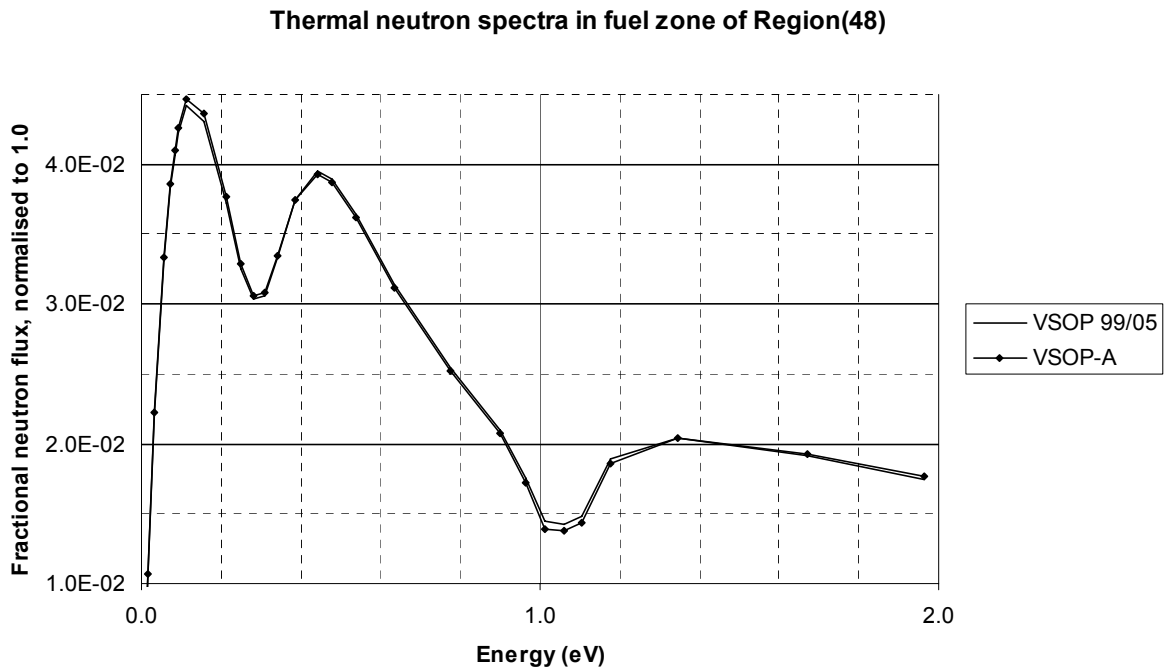

Figure 5: Comparison of the thermal neutron spectrum of VSOP-A to VSOP 99/05.

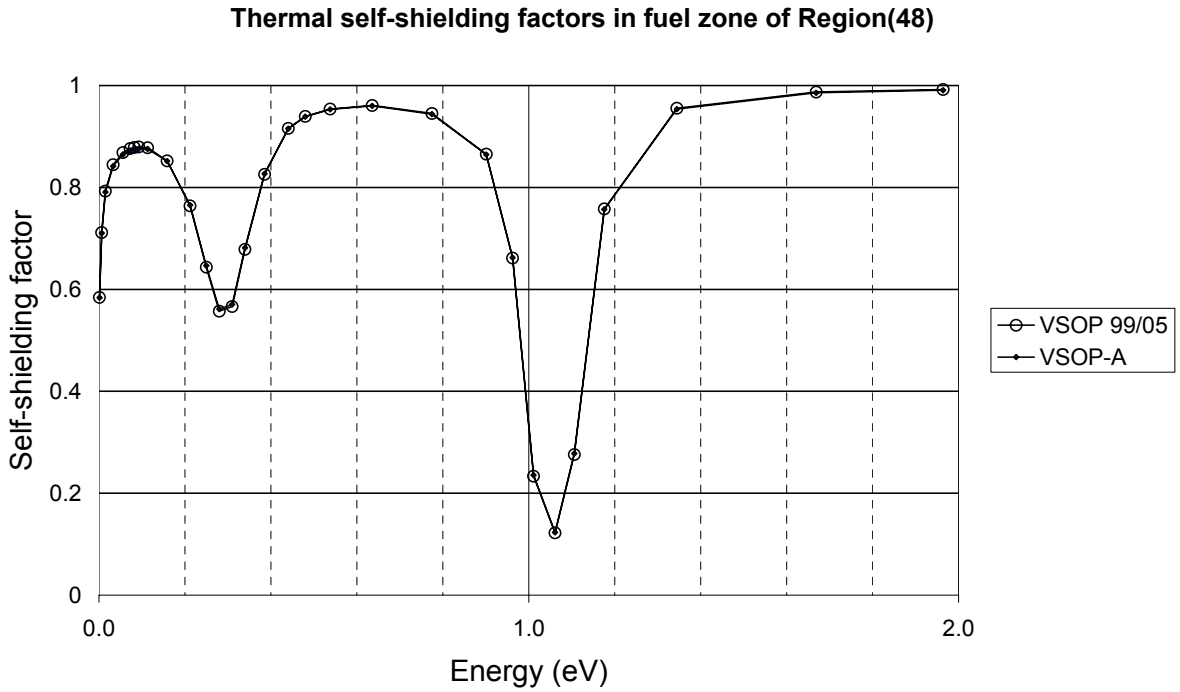

Figure 6: Comparison of the thermal self-shielding factors for VSOP-A to VSOP 99/05.

The notches in the graphs for the thermal spectra and for the self-shielding factors at the massive 1.05 eV capture resonance of ^{240}Pu are clearly visible. The thermal neutron spectra are virtually identical for VSOP-A and VSOP 99/05. The self-shielding factors for these codes are so similar that it is not possible to distinguish between the two graphs. Therefore these factors cannot explain the substantial differences in the global thermal absorption of ^{240}Pu.

Since Region(48) was purposely chosen far away from the reflectors, its thermal flux will be low, compared to Regions adjacent to the reflectors. Therefore its thermal spectrum may seem to be of less relevance to the global reactivity differences observed. However, it should be noted that the fluxes displayed are normalised. Therefore the meaning of these results pertain not to the total thermal flux, but rather to the mechanism of distribution of the down-scattered source neutrons. This is a global setting: since no large differences were observed between these distributions for VSOP 99/05 and VSOP-A in this Region, it thus follows that these settings for the whole core do not differ significantly between these codes.

2.2.4.1.4 Global scattering

In order to investigate the possibility that differences in the neutron flux distributions between the broad energy groups are responsible for these differences, the global neutron balance is shown in Table 9.

Table 9: Neutron balance per one lost neutron.

Parameter	Code	Energy Group 1 (Fast)	Energy Group 2	Energy Group 3	Energy Group 4 (Thermal)
Absorption	VSOP 99/05	0.0070	0.0904	**0.1302**	**0.6791**
	VSOP-A	0.0070	0.0905	**0.1366**	**0.6727**
Scattering out	VSOP 99/05	**0.7184**	**0.5250**	**0.4036**	0.0000
	VSOP-A	**0.7358**	**0.5421**	**0.4105**	0.0000
Source	VSOP 99/05	0.9838	**0.7346**	**0.5250**	**0.4036**
	VSOP-A	0.9838	**0.7520**	**0.5421**	**0.4105**
Leakage	VSOP 99/05	**0.2583**	**0.1192**	**-0.0088**	**-0.2755**
	VSOP-A	**0.2410**	**0.1195**	**-0.0051**	**-0.2621**

It can be seen from this table that several elements of the global neutron balance differ substantially between the codes (**see highlighted elements**). It seems probable that the difference in the scattering behaviour may be the source of this phenomenon. It is clear that in VSOP-A about 2% more neutrons are scattered down in each broad group, compared to VSOP 99/05, which led to similar increases in the neutron source term in the lower energy groups. Logically this should have increased the resonance escape probability, which possibly was the cause of the 18% increase in the average thermal neutron flux for VSOP-A reported in Table 6. Since ^{240}Pu mainly captures neutrons in the thermal region, this enhanced down scattering and thermal flux in VSOP-A might explain the enhanced capture in ^{240}Pu for VSOP-A seen in Table 6 and Table 7.

The two codes used the same THERMOS scattering matrixes for this specific calculation and this factor can thus be eliminated as a source for the observed differences in scattering behaviour. The temperature range of the scattering matrixes (300 K to 1500 K) enveloped that of the equilibrium core.

In order to further investigate the possibility that differences in flux distribution are responsible for the differences in absorption between the codes, the thermal fluxes for the inner fuel flow Channel(1) against the central reflector and the central fuel flow Channel(3) are compared in Figure 7 and Figure 8.

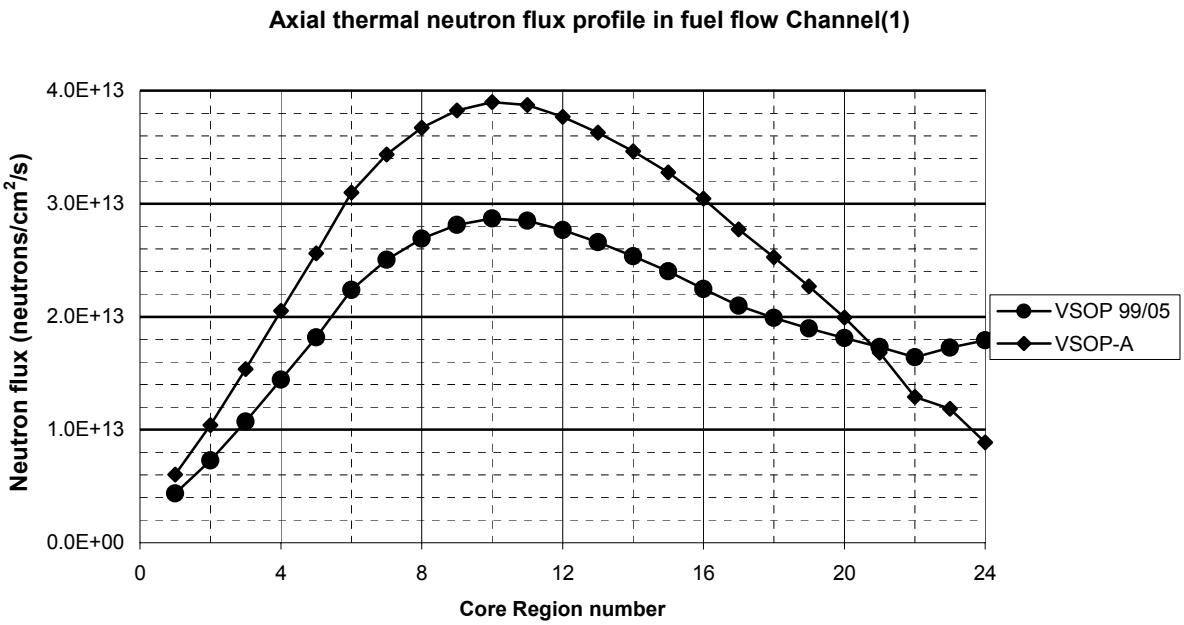

Figure 7: Comparison of axial thermal flux profile in Channel(1) for VSOP-A to VSOP 99/05.

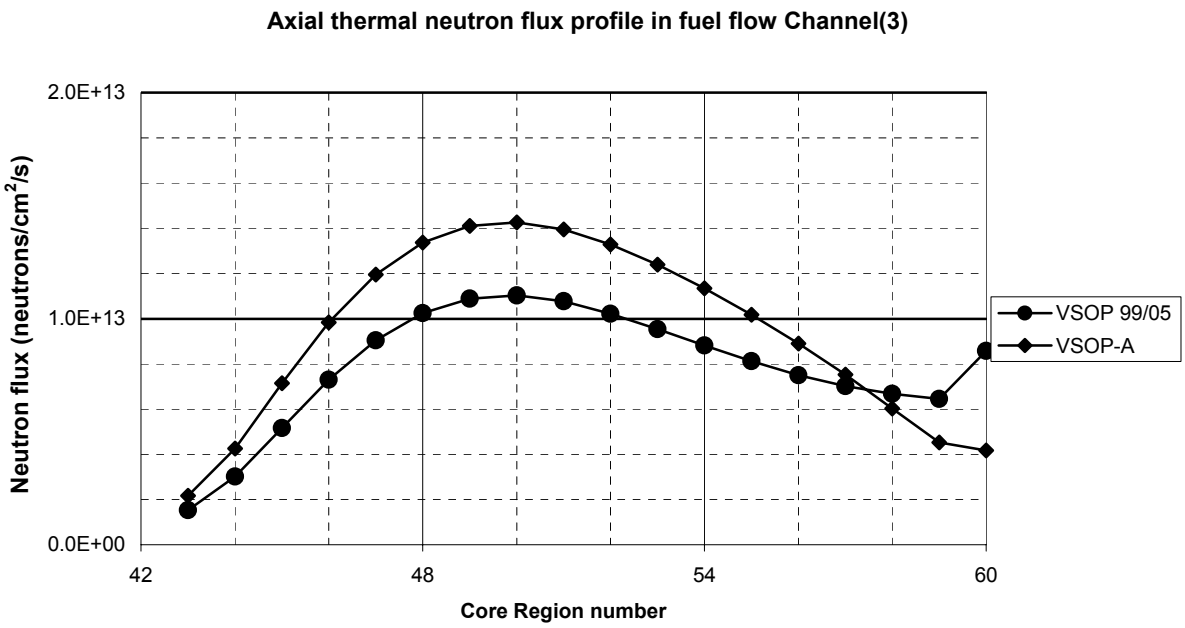

Figure 8: Comparison of axial thermal flux profile in Channel(3) for VSOP-A to VSOP 99/05.

It is clear from these charts that the thermal fluxes are much higher for VSOP-A, compared to VSOP 99/05. This can explain the markedly higher thermal capture in ^{240}Pu for VSOP-A. These huge differences justify investigation by means of an independent code, such as MCNPX. This is deferred to a follow-up study. The increase in the thermal flux for VSOP 99/05 at the bottom of the core was probably caused by the influx of thermal neutrons from the reflectors as the graphite cones of the fuel exit cones protrude inwards, thereby thinning the flow channels and thus bringing the fuel in both channels closer to the reflectors. This phenomenon is discussed in more detail in the main results in Chapter 3 below.

2.2.4.1.5 Leakage feedback

Brockmann *et al* (2004) demonstrated significant improvements in the accuracy of VSOP 99 simulations of LEU fuel cycles if the leakage (DB^2), in stead of the buckling (B^2) was used for the feedback. This improvement was obtained when the leakage feedback was calculated separately for each broad energy group (input parameter IBUCK = 1), instead of using a single average feedback for all the epithermal and fast groups (IBUCK = 2). However, it is well known that using separate feed back factors for each broad group often causes convergence problems. Brockmann *et al* (2004) solved these problems by:

- replacing the B^2-terms with DB^2 terms and
- increasing the upper energy limit of the first epithermal group to 130 eV, so that practically all the epithermal resonances for ^{238}U is contained in this group.

However the improved accuracy of separate feedback factors for each broad group cannot be implemented in the older versions of VSOP 99, since their use of the B2-term excludes this possibility due to the said iteration stability problems (Rütten *et al*, 2007: Par. 2.1.1). Therefore it was recommended that a single average feedback be used for these older codes.

Logically the advice to use a single feedback factor would also apply to VSOP-A, and indeed this was the option used in the present study. In an attempt to maintain equivalence between the two codes, the same option was used in VSOP 99/05 too, with only this difference that VSOP-A used B^2 and VSOP 99/05 DB^2. For both codes the traditional lower energy cut-offs for the three epithermal energy groups in the four group approach were used, i.e. 100000 eV, 29 eV and 1.860 eV.

In order to establish whether the B2- versus DB2 feedback terms might be responsible for the observed reactivity differences between VSOP-A and VSOP 99/05, the abovementioned simulations for the fresh fuel cores were repeated without any feedback by setting the input parameter IBUCK = 0 . The results are shown in Table 10.

Table 10: Comparison of k_{eff} for fresh Pu(PWR) core with and without leakage feedback.

Code	**Single average feedback (IBUCK=2)**	**No feedback (IBUCK=0)**
VSOP 99/05	1.1384	1.0016
VSOP-A	1.0008	1.0032

It is clear from this table that the very large difference in reactivity difference between the two codes virtually disappears when the feedback is switched off. This indicates that differences in how the feedback is calculated are the major contributing factors to the differences in reactivity. Switching the feedback off is, however, not an acceptable calculation option. Therefore a follow-up study is required to determine the optimal calculation options for the feedback for Pu fuel cycles.

2.2.4.1.6 Conclusion

It is clear that the large increase in thermal capture in ^{240}Pu for VSOP-A in the fresh Pu(PWR) fuel, compared to VSOP 99/05, was not caused by differences in the thermal capture cross-sections for ^{240}Pu, the lack of resonance integrals for ^{240}Pu in VSOP-A or by differences in the ways that THERMOS distributes the neutrons or calculates the self-shielding factors, once they have been scattered down into the thermal group, since these factors were virtually identical for the two codes. The differences in absorption were rather caused by the large differences between the neutron distributions of VSOP-A and VSOP 99/05, especially the fact that VSOP-A scatters the neutrons down faster, thereby causing a higher thermal neutron flux. Differences in how the two codes calculate the feedback of the leakage/buckling was shown to be the major source of these differences.

2.2.4.2 Verification of VSOP-A for the simulation of the Pu(PWR) equilibrium cycle

Now that the mechanisms that caused the difference in reactivity between the start-up cores of the two codes are better understood, they will be applied in the investigation of the difference in reactivity of the equilibrium cores. Similarly to Table 6, the global parameters that caused this difference is summarised in Table 11.

Table 11: Summary of factors responsible for the difference in k_{eff} between VSOP 99/05 and VSOP-A for the equilibrium fuel cycle

Parameter	VSOP 99/05	VSOP-A
k_{eff}	0.9591	0.9994
Avg. thermal flux (E+14/(cm2*sec))	**0.22**	**0.27**
Avg. total flux (E+14/(cm2*sec))	1.37	1.37
Fractional (%) neutron productions by:		
Pu-239	**48.96**	**46.69**
Pu-241	**50.24**	**53.11**
Neutron losses in heavy metals (%)	78.16	77.77
Esp. in fissile isotopes	**48.56**	**50.90**
Pu-238	0.78	-
Pu-239	26.46	26.42
Pu-240	**19.99**	**21.52**
Pu-241	**22.09**	**24.48**
Pu-242	**4.34**	**5.35**
Am-241	**1.32**	-
Am-243	**2.40**	-
Cm-244	**0.52**	-
in Fission products	9.49	10.80
Xe-135	1.24	1.02
Core-leakage	11.60	10.63

From the table it is clear that, even more so than was the case for the fresh fuel (Table 6), the average thermal flux is much higher for VSOP-A than for VSOP 99/05. However, the neutron absorptions in ^{240}Pu is now much lower than for the fresh fuel and is only slightly higher for VSOP-A at 21.52%, compared to 19.99% for VSOP 99/05. This sharp reduction in absorptions by ^{240}Pu for VSOP-A was apparently caused by the fact that the very high levels of captures in ^{240}Pu in the start-up core, and presumably during the rest of the burn-in cycles, significantly depleted the ^{240}Pu from 819.5 kg in the fresh fuel core to only 294.4 kg in the equilibrium core. This is also much lower than the 381.3 kg in the VSOP 99/05 equilibrium core. The enhanced number of captures in ^{240}Pu during the run-in to equilibrium similarly led to enhanced production of ^{241}Pu, which is reflected in the fact that the VSOP-A equilibrium core contains 452.8 kg of ^{241}Pu, compared to only 401.8 kg for VSOP 99/05. Where the higher thermal flux caused sharply increased captures in ^{240}Pu in the VSOP-A start-up core,

it now caused substantially higher absorptions in this enhanced concentration of fissile ^{241}Pu. This is reflected in the fact that 53.1% of the fissions in the VSOP-A equilibrium core was produced by ^{241}Pu, compared to only 50.2% for VSOP 99/05. Since ^{241}Pu produces a better neutron economy that ^{239}Pu, i.e. both σ_f and η are higher, these increased ^{241}Pu fissions can explain a substantial part of the higher value of k_{eff} = 0.9994 for VSOP-A, compared to only 0.9591 for VSOP 99/05.

Furthermore, the parasitic neutron losses in the MA amount to 4.24% in VSOP 99/05, which is not taken into account by VSOP-A.

Conclusion

The higher reactivity of the VSOP-A equilibrium core was logically explained on the bases of the same phenomena which caused the reduced reactivity of the VSOP-A start-up core, i.e. the enhanced scattering down of the neutrons, which was shown to be caused by differences in the calculation of the feedback of the leakage/buckling. This enhanced down-scattering caused an increased resonance escape probability for the epithermal resonances and thus an increased thermal neutron flux. Therefore, what appeared to be contradictory results have been shown to be logically compatible and are thus not seen as a matter of concern for the validity of the verification process.

2.2.5 Conclusion on the verification and validation of the Pu(PWR) VSOP models

The technique for the translation of the VSOP-A input models to VSOP 99/05 has been verified successfully for the LEU fuel cycle. Since the same technique was used to translate the Pu(PWR) models, their translation was assumed to have been verified too.

However, large differences between the values for k_{eff} for the Pu(PWR) fuel cycles for the two codes were obtained. Since VSOP 99/05 uses a calculation strategy for Pu fuel cycles that is theoretically more appropriate, its results were assumed to be the more accurate, unless proven otherwise. Therefore the set of tests, described above was conducted as a verification process for the use of VSOP-A for Pu(PWR) fuel cycles. Based on these results, the following are concluded:

1. One of the main assumptions of this verification strategy was that, on theoretical grounds, the exclusion of the resonance integrals for ^{240}Pu by VSOP-A was less appropriate than its inclusion by VSOP 99/05 and that this factor would significantly reduce the accuracy of VSOP-A for Pu(PWR) fuel cycle simulations. However, this assumption was not confirmed by the verification study:

a. The absorption in the epithermal resonances of ^{240}Pu was found to be so small as to be of little significance to the accuracy of the code.

b. Although VSOP-A excludes the resonance integrals, the results for the absorption by ^{240}Pu in the epithermal and fast windows were virtually identical for VSOP-A and VSOP 99/05.

c. The overwhelming majority of ^{240}Pu absorptions occurred in the massive 1.05 eV capture resonance in the thermal broad group. However, it was shown that, once the neutrons are scattered down into the thermal group, the two codes treat their distribution virtually identically.

d. Therefore it is concluded that no significant differences between the absorption cross-sections for ^{240}Pu of the two codes were found. Therefore this cannot be used as the basis for deeming the Pu simulations of VSOP-A as less accurate than those of VSOP 99/05.

2. However, the other main assumption, namely that radiative capture in the MA would be significant and that excluding it from its transmutation chain would cause VSOP-A to significantly over estimate k_{eff} for the equilibrium cycle, was confirmed.
   On the basis of this finding, it is preliminary maintained that VSOP 99/05 is more appropriate for the simulation of Pu(PWR) equilibrium fuel cycles than VSOP-A.

3. The very large difference in k_{eff} for the start-up cores of the two codes was due to differences in the distribution of the flux between the broad energy groups. The main cause of these differences was that VSOP-A scattered the neutrons down to the thermal group faster than VSOP 99/05, because of differences in how the feedback of the leakage/buckling is calculated. This caused VSOP-A to produce a substantially higher thermal flux and thus a much higher capture rate in the thermal capture resonance of ^{240}Pu.

4. It is well known that the PBMR Company and FZJ conducted substantial verification studies for the modifications that were introduced into the different VSOP 99 versions, as mentioned in the VSOP 99/05 manual (Rütten *et al*, 2007). However, these verification studies, for instance Brockmann *et al* (2004), have been conducted mainly for LEU fuel cycles. In the rest of this thesis it will be shown that Pu fuel cycles are generally substantially more sensitive to differences in, for instance, the neutron energy spectrum than LEU fuel cycles. Therefore influences that might have been found to be insignificant in LEU fuel cycle verification studies, might actually introduce

significant errors in Pu(PWR) fuel cycles. VSOP 99 was used to simulate Pu(PWR) fuel cycles in the NEA benchmark: Values for k_{eff} that was about 2% lower than for comparable codes were obtained (Organisation for Economic Co-Operation and Development, 2007). However, a lower upper boundary, which excluded the thermal capture resonance of 240Pu, was used for the thermal energy group. Therefore those results cannot be compared directly to the present study.

Therefore it is recommended that an appropriate set of the LEU verification studies for VSOP 99/05 should be repeated for Pu fuel cycles, in parallel with VSOP-A.

Especially important would be to repeat the verification studies regarding the influence of using either the B2 or DB2 terms for the feedback of the Buckling/leakage for Pu fuel cycles. Since the epithermal capture resonances of 242Pu and 240 Pu differ strongly from those of 238U, the results obtained for LEU fuel cycles cannot simply be transferred to Pu fuel cycles.

However, such verification studies will probably require a huge effort which falls outside the demarcated scope of the present study. Therefore it is referred to the list of follow-up studies (Par. 4.3).

5. Since the differences between the Pu(PWR) fuel cycle results for VSOP-A and VSOP 99/05 were found to be so large, it was deemed not viable to try and reconcile the Pu results for these codes in the present study. Therefore a choice was made to abandon the VSOP-A Pu calculations and to continue solely with VSOP 99/05.

2.3 Resonance and coated-particle structure treatment in VSOP

When the fuel is lumped together, as, for instance, in the 0.024 cm diameter Pu fuel kernels used in this study, the capture resonances of the fertile nuclides cause a reduction in the neutron flux in these lumps, at these resonance energies. This self-shielding significantly reduces the number of neutron captures in these resonances, which increases the resonance escape probability. This increases the fraction of neutrons that cause thermal fissions, thereby increasing k_{eff}, compared to the case where this same number of fuel atoms would have been diluted homogeneously throughout the fuel zone. Temperature increases in the fuel cause Doppler broadening of these resonances. This broadening lowers the height of the capture resonance peaks and thus reduces the amount of self-shielding in these resonances and consequently increases the number of captures, thereby decreasing k_{eff}.

This produces the desired negative temperature reactivity co-efficient, which is a very important inherent safety feature of HTRs.

2.3.1 Epithermal resonances

Lebenhaft (2002) gave a clear overview of the treatment methods of the double-heterogeneity and neutron resonances in HTRs. In the different VSOP versions the atom densities in the fuel zones are first homogenised for the neutron diffusion and fuel burn-up calculations. Background absorption cross-sections, i.e. cross-sections that are independent of the lumping effects and temperature, are supplied in the GAM-I-library. In VSOP 99/05 resonance integrals for the isotopes ^{232}Th, ^{238}U, ^{240}Pu and ^{242}Pu are evaluated by the VSOP-ZUT-section (Rütten *et al*, 2007: Par. A.1.), but in VSOP-A for ^{232}Th, ^{238}U only (Mulder and Teuchert, 2006a: 134 ff.). They are then transferred to the GAM-I code and stored with the background absorption cross-sections. Self-shielding factors for the resonances of these resonance absorbers are then automatically calculated from this data. The expected effect of the inclusion of these self-shielding factors is thus to decrease the calculated number of neutron captures in these resonances, i.e. to increase the resonance escape probability and thus increase k_{eff}.

Effective homogenised neutron reaction cross-sections are then derived by correcting the homogenised cross-sections by taking account of the collision probabilities of the average neutron in the coated particles. They are derived by explicit numerical calculation of the average path that all neutrons will travel between and through the coated particles. This average path is described in terms of the average distance that neutrons will travel through the graphite matrix between coated particles and the mean chord lengths that the neutrons will travail through the coating layers and the fuel kernels. (Hansen and Teuchert, 1971.) These parameters are calculated by the ZUT-DGL module from the geometry of the fuel spheres and coated particles, as specified on the D-cards and the ZUT-cards in VSOP. This includes the maximum and minimum fuel densities and maximum and minimum temperatures for each of the relevant resonance absorbers. This information is then used to interpolate for the values of the resonance integrals for the epithermal energy range for these four extremes, for each of the resonance absorbers, which are then stored on the disk for later use during the burn-up operating cycles. The resonance energy range can be specified by the user, with a maximum of the 68 energy groups in the GAM library, ranging from 10 MeV to 0.414 eV, with each group occupying a quarter lethargy unit. For the resolved resonances, the resonance integral is calculated separately for each resonance and these resonance integrals are then summed to obtain the total resonance integral in each energy group. However, the unresolved resonances in this range, for instance the range above

about 4 keV for ^{238}U, are treated as infinitely diluted by both VSOP 99/05 and VSOP-A, i.e. no self-shielding factors, due to the heterogeneity of the coated-particles, are calculated. Since the integrants in the resonance integrals are weighed by 1/E, the contribution of these higher energy resonances can usually safely be neglected for the moderate lumping in the tiny fuel kernels of HTR fuel. However, these codes do allow users the option of explicitly supplying pre-determined self-shielding factors for this unresolved energy range for high lumping cases.

The spectrum calculations in the VSOP module are performed at user-specified operating cycle intervals:
The nuclide densities in each spectrum zone are recalculated from the burn-up calculations. The temperatures may also be recalculated by calling THERMIX. The resonance integrals, for the nuclide densities of each specified resonance absorber and for each specified temperature, are then recalculated by interpolating between the abovementioned four extremes. From these resonance integrals, the relevant self-shielding factors for the resolved capture resonances for the said absorber nuclides are then recalculated. (Fixed self-shielding factors can also be supplied on the relevant input cards.) These parameters are then used to recalculate the neutron spectrum in the 68 GAM-energy groups, which are then used as weight factors for the calculation of the effective macroscopic reaction cross-sections in the coarse energy groups.

As was mentioned above, VSOP-A calculates the resonance integrals for ^{232}Th and ^{238}U only, while VSOP 99/05 includes ^{240}Pu and ^{242}Pu. For the U/Th and U/Pu fuel cycles, for which these codes were initially developed, the atom densities of ^{240}Pu and ^{242}Pu are small compared to ^{232}Th and ^{238}Pu and the resonance integrals for ^{240}Pu and ^{242}Pu can thus safely be neglected. However, in the Pu-fuel mixtures of the present study, all Pu-concentrations are increased by more than an order of magnitude and therefore these resonance integrals become important.

2.3.2 Thermal resonances

Neither the VSOP-A nor VSOP 99/05 manual provides a detailed description of how the resonances in the thermal energy region are treated. However, the VSOP-A manual states: “In the thermal energy range (< 2.05 eV) the resonances of ^{239}Pu, ^{240}Pu, and other nuclides cover multiple energy groups in the 96-group library. These are explicitly calculated and a temperature dependent broadening cannot be directly simulated. Earlier studies have shown, however, that the temperature dependent shift of the thermal energy spectrum, as contained in the moderator temperature coefficient, outweighs the effect of resonance broadening by far.” (Mulder and Teuchert, 2006a: 163.) Detailed simulation results for the calculation of the

self-shielding factors for the thermal capture resonance of ^{240}Pu is given in the verification section in Par. 2.2.3 – Par. 2.2.5. above. In addition to that, the following theoretical considerations are relevant:

In the absence of absorbers, the normalised distribution for neutrons that have reached thermal equilibrium with a moderator is given by the Maxwellian distribution (Lamarsh and Baratta, 2001: 37-39 and 72-74):

$$n(E) = N(E)/N = \frac{2\pi}{(\pi kT)^{3/2}} E^{1/2} e^{-E/kT} \qquad \text{(Eq. 1)}$$

where E is the neutron energy in eV, N(E) is the neutron density per unit energy, N the total thermal neutron density, T the temperature in K and k the Boltzman constant in eV/K.

With similar notation the thermal neutron flux per unit energy is then given by:

$$\varphi(E) = N(E)v(E) = N(E)\sqrt{2E/m_0} \qquad \text{(Eq. 2)}$$

where v(E) is the neutron speed corresponding to E and m_0 is the neutron mass. By combining these two equations, the normalised thermal flux per unit energy can then be conveniently defined as:

$\frac{\sqrt{m_0/2}}{N}\varphi(E) = \sqrt{E}.n(E) = \frac{2\pi}{(\pi kT)^{3/2}} Ee^{-E/kT}$, which is shown in Figure 9 for 1000°C.

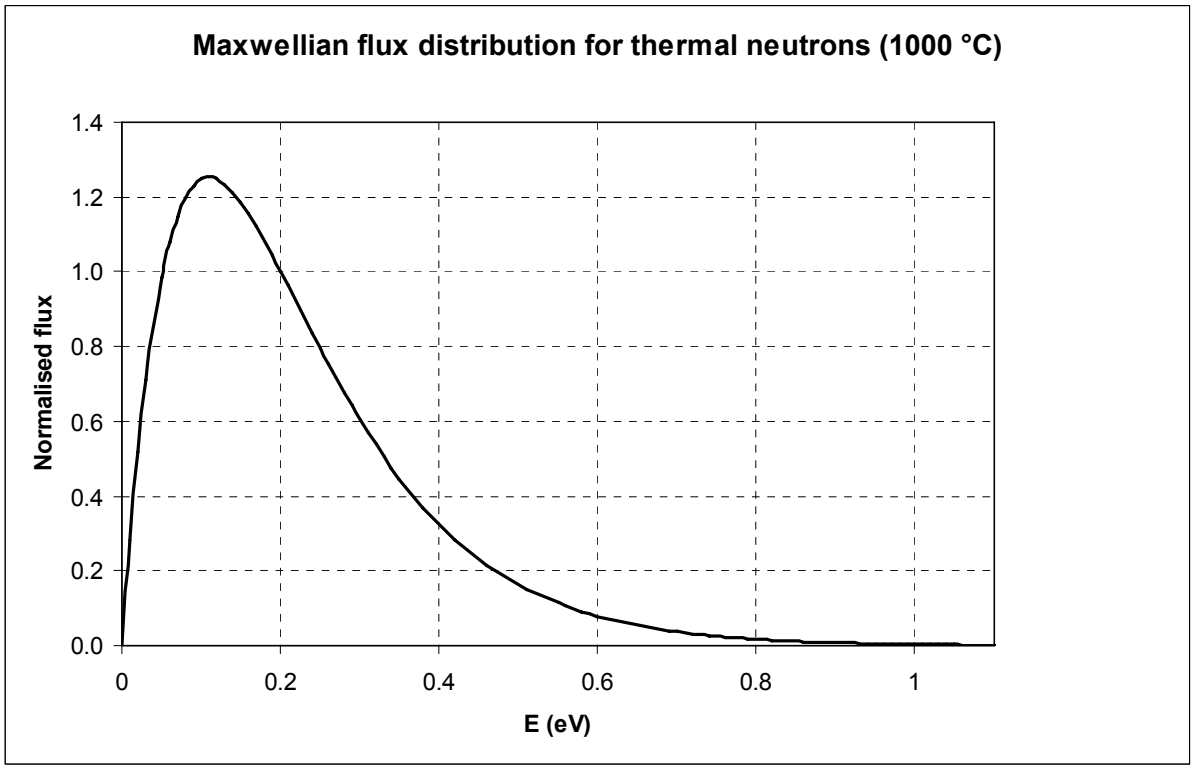

Figure 9: Theoretical normalised Maxwellian flux distribution for thermalised neutrons at 1000°C.

From this graph the following is clear: for the first fission resonance of ^{239}Pu at 0.3 eV the Maxwellian flux is significant and, more importantly, the magnitude of the negative gradient is large. This means that any increase in the moderator temperature will result in a significant increase in the fission rate, unless it is offset by increased capture in the resonances fertile isotopes, due to Doppler broadening. Therefore the statement that the temperature dependent shift of the thermal energy spectrum should outweigh the effect of resonance broadening, is probably accurate in this case.

However, at the massive 1.05 eV capture resonance of ^{240}Pu, the situation is very different: At this energy, both the magnitude and the gradient of the normalised thermal flux distribution approach zero. Therefore the increase in the capture rate in this resonance, due to the up-shift in the thermalised spectrum caused by a moderate increase in the temperature, will be relatively small. However, in spite of the fact that the flux of up-scattered thermalised neutrons approaches zero at the peak of this resonance, the non-thermalised spectrum, i.e. neutrons that are still in the process of being scattered down to thermal energies, is strong, as can be seen in Figure 10 (Kim *et al*, 2007: Fig. 3).

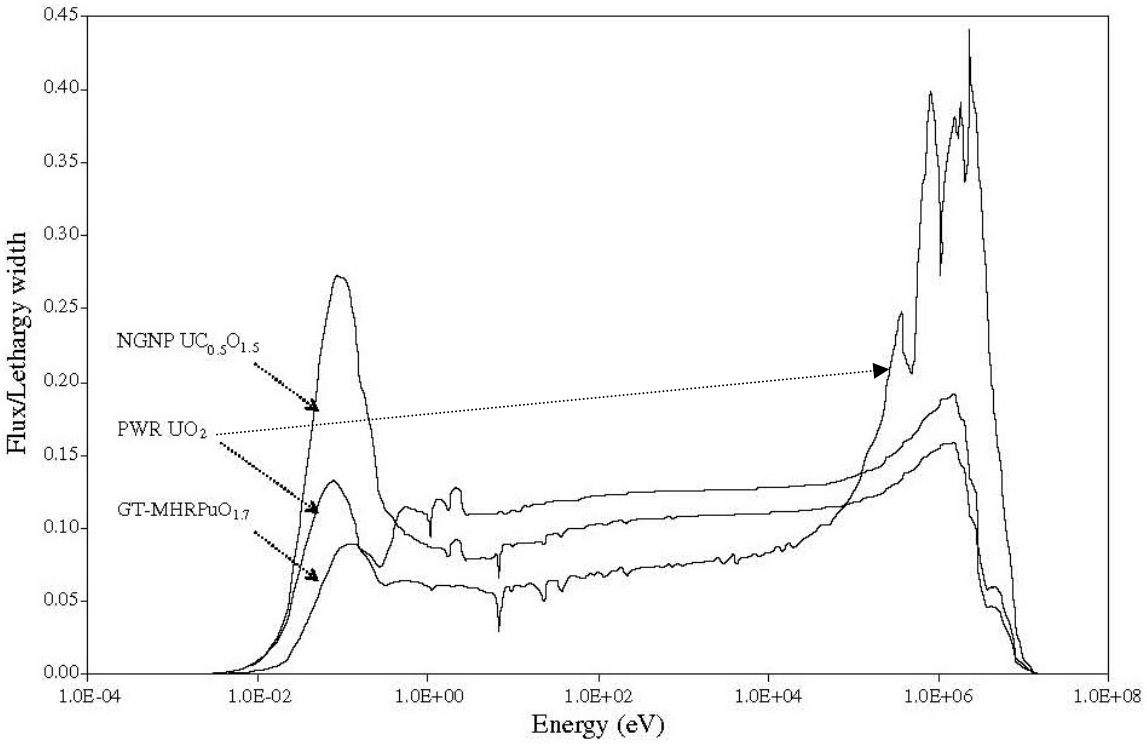

Figure 10: Neutron spectra of the PWR and VHTR fuels at beginning of life.

This means that while the effect of the temperature dependent shift of the thermal energy spectrum into this resonance may be negligible, the effect of resonance broadening on neutrons that are still being scattered down will probably be very significant.

Therefore it will be useful to do a follow-up study in which the accuracy of the treatment of this capture resonance of ^{240}Pu in VSOP 99/05 is tested against MCNPX or using a unit cell calculation with SCALE or another lattice code.

2.4 Geometry of the reactor

The geometry for the PBMR-400 input model for VSOP 99/05, is shown in **Figure 11**.

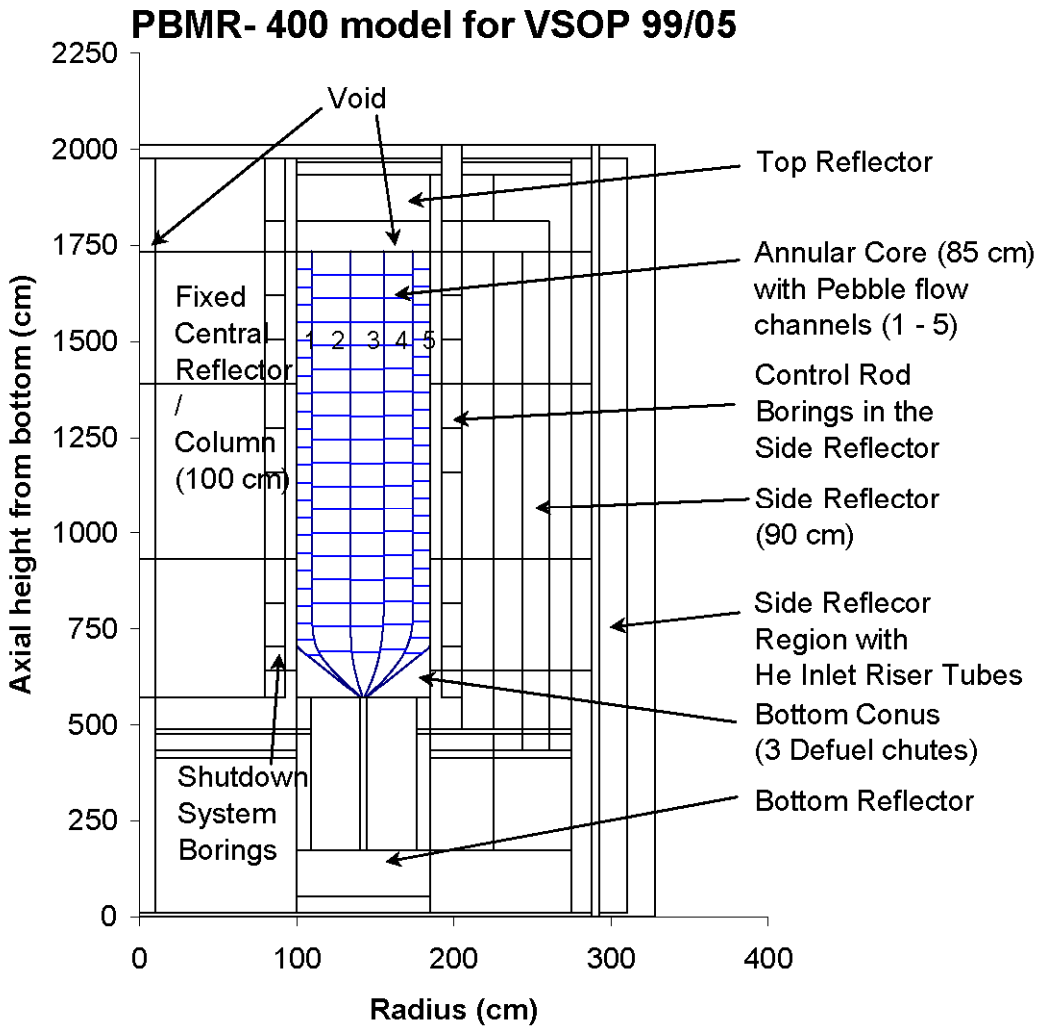

Figure 11: Physical layout of the PBMR-400 reactor, as modelled in VSOP 99/05.

2.5 Simulation of control rods

The data and methods for the simulation of the control rods were inherited from E.J. Mulder and was used “as is”. Therefore they do not form part of the original contribution of the author. Therefore these calculations are not presented for the purpose of being examined with a view to claiming them as part of the author’s contribution. Therefore the details of the calculations was moved out to the appendix (Par. 7.2). However, a summary of the obtained results are published here for the sake of demonstrating the control characteristics of the Pu(PWR) fuel cycle.

2.5.1 Introduction

A description of the reactor geometry that was used for these control rod calculations is given in the previous section and of the fuel cycles in Chapter 3. The distribution of neutrons in a reactor is theoretically described by the transport equation. Since fully realistic numerical solutions to this set of equations are very calculation intensive, the diffusion approximation (Lamarsh and Baratta, 2001: 237) is normally applied and solved, as is the case in VSOP. However, the diffusion approximation is not valid in the following cases (Lamarsh and Baratta, 2001: 235):

- When a medium strongly absorbs neutrons.
- Within about three mean paths of a neutron source or the edge of a medium.
- When the scattering of neutrons is strongly anisotropic.

Therefore diffusion calculations are not valid in or near control rods (CRs). Various methods to correct diffusion calculations of control rod worths have been developed. Tyobeka *et al* (2008) checked two dimensional approximations for control rods by means of three-dimensional MCNP simulations and found good correlations. Reitsma and Naidoo (2003) and Sen *et al* (2006) implemented both the Method of Equivalence Cross-Sections (MECS) of Fen *et al* (1992) and the method of Equivalent Boron Concentrations (EBC), which in this study will be called the MEB (Method of Equivalent Boronation). Reitsma and Naidoo (2003) simulated these methods for a 3-D VSOP 94 model for LEU fuel in the ASTRA experimental facility and Sen *et al* (2006) for the PBMR DPP-400 reactor. They compared these results to measured control rod worths from the ASTRA and found that both methods gave satisfactory results. They warned, however, that these correction methods did not conserve either the neutron flux distributions or the neutron reaction rates throughout the reactor and should therefore be used with caution.

They implemented the simulation technique for the MECS by first simulating the neutron flux in a single control rod and its surrounding environment by means of a 1-D cylindrical unit cell transport calculation. Diffusion parameters and reaction cross sections were then derived from the results of the transport calculations in such a manner that the reaction rates for the transport and diffusion methods, in the absorber region and its surroundings, would be the same. This was done by relating the leakage rates in the two methods. These diffusion parameters and cross-sections were then entered as input data for a 3-D diffusion calculation of the ASTRA facility in VSOP. The control rod worths calculated with VSOP were then compared to those experimentally measured in the ASTRA facility.

In spite of the acceptable results obtained, Reitsma and Naidoo warned of several implementation challenges that they experienced with the MECS, limiting its practicality. It should further be noted that the fact that their method requires 3-D VSOP calculations of a representative slice of the full reactor geometry, presents a significant challenge because 3-D reactor simulations are calculation intensive, especially when thermal hydraulic effects are included in the simulations.

The MEB is a much simpler method in which the boron concentration in the control rod regions in VSOP is varied until the calculated control rod worths equal the experimentally measured values, or in cases where experimental worths are not available, they equal worths obtained from more sophisticated simulation technique, i.e. the MECS in this case..

2.5.2 Method

The following version, developed by E.J. Mulder, of this MECS + MEB method was used in this study:

Mulder added a 3-D MEB to the 3-D MECS, i.e. 24 3-D control rods was simulated in VSOP-A by varying the ^{10}B atom density in the control rod meshes in a 1/24 slice of the core until the calculated control rod worth equalled the value obtained with the 3-D MECS. Mulder then used this 3-D MEB to do temperature-coupled diffusion calculations for the core with the control rods inserted to various depths: This was done to simulate the adjustment of the control rods in order to counter the ^{135}Xe poisoning following the power variations during the 100%/ 40%/ 100% load following. While the equivalent ^{10}B concentrations, used for providing xenon-override during load following, from these simulations were inherited in the standard input models, these simulations were not repeated in the present study.

For the present study control rod simulations were limited to the calculation of the shut-down margins. Therefore only the 2-D MEB was combined with the 3-D MECS (Mulder, 2006). This 2-D equivalent boron concentration in VSOP-A was then transferred to the 2-D VSOP 99/05 equilibrium core models.

2.5.2.1 3-D MECS simulations in VSOP-A

For the 3-D MECS, diffusion simulations of 12 full length inserted control rods were simulated by performing these calculations for a single control rod in VSOP-A for a pie-slice comprising 1/12 of the core of the PBMR-400 reactor. By defining reflective boundaries for the surfaces where this slice was cut, results that are equivalent to a full reactor core with 12 control rods were obtained, based upon the assumption of azimuthal symmetry between the control rod slices. This 12 control rod simulation represents the situation where 12 of the PBMR DPP-

400's 24 half-length control rods were lowered into the bottom half of the core and 12 into the top half of the core, which is the equivalent to 12 full length control rods fully inserted over the whole length of the core. These simulations were implemented as follows for both the LEU and Pu(PWR) fuel cycles:

1. Fuel compositions:

    a. The 3-D MECS VSOP-A start-up core for the LEU case, with the control rod fully withdrawn from the reactor, was filled with the standard fresh 9 g heavy metal /fuel sphere LEU(9.71 a/o%) equilibrium fuel spheres, with the standard LEU fuel sphere geometry. However, a significant concentration of 3.0 E-6 atoms/(barn.cm) of natural boron was added, in order to reduce k_{eff}, as was also done in the TOTMOS driver fuel.

    b. For the LEU equilibrium core (see below), the same fuel as for the start-up core was used, except that the natural boron was removed and that the core was then burnt in to equilibrium.

    c. For the Pu(PWR) case, the standard shell-ball fuel with 2.92 g heavy metal/sphere and an atomic fuel composition of ^{239}Pu = 55.45%; ^{240}Pu = 24.26%; ^{241}Pu = 13.41%; ^{242}Pu = 6.88% was used. Since this was used to create an equilibrium core, no neutron poisons were added and the core was burnt in to equilibrium.

2. These core simulations were then developed in the following ways:

    a. The Pu(PWR) core was first burnt-in to equilibrium, using fresh equilibrium fuel, without natural boron. Thereafter the MECS and MEB calculations were performed.
    k_{eff} was then noted with the control rod fully withdrawn, as well as with the control rod fully inserted. The worth of the 12 control rods in the full core was defined as the difference in k_{eff} for the case where this one control rod was fully inserted and the case where it was fully withdrawn in the 1/12 slice of the 3-D core, for the respective fuel cycles.

    b. For the LEU case, the calculations were first performed for the start-up core at a constant temperature of 1000 K, i.e. 727°C. k_{eff} was then noted with the control rod fully withdrawn, as well as with the control rod fully inserted, as described below.

c. In order to investigate the sensitivity of the MECS and MEB to burn-up and more realistic temperatures, these calculations were repeated for an equilibrium core: The start-up core was burnt in to equilibrium, including the iterative calculation of the equilibrium temperatures by means of the THERMIX code. The control rod-worth calculations were performed at virtually zero power and after ^{135}Xe decay.

3. When the control rod was withdrawn, the effect of the empty control rod channel was simulated by inserting the set of cross sections and diffusion constants for the diffusion method for voids (Gerwin and Scherer, 1979), which is a standard feature in VSOP, into the control rod meshes.

   When the control rod was inserted, the set of cross sections and diffusion constants, pre-calculated with TOTMOS according to the MECS (Fen *et al*, 1992). These constants and cross-sections were automatically produced by the TOTMOS transport code, which was used to perform the 1-D cylindrical cell calculations for a control rod embedded in an annulus of graphite moderator and an outer annulus of fuel and graphite mixture, which served as driver fuel for the neutron reactions, as will be described in more detail below. This was repeated for LEU and Pu(PWR) driver fuel respectively.

2.5.2.2 2-D MEB simulations in VSOP-A.

The 3-D worth of the 12 control rods of the MECS was then translated to the 2-D MEB in VSOP-A. The same fuel cycles of the 3-D cases, were also run in the 2-D cases and with the equivalent core geometry. The 3-D approach of simulating the control rods by inserting equivalent cross-sections into the control rod regions, was replaced by inserting an equivalent ^{10}B concentration in the 2-D control rod regions. This ^{10}B atom density was then varied to yield the same control rod worth, as was obtained for the 3-D MECS. This 2-D method was thus the 2-D MEB appended to the 3-D MECS.

This equivalent ^{10}B concentration, for each 2-D MEB in VSOP-A, was subsequently transferred to the 2-D VSOP 99/05 equilibrium core for calculation of the shut-down balances for the control rods.

2.5.2.3 2-D control rod xenon transient override margin calculations in VSOP 99/05

Before the shut-down margins, with the 12 control rods fully inserted, could be calculated, the ability of the current insertion depths of the control rods into the equilibrium cores to provide the required xenon poisoning override, had to be evaluated. These should be inserted deep

enough to provide sufficient insertion of positive reactivity to override xenon poisoning by withdrawing these control rods during the standard required 100% / 40% / 100% load following for the PBMR DPP-400 reactor.

In the 2-D VSOP-A input models for both the LEU and Pu(PWR) fuel cycles, inherited from the pilot study and then translated to VSOP 99/05, the equivalent ^{10}B atom density for all 24 control rods in the external reflector, i.e. 6.75 E-6 ^{10}B atoms/(barn.cm) in the 2-D control poison annulus, was inserted to a depth of 195.1 cm below the top reflector for the equilibrium core.

The decrease in k_{eff}, due to the build-up of ^{135}Xe, during the reduction in power from 100% to 40%, was simulated in VSOP 99/05 in the following way:

1. Fuel shuffling in both the LEU and Pu(PWR) VSOP 99/05 equilibrium cores was stopped, while the core power was maintained at 400 MW_{th} and k_{eff} was maintained at criticality.

2. The time length/large burn-up time step was then reduced to virtually zero, in order to "freeze" this critical static equilibrium core. k_{eff} was then noted. The equilibrium temperature distribution was also retained.

3. The core power was then reduced from 100% to 40% (= 160 MW_{th}), in order to initiate the ^{135}Xe poisoning transient, caused by load following. After the burn-up cycle with the minimum k_{eff}, the length of the large burn-up time steps was reduced to virtually zero, in order to "freeze in" the maximum xenon-poisoning and k_{eff} was noted. The decrease in k_{eff} was defined as the effect of the ^{135}Xe poisoning that had to be overridden by the withdrawal of the 24 control rods.

4. The equivalent ^{10}B concentration of all 24 control rods was then withdrawn to the bottom of the top reflector and k_{eff} was again noted. The difference between this increase in k_{eff}, supplied by withdrawing the control rods, and the positive reactivity insertion required to override the xenon poisoning was then reported as the xenon override margin.

2.5.2.4 2-D control rod shut-down balance in VSOP 99/05

Once the 2-D MEB was calculated in VSOP-A, this ^{10}B atom density was transferred to the 2-D VSOP 99/05 model for the PBMR DPP-400 equilibrium core, for each fuel cycle. These were the equilibrium cores for the 9 g LEU and the 3 g Pu(PWR) fuel cycles respectively,

with the equilibrium temperature profiles, described in Par. 3.3. This was then used to calculate both the hot and cold shut-down balances for the control rods in the following way:

1. The fuel shuffling in the equilibrium core was stopped, as described above, in order to "freeze" the equilibrium core.

2. The core power was simultaneously reduced to virtually zero, in order to initiate the ^{135}Xe poisoning shut-down transient. The maximum reactivity was reached after four days, due to the decay of ^{135}Xe and other isotopes. k_{eff} was noted and Δk_{eff} defined the contribution of nuclide decay to the shut-down balance.

3. Temperatures:

    a. For the calculation of the hot shut-down margin, the equilibrium temperature distribution was retained.

    b. For the cold shut-down balance, the temperature throughout the core was reduced to 50°C, which was considered the long term cold shut-down temperature. k_{eff} was noted. Temperatures were reduced in the following sequence, and the contribution of each to the cold shut-down requirement was noted:

        i. Resonance absorbers in the fuel, i.e. Doppler effect for ^{238}U in LEU and for ^{240}Pu and ^{242}Pu in Pu(PWR).

        ii. Moderators in the fuel spheres, i.e. carbon and oxygen.

        iii. Graphite reflectors.

4. The contribution of the insertion of the control rods to the shut-down balance was subsequently calculated by fully inserting the MEB ^{10}B concentrations from VSOP-A for the 12 control rods. For the LEU equilibrium VSOP 99/05 core, the ^{10}B MEB concentrations from respectively the VSOP-A start-up and equilibrium cores were inserted, in order to investigate the sensitivity of the VSOP 99/05 shut-down balance to the nuclide composition of the VSOP-A core that was used for the MEB.

5. Δk_{eff} for each of these steps was noted and constituted the components of the shut-down balance.

6. The control rods were then totally withdrawn from the reactor, in order to compare the full length worth of the 12 control rods in the 2-D VSOP 99/05 core to that of VSOP-A.

2.5.3 Results for control rod calculations

2.5.3.1 3-D MECS control rod worths and 2-D MEB in VSOP-A

After entering the parameters from the TOTMOS transport calculations into the control rod meshes and loading the fuels, as described above, the control rod worths were calculated for the 3-D VSOP-A case. Thereafter the 2-D MEB was calculated in VSOP-A for Pu(PWR), as shown in Table 12. The equivalent ^{10}B atom density was varied until the difference between the control rod worth was < 1E-4.

Table 12: 3-D MECS control rod worths and 2-D MEB in VSOP-A for the equilibrium cores, without control rods and after ^{135}Xe decay.

Fuel Core	**k_{eff} (3-D MECS: 12 CRs out)**	**k_{eff} (3-D MECS: 12 CRs in)**	**3-D MECS CR worth** (Δk_{eff})	**k_{eff} (2-D MEB: 12 CRs out)**	**Maximum thermal neutron flux in external reflector** (10^3 neutrons/ cm^2/s /W_{th})	**k_{eff} (2-D MEB: 12 CRs in)**	**2-D MEB: Equivalent ^{10}B atom density** (10^{-6} atoms / (barn.cm))
LEU (Equi-librium)	1.02119	0.93476	**-0.0864**	1.02940	423.8	0.94297	**1.704**
Pu (PWR) (Equi-librium)	1.01471	0.96358	**-0.0511**	1.01642	154.5	0.96528	**2.292**

After transferring the 2-D equivalent ^{10}B MEB atom density from VSOP-A to the equilibrium cores of VSOP 99/05, the 12control rod worths were recalculated, as shown in Table 13.

Table 13: 2-D control rod worths in VSOP 99/05 equilibrium cores, with equilibrium temperatures, after ^{135}Xe decay and for 12 control rods completely out versus completely in.

VSOP 99/05 equilibrium core	**Equivalent ^{10}B atom density from VSOP-A MEB: Source and density** (10^{-6} atoms / (barn.cm))	**k_{eff} (12 CRs out)**	**Maximum thermal neutron flux in external reflector** (10^3 n** / $cm^2/s/W_{th}$)	**k_{eff} (12 CRs in)**	**2-D 12 CR worth** (Δk_{eff})
LEU	**LEU** (Eq*) = **1.704**	1.04556	467.5	0.95251	-0.0763
Pu(PWR)	**Pu(PWR)** (Eq*) = **2.292**	1.03267	170.7	0.96151	-0.0547
	LEU (Eq*) = **1.704**			0.97077	-0.0454

Acronyms: *: Eq =Equilibrium core; **: n = neutrons.

2.5.3.2 2-D control rod xenon transient override margin calculations in VSOP 99/05

The results for the xenon override margin calculations are shown in Table 14.

Table 14: 2-D control rod xenon override margins in VSOP 99/05 for partial insertion of 24 control rods into equilibrium cores.

Fuel Core	**k_{eff}** (Eq. with 24 CRs in 195.1 cm below top reflector)	**k_{eff} -Min** at Max ^{135}Xe	**Δk_{eff}** (^{135}Xe tran-sient to be over-ridden)	**k_{eff}** (CRs out to bottom of top reflec-tor)	**Δk_{eff}** (over-ride ability of CRs)	**Over-ride margin** (Δk_{eff})
LEU	1.00008	0.98455	**-0.0155**	0.99870	**+0.0142**	**-0.0013** (Not sufficient)
Pu (PWR)	1.00005	0.99903	**-0.0010**	1.01463	**+0.0156**	**+0.0146**

Notes: *: Eq. stands for equilibrium core; **: n stands for neutrons.

In order to further investigate this much smaller xenon override requirement for the Pu(PWR) core, the ^{135}Xe concentrations for the two cores are compared in Table 15.

Table 15: ^{135}Xe atom density variations responsible for override requirement.

Fuel Core	^{135}Xe atom density (**Eq.** at **100%** power) (10^{-10} atoms/ (barn.cm))	^{135}Xe atom density (at k_{eff} **–Min,** i.e. at Max ^{135}Xe after reducing power to **40%**) (10^{-10} atoms/ (barn.cm))	**Increase (%)**
LEU	0.9139	1.252	**37.0**
Pu (PWR)	3.069	3.218	**4.9**

Discussion

It is clear from these results that inserting the 24 control rods to the same depth for both the LEU and Pu(PWR) fuel cycles, is sub-optimal from the perspective of supplying the minimum required ^{135}Xe-poisoning override:

The override abilities of the control rods are similar in the two cores, i.e. only slightly higher for the Pu(PWR) core (Table 14). Stable transient behaviour amidst ^{135}Xe power oscillations have been reported for the PBMR DPP-400 (Strydom, 2008). Even so, the override required by the increased ^{135}Xe poisoning is 15.5 times smaller for the Pu(PWR) core. Therefore, while this insertion depth provides only 91.7% of the required xenon override ability for the LEU equilibrium fuel cycle, it provides 1560% of the requirement for the Pu(PWR) core.

The cause of this much smaller override requirement for the Pu(PWR) core was revealed by the comparison of the increase in ^{135}Xe concentrations, during the power reduction from 100% to 40% (Table 15):

It should firstly be noted that the total negative reactivity inserted by ^{135}Xe poisoning (i.e. the negative of the positive reactivity inserted by four days of ^{135}Xe decay from Table 16) of -0.0287 for the equilibrium LEU core is about double the -0.0161 for the Pu(PWR) core. However, this larger reactivity effect in the LEU core is caused by a ^{135}Xe concentration of only 0.9139 x 10^{-10} atoms/ (barn.cm), compared to the more than three times larger 3.069 x 10^{-10} atoms/ (barn.cm) of the PU(PWR) core (Table 15). This larger reactivity effect, paradoxically caused by a lower ^{135}Xe concentration, is explained in part by the maximum thermal neutron flux in the external reflector for the LEU core, which is about double the value of the Pu(PWR) core (Table 14) and which is used here as a proxy for the thermal neutron flux in the core. It is further explained by the well known fact that the thermal neutron

spectrum is much harder for Pu than for LEU, which sharply reduces the thermal neutron capture, due to the fact that the thermal microscopic capture cross-section of ^{135}Xe decreases sharply with increasing energy. The 15.6 times smaller xenon override requirement for Pu thus stands in sharp contrast to the total xenon poisoning effect which is smaller by only a factor two. The additional factor 7.8 can be explained in the following way:

Because of the lower and harder thermal neutron flux in the Pu core, much less ^{135}Xe nuclides capture neutrons and thus the removal rate of ^{135}Xe through capture is much smaller than in the LEU core. Since the ^{135}I production rates, i.e. the fission product yields (Lamarsh and Baratta, 2001: Table 7.7), are similar from the fissioning of ^{239}Pu and ^{235}U, the production rates of ^{135}Xe, through decay of ^{135}I, would also be similar for the two cores. Therefore the reduced ^{135}Xe removal rate is what caused the equilibrium ^{135}Xe concentration in the Pu core to build up to more than three times that of the LEU core. This means that the decay rate of ^{135}Xe in the Pu core is also more than three times that in the LEU core. If the power of both cores were to be shut down completely, the evolution of the ^{135}Xe concentrations would be determined solely by the production rates from ^{135}I decay, which would be similar for both cores, and the decay rates of ^{135}Xe, which would be three times higher in the Pu core. In both cases the production rates would be higher than the decay rates and thus ^{135}Xe would build up. However, because of the much larger decay rate in the Pu core, the difference between the production and decay rates would be much smaller, and thus the build up of ^{135}Xe would occur much slower and peak at a much lower value in the Pu core. The dynamics of the power reduction from 100% to 40% are similar to those of a total shut-down, and thus the much smaller ^{135}Xe override requirement of the Pu core can similarly be explained by its higher ^{135}Xe decay rate.

This large excess reactivity, due to the deep insertion of the control rods, means that if the control rods were to be accidentally withdrawn during equilibrium operation of the Pu(PWR) core, a large+0.0156 Δk_{eff} reactivity will be inserted into the core. The factor 15.5 smaller xenon override requirement of the Pu(PWR) core provides the opportunity to strongly reduce this excess reactivity, which will then virtually eliminate the safety risk associated with accidental withdrawal of the control rods. Such a reduced insertion of the control rods into the equilibrium core will also improve the shut-down margins correspondingly by providing a larger reserve length of control rod insertion that could be added by fully inserting the control rods during shut-down.

The much smaller ^{135}Xe-override requirement of the Pu(PWR) core also introduces the opportunity to design a Pu-based reactor that can produce peak following, i.e. much more

aggressive load following than the current 100% / 40% / 100% for the LEU-fuelled PBMR DPP-400. This is also referred to the follow-up study.

2.5.3.3 2-D 12 control rod shut-down balance in VSOP 99/05

The 2-D zero power, hot as well as cold, shut-down balances, after four days of ^{135}Xe decay, for both the LEU and Pu(PWR) equilibrium VSOP 99/05 cores are shown in Table 16. The shut-down balances were calculated for the different equivalent ^{10}B atom densities, obtained from the 2-D VSOP-A MEB, described above.

Table 16 2-D 12 control rod shut-down balance in VSOP 99/05.

		VSOP 99/05 equilibrium core	
Parameter	**Unit**	**LEU (Low ^{10}B)**	**Pu(PWR)**
k_{eff} (Eq. with 24 CRs in 195.1 cm below top reflector)		1.00008	1.00005
Hot shut-down capability: 12 CRs fully in after 4 Days ^{135}Xe decay (see below)	Δk_{eff}	-0.076	-0.055
Hot shut-down margin	Δk_{eff}	**-0.048**	**-0.039**
Max. thermal neutron flux in external reflector before hot shut-down	10^3 n^{**}/cm^2 $/s/W_{th}$	467.5	170.7
Contributions to cold shut-down requirement:			
4 Days of ^{135}Xe decay (= **Hot shut-down requirement**)	Δk_{eff}	+0.0287	+0.0161
Reduction of eq. temperatures to 50°C:			
Resonance absorbers in fuel (Doppler)	Δk_{eff}	+0.0362	+0.0033
Moderators (C + O) in fuel	Δk_{eff}	+0.0324	+0.0140
Graphite in reflectors	Δk_{eff}	-0.0325	-0.0220
Total (= Cold Shut-down requirement)	Δk_{eff}	**+0.0648**	**+0.0115**
Max. thermal neutron flux in external reflector before insertion of CRs	10^3 n^{**}/cm^2 $/s/W_{th}$	362.2	195.7
Cold shut-down capability of 12 CRs:			
Equivalent ^{10}B atom density for 12 CRs from VSOP-A MEB: (**Source + density**)	10^{-6} Atoms / (barn.cm)	**LEU(Eq*) = 1.704**	**Pu(PWR)(Eq*) = 2.319**
Full insertion of 12 CRs	Δk_{eff}	**-0.0825**	**-0.0604**
Cold shut-down margin	Δk_{eff}	**-0.018**	**-0.049**

Notes: *: Eq stands for equilibrium core; **: n stands for neutrons.

2.5.4 Discussion of the control rod performance

2.5.4.1 Uncertainties in the results

The verification process, as described in the appendix (Par. 7.2.4.1) revealed significant uncertainties in the results that were obtained. Measures to mitigate these uncertainties was proposed for a follow-up study (Par. 7.2.6 in the appendix).

2.5.4.2 Safety analysis

The effects of these uncertainties in the ^{10}B concentrations were mitigated by the fact that these annuli were significantly "black" i.e. the poison concentrations were so high that significant self-shielding occurred in these. Therefore relatively large variations in ^{10}B concentrations produced smaller variations in the control rod worths (Table 16):

- The 40.6% increase in ^{10}B concentration from the low to the high LEU MEB cases, caused only a 21% increase in the hot shut-down capability for the LEU equilibrium core in VSOP 99/05 and
- only a 15.8% increase in the cold shut-down capability.

In view of these uncertainties, a conservative measure was introduced: the shut-down margins were also calculated with the lowest poison concentration (1.704 ^{10}B atoms/(barn.cm)) for the MEB obtained from all the different cases. With this conservative ^{10}B concentrations:

- All the cores could be safely shut down under all the simulated conditions.
- The cold shut-down margin for the Pu(PWR) core (Table 16) was better than for the LEU core.
- Although the hot shut-down margin, with the high ^{10}B concentration, of the LEU core was better than for the Pu(PWR) core, the Pu margin was still adequate.
- As was pointed out in the discussion of the xenon override margins (Table 14), the Pu core has an override margin of +0.0146 k_{eff}. If the excess reactivity were to be reduced accordingly by inserting the control rod less deeply into the core, the shut-down margins could be improved by a similar amount. This would make the Pu hot shut-down margin similar to that of the LEU core and will improve the lead of the Pu(PWR) cold shut-down margin even further.

2.5.5 Verification and validation of control rod calculations

It is clear from the results presented by Reitsma and Naidoo (2003), Sen *et al* (2006) and Mulder (2006) that in their 3-D VSOP simulations, both the MECS and MEB gave acceptable results. Their verification process included comparison to MCNP simulations.

When the 2-D MEB is added onto the 3-D MECS, as was done in the present study, the MEB will, by definition reproduce the results of the MECS, for the calibration core. It is, however, to be expected that the 2-D MEB will be more sensitive to variations in the core composition, compared to the 3-D MECS:

In the 3-D MECS, the only significant non-physical assumption is the diffusion approximation, which was compensated for by correcting the diffusion parameters and reaction cross-sections via the transport results. However, apart from any calculational errors this might introduce, replacing the individual 3-D control rods with a smeared out control poison annulus should significantly alter the neutron reactions in physical reality:

For 3-D control rods the spaces between the control rods are much larger than the thickness of the control rods. Therefore a significant fraction of the neutrons in the external reflector may diffuse back to the fuel core, without having passed through one of the control rods. The energy spectrum of a significant fraction of the neutrons that do diffuse back to the fuel will thus be unaffected by the presence of the control rods. Therefore the interactions between these neutrons and the fuel will not be affected by the presence of the control rods, for instance their capture-to-fission ratios will not be affected. However, when the control rods are replaced with a control poison annulus, which in the case of the PBMR DPP-400 is very close to the fuel core, almost all thermal neutrons that return from the external reflector to the fuel core, will have passed through this poison annulus. Since σ_γ for ^{10}B is very high at the lower end of the thermal energy range and then decreases rapidly with increasing energy, the lower part of the thermal neutron spectrum will be reduced sharply upon passing through this annulus, while higher energy neutrons will be much less affected. The annulus will act as a high pass neutron energy filter and the spectrum of the neutrons that diffused back to the fuel will thus be significantly harder, compared to the case for the control rods. Since LEU fuel is not very sensitive to changes in the neutron spectrum, this hardening of the spectrum should not significantly alter the core physics for the LEU case. This was confirmed by the fact that Tyobeka *et al* (2008) checked two dimensional approximations for control rods by means of three-dimensional MCNP simulations for a LEU case and found good correlations. However, as will be shown in the burn-up calculations below, Pu(PWR) is very sensitive to changes in the neutron spectrum:

Both ^{241}Pu and ^{239}Pu have a very high thermal fission resonance. Since this resonance of ^{241}Pu peaks at a lower energy than ^{239}Pu, a hardening of the spectrum will reduce the number of ^{241}Pu fissions more than the ^{239}Pu fissions. However, the physics characteristics of these nuclides differ significantly, for instance ^{241}Pu gives a positive Uniform Temperature Reactivity Coefficient (UTC) below 500°C (see Par. 3.4.1 below), while ^{239}Pu gives negative uniform temperature reactivity coefficient at all relevant temperatures. Therefore, replacing the 3-D control rods with a 2-D ^{10}B-annulus will create a reduction in the magnitude of the positive uniform temperature reactivity coefficient of the core at low temperatures, and will thus affect the shut-down margins. By similar logic, it may affect other core parameters, such as the radial power profile during normal operation, with the control rods partially inserted for reactivity control.

The 2-D MEB method should therefore be used with more caution for Pu cores, compared to the LEU for which the verification studies, mentioned above, were performed. Pu verification studies should thus be repeated with MCNP simulations. However, a detailed verification programme would cause too much of a diversion from the main focus of the present study and was therefore excluded by the demarcation of this study and is thus left for a follow-up study.

For more details, see Par. 7.2.4 to 7.2.5 in the appendix.

2.5.6 Conclusions

1. It was shown from the literature that the MECS + MEB simulation techniques for the control rod shut-down margins have been verified sufficiently for LEU fuel cycles.

2. However, significant uncertainties/errors have been pointed out in the present results for the Pu(PWR) fuel cycle. In spite of these uncertainties, it was shown, under conservative assumptions, that all simulated cores could be safely shut down under all simulated core conditions. Therefore it is concluded that shut-down margins for the Pu(PWR) fuel cycle are not an issue of significant concern.

3. Correction techniques for the uncertainties/errors in the present results have been referred to a follow-up study (Par. 7.2.6 in the appendix.)

4. Since the technique for the simulation of the control rods has explicitly been excluded, in the demarcation section, from the list of original contributions claimed for this study, any shortcomings in this technique should not affect the validity of the claims that an original contribution has been made by the present study.

3 Results

3.1 Comparison of calculation speed of VSOP-A and VSOP 99/05

VSOP-A contains the following features that allow it to execute faster than VSOP 99/05:

- The ability to initially run BIRGIT with a fine grid, in order to accurately calculate the volume matrix and store it for subsequent use. In subsequent runs a much coarser grid can then be used to save calculation time. Since the three modules of VSOP have been fused together into one code with one input file in VSOP 99/05, this ability has been lost.

- VSOP-A has the option to combine several regions into a single spectrum zone. By carefully combining regions that can be expected to contain similar neutron energy spectra end fuel compositions, the number of spectrum zones can be reduced, which reduces the number of calculations. VSOP 99/05 does not offer this feature.

- With a view to greater accuracy, VSOP 99/05 calculates the whole trans-plutonic transmutation chain, up to the point where ^{244}Cm captures a neutron in order to become ^{245}Cm. With a view to improving calculation speed, VSOP-A terminates this chain at the point where ^{242}Pu captures a neutron in order to become ^{243}PU.

The central processor unit(CPU)-time used for the calculation of a simple 342 operating cycle burn-in sequence, in order to create the equilibrium core, was tested on an Intel Centrino Duo Laptop computer with a T2500 Genuine Intel CPU with a 2 GHz processor and 2 GB RAM. The results were:

VSOP-A

Calculation of the volume matrix with the fine grid using BIR_A.EXE = 9.97 s.

Calculation of the volume matrix with the coarse grid using BIR_A.EXE = 0.03 s.

Calculation of the fuel properties etc. using DAT_A.EXE = 0.00 s.

Calculation of the 342 operating cycles towards the equilibrium core using VSOP_A.EXE = 198 s.

Total = 208 s.

VSOP 99/05:

All steps from the calculation of the volume matrix with a fine grid to the 342 operating cycles towards the equilibrium core were executed continuously and used 431 s CPU time.

VSOP-A thus used only 48.3% of the CPU time, compared to VSOP 99/05.

3.2 k_{eff} as a function of burn-up

The rate of decrease of the multiplication factor (k_{eff}), as a function of burn-up, determines how many recirculation passes will be required to flatten the axial power profile to a desired level. Therefore this parameter was investigated before designing the specific fuel cycles.

3.2.1 VSOP-A results from the pilot study

During the pilot study, the evolution of the infinite multiplication factor (K_∞) as a function of burn-up was calculated with VSOP-A (Mulder *et al*, 2008) for a simplified core configuration with a volume of 10 m^3 (R = 1 m, H = 3.18 m) at a constant temperature of 500°C. Fresh fuel was loaded into this core and was then kept static during burn-up.

When fuel spheres from the conventional 9 g LEU (9.6%) per fuel sphere U/Pu fuel cycle were loaded, K_∞ decreased almost linearly with burn-up from 1.35 to 0.83, as can be seen in **Figure 12** (Mulder *et al*, 2008: Fig. 2). However, for the 3 g Pu_{HM}(LWR) fuel spheres, K_∞ remained almost constant at a value of about 1.16 up to about 85% of its target burn-up, and then decreased rapidly towards the end.

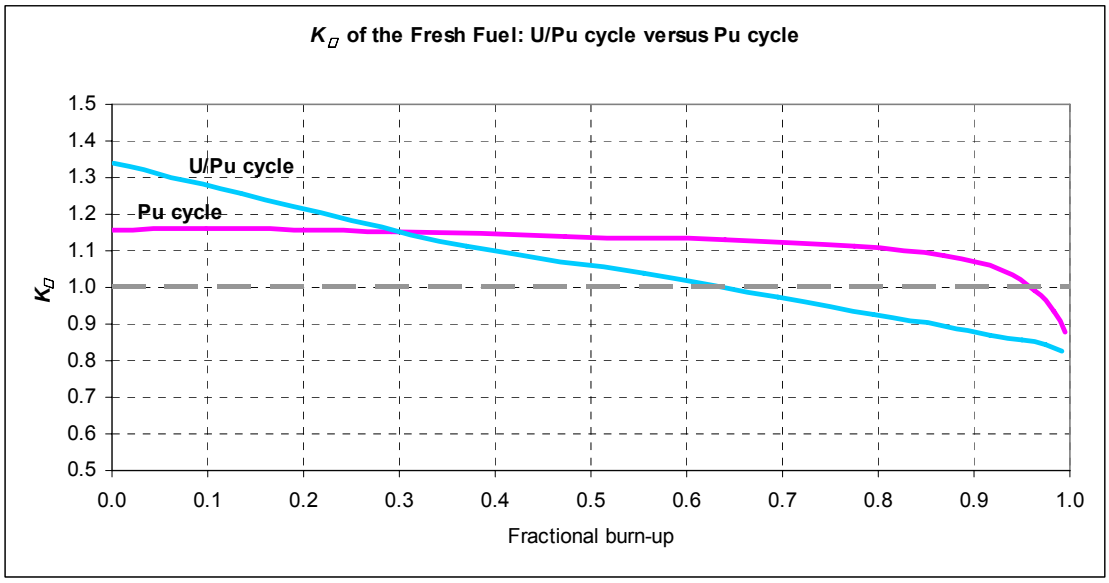

Figure 12: Decrease of K_∞ during burn-up. ($K_\infty = \nu\Sigma_f/\Sigma_a$.) Target burn-up: U/Pu Cycle 95 MWd/kg_{HM}, Pu Cycle 692 MWd/kg_{HM}.

This phenomenon was explained by the fact that the concentration of the main absorber, ^{240}Pu, decreased strongly from about 23.6 wt% in fresh fuel to almost zero at high burn-up, while the concentration of ^{241}Pu initially increased, as is shown in **Figure 13** (Mulder *et al*, 2008: Fig. 3).

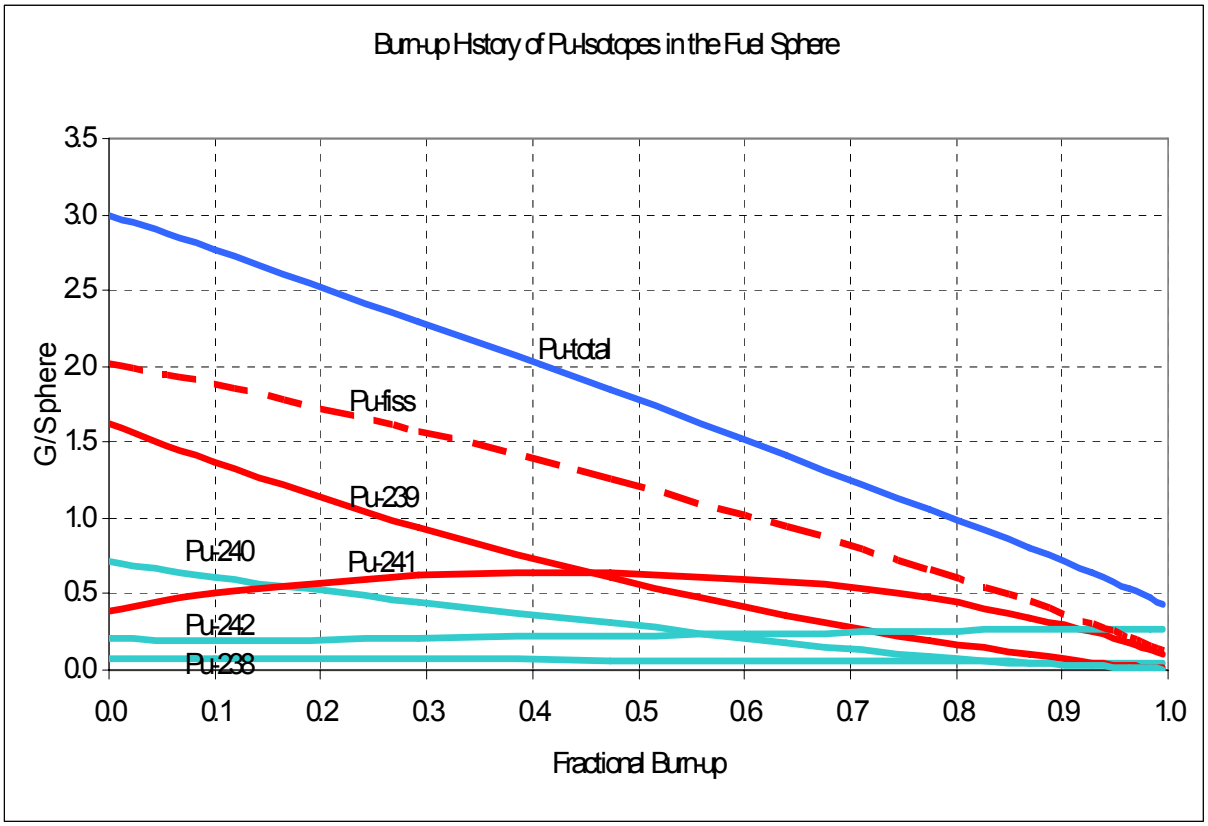

Figure 13: Pu-Cycle - Burn-up history of Pu-isotopes with target burn-up of 692 MWd/kg_{HM}.

In this way the reduction in the fissile concentration was offset by the reduction in the fertile absorber concentration, which assisted in sustaining the K_∞-curve. The moderation ratio, N_C/N_{HM}, also increased strongly by a factor 6.7, due to depletion of heavy metals by the very high burn-up, and this also supported K_∞.

The reason for this investigation was to gain insight into the physics characteristics of the Pu fuel cycle in order to improve insight into optimising the cycle.. The purpose of the six passes in the standard LEU fuel cycle is to combat the sharp reduction in K_∞ with burn-up. The high number of passes thus flattens the axial power profile. Therefore the flatter K_∞ curve for the Pu fuel cycle allowed for the reduction to three passes in the pilot study, while still maintaining a flatter axial power profile, compared to LEU.

3.2.2 Simulation parameters for VSOP 99/05

The fuel compositions are shown in **Par. 3.2.2** below. For the present study, the author opted to evaluate the evolution of k_{eff} as a function of burn-up in the PBMR DPP-400 core, rather

than K_∞ in the simplified core of the pilot study. This was done in order to take the influence of the full reactor geometry, as well as a more realistic fuel temperature distribution, into account. Therefore the PBMR DPP-400 core was loaded with fresh fuel and simulated with VSOP 99/05, using the equilibrium temperature distribution of the PBMR DPP-400 core with the 3-pass fuel cycle for Pu(PWR) from the VSOP-A simulations of the pilot study. The isotopic composition in the well-thermalised neutron spectra next to the reflectors can be expected to evolve quite differently, compared to the more epithermal spectra in the central flow channels. Therefore keeping the fuel static during burn-up might have introduced substantial differences between the fuel compositions adjacent to the reflector and those in the central fuel flow channels, which do not correspond to the situation in a normal reactor with multi-pass fuel recirculation. This potential problem was therefore circumvented by constantly recirculating the same fuel spheres during burn-up, without adding fresh fuel or discarding spent fuel. This produced mixing of the fuel in order to smooth out the effects of these location-dependent spectrum and burn-up patterns. These calculations were then performed for U/Pu(LEU), Pu(PWR), Pu(PWR)+MA and Pu(WGR). In order to be able to compare results, the composition of weapons-grade plutonium (Pu(WGR)) was chosen identical to the IAEA's Pu driven Th fuel cycles, i.e. 94% ^{239}Pu + 6% ^{240}Pu (IAEA, 2003: Table 3.2.1)

3.2.3 VSOP 99/05 results for k_{eff} for U/Pu(LEU), Pu(PWR) and Pu(WGR)

The evolution of k_{eff} as function of the core residence time at full power, is shown in Figure 14 for the different fuel cycles. If the time it takes for k_{eff} to decrease to 1.00 is compared, it is clear that all the Pu fuel cycles will be able to maintain much longer average core residence times than LEU. Of these Pu(WGR) will produce the longest and PU(PWR)+MA the shortest core residence times.

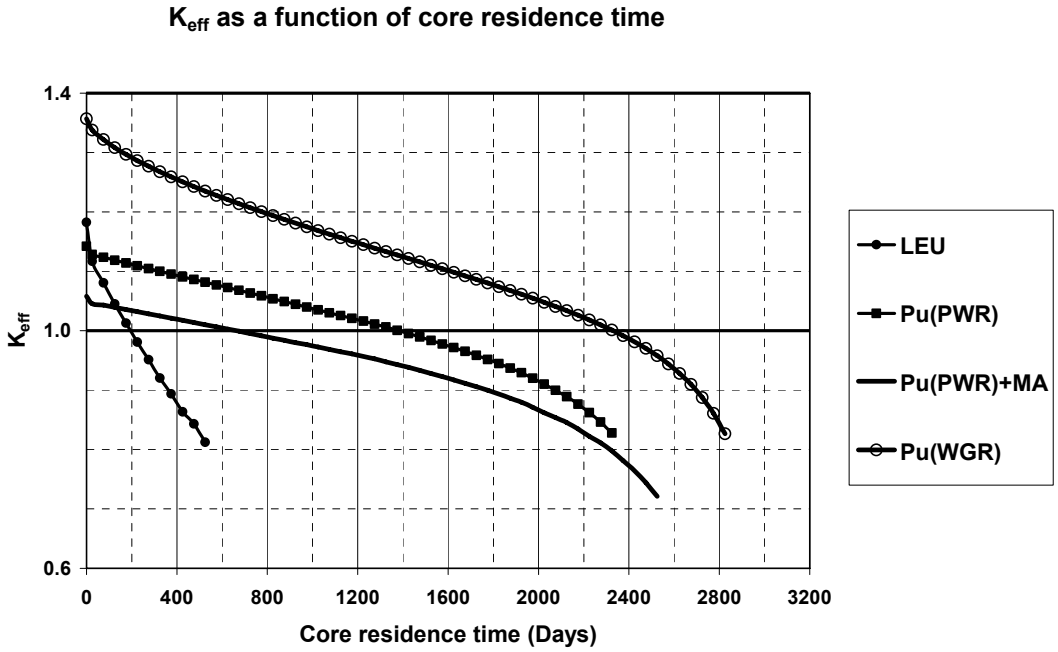

Figure 14: Comparison of evolution of k_{eff} with core residence time for different fuel cycles.

Interpolation between the points where k_{eff} is just larger and just smaller than 1.00 showed that Pu(PWR) takes 1380.8 days to reach k_{eff} =1.00, compared to only 194.9 days for the LEU fuel cycle. It would appear from this that, since Pu(PWR) maintains it reactivity much longer, it is a foregone conclusion that less recirculation passes will be required to flatten the axial power profile to the same level as for LEU. However, it should be borne in mind that the issue is not how much k_{eff} decreases per day, but per recirculation pass. For a 3-pass cycle, one should thus investigate the decrease in k_{eff} during a third of the average core residence time. Therefore, in order to investigate this feature for all the fuel cycles on an equal basis, their respective core residence times were normalised to the time it took for k_{eff} to decrease to 1.00, as is shown in Figure 15.

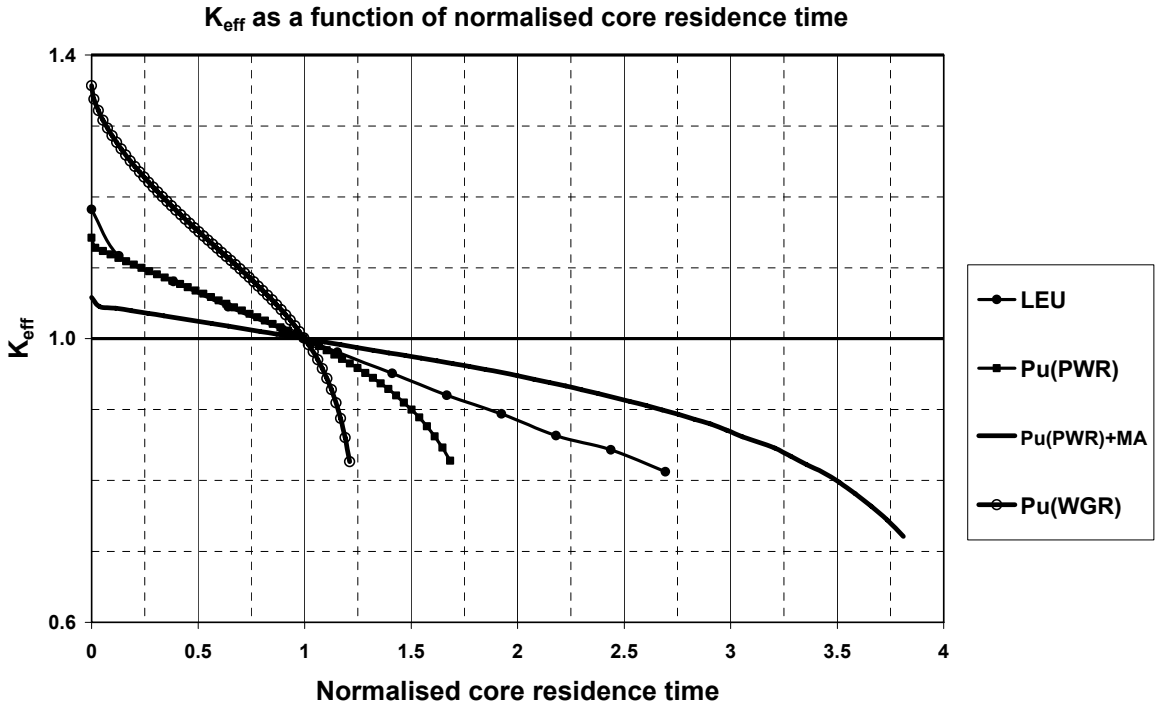

Figure 15: Evolution of k_{eff} as a function of the core residence time, normalised to the time it takes for k_{eff} to decrease to 1.00.

This time is of course shorter than the average residence time, but since it would be complicated to estimate which value of k_{eff} would correspond to the average residence time, the time to k_{eff} = 1.00 was used as a convenient proxy, based on the assumption that these two times would roughly be proportional to each other.

3.2.4 Discussion of results for k_{eff}

The surprising result from the normalised core residence times in Figure 15 is that for the phase towards k_{eff} = 1.00, the evolution of k_{eff} is virtually identical for Pu(PWR) and LEU, and after k_{eff} = 1.00, Pu(PWR) even decreases faster. This suggested that the number of recirculation passes should either be identical, or otherwise slightly more passes should be used for Pu(PWR). Each pass would of course be much longer for Pu(PWR).

This result contrasts sharply with the VSOP-A results from the pilot study in Figure 12, where K_∞ for Pu(PWR) decreased much slower than for LEU, per normalised time unit. The reason for the flattened profile for Pu(PWR) was that VSOP-A calculated the capture in ^{240}Pu in fresh Pu(PWR) fuel much higher, and thus k_{eff} much lower, than VSOP 99/05. Due to this higher estimate of the capture rate, ^{240}Pu burnt away much faster and ^{241}Pu was produced much faster in VSOP-A. This led to the slight increase, and later much slower decrease in K_∞. The

reason for this difference in the capture results between VSOP-A and VSOP 99/05 has been explained in detail in the verification study (Par. 2.2.4 to 2.2.5) above.

The decision to reduce the 6-pass cycle for LEU to three passes for Pu(PWR) in the pilot study was based on this flat K_∞ profile from VSOP-A. Due to the very different VSOP 99/05 result of the present study, it was decided that the 3-pass cycle would not be appropriate for the VSOP 99/05 simulations of Pu(PWR) in the present study. Therefore the cycle was reverted to the 6-passes of the LEU cycle. Differences between the details of implementation for LEU and Pu(PWR) are provided in the Appendix.

Since the comparison of Pu(PWR) to LEU formed the core of the present study, the Pu fuel cycle was only optimised for Pu(PWR) and used for Pu(WGR) and Pu(PWR)+MA as well.

3.3 Burn-up calculations for the incineration of U/Pu(LEU) Pu(PWR), Pu(WGR) and Pu(PWR)+MA

3.3.1 Simulation parameters and fuel compositions

The core neutronics reactor model of the pilot study was retained, except for a slight increase in the packing fractions of the coated fuel particles, necessitated by the slightly different manner in which VSOP-A and VSOP 99/05 calculate the heavy metal content of the fuel spheres, as described in the Appendix. Substitution of Mulder's VSOP-A PBMR-400 THERMIX model with the PBMR DPP-400 VSOP 99/05 THERMIX model changed the He coolant inlet/outlet temperatures from 500°C in and 900°C out to 500°C in and 944°C out for U/Pu(LEU) and 941°C out for Pu(PWR). These differences were due to the simulation of the bypass flow, as will be explained below. Key parameters for the two reference fuel spheres, i.e. the standard 9 g/fuel sphere 9.6 wt% enrichment LEU fuel sphere with the standard TRISO coated particles with the 0.05 cm diameter UO_2 fuel kernels for the PBMR-DPP-400 and the 3 g/fuel sphere Pu(PWR) shell ball from the pilot study, with its smaller 0.024 cm diameter PuO_2 fuel kernels, are summarised in **Table 17** and **Table 18**. These are the two reference cases. The other fuel spheres that were used lower down in an effort to optimise the Pu(PWR) fuel cycle, are combinations and perturbations of these reference fuel spheres. While the dimensions of the shell ball were retained, the heavy metal loading/fuel sphere was varied by either modifying the packing fraction of the coated particles, or the density of the fuel in the fuel kernels, or by switching between these large or small fuel kernels, as was indicated in each case. Whenever these parameters were modified, the resonance integrals were recalculated accordingly by modifying cards DZ4 to DZ9 and VSOP 99/05 was run, using the new resonance integral file. These modifications were also entered into the fuel descriptions on cards D8 to D17. On the THERMOS cards, the fuel type (FUTYP) was specified on card T7 and from there onwards the options to automatically read the fuel

sphere geometries from the output of the D-cards (dataset 29) were selected on cards T8 and T10. Therefore the only THERMOS card that had to be changed, was MTBL on card T8, where a selection had to be made between the two cell zones of the 'normal' LEU fuel sphere and the three zones of the shell ball that was used for all the Pu-based fuels.

Key parameters for the PBMR DPP-400 reactor core are summarised in **Table 19.**

For the few-group approximation to the solution of the neutron diffusion equation, the traditional lower cut-off energies for the three epithermal energy groups, in the four group approach, on VSOP 99/05 card G6 were used, i.e. 100000 eV, 29 eV and 1.860 eV.

Table 17: Lay-out of the reference fuel elements

Parameter			**Unit**	**U/Pu(LEU)**	**Pu(PWR)**
Heavy metal loading. (See Note [1] with Table 25)			g/sphere	9	3
Outer radius of zones: graphite centre / fuel matrix / graphite shell			cm	0.0 / 2.5 / 3.0	Shell ball: 1.8 / 2.5 / 3.0
Volume of fuel sphere			cm3	113.097	113.097
Volume of fuel matrix			cm3	65.450	41.021
Volume fraction of coated particles in matrix			%	9.3450	18.452
Coated particles:					
Diameter of fuel kernels			cm	0.05	0.024
Material				UO_2	PuO_2
Density			g/cm3	10.4000	10.1287
Enrichment				9.6 wt%	See Table 20
Number of coated particles in fuel sphere				15001	46383
TRISO coatings:	**U/Pu(LEU)**			**Pu(PWR)**	
	Thickness (cm)	Density (g/cm3)		Thickness (cm)	Density (g/cm3)
(1) Inner porous carbon buffer	0.0095	1.05		0.0095	1.05
(2) Inner pyrolytic carbon	0.0040	1.90		0.0049	1.90
(3) SiC	0.0035	3.18		0.0035	3.18
(4) Outer pyrolytic carbon	0.0040	1.90		0.0040	1.90
Coated particle radius (cm)	0.0460			0.0339	
Coated particle volume (cm3)	4.0772E-04			1.6319E-04	

For the temperature calculations in THERMIX, the fuel spheres were divided radial meshes (DI(I) on VSOP 99/05 cards TX11), as shown in Table 18.

Table 18: Radial mesh intervals in fuel spheres for THERMIX

	Fuel sphere	
	Standard U/Pu(LEU)	Shell ball for Pu(PWR)
Radial Mesh Interval nr.	Inner diameter (cm)	Inner diameter (cm)
1	5.0	5.00
2	3.0	4.53
3	1.0	4.06
4	0.3	3.60
5	0.0	0.0

The outer radial Mesh Interval[nr. 1] represents the outer 0.5 cm thick fuel free shell. For the standard 9 g LEU fuel sphere, all the inner meshes contain fuel and thus produce heat. Thermix reports the temperature at the outside surface of each mesh (Z.1 to Z.5). Since, for heat producing meshes, the maximum temperature will always occur at the inner surface, THERMIX underestimates the maximum temperature in such meshes. However, the choice of an inner diameter of only 0.3 cm for the 4-th Mesh Interval for the LEU fuel sphere meant that the inner Mesh Interval[5] was very small and the temperature at its outer surface thus approached the maximum temperature at its centre and therefore provided a good estimate of the maximum fuel temperature in the sphere. For the shell ball for the Pu cases, the inner Mesh Interval was chosen to coincide with the 1.8 cm radius inner fuel free graphite sphere. Since, based on the local heat deposition approximation, no heat is produced in this sphere, no heat entered or exited this mesh during equilibrium, and thus its temperature was assumed to be constant and equal to the temperature at the inner surface of Mesh Interval[4], which corresponds to the maximum fuel temperature in the sphere.

It was found that the temperature calculations were very sensitive to these mesh division in that, when the LEU mesh divisions were erroneously applied to the Pu shell ball, and thus lumped all the fuel together into Mesh Interval[2], the maximum fuel temperature in the reactor core increased by about 100°C.

Key parameters for the PBMR DPP-400 reactor core are summarised in **Table 19.**

Table 19: Design of PBMR DPP-400 reactor core

Volume of fuel core	**m^3**	**83.73**
Packing fraction of fuel spheres		**0.61**
Number of fuel spheres in core		**451,606**
Height	**m**	**11.625**
Radii of fuel core annulus, inner / outer	**m**	**1.00 / 1.85**
Number of flow zones		**5**
Flow pattern	**steps**	**24 / 18 / 18 / 18 / 24**
Pressure of helium	**Bar**	**90**
Heating of helium	**°C**	**500 → 944(U/Pu(LEU))** **500 → 941(Pu(PWR))**
Helium mass flow after reduction for cold bypass	**kg/s**	**173.4**
Cold bypass	**%**	**10.0**

The cold He bypass flow through the reflector blocks was simulated by simply reducing the He mass flow through the fuel core to 173.4 kg/s, from 192.68 kg/s, which would correspond to a He temperature increase from 500 to 900 across the core for the nominal 400 MW_{th} power, for the He specific heat capacity of 5189.94 J/kg/°C, with no bypass flow. No actual He flow through the reflector blocks was thus simulated. This reduction in coolant flow caused the He outlet temperature to increase from the expected 900°C to the range of 941 - 944°C. This is an approximation to the full simulation of bypass flow: If the 10% bypass flow was in actually simulated as flowing through the reflectors, it would, of course, have lowered the reflector temperature, as occurs in reality. However, in reality, this cooling of the reflectors is limited by non-local heat deposition, due to absorption of $\gamma-$rays from the fission and decay reactions, in the reflectors. Since the simulation of non-local heat deposition is not yet available in VSOP 99/05, the said approximation was used.

The isotope vector of the OECD benchmark, as shown in Table 20, was used for all the Pu(PWR) cases, except in specialised cases where modifications were specifically stated.

Table 20: Isotopic composition for simulations with reactor-grade plutonium (41.2 GWd/t burn-up + 3 years cooling) from the OECD benchmark (from Organisation for Economic Co-Operation and Development, 2003b: Figure 6).

Isotope	Weight fraction (%)	Atom fraction (%)
^{238}Pu	2.59	2.8586
^{239}Pu	53.85	55.4481
^{240}Pu	23.66	24.2604
^{241}Pu	13.13	13.4072
^{242}Pu	6.77	6.8843

A case where the associated MA were added to the Pu(PWR), was also calculated. Since this OECD benchmark does not supply the fractions of the MA, which were associated with this Pu mixture during chemical reprocessing, these were derived in the following way:

An isotope vector for fresh PWR spent fuel with a burn-up of 53 MWd/kg$_{HM}$, which included the MA, was received by personal communication from Lahoda (2006). The evolution of this isotope vector after 3 years of cooling was then calculated. Especially important was the β-decay of ^{241}Pu to ^{241}Am, with a half life of 14.29 years, because ^{241}Am has two strong thermal capture resonances and thus reduces k_{eff} and the attainable burn-up significantly. These thermal capture resonances may also influence the moderator temperature reactivity coefficient by countering the positive contribution of the thermal fission resonances of ^{239}Pu and ^{241}Pu, as will be investigated below. It should also be kept in mind that in cases where pure Pu(PWR) is used, this decay reaction will strongly reduce the reactivity of the fuel, if a significant amount of time elapses between chemical reprocessing and the irradiation of the fuel. These evolved atom densities of the MA were then normalised relative to the ^{239}Pu atom density of this mixture. The MA vector from the Lahoda data was then appended to the Pu(PWR) vector of the OECD benchmark by multiplying these normalised atom densities with the ^{239}Pu atom density of the OECD benchmark, as shown in **Table 21**.

Table 21: Atom fractions for Pu(PWR) + MA.

Nuclide	GAM-I Id. Nr.	VSOP Id. Nr.	a/o %
Np-237	133	11	4.998
Pu-238	177	15	2.46
Pu-239	14	16	45.784
Pu-240	15	17	22.255
Pu-241	16	18	12.372
Pu-242	17	19	7.822
Am-241	178	21	2.337
Am-243	181	24	1.966
Am-242	179	23	0.005
Cm-244	184	28	4.998

For **Pu(WGR)** mass fractions of 94% ^{239}Pu and 6% ^{240}Pu were used.

3.3.2 VSOP-A results from the pilot study

The VSOP-A results from the pilot study are summarised in **Table 22** and **Table 23**.

Table 22: Characteristics of the U/Pu-cycle vs. the Pu(PWR)-cycle from the VSOP-A calculations of the pilot study.

Fuel cycle		9 g U/Pu	3 g Pu(PWR)
Fuel element passes through the core		6	3
Core physics:			
Fuel residence time	days	961	2362
Fuel shuffling	spheres/day	2821	492
Submitting of fresh fuel elements	spheres/day	470	191
Target burn-up	MWd/kg_{HM}	95.5	692.6
Fast neutron fluence of spent fuel (E>0.1 MeV)	$10^{21}/cm^2$	2.74	7.18
Average thermal neutron flux	$10^{14}/(cm^2 \cdot sec)$	0.79	0.27
Neutron leakage	%	15.21	10.60
Thermal properties:			
Maximum power per sphere	KW/sphere	2.77	3.77
Maximum fuel temperature	°C	1069	1058
DLOFC-maximum temperature	°C	1577	1501
Time of max. temp. after DLOFC	h	45	57
Relative decay heat at max. temp.	%	0.470	0.398
Temperature coefficient at equilibrium T :			
Resonance absorber (Doppler)	$10^{-5}\ \Delta k_{eff}/°C$	- 3.4	-
Moderator		- 2.4	- 5.0
Reflector		+ 3.2	+ 1.8
Total		- 2.6	- 3.2
Shut-down balance:			
Decay of ^{135}Xe and other nuclides over 3 days	Δk_{eff}	+ 0.0279	+ 0.0177
Insertion of 24 rods to 688 cm		- 0.0532	- 0.0314
Temperature reduction to 50°C		+ 0.0328	- 0.0232
Total		+ 0.0075	- 0.0369

During a DLOFC, the maximum temperature of the Pu-cycle was lower than for the U/Pu-cycle, which resulted from the lower decay heat of the fission products of the plutonium in comparison with those of uranium.

Table 23: Fuel materials balance for the U/Pu-cycle vs. the Pu(PWR)-cycle from the VSOP-A calculations of the pilot study

Fuel cycle		**9 g U/Pu(LEU)**			**3 g Pu(PWR)**		
Fresh fuel supply		470 balls/day			191 balls/day		
		loading →	unloading	reduction			
^{234}U	g/sphere	0.0084 →	0.0052	- 38.7%			
^{235}U	g/sphere	0.8640 →	0.1499	- 83.7%			
^{236}U	g/sphere	0 →	0.1148				
^{238}U	g/sphere	8.1276 →	7.7136	- 5.1%			
Total U	g/sphere	9.0000 →	7.9835	- 11.3%			
Fissile U enrichment		9.6%	1.9%				
					loading →	unloading	reduction
^{238}Pu	g/sphere	0 →	0		0.0780 →	0.0375	- 52.0%
^{239}Pu	g/sphere	0 →	0.0462		1.6154 →	0.0079	- 99.5%
^{240}Pu	g/sphere	0 →	0.0275		0.7097 →	0.0169	- 97.6%
^{241}Pu	g/sphere	0 →	0.0220		0.3938 →	0.0840	- 78.7%
^{242}Pu	g/sphere	0 →	0.0197		0.2031 →	0.2643	+ 30.1%
Total	g/sphere	0 →	0.1153		3.0000 →	0.4106	- 86.3%
Fissile Pu enrichment			59.1%		66.7%	22.4%	
Total fissile enrichment		9.6%	2.6%		66.7%	22.4%	

A consequence of the relatively low thermal flux is a reduction in the shut-down balance. The reduction in thermal flux reduces both the effect of ^{135}Xe poisoning and the capture of neutrons in the control rods. Therefore both the negative reactivity requirement, due to the positive reactivity added by ^{135}Xe-decay, and the capability of insertion of the control rods to supply negative reactivity, are smaller than for the U/Pu-cycle. It is an interesting result that the reactor could be kept sub-critical solely with the regular control system.

An undesirable result was that cooling down to 50°C decreased the reactivity for the Pu-cycle, indicating that, in the lower temperature range the total temperature coefficient switches to a positive value. This positive temperature reactivity coefficient of the Pu-cycle at low temperatures will probably raise regulatory issues for the start-up procedure from cold conditions. This may necessitate preheating the core and reflector, before starting the fission

reaction. Due to these possible implications, the mechanism and effect of these temperature induced spectrum shifts will be investigated further in the present study.

3.3.3 Summary of VSOP99/05 results

While the details for the calculations of the temperature reactivity coefficients, the control rod shut-down margins and the maximum temperatures are given in separate sections below, the main characteristics of burn-up results for U/Pu(LEU) vs. the Pu(PWR), Pu(PWR)+MA and Pu(WGR) are summarised in **Table 24** to **Table 26**.

In order to better understand the factors that influenced the different parameters, 2 g and 1 g per ball cases were added to the standard 3 g Pu(PWR) case. The fuel compositions of these were obtained by lowering the coated particle packing fractions in the fuel zone.

3.3.3.1 Burn-up and fuel cycle characteristics

The burn-up characteristics and materials balances are summarised in Table 24 and Table 25**.**

Table 24: Characteristics of the U/Pu vs. Pu-fuel cycles for VSOP 99/05.

Fuel cycle		9 g U/Pu(LEU)	3 g Pu(PWR)	3 g Pu(PWR)+MA	3 g Pu(WGR)	2 g Pu(PWR)	1 g Pu(PWR)
Core physics:	**Unit**						
Number of passes through the core		6	6	6	6	6	6
Average fissile enrichment of core	%	5.22	50.23	53.27	56.89	41.43	32.98
Average fuel residence time	days	994.7	2095.0	1234.1	2902.4	1538.7	763.8
Fuel shuffling	spheres/day	2724	1333	2508	939	1814	3655
Submitting of fresh fuel elements	spheres/day	453	222	418	156	302	609
Average burn-up	MWd/kg_{HM} [1]	97.9	601.0	319.0	852.4	661.6	656.6
Fast neutron fluence of spent fuel (E>0.1 MeV)	$10^{21}/cm^2$	2.87	6.32	3.60	9.01	4.76	2.40
Average thermal neutron flux	$10^{14}/(cm^2.sec)$	0.79	0.18	0.13	0.27	0.33	0.75
Conversion ratio (C)		0.447	0.413	0.407	0.314	0.395	0.366
Neutron leakage from core	%	14.88	10.45	9.81	12.29	11.84	15.53
Maximum power per sphere	kW/sphere	2.94	4.89	3.00	9.26	5.74	6.49
Maximum fuel temperature	°C	1050	1182	1164	1367	1116	1173
Max. Uniform Temperature Coefficient (UTC)	$\Delta k_{eff}/°C * 10^{-5}$	-4.49	+2.30	+0.6	+5.3	+7.5	+16.9
Shut-down balance:						-	-
Decay of ^{135}Xe and other nuclides over 4 days	Δk_{eff}	+0.0287	+0.0161				
Temperature reduction to 50°C	Δk_{eff}	+0.0361	+0.0047				
Full insertion of 12 rods	Δk_{eff}	-0.0955	-0.0604				
Total	Δk_{eff}	-0.0307	-0.0396				

Note: 1 See note [1] at the end of Table 25 for the different definitions of HM, used by VSOP 99/05.

3.3.3.2 Fuel materials balance

Table 25: Materials balance for Pu(PWR) vs. U/Pu(LEU) fuel for the PBMR-400 MW_{th}

Fuel cycle		U/Pu(LEU)			Pu(PWR)		
Average burn-up		97.9 MW.d/kg_{HM}			601.01 MW.d/kg Pu_{HM}[1]		
Fresh fuel supply		453 balls/day * 9 g U/ball			222 balls/day * 3 g Pu_{HM}[1]/ball		
		loading →	unloading	change			
^{234}U	(kg/GW_{th}d)	0.0096 →	0.0057	- 41%			
^{235}U	(kg/GW_{th}d)	0.9807 →	0.1560	- 84.1%			
^{236}U	(kg/GW_{th}d)	0 →	0.1319				
^{238}U	(kg/GW_{th}d)	9.2250 →	8.7359	- 5.3%			
Total U	(kg/GW_{th}d)	10.215 →	9.0295	- 11.6%			
Fissile U enrichment		9.60%	1.73%				
					loading →	unloading	change
^{237}Np		0 →	0.0092		0 →	0.0001	
^{238}Pu	(kg/GW_{th}d)	0 →	0.0038		0.046 →	0.0491	+6.7%
^{239}Pu	(kg/GW_{th}d)	0 →	0.0525		0.8948 →	0.0393	-95.6%
^{240}Pu	(kg/GW_{th}d)	0 →	0.0404		0.3931 →	0.1135	-71.1%
^{241}Pu	(kg/GW_{th}d)	0 →	0.0243		0.2182 →	0.1430	-34.5%
^{242}Pu	(kg/GW_{th}d)	0 →	0.0219		0.1125 →	0.1665	+48.0%
^{241}AM	(kg/GW_{th}d)	0 →	0.0018		0 →	0.0268	
^{242m}AM	(kg/GW_{th}d)	0 →	0.0000		0 →	0.0008	
^{243}AM	(kg/GW_{th}d)	0 →	0.0035		0 →	0.0572	
^{242}CM	(kg/GW_{th}d)	0 →	0.0000		0 →	0.0008	
^{243}CM	(kg/GW_{th}d)	0 →	0.0000		0 →	0.0002	
^{244}CM	(kg/GW_{th}d)	0 →	0.0008		0 →	0.0409	
Total Pu[1]	(kg/GW_{th}d)	0 →	0.1429		1.6646 →	0.5115	-69.3%
Fissile Pu enrichment%		- →	53.74		66.86% →	35.74%	
Total fissile enrichment%		9.60 →	2.53				

Note: [1] VSOP nomenclature for HM: in the bookkeeping for the mass of heavy metals for the specification of the heavy metal content of fresh fuel spheres, VSOP 99/05 include only those heavy metals that are specified on the input cards that describe the contents of the fuel kernels, i.e. cards D7 to D12. The heavy metals specified as homogenised atom densities on VSOP 99/05 Card D17 are thus excluded, for instance ^{237}Np, ^{238}Pu and all MA. The loadings of these MA are therefore also not affected by adjustment of the packing fraction of the coated fuel particles (FF1) or the homogenised heavy metal density in the fuel zone (ROSM) on card D12. The DATA-2-module thus treat these heavy metals as if they are impurities in the matrix graphite, although their distribution, i.e. in the fuel kernels, matrix graphite etc. can be specified for

THERMOS on card T10. The output of the DATA-2-module consequently always underestimates the heavy metal content of the fuel sphere types. This becomes highly significant when significant quantities of other heavy metals are included in fresh fuel, as happened in the present Pu(PWR)+MA mixture. In this study this exclusive HM definition was retained for the specification of fresh fuel types, i.e. Pu_{HM} refers to Pu excluding ^{238}Pu, as opposed to "Total Pu", which will refer to Pu_{HM} + ^{238}Pu and "Total HM", which will include all heavy metals.
However, when burn-ups are reported, the VSOP-module includes ^{238}Pu and the MA in its summation of the HM mass supplied to the reactor. For more detail, see Par. 6.5.5.3 below.

Incineration results for Pu(PWR)+MA

The mass balance, for the case of pure Pu(PWR) and the case where the associated MA were added to the fuel (Pu(PWR)+MA) is shown in Table 26.

Table 26: Materials balance for Pu(PWR)+MA vs. Pu(PWR) fuel.

Fuel cycle		Pu(PWR)			Pu(PWR)+MA		
Average burn-up ($MW.d/kg_{HM}$)		601.0			319.0		
Fresh fuel supply		191 balls/day * 3 g Pu_{HM}[1]/ball			222 balls/day * (3 g Pu_{HM}[1]+ 0.31 g MA)/ball		
		loading →	unloading	ΔHM	loading →	unloading	ΔHM
^{237}Np		0 →	0.0001	+0.0001	0.1642 →	0.1019	-0.0623
^{238}Pu	($kg/GW_{th}d$)	0.046 →	0.0491	+0.0031	0.0812 →	0.1586	0.0774
^{239}Pu	($kg/GW_{th}d$)	0.8948 →	0.0393	-0.8555	1.5174 →	0.4771	-1.0403
^{240}Pu	($kg/GW_{th}d$)	0.3931 →	0.1135	-0.2796	0.6667 →	0.4581	-0.2086
^{241}Pu	($kg/GW_{th}d$)	0.2182 →	0.1430	-0.0752	0.3700 →	0.4350	0.0650
^{242}Pu	($kg/GW_{th}d$)	0.1125 →	0.1665	+0.0540	0.1908 →	0.2307	0.0399
^{241}AM	($kg/GW_{th}d$)	0 →	0.0268	+0.0268	0.0781 →	0.0908	0.0127
^{242m}AM	($kg/GW_{th}d$)	0 →	0.0008	+0.0008	0 →	0.0031	0.0031
^{242}AM	($kg/GW_{th}d$)	0	0.0000	0.0000	0.0002 →	0.0000	-0.0002
^{243}AM	($kg/GW_{th}d$)	0 →	0.0572	+0.0572	0.0662 →	0.0903	0.0241
^{242}CM	($kg/GW_{th}d$)	0 →	0.0008	+0.0008	0 →	0.0024	0.0024
^{243}CM	($kg/GW_{th}d$)	0 →	0.0002	+0.0002	0 →	0.0005	0.0005
^{244}CM	($kg/GW_{th}d$)	0 →	0.0409	+0.0409	0 →	0.0530	0.0530
Total Pu[1]	($kg/GW_{th}d$)	1.6646 →	0.5115	-1.1531	2.9903 →	1.8614	-1.1289
Fissile Pu enrichment	%	66.86 →	35.74		66.78 →	51.84	
Total HM	($kg/GW_{th}d$)	1.6646 →	0.6382	-1.0264	3.1348 →	2.1015	-1.0333

Note: [1] See Table 26

3.3.4 Discussion of summary of VSOP 99/05 results

3.3.4.1 Limits of TRISO fuel

A large amount of data has been published on the performance limits of TRISO fuel, especially on the German experience (IAEA, 1997; Venter, 2004 and Venter and Nabielek, 2006). While these documents describe a large number of fuel compositions that performed well, as well as others that performed less well, the German experimental programme was more focused on finding fuel compositions that would perform well, than on determining the limits beyond which the fuel would not work well. In the words of Venter and Nabielek (2006): "Even though a large body of experimental data exists on German LEU-TRISO fuel, the actual performance limits of this fuel type have never been established." This leaves one with the problem that, as soon as you move out of the tried and trusted parameters of the German experience, it becomes very difficult to predict where the limits will be. Since German programme did not focus on Pu fuel and concentrated on much lower burn-ups than the 600 to 700 MWd/kg heavy metal, which is typical for pure Pu(PWR) fuels, the German experience cannot be used to predict these limits with confidence. Therefore, until a focused experimental programme can determine these limits with confidence, these limits should be shunned in reactor designs. Based on this philosophy, the following design target limits were chosen for the present study:

Power density: Although the PBMR (Pty.) Ltd. never established a firm limit, the design team widely accepted that a maximum power of 4.5 kW/fuel sphere should not be exceeded. For the 15,000 coated particles (CPs) in the standard 9 g LEU(10%) pebble, this amounts to a limit of 300 mW/coated particle. There exists a difference of opinion as to whether the safety limit should be imposed on the power/sphere or on the power/coated particle. Since resolving this issue falls outside the scope of the present study, both these limits will be imposed.

Maximum temperatures during normal operation: The internal design target of 1130°C, which was adopted by the PBMR (Pty.) Ltd. for the PBMR DPP-400, will be used. This matter will be discussed in more detail in Par. 3.3.4.3 below.

Maximum fast fluence on the coated particles of spent fuel elements: The limit of 8.0 E+21 n/cm^2, proposed by Boer and Ougouag (2010b: 7), will be accepted, based on their statement that experience with TRISO fuel above this limit is unavailable. (See also IAEA (1997); Venter (2004) and Venter and Nabielek (2006).)

Maximum fuel temperature during a DLOFC: Although DLOFC temperatures were not calculated in the present study, the generally accepted limit of 1600°C will be adopted. Minimising the maximum DLOFC temperatures will be borne in mind when proposals for the redesign of the PBMR-400 will be given in the list of suggested follow-up studies.

3.3.4.2 Burn-up

The average burn-up of 601.0 MWd/kg_{HM} obtained with VSOP 99/05 for the reference 3 g per pebble Pu(PWR) case, was much lower than the 692.6 MWd/kg_{HM} obtained with VSOP-A in the pilot study. This was to be expected due to the fact that VSOP-A does not include the MA, which builds up during burn-up in its calculations, and because of the other differences discussed above. More surprising was the fact that the 661.6 MWd/kg_{HM}, obtained with VSOP 99/05 for 2 g Pu(PWR), was significantly lower than the burn-up of 702 MWd/kg obtained by Boer and Ougouag (2010a): They simulated the irradiation of 2 g heavy metal per pebble Pu(PWR) and Pu(PWR) + MA, excluding Am, in a standard PBMR DPP-400 core and obtained maximum fuel temperatures, for the first pebble pas, during normal operation of 1316°C (Boer and Ougouag, 2010b) and 1359°C respectively. These are much higher than the 1116°C obtained for the 2 g Pu(PWR) with VSOP 99/05. The reason why these differences are surprising is that Boer and Ougouag used parameters for their simulation similar to those used in the present study, i.e. they also included the build-up of the MA and used resonance integrals for ^{240}Pu and ^{242}Pu. It should, however, be noted that they used 200 µm diameter fuel kernels, compared to the 240 µm for the present study. They also used the standard fuel spheres, while shell-ball fuel spheres were used in the present study. Since shell fuel improves the heat conduction to the surface of the sphere, this might have been responsible for the lower temperature in the present study. However, the shell fuel and larger fuel kernels should have led to better moderation, through better lumping, in the present study, which should have increased the burn-up for the present study. On the other hand, the codes used by Boer and Ougouag did include the fissioning of ^{245}Cm, which was excluded by VSOP 99/05. Since the build-up of ^{245}Cm is very low, this can explain only a small part of their higher burn-up. A more detailed comparison with the temperature coefficients obtained by Boer and Ougouag will be given below. Since their papers do not give enough detail on the parameters used in their codes and the results obtained, it is not presently possible to resolve these differences in our results, and therefore this is left for a follow-up study.

The burn-up results for PU(PWR)+MA were also disappointing. Taken on face value, **Table 26** seems to suggest that ΔHM improved slightly from -1.0264 to -1.0333 kg/GW_{th}d when the associated MA were added to the Pu(PWR). However, the total heavy metal in the spent fuel increased from 0.6382 to 2.1015 kg/GW_{th}d, when the associated MA were added to the fresh

fuel. It should, however, be noted that the 0.1718 kg/GW_{th}d MA associated with the 1.6646 kg/GW_{th}d fresh pure Pu(PWR) loaded was not included in the 0.6382 kg/GW_{th}d heavy metal in its spent fuel, because it did not physically enter the reactor. In reality the associated MA still need to be disposed of by society, and could thus be added to the heavy metal of the spent fuel for the pure Pu(PWR), in which case it would increase to 0.810 kg/GW_{th}d, which is still only 48.7% of the 2.1015 kg/GW_{th}d for the case where the associated MA actually entered the reactor. The main effect of the added MA was to almost halve the burn-up from 601.0 to 319.0. The main reason for this very negative effect of the MA is that, while they significantly capture neutrons, they do not contribute significantly to fission. The total fraction of fissions coming from MA was only 0.21% for the Pu(PWR)+MA case. This is because their thermal fission cross-sections are negligible With each capture they only move along one step in the transmutation chain, mostly without producing a fissile nucleus. It should be noted that a small fraction of the ^{243}Am in a PBR will be transmutated to ^{245}Cm, which can easily be fissioned. The problem, though, is that ^{244}Cm has a very small capture cross-section and thus forms a bottleneck in the transmutation chain towards ^{245}Cm. The other problem is that VSOP 99/05 does not include ^{245}Cm in its libraries and therefore this small fraction of fissions is neglected. The reduction in burn-up, caused by adding the associated MA, strongly reduces the fraction of fissions in the Pu. For pure Pu(PWR) the total Pu mass is reduced by 69.3%, but when the MA is added, the Pu reduction decreases to 37.8%. The biggest effect of this premature termination of the burn-up process is that the mass of ^{241}Pu in the spent fuel approximately triples from 0.143 to 0.435 kg/GW_{th}d. As has been pointed out earlier, this is an undesirable result, since this ^{241}Pu will in the long term decay to ^{237}Np, which will significantly increase the long term radiotoxicity and proliferation risk.

The fact that for the Pu(PWR) case the associated MA did not enter the reactor, is very desirable, because it means that the associated and separated MA is still uncontaminated and can thus be stored safely until fast reactors come online. It has been pointed out earlier that Am does not pose a significant proliferation risk, and thus storing it in uncontaminated form, is not a problem. ^{237}Np, however, does pose a significant proliferation risk and therefore a separate study will be done (see below) where only the ^{237}Np will be added to the Pu(PWR), in order to increase the proliferation resistance. In fast reactors, both ^{237}Np and Am will contribute significantly to the fast fissions, because they have large fast fission cross-sections, and therefore these will not have the same negative impact on the neutron economy, as was reported here for the PBMR DPP-400.

The fact that, for the Pu(PWR)+MA case, the MA have now been contaminated by the radioactive fission products, means that chemical reprocessing will be required if the

resulting MA in the spent fuel are to be burnt in a fast reactor at a later stage. However, this will bring about a large and unnecessary increase in cost and it will deprive the Pu incineration option from its most desirable asset, namely that Pu can be incinerated almost completely, and the spent fuel can thus be sent directly to a final deep geological repository, without chemical reprocessing.

In conclusion, the addition of the MA to the Pu(PWR) in a PBMR DPP-400 produces mainly undesirable results and is thus not advisable. This corresponds with the view of Kloosterman and Li (1995) that Am should preferably be transmutated in fast reactors, where it will make a positive contribution to the neutron economy. However, in thermal reactors, including LWRs, it acts mainly as a radiative capturer and therefore strongly erodes the neutron economy and therefore requires a higher fissile enrichment. While ^{241}Am can be transmutated to ^{238}Pu in a thermal spectrum, thereby enhancing the proliferation resistance of the spent fuel mixture, the thermal irradiation of ^{243}Am is pointless.

The lesson from these results is that, due to the high leakage and the lack of fast fission in small PBRs, deep burn of Pu(PWR) can only occur if the available neutrons are carefully conserved. Any action that reduces the neutron economy, like adding neutron poisons or MA to the fuel, will reduce the level of burn-up and will consequently increase the mass of heavy metal in the spent fuel.

The view within PUMA is that the only practical way to transmutate Cm is to store it for about 100 years, at which time most of it will have $\alpha-$ decayed to Pu, which can readily be transmutated in other reactors (Somers, 2007). This was also the main reason why the associated Cm was excluded from the fresh fuel for the Pu(PWR)+MA case.

3.3.4.3 Maximum temperatures during normal operation

The maximum fuel temperature of 1182°C during normal operation for the 3 g Pu_{HM}/ball case was disappointing, since this exceeds the internal design target of 1130°C adopted by the PBMR (Pty.) Ltd. for the PBMR DPP-400 (Reitsma, 2011). This maximum value was defined to limit the diffusion of ^{110m}Ag through intact coated particles as to limit the plate-out on the turbine blades in order to facilitate lower radioactivity and therefore dose rates during maintenance.

Since diffusion through the SiC coating is the mechanism of escape of the radioactive fission product gasses from the coated particles and since the rate of diffusion normally increases exponentially with temperature, a small increase in the maximum temperature will cause a large increase in the leakage rate in these areas of increased temperature. While the details

probably remain proprietary information, it is well known that PBMR (Pty.) Ltd. invested significant resources into research projects to try and solve the problem of ^{110m}Ag leakage. In view of the fact that an increase in coated particle temperature from 1100°C to 1200°C, causes an approximate tripling of the leakage rate (**Figure 16** (Slabber, 2004: Fig. 3)), and the fact that the fissioning of ^{239}Pu produces at least an order of magnitude more ^{110m}Ag than the fissioning of ^{235}U, the leakage rate in the present high maximum temperature Pu fuel cycles may be between one and two orders of magnitude larger than that for the LEU fuel cycle of the PBMR DPP-400 and may thus present a serious concern.

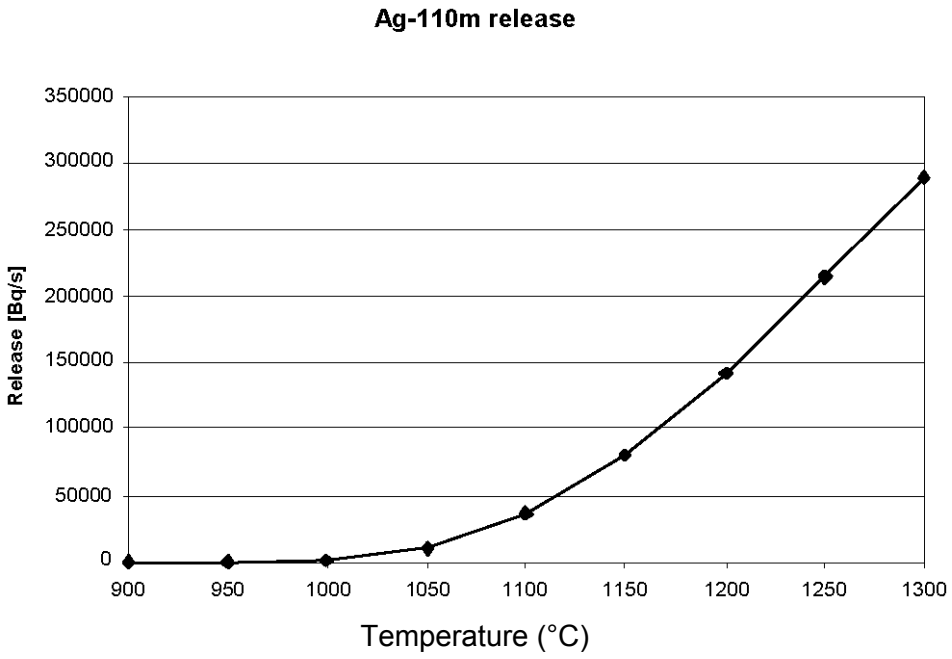

Figure 16: Release rate of radioactive ^{110m}Ag out of the coated fuel particles, as a function of temperature.

However, since these maintenance requirements for the radioactive He turbine blades do not apply to Rankine steam cycles, this temperature problem can be circumvented by switching to a steam cycle. A steam cycle will also lower the He inlet and outlet temperatures to about 250 and 750°C respectively, which would strongly reduce the maximum fuel temperatures. However, since k_{eff} for Pu fuel cycles increases more strongly with increasing neutron moderation, compared to U/Pu(LEU) fuel cycles, the possibility of water ingress into the core will require special attention for Pu cycles.

3.3.4.4 Maximum power per fuel sphere

It is clear from **Table 24** that, with the exception of Pu(PWR)+MA with a maximum power density of 3.00 kW/sphere for the equilibrium core, all the Pu cases exceeded the adopted

limit of 4.5 kW/sphere and that the maximum power/sphere increased with decreasing heavy metal loading. Of the Pu(PWR) cases, 3 g/sphere fared the best with 4.89 kW/sphere. The increasing maximum power density with decreasing heavy metal loading, increases the severity of the power peak when it is expressed in power/coated particle.

For 3 g Pu(WGR), this number jumped to 9.26 kW/sphere. This suggests that the maximum power density is constrained by the negative uniform temperature reactivity coefficient at the equilibrium temperature distribution, supplied by captures in the epithermal resonances of ^{240}Pu and ^{242}Pu, which will tend to suppress hotspots in the power and temperature profiles. The low fractions of these fertile isotopes in the equilibrium core of Pu(WGR), caused Pu(WGR) to have the most positive uniform temperature reactivity coefficient, across the whole temperature range, i.e. the negative uniform temperature reactivity coefficient with the smallest magnitude at equilibrium temperatures. This probably caused the extreme power and temperature peaks for Pu(WGR).

In order to investigate the idea that there is a link between the uniform temperature reactivity coefficient and the peak in power density, the maximum uniform temperature reactivity coefficient and maximum power/coated particle for Pu(PWR) are shown in **Figure 17**, on separate axes.

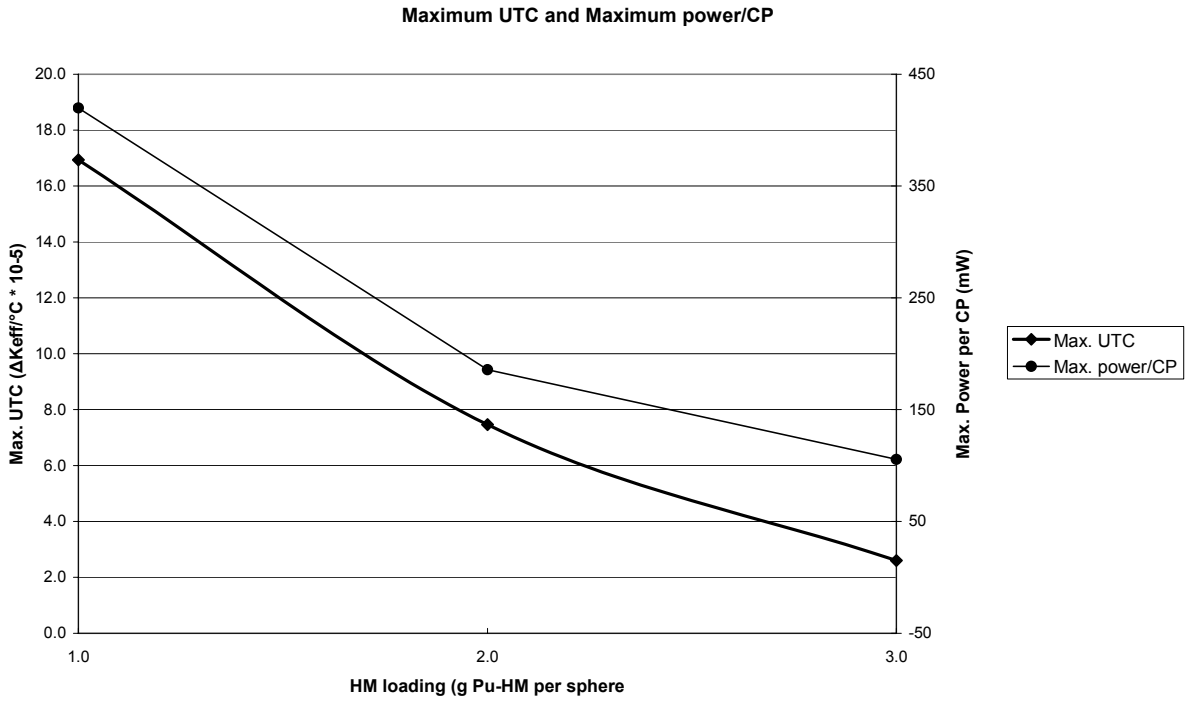

Figure 17: Maximum uniform temperature reactivity coefficient (UTC) and power/coated particle (CP) for different heavy metal loadings for Pu(PWR).

It is obvious from this chart that there is a strong correlation between the maximum uniform temperature reactivity coefficient and the maximum power/coated particle. However, it should be noted that the maximum power/coated particle was simulated at equilibrium temperatures, while the maximum uniform temperature reactivity coefficient occurred at about 100°C, and can thus not necessarily be linked causally. However, they are probably driven by the same causes. Decreasing heavy metal content increases the resonance escape probability, which makes the capture resonances less effective in creating a large negative fuel temperature reactivity coefficient. It also causes a higher thermal flux. This again increases the effect of the thermal fission resonances of ^{239}Pu, and especially ^{241}Pu, which is responsible for the positive moderator temperature reactivity coefficient (and thus uniform temperature reactivity coefficient) at low temperatures. This more positive uniform temperature reactivity coefficient then undermines the ability to suppress hotspots, even at equilibrium temperatures, which then enhances the spikes in power density.

Although all three cases exceeded the 4.5 kW limit on the maximum power/sphere. Only the 1 g Pu(PWR) case with 420 mW/coated particle exceeded the adopted limit of 300 mW/coated particle. This is because the number of coated particles for the 2 g and 3 g cases are respectively about twice and triple that for the 9 g U/Pu(LEU) fuel sphere.

3.3.4.5 Maximum fluence in spent fuel

Only the 3 g Pu(WGR) case, with a fluence of 9.01E+21 n/cm^2, exceeded the adopted limit of 8.0E+21 n/cm^2, because of its very high burn-up of 852.4 MWd/kg$_{HM}$. Especially surprising was that the 3 g Pu(PWR) case reached only 6.32 E+21 n/cm^2, while Boer and Ougouag (2010a) reported exceeding 8.0E+21 n/cm^2, for 3 g Pu(PWR). This difference is much larger than can be explained by the higher burn-up reported by them. Perhaps the lower fluence in the present study can be explained by the larger fuel kernels and by the shell-ball fuel, which would both improve lumping, and thus the probability that a fast neutron will be moderated to below the fast range, before hitting the next coated particle. Resolution of this difference is also referred to a follow-up study. If Boer and Ougouag's results would prove to be accurate, this would impose another serious constraint for the fuel design, as is shown in **Figure 18**.

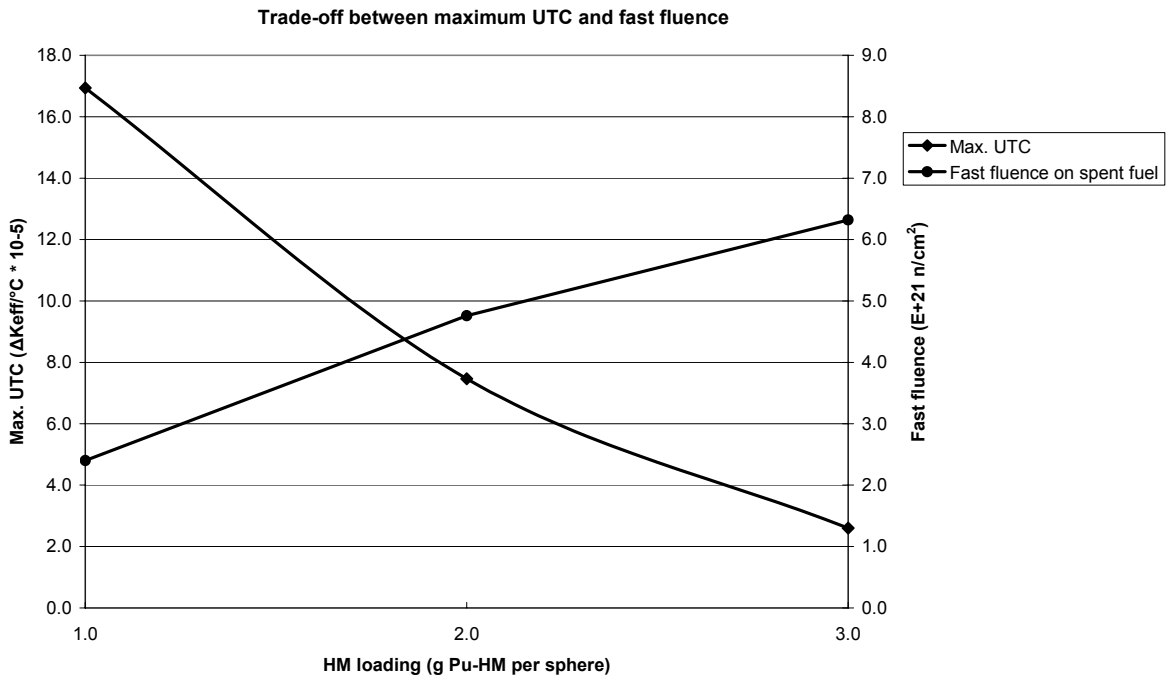

Figure 18: Trade-off between the maximum uniform temperature reactivity coefficient (UTC) and the fast fluence on the spent fuel, as a function of the Pu(PWR) heavy metal loading/sphere.

From this chart it is clear that, in order to obtain a negative maximum uniform temperature reactivity coefficient, one would like to increase the heavy metal loading to above 3 g Pu/sphere. However, that may cause the limit on the fast fluence to be exceeded.

In any case, the problem seems serious enough to warrant further efforts to modify the fuel cycle in order to reduce the maximum fuel temperatures during normal operation, as will be spelled out in the proposals for follow-up studies below.

3.3.4.6 Proliferation resistance

From Table 26 it can be deduced that the ^{238}Pu fraction in the spent fuel for the fresh 3 g Pu(PWR) case, is 9.6%. This is above the 9% target adopted in the literature study, above which the decay heat will be so severe that it will not be possible to use the Pu mixture to fuel an implosion-type nuclear weapon. A high yield weapon is thus excluded. Furthermore, the ^{240}Pu fraction is 22.2%, which means that, even if someone would in some way manage to build an implosion-type weapon with this mixture, it will very probably predetonate, which will also reduce the yield to fizzle yields. Normally these fractional criteria are accepted as sufficient safeguards against proliferation, even for Pu mixtures with high fractions of ^{239}Pu. However, in this case the ^{239}Pu has been incinerated down to 7.7%, while ^{242}Pu is now the dominant isotope with 32.6%. However, ^{242}Pu is the single isotope amongst the Pu isotopes and MA with the highest critical mass, and thus the least attractive proliferation fuel of all the competing candidates. This means that the spent fuel is already so extremely proliferation resistant that it would not make sense to add other nuclides to the fresh fuel, in order to try and increase its proliferation resistance even further.

3.4 Optimisation of fuel cycle

Based on the above analysis of the summary results, the following more detailed studies were conducted in VSOP 99/05 in order to attempt improvement of the specific parameters.

3.4.1 Temperature reactivity coefficients

3.4.1.1 Calculation methods for temperature reactivity coefficients in VSOP 99/05.

Isodeltic temperature reactivity coefficients for the whole core were calculated: the temperature coefficients were separated into the fuel temperature reactivity coefficient (FTC), i.e. the Doppler coefficient for the resonance absorbers in the fuel, the moderator temperature reactivity coefficient (MTC) for the graphite in the fuel spheres, the uniform temperature reactivity coefficient (UTC), where the fuel and moderator temperatures are varied together, and reflector temperature reactivity coefficient (RTC), where the temperatures of the two radial graphite reflectors were varied together. In each case the temperatures of all the material not of interest, i.e. for the fuel temperature reactivity coefficient, the temperatures of the moderator and reflectors were kept unchanged at the equilibrium core temperatures, while all the temperatures of interest, i.e. the fuel

temperatures in this case, were first reset to 50°C, where after they were increased by a constant difference, i.e. 100°C/step, up to 1850°C.

Conceptually, the fact that an unrealistic flat temperature profile was used for the material of interest may be an important deviation from reality. However, in practice it was found that these coefficients changed minimally when the variation was rather carried out around the realistic equilibrium temperature profile, for the material of interest. Therefore, for the sake of simplicity, the flat temperature profiles were retained.

The moderator temperature reactivity coefficient, and thus the uniform temperature reactivity coefficient, is mainly determined by the up-shift of the Maxwellian thermal neutron spectrum, due to increases in the temperature of the graphite moderator. This up-shift is modelled my means of the selection of the carbon scattering matrices on VSOP 99/05 Card T3, from the Thermos Library (Rütten *et al*, 2007: Table III). The VSOP-A manual, and thus the VSOP-A input models from the pilot study, contained only the carbon scattering matrices with identification numbers 1600 to 1612, representing the Young Phonon spectrum for the temperatures 300 K to 1500 K (Mulder and Teuchert, 2006a: Table IV). This meant that when the graphite temperature was increased above 1500 K, the thermal spectrum up-shift abruptly ceased and thus the magnitude of the moderator temperature reactivity coefficient suddenly fell back to zero. This problem was solved by manually adding the carbon scattering matrix identification numbers 1613 to 1616 to the translated VSOP 99/05 input model. These represent the results for the Brown-St.-John free gas model (Caspers, 1968: 38) for 1650 K to 2200 K. This transition to the Brown-St.-John free gas model caused the bump in the moderator temperature reactivity coefficient and uniform temperature reactivity coefficient charts, visible at 1300°C.

In order to handle the wide variety of fuel temperatures for the calculation of the fuel temperature reactivity coefficient, the following temperatures and Id.-numbers were used for maximum nuclide densities for the finite resonance integral calculations on VSOP 99/05 cards G5, as shown in Table 27. For the minimum densities, the last zero of each Id. number was replaced by “1”.

Table 27: Temperatures for resonance integral calculations for VSOP 99/05

	Id. numbers of finite resonance integral sets (Max. density)		
Temperature (°C)	**^{238}U**	**^{240}Pu**	**^{242}Pu**
20	120020	150020	170020
200	120200	150200	170200
400	120400	150400	170400
600	120600	150600	170600
800	120800	150800	170800
1000	121000	151000	171000
1200	121200	151200	171200
1600	121600	151600	171600
2000	122000	152000	172000

The temperature dependent resonance integrals for these datasets are shown in Figure 19 for the standard 9 g LEU and 3 g Pu(PWR) cases.

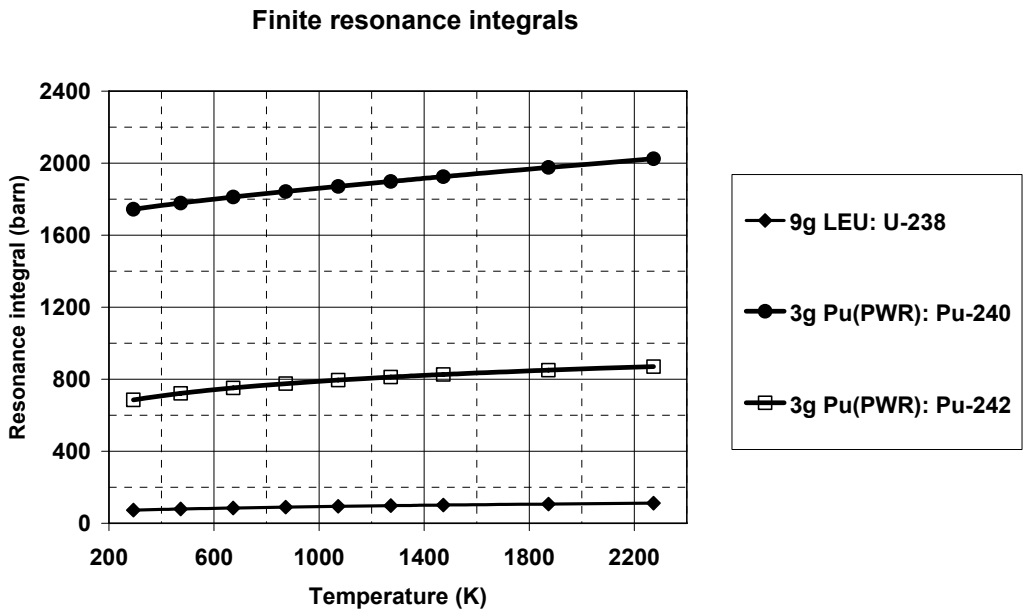

Figure 19: Comparison of the finite resonance integrals for the standard 9 g LEU and 3 g Pu(PWR) fuel spheres.

It should, however, be noted that virtually all the resonance captures in ^{240}Pu takes place in the massive 1.05 eV capture resonance in the thermal broad group. The capture in this

resonance is thus explicitly calculated by the THERMOS code, instead of being corrected in the epithermal or fast windows, on the basis of the resonance integrals.

3.4.1.2 Results for temperature reactivity coefficients

3.4.1.2.1 Verification

Firstly the coefficients for the standard U/Pu(LEU) case were calculated (**Figure 20**) , in order to verify the calculations against published data for the PBMR-400 (**Figure 21** (Reitsma, 2004: Fig. 7)).

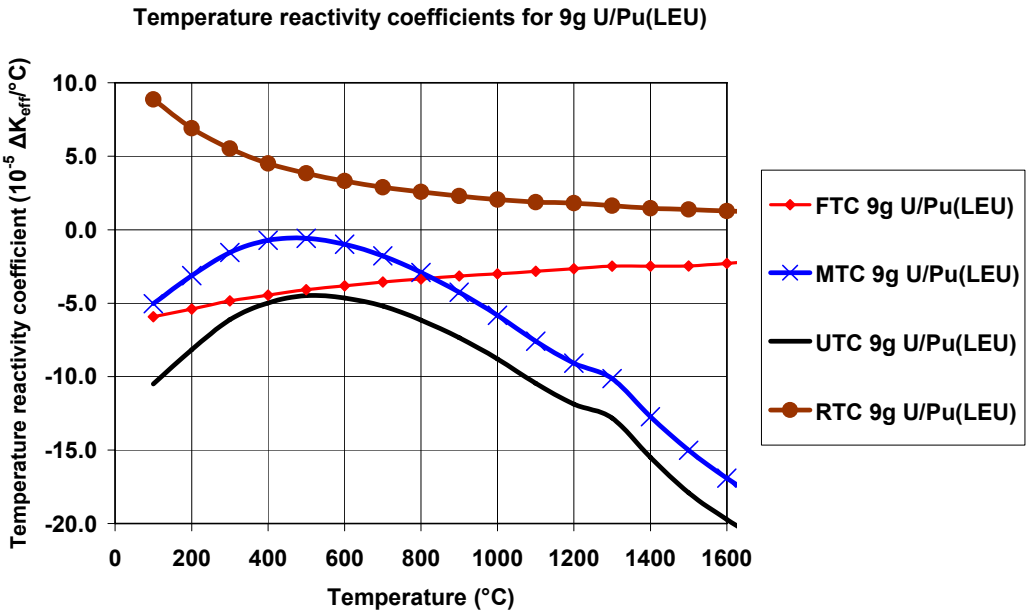

Figure 20: Temperature reactivity coefficient for the standard U/Pu(LEU) case, for verification against Figure 21.

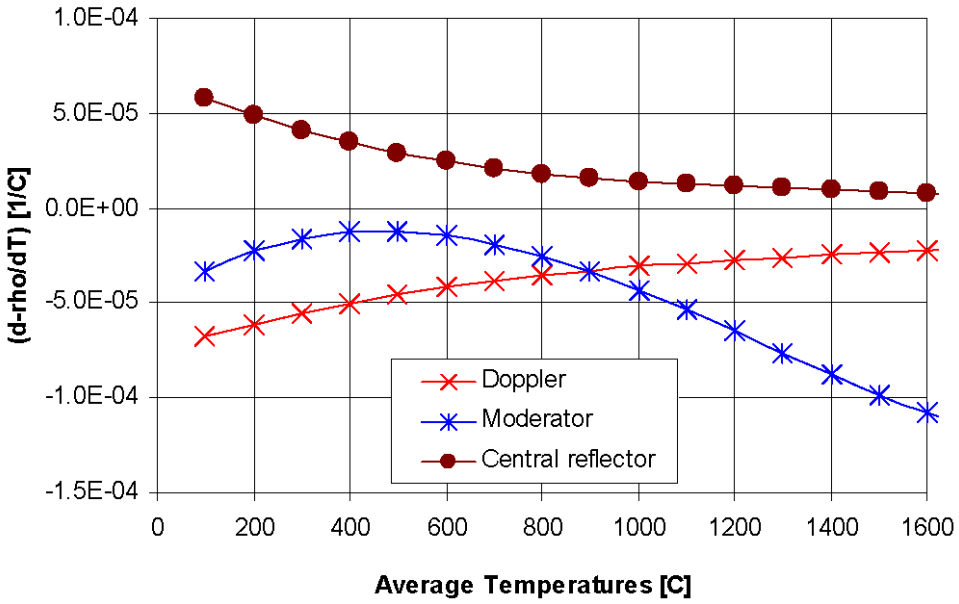

Figure 21: Published temperature reactivity coefficients for the standard U/Pu(LEU) fuel in the PBMR-400.

It is clear from these graphs that the magnitudes of the coefficients differ significantly, for instance at 200°C the:

- calculated reflector temperature reactivity coefficient = 6.9 E-5 Δk_{eff}/°C, compared to about 5.0 E-5 Δk_{eff}/°C for the published data;
- calculated moderator temperature reactivity coefficient = -3.1 E-5 Δk_{eff}/°C, compared to about -2.0 E-5 Δk_{eff}/°C for the published data;
- calculated fuel temperature reactivity coefficient = -5.4 E-5 Δk_{eff}/°C, compared to about -6.5 E-5 Δk_{eff}/°C for the published data.

Possible reasons for these differences may be:

- Reitsma (2004) reported the reflector temperature reactivity coefficient for only the central reflector, while the present results combined both the central and external reflectors.
- Reitsma used an older version of VSOP 99 for the calculation of the published data. As was pointed out above, significant differences in results were published between the various versions of VSOP 99.

- Different epithermal energy windows were used, and the calculation models differed slightly, as was pointed out above.

- No neutron poisons were included in the fuel in the present study.

- It is possible that Reitsma may have varied the temperatures of the materials of interest around the equilibrium temperature distribution, while flat temperature profiles were used in the present study.

3.4.1.2.2 Conclusion on verification

As was pointed out above, a detailed reconciliation between the different codes and models falls outside the scope of the present study. Therefore the purpose of the verification efforts is not to attempt to obtain identical results, but only to guard against errors in the translation of the input models. In spite of the differences between the codes and models, similar, although not identical, results were obtained for the U/Pu(LEU) case. This suggests that probably no significant errors were introduced into the present input models during the translation process and that it is thus safe to proceed to use these same methods for the Pu-cases.

3.4.1.2.3 Comparison of Pu(PWR) to U/Pu(LEU)

The temperature reactivity coefficients for the standard 9 g U/Pu(LEU) and the reference 3 g Pu(PWR) cases are compared in **Figure 22** below.

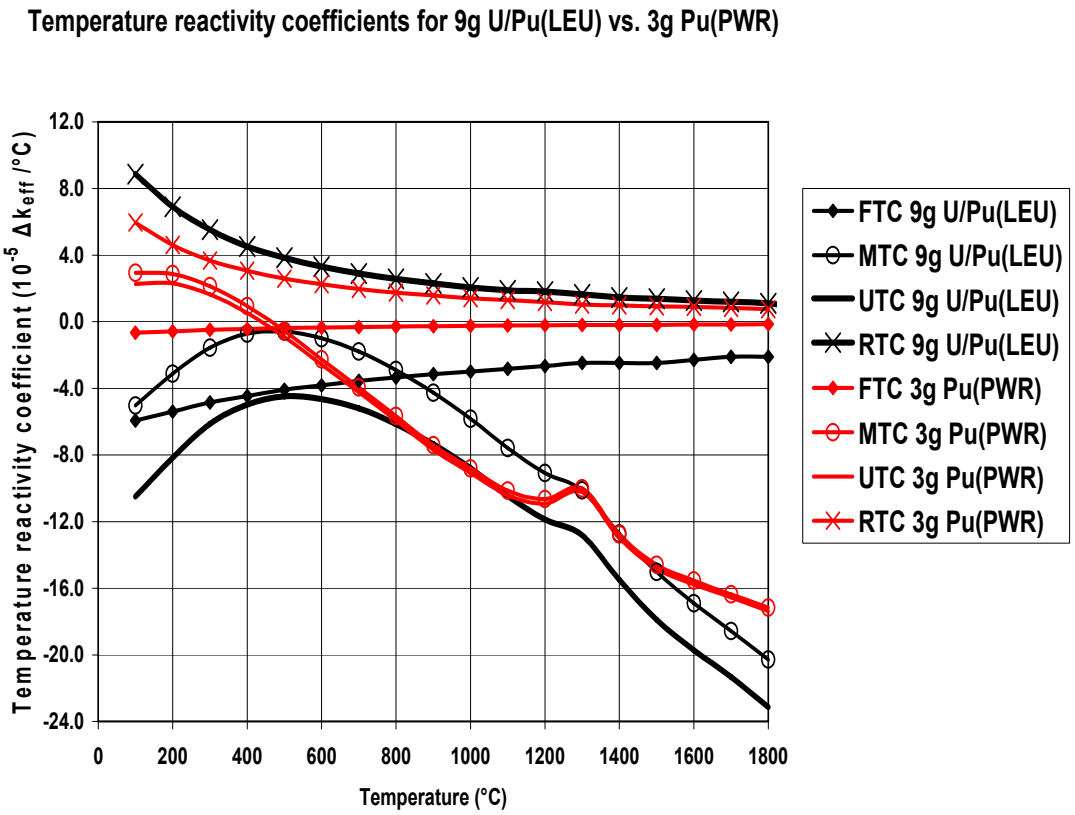

Figure 22: Comparison of temperature reactivity coefficients for 3 g Pu(PWR) to 9 g U/Pu(LEU).

3.4.1.3 Discussion of temperature reactivity coefficients

From **Table 24** and the chart of the temperature reactivity coefficients (**Figure 22**), it is clear that, across the whole temperature range, the uniform temperature reactivity coefficient (UTC) for 3 g Pu(PWR) is greater, i.e. more positive, than for the standard 9 g U/Pu(LEU) fuel cycle. The fact that the UTC for Pu(PWR) is positive below about 450°C is disconcerting. This was partly caused by the positive moderator temperature reactivity coefficient in this range and partly by the fact that the magnitude of the fuel temperature reactivity coefficient, which remained positive across the whole temperature range, was so small, also compared to the U/Pu(LEU) case that its contribution to the uniform temperature reactivity coefficient was virtually negligible and thus it could not significantly offset the positive moderator temperature reactivity coefficient. Probable reasons for this small fuel temperature reactivity coefficient for Pu are:

- The much lower heavy metal loading of 3 g Pu(PWR), compared to 9 g LEU, strongly increased the moderation ratio. This, together with the much lower fraction of fertile nuclides (^{240}Pu and ^{242}Pu), strongly increased the resonance escape probability in the epithermal resonances.

- The fissile enrichment of the core was about an order of magnitude higher for Pu(PWR) than for U/Pu(LEU). While, due to the Doppler effect, increasing temperature for the U/Pu cases mainly caused increased capture in the epithermal capture resonances of the dominant fertile ^{238}U, a large fraction of the epithermal resonances for the Pu(PWR) core were fission resonances in the dominant fissile ^{239}Pu and ^{241}Pu. Therefore the Doppler effect in the Pu case increased epithermal fissions with increasing temperature, so that the increase in fission neutrons assisted in offsetting the increased number of neutron captures in ^{240}Pu and ^{242}Pu.

3.4.1.4 Comparison of uniform temperature reactivity coefficient to results by Boer and Ougouag (2010a and 2010b)

3.4.1.4.1 Methods and results

Boer and Ougouag (2010a) simulated the irradiation of 2 g heavy metal per pebble Pu(PWR) and Pu(PWR) + MA, excluding Am, in a standard PBMR DPP-400 core and obtained maximum average fuel temperatures during normal operation of 1003°C for Pu(PWR) and 1046°C for Pu(PWR) + MA. These corresponded to maximum temperatures for the first pebble pass of 1316°C (Boer and Ougouag, 2010b) and about 1359°C respectively. The maximum DLOFC fuel temperatures were 1682°C and 1769°C for Pu and Pu + MA fuel, respectively. The average discharge burn-up was 702 MWd/kg for Pu(PWR) and 560 MWd/kg for Pu(PWR) + MA, with corresponding average heavy metal discharges of 136 g/d and 287 g/d. Very high maximum fuel temperatures during a DLOFC of 1770°C for the Pu(PWR) fuel and 1682°C for the Pu(PWR) + MA were obtained.

The fuel (i.e. Doppler) temperature reactivity coefficient (FTC_∞) is always negative, but, for Pu pebble fuel, its magnitude is about an order smaller than that of the moderator temperature reactivity coefficient (MTC_∞). (See the discussion below for the definitions of these coefficients.) The MTC_∞ for ^{239}Pu depends mostly on the moderation ratio, which changes with burn-up, and therefore the MTC_∞ may be negative at certain burn-ups and positive at others (Boer and Ougouag, 2010a). However, the positive contribution to the MTC_∞ is limited by the fact that, as the moderator temperature increases, the capture to fission ratio also increases.

For ^{241}Pu, the case is less favourable – as the moderator temperature increases, the capture-to-fission ratio first decreases and then increases above 0.1 eV, as it nears the thermal resonance. This creates a strong positive contribution to the MTC_∞ at low temperatures and a negative one at high temperatures. As burn-up increases and the ^{239}Pu starts to get depleted, the fraction of ^{239}Pu fissions decreases and that of ^{241}Pu increases. Therefore, at high burn-ups and low temperatures, the positive contribution of ^{241}Pu to the MTC_∞ dominates the negative contribution of ^{239}Pu and thus the MTC_∞ becomes slightly positive, as shown in **Figure 23** (Boer and Ougouag, 2010a: Fig. 4).

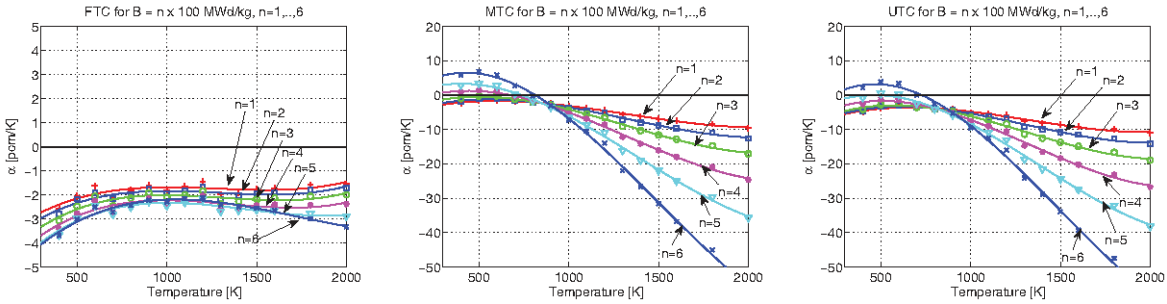

FTC_∞ MTC_∞ UTC_∞

Figure 23: Temperature reactivity coefficients for fuel spheres of different burn-ups, in an infinite cylinder.

The temperatures at which this switch occurred varied between 427°C (700 K) for 400 MWd/kg burn-up and 527°C for 600 MWd/kg. For 600 MWd/kg and below 427°C, even the uniform temperature reactivity coefficient (i.e. the coefficient when the moderator and fuel temperatures are varied by the same ΔT) becomes slightly positive.

Boer and Ougouag invested significant design effort into guaranteeing that the UTC_∞ remains negative at all axial locations in the equilibrium core, over all probable temperatures. This they investigated by obtaining the nuclide compositions of the fuel spheres from the PEBBED code (Gougar *et al*, 2010), as these evolved over the six passes. Then they separated representative individual fuel spheres at different burn-up stages and entered the nuclide composition for each pebble into a 1-D transport code. The transport calculations were performed successively for a TRISO particle, a pebble and a radial slab of the core, for a broad range of temperatures, using SCALE-6. Since this reactor slice had white upper and lower boundaries, it represented an infinite cylinder, filled with this single pebble type. From

these results, they calculated the FTC_∞, MTC_∞ and UTC_∞ for each pebble type. Subsequently they performed realistic calculations where the nuclide mixes of fuel spheres from the six passes were averaged, at representative axial positions. The transport calculations for the TRISO, pebble and radial slab (i.e. infinite cylinder) were then repeated for this mixture, at every axial position. Lastly the UTC_∞, as a function of temperature, was calculated at each axial position. They found that about the lower 75% of the core had a slightly positive UTC_∞, at temperatures below about 400°C, as shown in **Figure 24** (Boer and Ougouag, 2010a: Fig. 5).

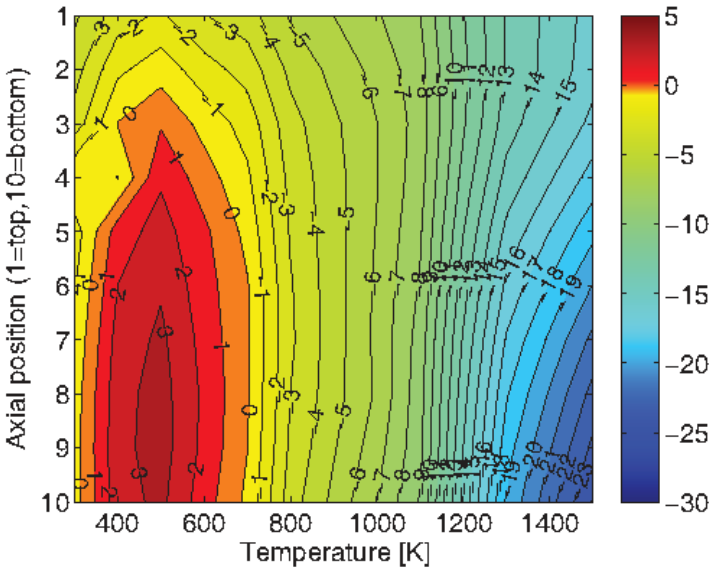

Figure 24: Uniform Temperature Coefficients (UTC_∞) of reactivity in the deep-burn Pu(PWR)-fuelled PBMR DPP-400, as a function of the axial core position and temperature; for the reference case without addition of Er. The core has a positive UTC_∞ at low temperatures, except near the top of the core.

They addressed this challenge by adding 1.5E−6 $(b.cm)^{-1}$ ^{167}Er, which restored the UTC_∞ to negative values for all temperatures and axial positions, but at the price of reducing the average discharge burn-up to 600 MWd/kg. Similar results were found for their Pu+MA fuel.

Boer and Ougouag (2010b) did a follow-up study where they also simulated the tangential stress in the SiC layer of the coated particles, during a DLOFC, but found an unacceptable failure probability of 2.6E-4 for a high burn-up pebble.

They tried to lower the peak in the power density, and thus the fuel temperature, as well as to restore a negative UTC_{∞} over all operating conditions and all axial core heights, by increasing the heavy metal loading to 3 g/pebble and/or by adding ^{167}Er to the fuel kernels. These they employed in a PBMR DPP-400, which had been modified by replacing the central reflector with very low (i.e. 5% of normal) density graphite, in order to remove the peaks in the thermal flux, the power and temperature next to the central reflector (Boer and Ougouag, 2010a). As they pointed out themselves, this is not a realistic solution, since removal of these peaks requires graphite densities below 20% of the normal density, which will present manufacturing challenges. Nonetheless, these interventions delivered improved results in that the low density central reflector completely removed the power and temperature peaks next to this reflector. Increasing the heavy metal density and adding ^{167}Er each managed to make the UTC_{∞} negative over all core conditions. However, increasing the heavy metal loading to 3 g/pebble increased the fast fluence on the coated particles to 8.0E+21 n/cm^2, for which experience with TRISO fuel is unavailable. The addition of ^{167}Er also substantially reduced the burn-up to 600 MWd/kg and thus increased the disloading of heavy metal. They also simulated the same Pu fuels in the Chinese HTR-PM reactor, with its cylindrical core and Rankine cycle. Since this reactor does not have a central reflector, the pebble passes were increased from 6 to 15, and the power reduced from 400 to 250 MW_{th}, the peak power density in the centre was much reduced from 17.2 to 8.1 MW/m^3 and the average discharge burn-up increased slightly to 715 MWd/kg. Adding to this the lower He inlet and outlet temperatures of 250 and 750°C respectively, they, understandably, obtained lower temperatures of 1120°C for the first pebble pass during normal operation and 1764°C maximum fuel temperature during a DLOFC.

3.4.1.4.2 Discussion

Boer and Ougouag stated that the positive UTC_{∞} would be problematic during start-up and shut-down of the reactor. They also aimed to keep the UTC_{∞} negative over all axial positions in the core and over all probable temperatures.

In the present study, results for the uniform temperature reactivity coefficient, calculated over the whole core, were obtained that differed significantly from those of Boer and Ougouag in that, at low temperatures, the uniform temperature reactivity coefficient was positive for all Pu based fuels and configurations that were studied, while Boer and Ougouag reported negative values of UTC_{∞} across the whole core and over all temperatures for a heavy metal loading to 3 g Pu(PWR)/sphere. It should, however, be noted that they obtained these results for a low density central reflector, which was very different from the normal density reflector used in

the present study. Using the results of Boer and Ougouag as the basis for the discussion, another possible view of the role of the UTC_∞ in practical reactor control will now be presented.

It should be borne in mind that the problem with the positive UTC_∞ only occurred at high burn-up and low temperatures. This means that during the low temperatures of the first start-up core, the fuel will be fresh and thus the high burn-up challenge will not be present. This challenge will thus only occur if an equilibrium core is shut down and is then restarted after it has been allowed to cool down for a long time. This case will be discussed in more detail below.

During normal operation, fresh fuel pebbles are loaded at the top, where they experience low temperatures, but due to low burn-ups of the mixture of different pebble passes, the positive UTC_∞ for the average pebble composition will not occur at the top of the reactor, as Boer and Ougouag indeed showed. The positive UTC_∞ is mainly brought on by the large influx of moderated neutrons from the two reflectors, combined with the fast depletion of ^{239}Pu, i.e. the early switch to mainly ^{241}Pu fissions which occurs close to the reflectors. However, the power peaks next to the reflectors also cause rapid temperature increases in the fuel, as the fuel travels down the flow channels. This means that, by the time that the fuel has travelled far enough downwards to have reached a high enough burn-up to have made the switch to predominantly ^{241}Pu fissions, and thus to a positive UTC_∞ at low temperatures, the fuel will have attained high temperatures, at which the positive UTC_∞ would not apply, under the expected operating conditions.

It should further be noted that the scope of applicability of the concept of location dependent UTC_∞ is limited in reactor control. The UTC_∞ is calculated by averaging the nuclide concentration at each axial position and performing 1-D transport calculations of a radial slice at each axial position, with white boundaries at the upper and lower boundaries of each slice. It thus mimics the UTC_∞ for an infinitely elongated reactor, consisting of a cylinder with the radius and nuclide composition of the said radial slice. What was termed the uniform temperature reactivity coefficient (UTC), which is normally defined as $\alpha_{T(Mod+Fuel)} = \frac{d\rho}{dT} = \frac{1}{K_{eff}^2}\frac{dK_{eff}}{dT}$ (Lamarsh and Baratta, 2001: 365), was thus actually calculated by Boer and Ougouag as $\frac{1}{K_\infty^2}\frac{dK_\infty}{dT}$, where K_∞ here indicates the neutron

multiplication factor of the infinite cylinder, filled with the material composition of the said radial slice of the reactor at a specific axial position. It is because of this difference in definitions that, for the sake of clarity in this discussion in the present thesis, it was decided to call the concepts that Boer and Ougouag called the FTC, MTC and UTC, the FTC_∞, MTC_∞ and UTC_∞. In order to remove any possibility of confusion, these temperature reactivity coefficients, when they were calculated over the whole finite reactor core, as defined above by Lamarsh, will here be referred to as FTC_c, MTC_c and UTC_c., where the "c" represents "core".

This is an important distinction, due to the fact that, while K_∞ and the UTC_∞ are valuable tools to study the properties of the fuel at different locations and burn-ups in a reactor, they are not always appropriate with respect to the control of a whole reactor, since the behaviour of the whole reactor is determined by k_{eff} and the UTC_c. This statement is based on the view that no matter how high K_∞ may be at a specific location in a reactor, if k_{eff} for the whole reactor is < 1.0, the whole reactor will be subcritical and the average neutron flux and power in the reactor will decrease with time and a power excursion will thus not be possible. Similarly, no matter how strongly positive the UTC_∞ may be at specific locations in a reactor, as long as the UTC for the total reactor remains negative, k_{eff} will decrease with increasing temperature, and thus increasing temperature will not cause a reactivity excursion.

The most probable scenario where the low temperatures and high burn-ups, and thus positive UTC_∞ for the lower 75% of the core, can be expected to occur, is the restart of an equilibrium core, after it has been allowed to cool down to these low temperatures. It should firstly be noted that this will take a long time, i.e. more than a week, for the core to cool down to these low temperatures. A short reactor shut-down for only a few days, for instance to do maintenance to the turbines, will thus not induce enough cooling to induce the low temperature challenge. If, however, the reactor is shut down for a long time, provided that the UTC_c remains negative, the main effect of an increasing temperature, combined with the UTC_∞-profile reported by Boer and Ougouag, will be to suppress the flux and power at locations with a negative UTC_∞ and to elevate it at locations with a positive UTC_∞, i.e. to suppress the power at the top of the reactor, where the axial power profile normally peaks, and to elevate it at the bottom, where it is normally very low. The UTC_∞ profile will thus assist in flattening the axial power profile, which is desirable. Figure 24 may seem to suggest that, since 75% of the core has a positive UTC_∞, the UTC_c may also be positive. It should, however, be kept in mind that the ^{135}Xe, which makes a substantial positive contribution to

the MTC_c, will have decayed by then, which might be enough to restore negative UTC_∞ to the whole core. Since the reactivity in this restart core will also be very high, due to the absence of ^{135}Xe, the ^{10}B control rods will have to be inserted significantly during the restart. While the presence of ^{10}B normally contributes positively to the MTC_c, it will also strongly reduce the thermal neutron flux in the external reflector. Since the influx of these neutrons is a main cause of the positive UTC_∞ next to the reflectors, the insertion of the control rods may, in this case, even help to restore a negative UTC.

Regarding the UTC_∞ of the individual pebble passes (**Figure 23**) in the pebble mixture, the following analysis applies:

Regarding the MTC_∞, it should be remembered that it takes many collisions to bring the neutrons into thermal equilibrium with the graphite moderator. Therefore the temperature of the Maxwellian neutron spectrum is not determined mainly by the temperature of the considered fuel pebble, but rather by the temperature of the moderator in the area surrounding this pebble, especially the reflectors. This fact brings a significant safety benefit. The reason why positive reactivity coefficients are justly feared, is that they normally cause any aberration which triggers a reactivity excursion to amplify itself in a vicious spiral, as happened with the steam bubble and the positive void reactivity coefficient at Chernobyl.

However, in the present case, the mechanism is different. The FTC_∞ for a specific fuel pebble is largely determined by the resonance escape probability, which decreases with increasing temperature, due to Doppler broadening of the capture resonances. Since neutrons, depending on the graphite and fuel properties, on average travel about half a meter from the place where they were born to the place where they are finally moderated, a specific pebble cannot contribute significantly to the moderation of the thermal neutrons that will be the main source of fissions in that specific pebble. The FTC_∞ for a specific pebble will thus be determined by the temperature and nuclide composition of the fuel and moderator in a sphere with a radius of roughly half a meter surrounding that pebble.

Similarly, the MTC_∞ of a specific pebble is determined by a combination of its own nuclide composition (where the increasing ratio of ^{241}Pu to ^{239}Pu is the main controlling factor in Pu(PWR) fuel), together with the temperature of the thermal neutron spectrum in this pebble. By the same reasoning as above, any single pebble cannot significantly contribute to the temperature of the neutron spectrum in it, since this is rather determined by the temperature

of the larger graphite zone surrounding this pebble. The temperature in the reflectors is especially important, since they are the main moderating agents in the PBMR DPP-400 core.

This means if a local temperature increase occurs in a specific pebble with a positive MTC_∞ and UTC_∞, as will be the case for a high burn-up pebble at low temperatures at the top of the core, since this pebble does not contribute significantly to the thermalisation of the thermal neutrons that enters it, its own rise in temperature will not lead to a significant rise in the temperature of the thermal neutron spectrum that enters it, and thus its positive MTC_∞ and UTC_∞ will not be able to amplify this temperature excursion in this pebble. Such amplification can only come from the collective contributions of the large number of pebbles, and the reflectors, surrounding this pebble. However, since these pebbles will consist of a mixture of the burn-ups for the six passes, they will, on average have a negative UTC_∞, as was shown in Figure 24 above. The original temperature excursion will thus cause the surrounding pebbles to capture more neutrons and produce less fissions and thus less power, which will then halt this local temperature excursion.

If a core design and fuel cycle that have a negative UTC_c are implemented, the total effect of an increase in temperature will be a reduction in power and neutron flux, which will eventually feed back to the original pebble of interest and will thus limit its temperature increase too. The positive UTC_∞ in a specific pebble will thus be countered by the, on average, negative UTC_∞ of the pebbles that surround it, and thus a single pebble, or by the same reasoning, a small cluster of pebbles with positive UTC_∞, will not cause a self-amplifying reactivity, power or temperature excursion.

3.4.1.4.3 Conclusion

Therefore, in the present study, the requirement of a negative reactivity coefficient, across all probable temperatures, will be imposed on the UTC_c for the whole core, rather than on the UTC_∞ at certain locations or for certain pebbles or certain temperature regions. However, since positive values for the UTC_c were in fact obtained in the present study, further attempts to restore negative UTC_c over all relevant temperatures will now be presented. Since the comparison to the results of Boer and Ougouag ends here, the UTC_c will now again be referred to as the UTC only, etc.

3.4.2 Optimisation of the uniform temperature reactivity coefficient

From **Figure 22**, it was clear that in the 3 g Pu(PWR) case, the contribution of the fuel temperature reactivity coefficient to the uniform temperature reactivity coefficient was virtually negligible. It would also be easier to interpret the data when a single phenomenon is studied. Therefore optimisation of the uniform temperature reactivity coefficient for the Pu(PWR) cases was replaced with optimisation of the moderator temperature reactivity coefficient.

3.4.2.1 Theoretical considerations

During the pilot study for the present work, Mulder *et al* (2008: Table 8) found an increase in k_{eff} of +0.0232 when the temperature of the reactor-grade Pu-fuelled PBMR DPP-400 was increased from 50°C to the full power equilibrium temperature distribution which has an average of just over 800°C. Such positive temperature reactivity coefficients for Pu(PWR) may pose serious licensing challenges since positive temperature coefficients are generally forbidden by nuclear regulations. The source of this problem and possible solutions will be discussed in more detail in the exposition of the results of the present study. The source of this problem can be seen from the first fission resonance for ^{239}Pu shown in Figure 25.

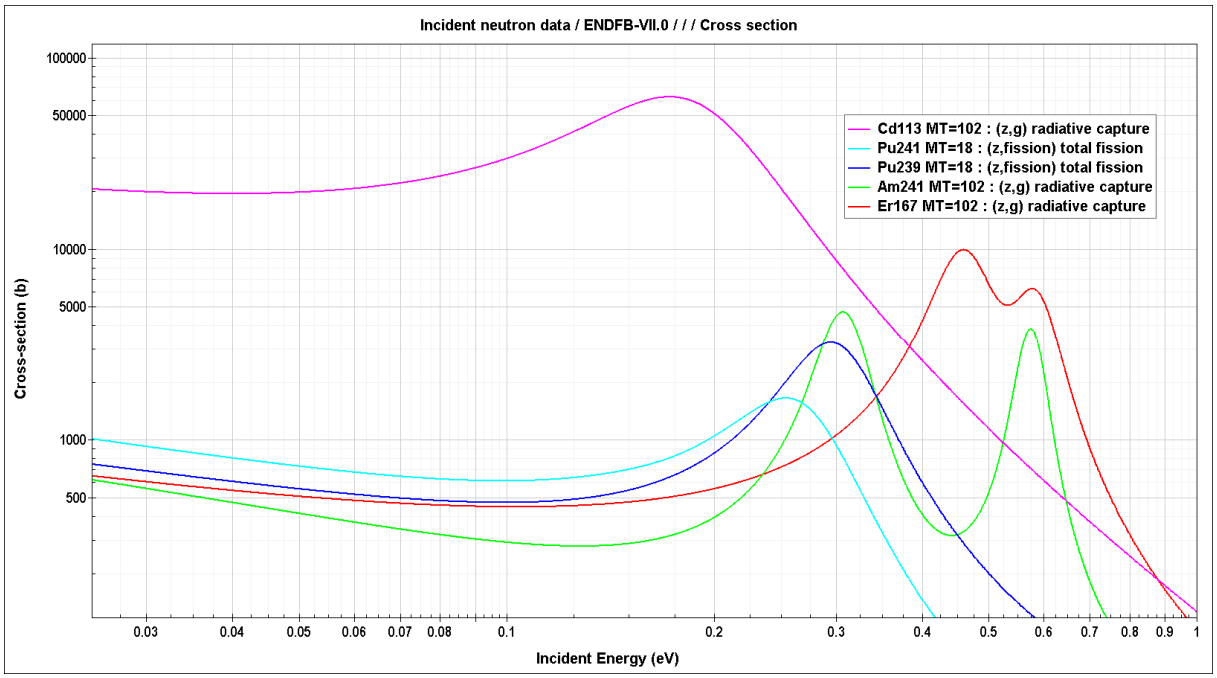

Figure 25: Thermal (0.25 to 1.0 eV) fission resonances for ^{239}Pu and ^{241}Pu and σ_γ for the neutron capturers with thermal capture resonances. (ENDFB 7.0 from JANIS.)

At low temperatures, where the uniform temperature reactivity coefficient is positive for Pu(PWR), for instance at 100°C, the peak of the Maxwellian thermal neutron spectrum will lie

at 0.016 eV and the average energy at 0.048 eV and thus only a small part of the high energy tail of the thermalised neutron spectrum will reach the strong fission resonances of ^{239}Pu and ^{241}Pu at 0.293 eV and 0.253 eV, respectively. As the temperature increases, absorption, both in the fission and associated capture resonances of ^{239}Pu and ^{241}Pu, will increase strongly. This competition will reduce neutron capture in ^{135}Xe, which will increase k_{eff}, and will thus make a positive contribution to the temperature reactivity coefficient. The precise evolution of k_{eff} with temperature will also depend on the capture-to-fission ratio in these resonances, which is higher for ^{239}Pu than for ^{241}Pu and which changes with temperature. It is clear that this up-shift in the tail of the thermal spectrum will not to a substantial degree reach the very strong capture resonance of ^{240}PU at 1.05 eV and thus this capture resonance will not be able to cancel the effect of these fission resonances. If, however, an isotope with a capture resonance that overlaps with these fission resonances, or even better lies slightly below them, could be added to the fuel, it would assist to counter this reactivity problem. The parasitic absorber, erbium-167, also shown in Figure 25, has two strong radiative capture resonances with peaks at 0.46 to 0.58 eV and is therefore often used as a burnable poison in reactor simulations. Unfortunately, these resonances are situated far above the fission resonances of ^{239}Pu and ^{241}Pu. The part of the high energy tail of the thermal neutron spectrum that will push up into the first of these two capture resonances will thus be much smaller than at these fission resonances. Therefore these capture resonances will be less effective at countering the positive contribution to the temperature reactivity coefficient from the fission resonances, compared to a poison with a thermal capture resonance at a lower energy. Nonetheless, the thermal capture cross-section of ^{167}Er seems more favourable than that of ^{151}Eu: while their thermal capture resonances are similar (Tran and Kato, 2009: Fig. 1), the capture cross-section of ^{151}Eu below 0.1 eV is about an order of magnitude larger than that of ^{167}Er, and decreases strongly with increasing energy, compared to a much flatter curve for ^{167}Er. This means that ^{151}Eu will probably display stronger 1/v behaviour at low temperatures, i.e. the capture rate will be independent of temperature, compared to ^{167}Er where the flat capture cross-section curve will cause increasing absorption with increasing temperature, meaning that ^{167}Er will start to combat the positive moderator temperature reactivity coefficient, even at low temperatures, well before the tail of the Maxwell spectrum strongly pushes into the capture resonance. In Par. 3.4.1.4 above, where the results of Boer and Ougouag were summarised, success was reported with using ^{167}Er to restore a negative UTC_{∞} across the whole core, although that was achieved in a PBMR-400 with a low density central reflector and the addition of ^{167}Er significantly reduced the burn-up. While gadolinium does not have a thermal capture resonance, it is a burnable poison that can be used to restore a negative fuel temperature reactivity coefficient (Somers, 2007: 12), probably due to the Doppler effect in its epithermal

capture resonances. ^{113}Cd, on the other hand, does have a very strong capture resonance at 0.172 eV, which falls between the peak and average of the thermal neutron spectrum. This resonance will thus strongly absorb the high energy tail of the thermal spectrum and may thus, theoretically, be valuable in countering the effects of the two fission resonances.

Kloosterman (2003) simulated the use of boron and gadolinium burnable poison particles in UO_2 and PUO_2 fuels in to successfully control reactivity swings in HTRs. Tran and Kato (2009) simulated a number of burnable poisons, including natural CdO, to flatten the axial power profile for OTTO-cycle HTRs. Unfortunately, they found that, since σ_γ is so large and ^{113}Cd comprises only 12% of natural cadmium, the ^{113}Cd in "small" (2 mm diameter) kernels burnt away almost completely at burn-ups of as little as 60 MWd/kg$_{HM}$. Therefore they also added large (3.8 mm diameter) kernels in order to control to reactivity swings up to larger burn-ups and found that they could control the swing in k_∞ to about 4%, over a burn-up range of 0 to 100 MWd/t$_{HM}$. This burn-up range, however, is much smaller than the 0 to 700 MWd/t$_{HM}$ required for the incineration of pure Pu(PWR). They also pointed out that larger kernels are advantageous with respect to the manufacturing process. It might therefore be possible to experiment with even larger CdO kernels, in order to cover the required burn-up range for Pu(PWR). Unfortunately, the need for large CdO kernels means that it would not be possible to insert the CdO into the Pu fuel kernels. Tran and Kato concluded that they obtained the best results with Gd_2O_3, since the ^{155}Gd and ^{157}Gd burned away slower than ^{113}Cd, allowing a reduction in the swing in k_∞ with burn-up to 2.5%, using a single kernel diameter of 1.9 mm. However, since ^{155}Gd and ^{157}Gd do not have any thermal capture resonances, they will not be useful for manipulating the thermal spectrum, in order to counter the thermal fission resonances of ^{239}Pu and especially ^{241}Pu. ^{237}NP has a capture resonance at 0.488 eV, which lies even higher than the capture resonance of ^{167}Er and will therefore not be suitable to counter the reactivity increases in the fission resonances of ^{239}Pu and ^{241}Pu. However, since the neutron captures in ^{237}Np will cause β^--decay to the fertile ^{238}PU, which is valuable for increasing the proliferation resistance of the Pu-mixture in the spent fuel, as has been shown above, adding ^{237}NP to the fresh fuel will be investigated below as a possible way to get rid of the ^{237}Np, which carries a significant proliferation risk, while simultaneously increasing the proliferation resistance of the spent fuel through increasing the ^{238}Pu content.

The first capture resonance of ^{241}Am at 0.305 eV appears promising, because it significantly overlaps with the fission resonance of ^{239}Pu and therefore may help to counter its effect on the temperature reactivity coefficient. The option of letting a substantial part of the ^{241}Pu β^--decay to ^{241}Am before inserting the fuel into the reactor will thus be investigated as a means

of countering the positive moderator temperature reactivity coefficient. Not only may the capture resonance of ^{241}Am absorb a significant part of the high energy thermal tail, but the loss of ^{241}Pu will also reduce the ^{241}Pu/^{239}Pu ratio in the fresh fuel. Since it is the increase in ^{241}Pu fissions, with increasing temperature at low temperature, which causes the positive moderator temperature reactivity coefficient, a reduction in the available ^{241}Pu may also help to reduce this problem. As has been pointed out above, the transmutation of this ^{241}Am will also increase the proliferation resistance by producing ^{238}Pu. For these reasons, decay of ^{241}Pu to ^{241}Am, rather than the addition of the parasitic absorber ^{167}Er, will be used to attempt to restore a negative uniform temperature reactivity coefficient at low temperatures.

Of course the positive temperature coefficient due to the thermal fissioning resonance of ^{239}Pu and ^{241}Pu does not only have to be countered in the thermal energy region, but can also be countered by the Doppler effect in the epithermal resonances of fertile isotopes like ^{232}Th or ^{238}U. Since adding ^{232}Th to the Pu for this purpose is the subject of a Master's degree study which is currently also being conducted at the Postgraduate School of Nuclear Science and Engineering at the NWU, this option will not be investigated in the present study.

3.4.2.2 Simulation parameters and fuel compositions

3.4.2.2.1 Standard cases

In order to gain a better understanding of the phenomenon of the positive uniform temperature reactivity coefficient at low temperatures, the uniform temperature reactivity coefficient was calculated for all the pure Pu(PWR) cases reported in **Table 24**, according to the method described in that section. The standard cases, i.e. 3 g Pu(PWR), 2 g Pu(PWR), 1 g Pu(PWR), 3 g Pu(PWR)+MA, 3 g Pu(WGR) were thus calculated. The 3 g Pu(PWR) case served as the reference case.

In an effort to restore a positive uniform temperature reactivity coefficient at low temperatures, the following optimisation cases were added, and all the cases are displayed in **Figure 26**.

3.4.2.2.2 Decay of ^{241}Pu to ^{241}Am

As motivated above in the theoretical considerations, an attempt was made to use the thermal capture resonances of ^{241}Am to counter the positive uniform temperature reactivity coefficient, caused by the thermal fission resonances of ^{239}Pu and, especially, ^{241}Pu. This was done by using the standard 3 g Pu(PWR) fuel spheres, but simulating enough delay (i.e. just less than half of the half-life) after chemical separation of the Pu(PWR) for 25% of the

^{241}Pu to decay to ^{241}Am, at which point the fuel entered the reactor. This fuel type is indicated by the acronym "**UTC 3g PU(PWR) - 25% decay**".

The 3 g Pu(PWR)+MA had the smallest positive uniform temperature reactivity coefficient in **Table 24**, and would seem like the best candidate to use as the basis from which to optimise towards a positive uniform temperature reactivity coefficient. However, this fuel type was excluded from the experiment with the decay of ^{241}Pu: the Pu(PWR)+MA case already produced a disappointing reduction in burn-up and associated increase in heavy metal to be discarded in the spent fuel, as reported above. Since allowing a substantial fraction of its ^{241}Pu to decay to ^{241}Am, would only worsen this problem, this option was not explored for this case.

3.4.2.2.3 Low density kernels

Based on the warning by Jonnet, Kloosterman and Boer (2010), discussed above, that significant coated particle failure might occur at very high burn-ups for pure Pu(PWR), their recommendation to use diluted kernels was explored. While they proposed 500 μm diameter kernels, consisting of 10% Pu diluted in inert matrix materials, a simplified version of this proposed kernel was simulated here. The standard 240 μm diameter PuO_2 kernel was diluted to 500 μm by simply reducing its density accordingly, without adding any inert matrix material. While this is not physically realistic, it was simply used as a first attempt to gain an understanding of the potential effect of dilution of the fuel kernels, with a view to conducting more realistic simulations in a follow-up study.

When the larger coated particles were inserted into the standard 3 g/pebble shell-ball for this study, i.e. when the same number of coated particles were retained, the increased volume of the diluted coated particles, increased the packing fraction to 46%. Realising that such a packing fraction would be unrealistically high, since it would cause many coated particles to press against each other and thus crack, the packing fraction was reduced by two thirds, in order to obtain a 1 g/pebble, low density, Pu(PWR) fuel sphere, indicated by the acronym "**UTC 1g Pu(PWR) Low Density**".

3.4.2.2.4 Results

The uniform temperature reactivity coefficients for all the Pu fuel compositions investigated are shown in **Figure 26** as a function of temperature. In order to better focus on the area where the positive uniform temperature reactivity coefficient occurs only the temperatures up to 1100 ° are shown.

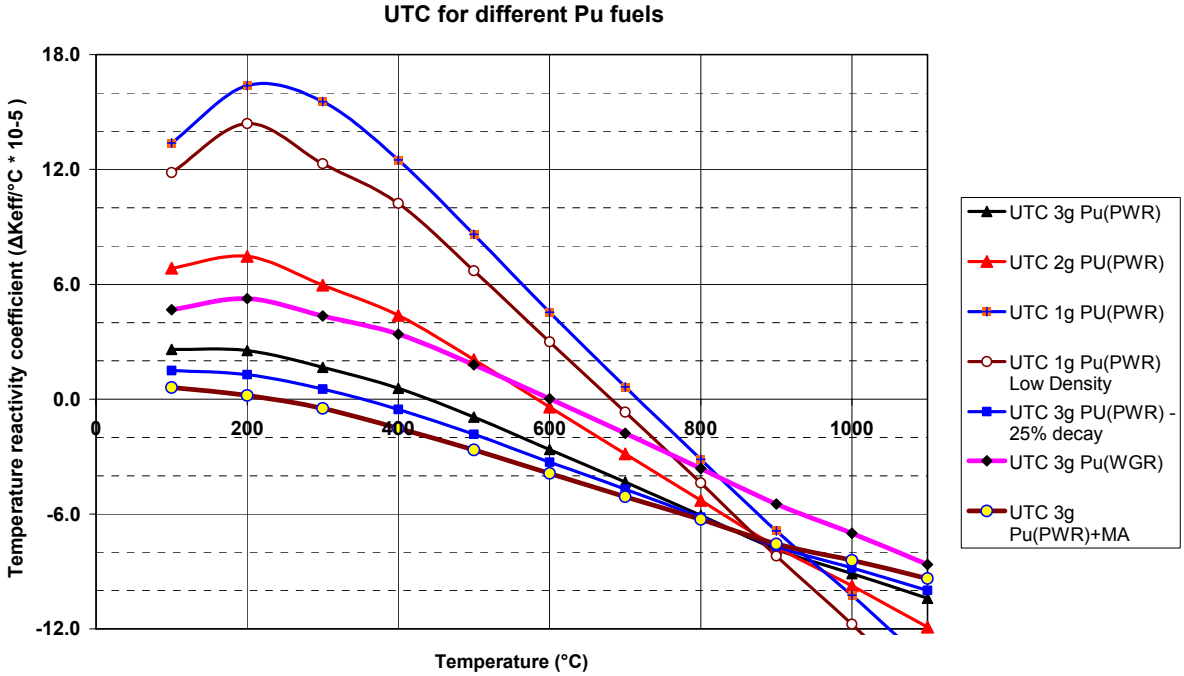

Figure 26: Uniform temperature reactivity coefficient (UTC) for all the Pu fuel compositions, as function of temperature.

3.4.2.2.5 Discussion

From this chart, the following trends are clear:

1. The magnitude of the positive uniform temperature reactivity coefficient at low temperatures increased strongly with decreasing Pu(PWR) heavy metal loadings, which is the reason why the 1 g Pu(PWR) fared the worst.

2. The magnitude of the positive uniform temperature reactivity coefficient decreased strongly with increasing fractions of the fertile Pu isotopes, i.e. ^{240}Pu and ^{242}Pu. Therefore 3 g Pu(PWR) had a lower uniform temperature reactivity coefficient than Pu(WGR) and Pu(PWR)+MA fared the best and almost achieved a zero uniform

temperature reactivity coefficient at low temperatures. From **Table 24**, above, it was clear that the price for this reduction in the uniform temperature reactivity coefficient is a large reduction in the burn-up and thus a strong increase in the radiotoxic heavy metal in the spent fuel to be discarded.

3. Most disappointing was the **3 g PU(PWR) - 25% decay of ^{241}Pu** case: this decay strongly reduced the burn-up from 601 to 473.6 MWd/kg$_{HM}$, yet it only reduced the maximum positive uniform temperature reactivity coefficient from +2.6 to +1.5 Δk_{eff}/°C * 10^{-5}. The reason for this failure will be investigated in the next section.

   It should further be kept in mind that VSOP expresses burn-up only as per kg Pu$_{HM}$. Thus the 25% ^{241}Pu that decayed to ^{241}Am is excluded from this number. If the total energy produced per sphere were to be compared to the pure Pu(PWR) case, the 25% decay case would thus fare another 25% worse than its burn-up figure suggests. This is therefore clearly an inefficient way to reduce the uniform temperature reactivity coefficient.

   If the Pu(PWR) is stored for a substantial time before being irradiated in the reactor, this undesirable decay will occur unintentionally: from the half-life of 14.29 years for ^{241}Pu, it follows that 25% will decay in less than 7.15 years. In order to avoid the consequential reduction in burn-up, the time between chemical separation of the Pu and the onset of irradiation will thus have to be reduced to substantially less than this period. For separated Pu(PWR) mixtures that have already been stored for a long time, reseparation shortly before irradiation will thus be advisable. This can be expected to complicate logistics and increase cost.

4. The dilution of the kernel somewhat reduced the positive uniform temperature reactivity coefficient, compared to the normal density 1 g Pu(PWR) case. However, it still fared much worse than the standard 2 g Pu(PWR) case, and thus the dilution of the kernel cannot be seen as the most efficient way of reducing the uniform temperature reactivity coefficient.

   Encouraging was the fact that the dilution of the kernel increased the burn-up significantly from 656.6 to 682.9 MWd/kg and strongly reduced the maximum power/sphere from 6.49 to 5.45 kW/sphere and the maximum fuel temperature from 1173 to 1105°C, which is the lowest of all the Pu fuel types and also falls below the design target of 1130°C.

The reason for this improvement is not obvious. All the neutronic parameters appeared somewhat better for the low density kernels. However, the one factor that stood out is the reduction in neutron leakage from 15.53% to 14.16%. The reason for this is probably the following: from **Table 24** it can be seen that the neutron leakage spiked from 11.8% to 15.5%, from the 2 g to the 1 g cases for the standard Pu(PWR) kernel. The obvious explanation is that since the packing fraction halved from 2 g to 1 g, the fuel became much more transparent to the neutrons and thus more of them escaped absorption in the resonances and passed straight through the fuel into the reflectors. There they were moderated and thus many were captured in the reflector graphite, due to the increased capture cross-sections at thermal energies. This scenario is also reflected in the fact that the average thermal flux for the 1 g case is approximately double that of the 2 g case. With the switch to the diluted kernels, the number of kernels remained the same, but since they became much larger, the lumping decreased and thus the resonance escape probability decreased. This caused an increase in the fissions in the epithermal fission resonances, which improved the production of fission neutrons. The decreased resonance escape probability also reduced leakage into the reflectors.

While 1 g/pebble is obviously too low, these results are encouraging in that it seems certain that if the heavy metal loading with the diluted kernels can be increased to, for instance, 2 g/pebble, the neutronic parameters might improve significantly.

3.4.2.3 Investigation into mechanism of the positive uniform temperature reactivity coefficient

An investigation was performed in order to determine the mechanisms the different phases uniform temperature reactivity coefficient chart for Pu(PWR), i.e.:

1. the positive uniform temperature reactivity coefficient at low temperatures,

2. the negative uniform temperature reactivity coefficient at intermediate temperatures.

3.4.2.3.1 Method

Since the fuel temperature reactivity coefficient for Pu(PWR) is virtually negligible and since it would be easier to interpret the data if a single phenomenon was studied, the moderator temperature reactivity coefficient was used as proxy for the uniform temperature reactivity coefficient. Since the chart for the uniform temperature reactivity coefficient for the 1 g

Pu(PWR) case (**Figure 26**) displayed these characteristics the clearest, this case was selected for investigation.

The temperatures of the moderators in the reflectors were kept constant at 50°C. The temperature of the graphite moderator in the fuel was first reduced to 100°C and was then raised in increments of 100°C, up to 1600°C.

3.4.2.3.2 Results

The main components of the neutron balance are shown in **Figure 27**. Since only the changes in these parameters will affect changes in k_{eff}, and thus the moderator temperature reactivity coefficient, the parameters for the whole core were used as proxy for the parameters that were directly affected by the changes in the moderator temperature in the fuel: these included the fast and epithermal fissions that are independent of the variations of the moderator temperature in the fuel and were thus assumed to remain constant.

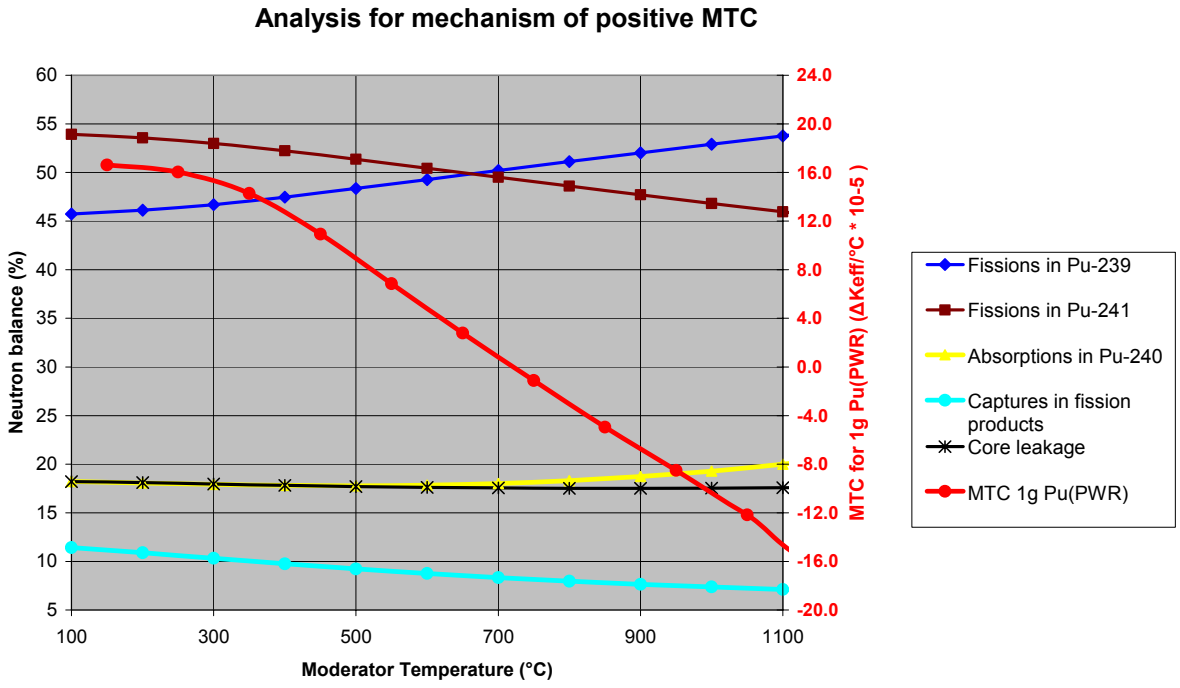

Figure 27: The relevant components of the neutron balance for the analysis of the mechanism of the variations in the moderator temperature reactivity coefficient for the 1 g Pu(PWR) case, with the moderator temperature reactivity coefficient displayed as reference on the separate axis on the right.

3.4.2.3.3 Discussion and conclusion

1. **Positive moderator temperature reactivity coefficient below 700°C**: From the chart it is clear that below about 650°C ^{241}Pu fissions substantially dominated ^{239}Pu fissions. Boer and Ougouag, as quoted above, pointed out that at low temperatures ^{241}Pu has a positive moderator temperature reactivity coefficient. This is because the fission resonance first rises faster than the capture resonance, with increasing neutron energy, and thus a rise in temperature reduces the capture-to-fission ratio, up to the point where the capture resonance starts to rise faster than the fission resonance and this phenomenon then reverses. ^{239}Pu, in the absence of other nuclides, has a negative moderator temperature reactivity coefficient at all temperatures. However, since ^{241}Pu fissions dominate at low temperatures, the total moderator temperature reactivity coefficient is positive at these temperatures.

   Furthermore the rise in temperature caused a significant reduction in the capture in the fission products, which also contributed to the positive moderator temperature reactivity coefficient.

2. **Negative moderator temperature reactivity coefficient above 700°C**, where the magnitude increased with temperature, was caused by the following three phenomena:

   a. ^{239}Pu fissions, which inherently contribute to a negative moderator temperature reactivity coefficient, increasingly dominated ^{241}Pu fissions.

   b. Captures in the fission products started to bottom out, and thus the decrease in captures with rising temperature slowed down, thereby reducing the contribution of this driver of a positive moderator temperature reactivity coefficient.

   c. Captures in ^{240}Pu started to rise significantly with temperature, which contributed to a negative moderator temperature reactivity coefficient.

Failure of decay of ^{241}Pu to ^{241}Am to restore negative uniform temperature reactivity coefficient

These results also explain the failure of the attempt to restore a negative uniform temperature reactivity coefficient at low temperatures by first allowing a significant fraction of the ^{241}Pu to decay to ^{241}Am, reported above:

1. Since the first thermal capture resonance of ^{241}Am overlaps significantly with the fission resonance of ^{239}Pu (Figure 25), and actually peaks slightly above that of ^{239}Pu, increased capture in ^{241}Am will coincide with the upper temperature range where ^{239}Pu fissions dominate ^{241}Pu fissions (**Figure 27**), i.e. the range above about 900°C. Therefore the contribution of captures in ^{241}Am at the low temperatures will be too small to counter the positive moderator temperature reactivity coefficient provided by ^{241}Pu fissions in this range.

2. Since the ^{241}Am capture resonance overlaps with the ^{239}Pu fission resonance and therefore lies significantly above the ^{241}Pu resonance, captures in ^{241}Am will significantly compete with and thus reduce fissions in ^{239}Pu, but will cause a much smaller reduction in ^{241}Pu fissions. Therefore the presence of the ^{241}Am may actually increase the ^{241}Pu to ^{239}Pu fission ratio, especially at higher temperatures. Since ^{241}Pu fissions contribute to a positive and ^{239}Pu fissions to a negative moderator temperature reactivity coefficient, this increase in the dominance of ^{241}Pu fissions may actually be counter-productive. This was actually observed in **Figure 26** where the ^{241}Am made the uniform temperature reactivity coefficient more positive at higher temperatures.

3.4.2.4 Conclusion on optimisation of the uniform temperature reactivity coefficient

- It is clear that efforts to restore a negative uniform temperature reactivity coefficient by adding a neutron capturer with a thermal capture resonance, i.e. ^{241}Am, to the fuel were inefficient, mainly because its capture resonance peaked at too high an energy and thus competed with ^{239}Pu, rather than with ^{241}Pu, fissions.

- Since none of the other capturers investigated had thermal capture resonances that were better positioned, it is concluded that trying to restore a negative uniform temperature reactivity coefficient by interventions in the thermal energy region is not the best option.

- Adding capturers with strong epithermal capture resonances will make the fuel temperature reactivity coefficient more negative, due to the Doppler effect, which may solve the problem. If these captures add no value to the neutron economy, as will be the case for parasitic absorbers like ^{167}Er, the price in terms of a reduced burn-up will probably be unacceptably high. If, however, epithermal captures in ^{232}Th were to be used to supply the negative uniform temperature reactivity coefficient, ^{233}U will be produced. Fissions of ^{233}U will make a valuable contribution to the neutron economy of the reactor, which will help to counter the neutron losses in ^{232}Th. Thus the burn-up

of the Pu will not be reduced so strongly. More detailed proposals for the redesign of the reactor and fuel cycle will be given in the final conclusions of this thesis below.

- The performance of the diluted fuel kernels was encouraging. However, this dilution with inert materials to 10% heavy metal will significantly limit the maximum heavy metal loading that can be achieved. Reducing the Pu loading to 1 g/pebble, as was done for the present case, may reduce the total energy that can be obtained from a pebble to the extent that it may significantly limit the fuel economics. Therefore a techno-economic optimisation of the dilution fraction and the packing fraction is advisable.

3.4.3 Power and temperature peaks

Since for all the Pu fuel cycles investigated, either the maximum power density or the maximum fuel temperature exceeded the adopted safety limits, the following investigation was executed in order to establish the cause of these extreme peaks, in order to propose solutions.

3.4.3.1 Method

From the THERMIX output for the reference 9 g U/Pu(LEU) and the 3 g Pu(PWR) cases, the hottest fuel temperatures, i.e. the temperatures in the centre of the spheres for the first pebble pass, as well as the He coolant temperatures, were selected. The average power densities for the mixtures of all six passes were also obtained from the POWFORM output files for these cases. The temperature and power peaks were investigated by plotting the axial and radial profiles, for the relevant parameters, through the spatial locations of these peaks.

3.4.3.2 Results

The maximum fuel temperatures and average power densities, averaged over the mixture of six fuel sphere passes present at any region in the core, for two sets of axial profiles are shown in **Figure 28**. The average power density for the Pu(PWR) peaked at an axial height of about 2.5 m below the top of the fuel core, right next to the central reflector (R = 102.3 cm in the centre of the radial mesh). This caused a peak (just above 3 m) in the maximum fuel temperature at the same radius and therefore the axial profiles at this radius were selected. However, the highest temperature was observed in single mesh near the radial centre of the fuel annulus at R = 139.1 cm at the bottom of the core, directly adjacent to the cones for the spent fuel outlet cones, and therefore profiles through this point were also investigated.

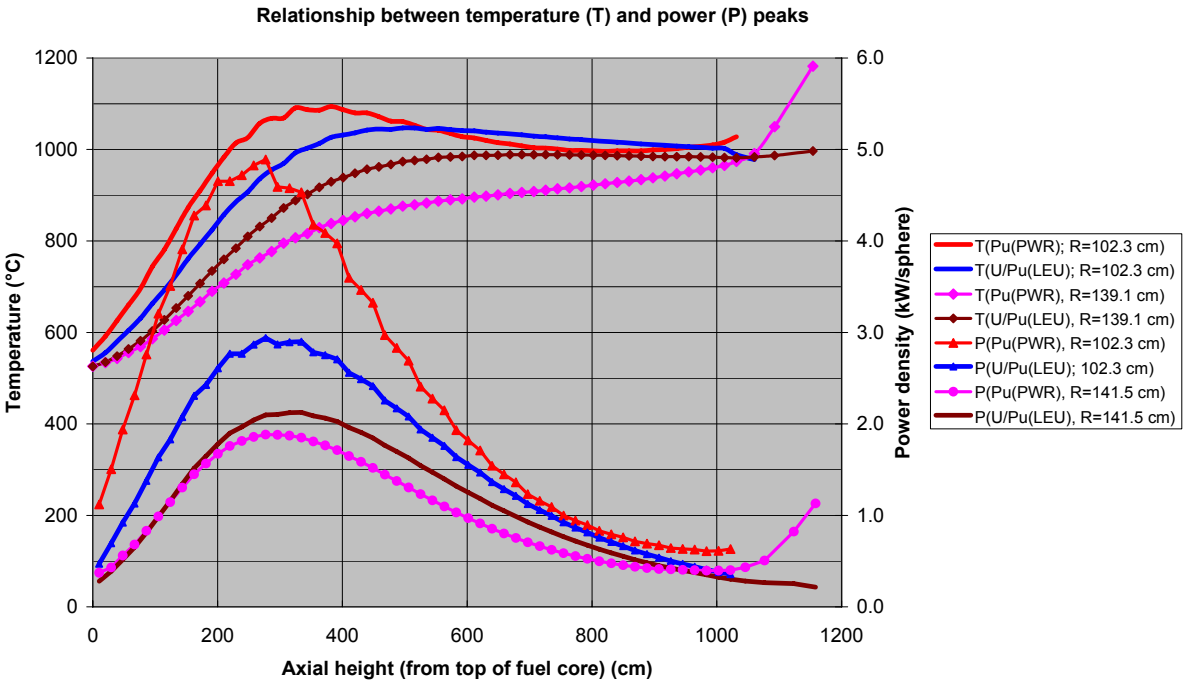

Figure 28: Axial profiles for the maximum fuel temperatures and power densities for 3 g Pu(PWR) and the reference 9 g U/Pu(LEU) at two radial positions.

In order to gain a better understanding of the heat transfer between the fuel and the coolant on the temperature peaks, the He coolant temperatures were added for the Pu(PWR) case, as shown in **Figure 29**.

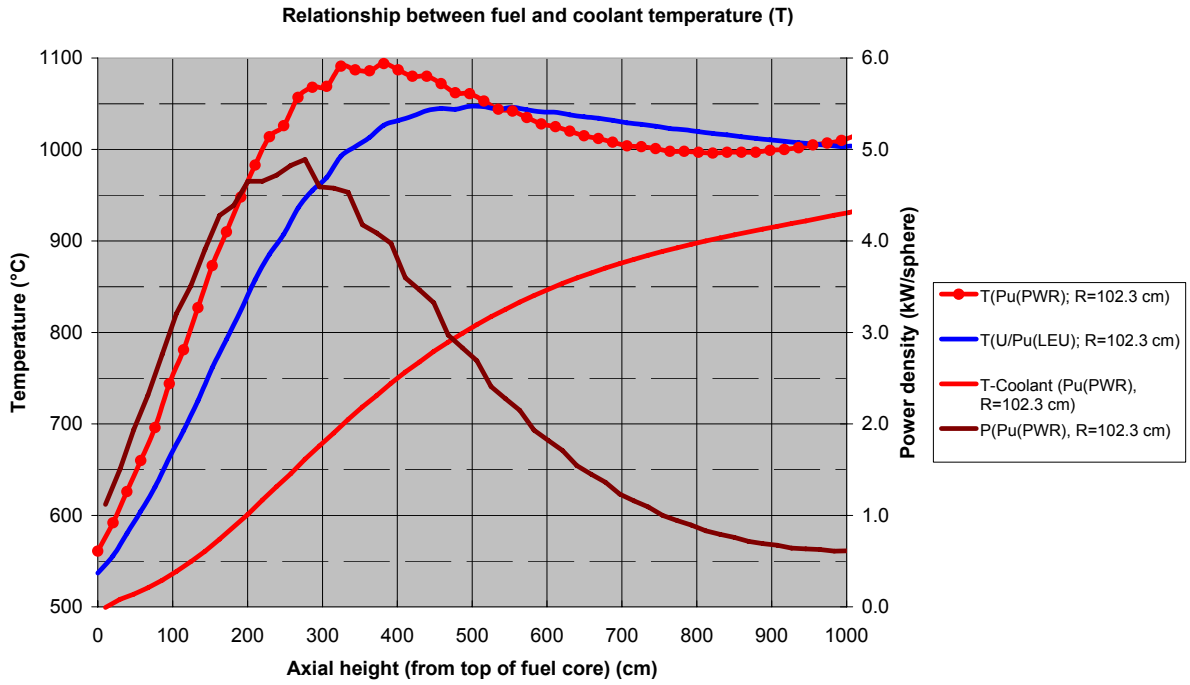

Figure 29: Axial profiles for the maximum fuel temperature, He coolant temperature and power densities for 3 g Pu(PWR) and the reference maximum fuel temperature for the 9 g U/Pu(LEU) at R = 102.3 cm, next to the central reflector.

With a view to the optimisation of the power distribution near the power peaks, the axial power profiles are compared in **Figure 30** and the radial profiles in **Figure 31**.

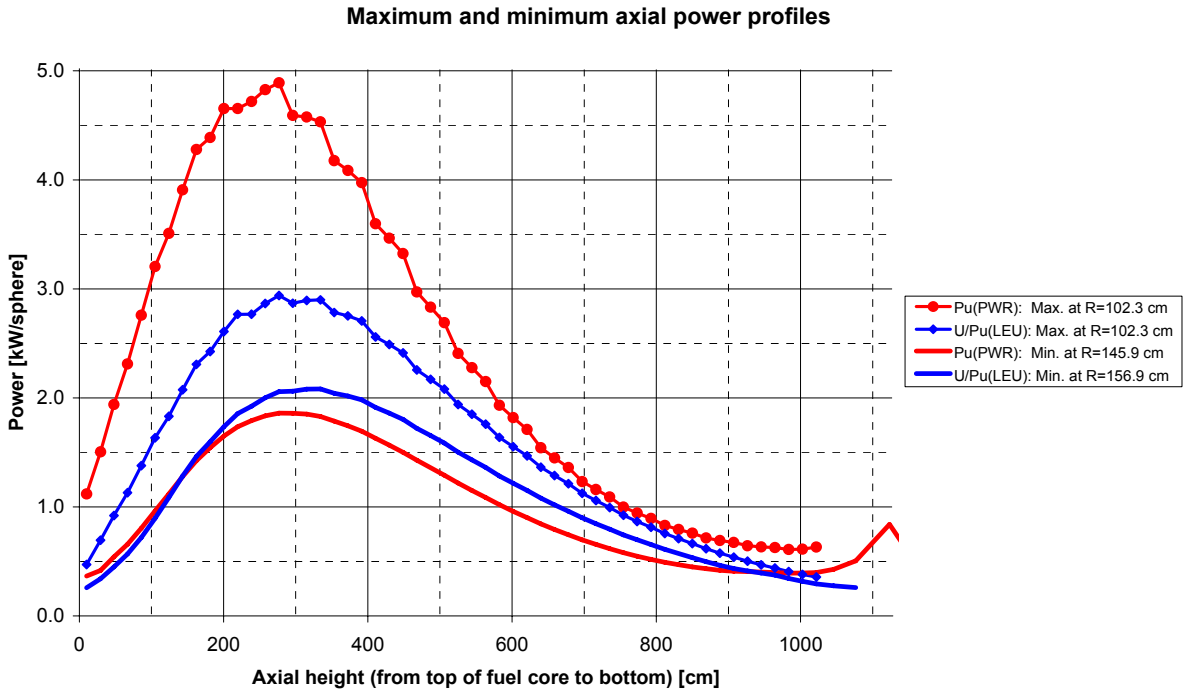

Figure 30: Axial power profiles at the radius at maximum power density (R = 102.3 cm) next to the central reflector and the minimum power densities (R = 145.9 cm for 3 g Pu(PWR) and R = 156.9 cm for 9 g U/Pu(LEU)), near the centre of the fuel annulus.

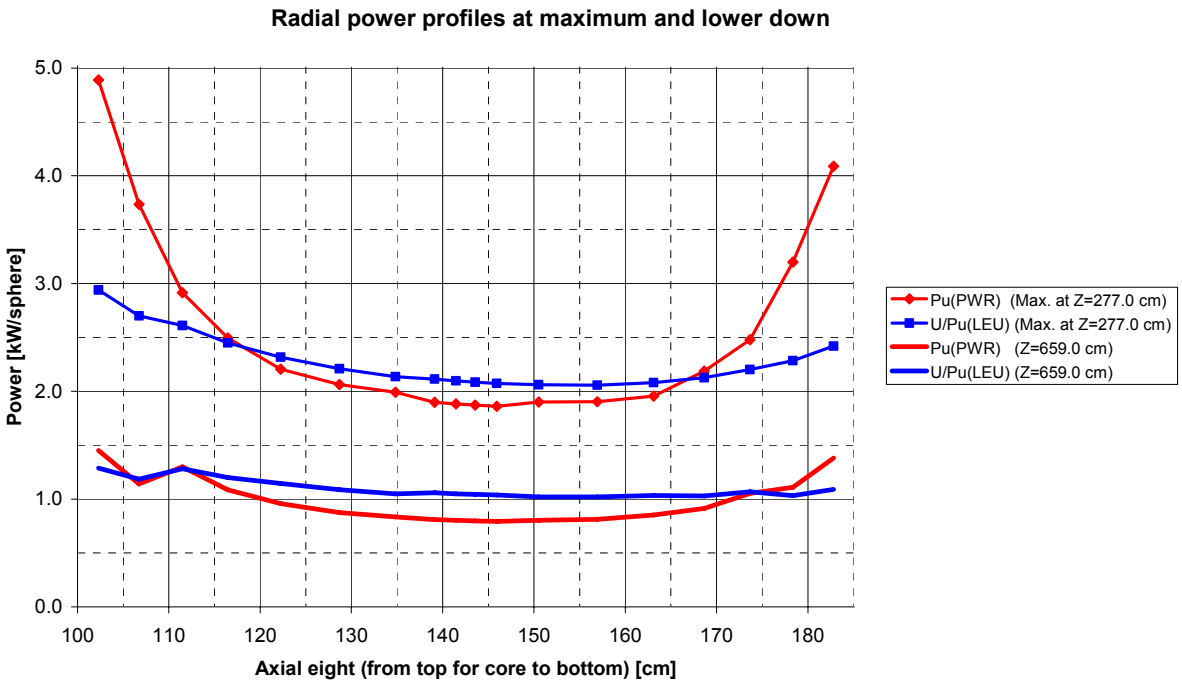

Figure 31: Radial power profiles at the maximum axial power density (Z = 277.0 cm) and in the lower half of the core (Z = 659.0 cm) for 3 g Pu(PWR) and the reference 9 g U/Pu(LEU)).

3.4.3.3 Discussion

3.4.3.3.1 Maximum fuel temperatures

From **Figure 28** it is clear that the power densities for the 3 g Pu(PWR) and reference 9 g U/Pu(LEU) fuel cycles peak at the same axial height (Z = 277.0 cm below the top of the fuel core), at the radial position directly adjacent to the central reflector (R = 102.3 cm). Although the maximum power density of 4.89 kW/sphere for Pu(PWR), which substantially exceeds the safety limit of 4.5 kW/sphere, is almost double the 2.94 kW/sphere of the U/Pu(LEU), the same axial temperature profile for Pu(PWR) peaks much lower down (Z = 382.0 cm) at 1094°C and is only slightly higher than the 1050°C for U/Pu(LEU), which peaked even lower at Z = 496.6 cm. This peak for Pu(PWR) is still well within the adopted safety limit of 1130°C. The reason for this acceptable temperature peak is that the power peaks very close to the top of the core, where the He coolant, which flows down from the top, is still much cooler than the fuel (about 650°C, compared to about 1060°C) as is shown in **Figure 29**. This large temperature difference drives effective conduction of the heat produced in the fuel to the coolant, and thus effective cooling of the fuel. This cooling, for identical temperature differences, would be more effective for the Pu(PWR), because it uses shell-ball fuel

spheres and thus the distance between the innermost fuel and the surface of the sphere is much shorter.

The other reason why the temperature peaks are similar is that, after the power density for Pu(PWR) has peaked, it drops rapidly with increasing axial distance, while U/Pu(LEU) maintains its power density much better. Therefore, at the height of peak Pu(PWR) temperature, the Pu(PWR) power density has decreased significantly from its peak, and at the height of peak U/Pu(LEU) temperature, the Pu(PWR) and U/Pu(LEU) power densities have become similar (**Figure 28**). The U/Pu(LEU) thus transfers its heat more efficiently to the coolant because the power profile is much less peaked and a larger part of the axial profile is therefore used to transfer the heat from the fuel to the coolant. A similar amount of energy is thus transferred at lower peak fuel temperatures.

3.4.3.3.2 Temperature peak in spent fuel outlet chute

Surprisingly, the maximum fuel temperature of 1182°C for Pu(PWR) did not occur at the radius of maximum power density next to the central reflector, but in single mesh near the radial centre of the fuel annulus at R = 139.1 cm at the bottom of the core (Z=1154.1 cm), in the outlet chute for the spent fuel (**Figure 28**). The reasons for this are probably as discussed in the following paragraphs.

Part of the reason for the sharp drop in the axial power density profile towards the bottom of the core, next to the central reflector, is that the fissile Pu isotopes get depleted. While on average it takes six passes of the Pu(PWR) pebbles to reach their target burn-up, the average power density in the inner flow channel, adjacent to the central reflector, is so high, that pebble passes two to six reach their target burn-up during a single pass in this flow channel and will thus be discarded as spent fuel. This high burn-up depletes the fissile isotopes so that the average fissile enrichment in this flow channel, near the bottom of the core, is much lower than for the central flow channels. Although the enrichment in the central channels is much higher, their power densities are severely limited by the fact that the influx of thermal neutrons from the two reflectors are strongly absorbed in the two flow channels next to these reflectors, so that the neutron spectrum is severely under-moderated in the three central channels. However, as the fuel enters the exit cones, all the flow channels are squeezed by the reflector cones, so that they become much thinner (**Figure 11**). Therefore the central flow channel fuel comes much closer to the reflector cones. Combined with the reduced ability of the external flow channel fuel to absorb this influx of thermal neutrons, due to the depletion of their fissile nuclides, this causes an increased influx of thermal neutrons

into the higher enriched fuel of the central flow channels, as was seen in Figure 8, and thus the spike in the power density shown in **Figure 28** at the bottom of the core.

Although the maximum power density in this spike is only about 1 kW/sphere, compared to the almost 5 kW/sphere in the large power peak next to the central reflector near the top of the core, the temperature of the He coolant has now risen to almost 950°C, compared to only about 650°C near the top of the core. Therefore the ability of the coolant to evacuate the produced heat is much lower at the bottom of the core, and therefore this tiny power peak caused the sharp temperature spike, also shown in **Figure 28** at the bottom of the core. It is ironic that this tiny power spike, in a small part of the core, which contributed very little to the total power output of the reactor, increased the maximum fuel temperature for Pu(PWR) from the acceptable 1094°C in the peak near the top of the core to 1182°C, which significantly exceeds the safety limit of 1130°C and thus rendered the design not licensable. Therefore it may be a good idea to insert neutron poisons into graphite outlet chutes.

3.4.3.3.3 Maximum power densities

It is clear from the discussion above that, except for the tiny part at the bottom of the core, the exceeding of the safety limits by the maximum power density in the Pu(PWR) fuel cycle was a much more serious problem than the maximum fuel temperatures. The nature of this problem is clear from axial and radial profiles in Figure 30 and Figure 31:

The safety performance of the U/Pu(LEU) fuel cycle was much better than the Pu(PWR) cycle. The reason was that its power profile was much less peaked, especially in the radial direction where the U/Pu(LEU) profile is almost flat. The reasons probably are the much lower thermal σ_f of ^{235}U, compared to both ^{239}Pu and ^{241}Pu, the better epithermal neutron economy (η) of ^{235}U and the much larger magnitude of the negative uniform temperature reactivity coefficient for LEU, compared to Pu(PWR). The lower σ_f of ^{235}U, combined with the much lower fissile enrichment, makes the LEU fuel kernels markedly more transparent to thermal neutrons than for Pu(PWR). While the influx of thermal neutrons are thus largely absorbed by the Pu(PWR) within the first 5 cm from the central reflector, i.e. within the first layer of pebbles, which causes the dramatic fission power spike in the radial direction between R = 100 and 105 cm (Figure 31), this influx of thermal neutrons is only partly absorbed by the first layer of LEU pebbles and thus this thermal fission spike is much more evenly spread out over more than 20 cm in the radial direction.

Furthermore, the strong negative uniform temperature reactivity coefficient of the U/Pu(LEU) assisted in suppressing any power density spikes, due to the associated temperature spikes.

3.4.3.4 Conclusions on maximum fuel temperature and power density

Since only a small part of the fuel exit cones was responsible for the exceeding of the maximum fuel temperature limit for the Pu(PWR), this problem can easily be solved by placing neutron poisons in these reflector cones.

However, such poisoning is necessitated by a more serious possibility, which was not investigated in this study, namely criticality of fresh fuel in the exit cones. The power spike in the exit chute served as a reminder of the volatile nature of Pu(PWR) in that its reactivity is mainly suppressed by under moderation of the neutron spectrum. Any increase in neutron moderation will thus cause a sharp increase in reactivity. Therefore, if an emergency should require that the reactor be shut down and the fuel evacuated from the core, the layer of fresh fuel at the top of the core will eventually reach the exit cones. Because of the increased moderation, due to the proximity of the reflectors, the probability that such fresh fuel may become critical in these cones is much larger for Pu(PWR) than for LEU. Therefore the safety assessment that was done for the exit cones of the PBMR DPP-400 for LEU may very well not hold for Pu(PWR), which emphasises the imperative for poison in these cones.

Since the large axial power peak for Pu(PWR) (Figure 30), adjacent to the central reflector, tapered off very quickly, both in the axial and radial directions, the area that exceeded the safety limit of 4.5 kW/sphere was only the axial region between Z = 140 cm and 380 cm, and in the radial direction, only in the first 5 cm next to the central reflector. This problem area comprises only 0.85% of the core volume and thus supplies only a few percent of the total core power. The corresponding power peak next to the external reflector is much smaller and thus even less of a problem. This means that neutron poisons will have to be introduced into only a small part of the reflectors in order to suppress these power density peaks. More detailed proposals for the redesign of the reactor for Pu(PWR) will be made in the final conclusion section of this thesis.

3.4.4 Maximising proliferation resistance

From the literature study above, the most important ways of improving the proliferation resistance of U/Pu and Pu fuel cycles were determined as:

- transmutation of the ^{237}NP from previous spent fuel and
- increasing the ^{238}Pu content of the Pu mixtures produced in the current Pu fuel cycles.

By adding the associated ^{237}Np, from reprocessed fuel, to the current Pu(PWR) in the fresh fuel, a significant fraction of the ^{237}Np should be transmutated to ^{238}Pu, which should achieve both these aims.

3.4.4.1 Simulation parameters

The ^{237}Np concentration of the Pu(PWR)+MA case was added to the 3 g Pu per fuel sphere Pu(PWR) case, as shown in the materials balance of the results in Table 28.

3.4.4.2 Results

Table 28: Materials balance for Pu(PWR)+ ^{237}Np vs. Pu(PWR) fuel

Fuel cycle		Pu(PWR)			Pu(PWR)+ ^{237}Np		
Average burn-up ($MW.d/kg_{HM}$)		601.0			488.9		
Fresh fuel supply		191 balls/day * 3 g Pu_{HM}[1]/ball			235 balls/day * 3 g Pu_{HM}[1]/ball		
		loading →	unloading	ΔHM	loading →	unloading	ΔHM
^{237}Np	($kg/GW_{th}d$)	0 →	0.0001	+0.0001	0.1123 →	0.0515	-0.0608
^{238}Pu	($kg/GW_{th}d$)	0.046 →	0.0491	+0.0031	0.0555 →	0.1061	0.0506
^{239}Pu	($kg/GW_{th}d$)	0.8948 →	0.0393	-0.8555	1.0375 →	0.1176	-0.9199
^{240}Pu	($kg/GW_{th}d$)	0.3931 →	0.1135	-0.2796	0.4558 →	0.1999	-0.2559
^{241}Pu	($kg/GW_{th}d$)	0.2182 →	0.1430	-0.0752	0.2530 →	0.2316	-0.0214
^{242}Pu	($kg/GW_{th}d$)	0.1125 →	0.1665	+0.0540	0.1304 →	0.1793	0.0489
^{241}AM	($kg/GW_{th}d$)	0 →	0.0268	+0.0268	→	0.0409	0.0409
^{242m}AM	($kg/GW_{th}d$)	0 →	0.0008	+0.0008	→	0.0012	0.0012
^{243}AM	($kg/GW_{th}d$)	0 →	0.0572	+0.0572	→	0.0568	0.0568
^{242}CM	($kg/GW_{th}d$)	0 →	0.0008	+0.0008	→	0.0010	0.0010
^{243}CM	($kg/GW_{th}d$)	0 →	0.0002	+0.0002	→	0.0002	0.0002
^{244}CM	($kg/GW_{th}d$)	0 →	0.0409	+0.0409	→	0.0346	0.0346
Total Pu[1]	($kg/GW_{th}d$)	1.6646 →	0.5115	-1.1531	2.0445 →	0.886	-1.1585
Fissile Pu enrichment	%	66.86 →	35.74		66.789 →	41.845	
Total HM	($kg/GW_{th}d$)	1.6646 →	0.6382	-1.0264	2.0445 →	1.0207	-1.0238

Note: [1] See Table 26

3.4.4.3 Discussion and conclusions

The addition of ^{237}Np caused a substantial increase in the ^{238}Pu fraction of the plutonium mixture in the spent fuel, from 9.6% to 13.3%, thereby adding significant value.

However, the resulting decrease in burn-up increased the heavy metal disloading by 59.9% from 0.6382 to 1.0207 kg/GW_{th}d. Especially undesirable is the disloading of ^{241}Pu that increased by 62.0% from 0.1430 to 0.2316 kg/GW_{th}d. This increased disloaded mass of ^{241}Pu will within a few decades decay to ^{241}Am, which will within a few centuries decay to ^{237}NP, which will significantly increase the long term radiotoxicity and proliferation risk, as was shown in the literature study. Therefore, in the long term, this intervention, aimed at reducing ^{237}Np, will actually increase it. Therefore adding ^{237}Np to the Pu(PWR) fuel for PBRs is not advisable.

Since, just as Am, ^{237}Np has a high fast fission cross-section, the more advisable route would be to incinerate it in fast reactors, LWRs or CANDU reactors, which all have much higher fast fission fractions than PBRs. Pu in the spent fuel of LWRs, and much more so for CANDU reactors, lacks the high level of proliferation resistance of PBR spent fuel. Therefore the increase in the ^{238}Pu fraction in the spent fuel Pu mixture from the transmutation chain of ^{237}Np may add more proliferation resistance value for those reactors, compared to PBRs that do not need it.

4 Discussions of study and conclusions

4.1 Assessment of the originality of the results

The author claims to have attained the North-West University's stated outcomes for obtaining a Ph.D. degree in that the following original contributions have been made:

1) An original research problem was formulated.

2) A critical literature survey was presented. From this literature survey the originality of the research aims and objectives was shown.

3) The originality of the research aims has already been motivated in Par. 1.5 above. The original aims achieved are now summarised:

    a. A computer code for the semi-automatic translation of VSOP-A input models to VSOP 99/05 input models was developed. While the development of codes and numerical procedures are normally viewed as contributing relatively little to the originality of a study, the development of these codes are claimed to have constituted an original contribution, due to the following problems that had to be solved in the process:

        i. Since 1994 when the original VSOP code, which ran only on a mainframe computer, split into the branch that was developed by E.J. Mulder to become VSOP-A and another branch that was developed by Kernforschungsanlage Jülich GmbH in Germany to become VSOP 99/05, there was little explicit contact between these code development efforts. Therefore, while the structures of their respective input cards remained largely similar, many small changes evolved independently in both codes, but without any cross-referencing to these differences in their respective input manuals (Mulder and Teuchert, 2006a and Rütten *et al*, 2007). Therefore it required skill (and patience) from the author to unravel these differences. Since in many instances, certain parameters in the VSOP-A cards were dropped from the VSOP 99/05 input cards and their functions replaced with new functions, which differed conceptually from the old functions, devising a way to automatically translate these old parameters into the new ones required original problem solving skills. Therefore the development of these translation codes is claimed as an original contribution.

ii. The discovery of the fluctuations of the VSOP batch volumes in the Pu fuel cycle of the pilot study and the solution to this problem by volume corrections in the fuel cycle input cards, are claimed as original contributions.

iii. The translation of input models (Par. 2.2 and Par. In the 6 in the appendix) and the accuracy of other calculations were verified and validated, on a continuous basis throughout the study.

b. The incineration of pure Pu(PWR), Pu(WGR), PU(PWR)+MA and the reference U/Pu(LEU) for a PBMR DPP-400 reactor have been simulated with the VSOP 99/05 codes. These results, as well as their comparison to each other and to the VSOP-A results from the pilot study, are claimed as original contributions.

c. From the literature survey the author established the importance of high fractions of ^{238}Pu in the spent fuel Pu-mixture, as well as the importance of transmutation of ^{237}Np to ^{238}Pu, for the maximisation of proliferation resistance. In previous Pu incineration studies, the proliferation resistance was mainly assessed in terms of the reduction of the total mass of Pu and the maximisation of the ^{240}Pu content of the spent fuel Pu-mixture. Therefore, exploring the optimising of the proliferation resistance of this fuel cycle with regards ^{238}Pu and ^{237}Np is claimed as an original contribution.

d. The proposed new design optimisations for the Pu(PWR) fuel cycle, the power conversion unit and the reactor geometry, given below, are claimed as original contributions.

4.2 Implications of the results

4.2.1 Development of a computer code for the translation of VSOP-A input models to VSOP 99/05

Since a large variety of input models has been developed and tested for VSOP-A, which has not yet been translated to the VSOP 99 format, the computer code for the semi-automatic translation of VSOP-A input models to VSOP 99/05 may possibly unlock some commercial and research value.

It may also aid design studies for regulatory purposes in providing both VSOP-A and VSOP 99/05 input models for the purpose of independent review codes. Such a semi-automatic

translation method may also be viewed by regulators as being more reliable than manual translation.

4.2.2 Comparison of VSOP-A and VSOP 99/05

The comparison of the simulation results of VSOP-A and VSOP 99/05 for the U/Pu(LEU) fuel cycle has confirmed that these two codes yield very similar results, which confirmed the confidence in the accuracy of translation of the input models between these codes. Confirmation of the actual accuracy of these codes will only be achievable once their results are compared to experimental data or to high fidelity computational benchmarks, which are not currently available, or to high fidelity codes, such as MCNPX, which is deferred to a follow-up study.

However, large differences were found when these codes were compared for the Pu(PWR) fuel cycle. This confirmed that there are important differences between their algorithms, which mainly consisted therein that:

- VSOP-A truncated the trans-plutonic transmutation chain after ^{242}Pu, while VSOP 99/05 continued it up to ^{244}Cm and
- VSOP-A scattered the neutrons down to the thermal group faster, thereby creating an elevated thermal neutron flux. This was shown to be caused by differences in how the leakage feedback is handled.

A more detailed verification and validation study for both codes, especially of the neutron energy spectra and the few-group cross-sections produced by GAM-ZUT-THERMOS, against MCNPX was referred to the list of suggested follow-up studies below.

4.2.3 Burn-up simulations for the different Pu fuel mixtures

4.2.3.1 Burn-up

Burn-up results were presented for Pu(PWR), Pu(PWR)+MA and Pu(WGR) and were compared to LEU. However, the average obtainable burn-up was found to be significantly constrained by the poor neutron economy of especially ^{239}Pu in PBRs. Therefore any modification to the fuel cycle that caused a deterioration in the neutron economy, such as the addition of extra neutron capturers, for instance MA or ^{237}Np, also caused a large reduction in the average burn-up. This caused an unacceptable increase in the amount of heavy metal to be disposed of in the spent fuel. Therefore the addition of MA to Pu(PWR) is not recommended. These nuclides should rather be burned in fast breeder reactors, where the

neutron economy is not constrained and where these isotopes can contribute positively to the neutron economy through fast fissions.

The constraints on the PBR neutron economy imply that the optimisation of the neutron economy, such as the minimisation of neutron leakage, should always be an integral component of the design of a Pu fuel cycle and of the associated reactor.

4.2.3.2 Safety

None of the Pu fuel cycles tested passed all safety requirements, i.e. every Pu cycle produced either maximum fuel temperatures or maximum power densities that were too high. Furthermore, all the Pu cycles displayed positive uniform temperature reactivity coefficient at low temperatures, which is unacceptable from a licensing point of view.

It might be possible to reinterpret the adopted safety limits, in order to attempt the justification of a safety case for some of the Pu fuel cycles in a PBMR DPP-400 reactor. For instance, the problem of the positive uniform temperature reactivity coefficient at low temperatures might be circumvented by operating protocols that stipulate that the fuel must always be pre-heated, for instance by means of electrical heaters, to a level above the critical low temperature range, before the neutron fission chain reaction is started. However, the safety of the reactor will then depend on the adherence of operators to this protocol. Such an approach will impair the cornerstone of the standard PBR safety case, which is inherent safety that is operator independent, because it is guaranteed solely by the laws of nature.

Therefore, the best approach will be to redesign the reactor and fuel cycles, with a view to improving the safety-performance of the Pu(PWR) fuel cycle to within acceptable standards. The guiding principles for such a redesign are described below.

4.2.3.3 Nuclear weapons proliferation resistance

The proliferation resistance of the spent fuel of the simulated Pu(PWR) fuel cycles was excellent, in that the ^{238}Pu and ^{240}Pu contents were high and the fissile enrichment was low.

However, when ^{237}Np was added to the fuel, for the sake of destroying the proliferation potential of the ^{237}Np, the transmutation fraction of the ^{237}NP was too low to make this strategy effective. The addition of ^{237}Np also caused an undesirable decrease in burn-up and thus an increase in the heavy metal in the spent fuel. Therefore it is recommended that ^{237}Np rather be burned in fast reactors or in LWRs or HWRs, in other fuel cycles such as U/Pu(LEU) where maximum neutron economy is less important and where the improvement of the proliferation resistance of the spent fuel Pu-mixtures, through increasing the ^{238}Pu

fraction, is more needed than in PBRs, that already possess excellent proliferation resistance.

4.3 Suggestions for future studies

4.3.1 Verification of VSOP-A vs. VSOP 99/05 with MCNP

Due to the large differences that were found between the results for VSOP-A and VSOP 99/05 for the Pu(PWR) fuel cycle, a MCNPX calibration study is proposed, in order to verify the sources of these differences and propose appropriate modifications to the codes, in order to reconcile their results. The focus should be on neutron energy spectra and the few-group cross-sections produced by GAM-ZUT-THERMOS in the respective VSOP codes.

Since the results of the present study showed that Pu(PWR) fuel cycles are much more sensitive to variations in the neutron energy spectrum, it is proposed that an appropriate selection of the verification studies for VSOP 99 with LEU fuel cycles be repeated with Pu(PWR) fuel cycles (Par. 2.2.4 - 2.2.5).

4.3.2 Reconciliation with the results of Boer and Ougouag

Significant differences were also found between the present VSOP 99/05 simulations and the simulations by Boer and Ougouag. A collaborative study with Boer and Ougouag is proposed, in order to resolve these differences.

4.3.3 Simulation of DLOFC temperatures, using the Multi-group TINTE code.

Simulation of the maximum temperatures, caused by the decay heat during a DLOFC, was excluded from this study, for the reasons stated in the demarcation section. Since these results are important, such a Multi-group TINTE simulation for Pu(PWR) is proposed.

4.3.4 Verification of the MEB for Pu fuel against MCNPX

The uncertainties in the calculated shutdown margins for the control rods have been spelled out in Par. 7.2.4 to 7.2.7 in the appendix. Therefore a MCNPX calibration study for the 2-D MEB with Pu fuel cycles is proposed.

4.3.5 Simulation of the reactivity of fresh Pu(PWR) fuel in the fuel exit cones

The power density spike in the fuel exit cones of the core for the Pu(PWR) fuel cycle suggests that there is a possibility that, if the fuel needs to be evacuated from the core, fresh fuel at the top of the core might become critical upon passing through the exit cones. A VSOP 99 simulation study is proposed to investigate this possibility.

4.4 Proposal for the redesign of the PBMR DPP-400 for Pu(PWR)

Since all the Pu mixtures failed at least one aspect of the safety limits, the following redesign of the reactor and fuel cycle is proposed in order to improve its safety performance with Pu fuel.

4.4.1 Pu fuel composition

4.4.1.1 Deep-burn pure Pu(PWR) fuel cycle

The aim for this fuel cycle will be very high burn-up, so that the spent fuel can be disposed of directly into a deep geological repository, without the need for chemical reprocessing.

It was clear from the results that pure Pu(WGR) fared the worst of all the Pu fuels in that it had a very high positive uniform temperature reactivity coefficient at low temperatures and by far exceeded the limits on the maximum fuel temperature and power density, as well as the fast fluence limit on spent fuel. It is clearly not suitable to be used in its pure form and should only be considered as driver material for, for instance, Th-based fuel cycles.

Since adding MA to the Pu(PWR) caused an unacceptable decrease in burn-up and thus an unacceptable increase in the heavy metal to be disposed of in the spent fuel, the addition of MA will not be considered. Although MOX-grade Pu was not tested in this study, it is well known that MOX-grade Pu gives a lower burn-up than Pu(PWR), and thus, for the same reasons will not be considered as fuel.

Pure Pu(PWR) thus seems to be the only promising fuel candidate. Since the magnitude of the positive uniform temperature reactivity coefficient increased strongly when the Pu(PWR) heavy metal loading was reduced significantly below 3 g Pu_{HM}/pebble, 3 g/pebble should be used as the point of departure for the optimisation studies.

For the sake of guaranteed coated particle integrity and a reduction in the positive uniform temperature reactivity coefficient, the small concentrated Pu fuel kernels should be replaced with large (500 µm diameter) diluted kernels. Kernels can be diluted either with inert matrix materials or ^{232}Th. Since a dilution down to 10% Pu requires an unrealistically high coated particle packing fraction of 46% in order to obtain a loading of 3 g Pu_{HM}/pebble, less severe dilution, down to, for instance, 20% or 30% Pu, should be investigated. Since the present results suggested that inert matrix materials alone might not be able to restore a negative uniform temperature reactivity coefficient, the addition of ^{232}Th, in order to supply a negative uniform temperature reactivity coefficient through the Doppler effect, should be investigated.

4.4.1.2 Pu-driven ^{232}Th fuel cycles

The aim for this fuel cycle will be maximum conservation of natural uranium resources. Since it is well known that ^{233}U is the only fissile nuclide that can produce a high enough conversion ratio in PBRs to produce a high level of conservation of natural uranium, the aim for this cycle should be to maximise the fraction of ^{233}U fissions and thus to minimise Pu fissions. Therefore the minimum possible Pu and maximum ^{232}Th loading in fresh fuel should be pursued. Due to the requirement of maximum ^{232}Th loading, dilution with inert matrix materials will not be an option, i.e. the Pu will have to be diluted solely with ^{232}Th.

Since the aim will be to maximise natural uranium conservation, the requirement of chemical reprocessing of the spent fuel will be a given fact, and thus maximum Pu destruction in a single burn-up cycle, with a view to direct disposal of the spent fuel, will not be a priority. Since a negative uniform temperature reactivity coefficient will be guaranteed by the high loading of ^{232}Th, Pu(WGR) should be added to the driver fuel options, together with Pu(PWR).

Extensive work on Pu-driven thorium fuel cycles in versions of the HTR MEDUL has been reported in the literature study above. However, the present author expects that the larger core of the PBMR-400, as will be modified according to the proposals below, will have lower leakage and may thus produce improved neutronic performance.

4.4.2 Power conversion system

Since high fuel temperatures during normal operation were problematic in the present study, switching from the direct Brayton cycle to the indirect Rankine steam cycle should be investigated. The much lower He inlet and outlet temperatures of the steam cycle will strongly lower the maximum fuel temperatures.

The steam cycle comes with an increased probability of a water ingress incident. Since the reactivity of Pu fuels increases much more when the neutron moderation increases, compared to LEU, the probability of water ingress causing a serious reactivity and power excursion will be elevated. Thus a strong negative uniform temperature reactivity coefficient will be required in order to bring such an excursion under control. Therefore the ^{232}Th content will probably need to be high, in order to maximise the Doppler effect.

4.4.3 Neutron poisons in the reflectors

While reports of relative success with the addition of neutron poisons like ^{167}Er to the fuel were discussed in the literature study above, the addition of neutron poisons to the reflectors can be expected be a more efficient way of flattening the power profiles and of reducing the

uniform temperature reactivity coefficient. Adding poisons to the fuel will have the effect of neutrons being captured in the desirable locations, such as next to the reflectors and at the axial regions where the power profiles peak. Unfortunately these poisons will also indiscriminately capture neutrons in the rest of the core as well. Therefore an unnecessary large number of neutrons will be sacrificed in order to achieve the desired results. This will reduce the burn-up and unnecessarily increase the heavy metal in the spent fuel. However, if the poisons are placed in the reflectors, the poison distribution can be adjusted to more efficiently target only the specific problem areas.

The strategic aims of the neutron poison placement should be:

1. To reduce the power density peaks to well within the safety limits.

2. However, the aim should not be to flatten the axial power profiles as much as possible: as has been shown above, the heat transfer from the fuel to the He coolant is much more effective near the top of the core where the He is still relatively cool. Therefore the current feature of an axial power peak in the top half of the core will be retained, but with a smaller peaking factor.

3. The axial power peaks should be suppressed to lower levels near the central, compared to near the external reflector. The reason for this is that the conduction of the decay heat to the core barrel is much more efficient for decay heat produced close to the external reflector, due to the shorter conduction path. Therefore concentrating the power density, during normal operation, next to the external reflector, should significantly reduce the maximum temperature during a DLOFC.

4. Optimisation of the poison placement should be aimed holistically at all the operational parameters, including the following ideal outcomes:

    a. Large cold shut-down margins after xenon decay.

    b. High total power output for the reactor.

    c. Low maximum fuel temperatures during a DLOFC.

    d. Large attainable variations in power output during load following. This can be maximised by minimising the reactivity swings, due to the variations in the ^{135}Xe concentrations, caused by load variations, as has largely been achieved for the Pu(PWR) fuel cycle in the present study.

5. In order to prevent depletion of the neutron poison concentrations over time, a mixture of burnable poisons, such as ^{10}B, and non-burnable poisons, such as hafnium, should be investigated. Hafnium will mainly capture epithermal neutrons, and will thus cause a softening of the neutron spectrum that flows back to the core, while ^{10}B will mainly capture low energy thermal neutrons and will thus lead to a hardening of the spectrum. For the same reasons, the Doppler effect will cause hafnium to capture more neutrons with increasing temperature, while the up-shift in the thermal spectrum will cause ^{10}B to capture less with increasing temperature. Therefore the composition of the poison mixture can be used to adjust both the neutron spectrum in the fuel adjacent to the poison in the reflectors, and the temperature coefficient of the reflectors. This may prove to be a powerful tool for the optimisation of the shape of the power profiles, temperatures, uniform temperature reactivity coefficient and the cold shut-down margins after decay of the ^{135}Xe.

4.4.4 Thinning of the central reflector

As has been pointed out above, the average burn-up attainable with Pu(PWR) decreases sharply whenever any action is taken that impairs the neutron economy. Therefore the proposed addition of poisons to the reflectors can be expected to cause an undesirable reduction in burn-up. In order to counter this, it is proposed that the central reflector be thinned, for instance from the present 2 m diameter to 1 m. Such a four-fold reduction in the reflector volume and a two-fold reduction in its cylindrical external surface area, where the fuel comes into contact with the poisoning potential of the reflector, should sharply reduce the number of neutrons captured in the central reflector. Such a thinning of the reflector will also substantially increase the fuel volume in the core, and thus the total power output attainable, for a given maximum power per fuel sphere (Serfontein *et al*, 2008.). The larger fuel volume will also cause a reduction in the leakage fraction. These measures will counter in the expected reduction in burn-up, due to the insertion of the neutron poisons into the reflectors.

The increase in fuel volume could be used to increase the total power output without increasing the power density. This could be useful where the aim is to supply higher levels of power for short periods, for instance in the case where a reactor is used to do peak-load following. However, if the average total power were to be increased significantly above 400 MW_{th}, the maximum fuel temperature during a DLOFC might exceed the 1600°C safety limit. Therefore the better use of the extra fuel volume might be to maintain the average power at 400 MWth, but at lower power densities, which would imply lower fuel temperatures during normal operation.

One of the original reasons for the 2 m thick central reflector was to “push” the neutron flux out towards the control rods in the external reflector. This was achieved by the pushing out of by inserting the thick central reflector. If a central reflector is not present, or is thinned as proposed her, the inner fuel layers may be positioned so far from the control rods in the external reflector that the rods will have minimal control over the neutron flux in these layers. This will reduce the worth of the control rods to the point where it will not be possible to maintain a cold shut-down of the reactor, after the ^{135}Xe has decayed.

However, the insertion of neutron poisons in the central reflector will counter this effect, in that the flux in the inner fuel layers will be suppressed, and thus the radial flux profile will be “pushed” out towards the external control rods, without having to push the fuel out.

The positive uniform temperature reactivity coefficient values, observed in the present study, were probably partly caused by the large influx of thermal neutrons from the central reflector. However, thinning the central reflector, increasing the fuel volume and inserting neutron poisons in the reflectors will all decrease the fraction of the total neutrons that are thermal neutrons from the reflectors, which should decrease the uniform temperature reactivity coefficient.

4.5 Final conclusions

The Pu fuel cycles investigated in the PBMR DPP-400 reactor did not meet the stated safety requirements. Therefore design modifications to the Pu(PWR) fuel cycle, the PBMR DPP-400 reactor geometry and its power conversion system were proposed in order to optimise both the safety and the techno-economic performance of the reactor and fuel cycle combination.

5 References

Australian Safeguards Office: John Carlson, John Bardsley, Victor Bragin and John Hill. 1997. Plutonium isotopics - Non-proliferation and safeguards issues. Canberra ACT, Australia. IAEA-SM-351/64. http://www.fas.org/nuke/intro/nuke/O_9705.htm Date accessed: 15 Jan. 2007.

Bell, William C. and Cham E. Dallas. 2007. Vulnerability of populations and the urban health care systems to nuclear weapon attack – examples from four American cities. International Journal of Health Geographics, 2007, 6:5. http://www.ij-healthgeographics.com/content/pdf/1476-072X-6-5.pdf Date accessed: 22 Sept. 2010.

Bende, Evert Eugène. 2000. Plutonium Burning in a Pebble-Bed Type High Temperature Nuclear Reactor. PhD Thesis. Delft University of Technology. Petten: Nuclear Research and Consultancy Group (NRG). http://www.tudelft.nl/live/binaries/b956b284-243e-4522-97f7-ba99e9b212f8/doc/bende.pdf Date accessed: 25 May 2007.

Boer, B. and A.M. Ougouag. 2010a. Core analysis, design and optimisation of a Deep-Burn Pebble Bed Reactor. Proceedings of PHYSOR 2010, May 2010, Pittsburgh, Pennsylvania.

Boer, B. and A.M. Ougouag. 2010b. Core optimization of a Deep-Burn Pebble Bed Reactor. Proceedings of ICAPP '10, 13-17 June 2010, San Diego, CA, USA. Preprint of Paper 10290.

BGR (Bundesanstalt für Geowissenschaften und Rohstoffe – German Federal Institute for Geosciences and Natural Resources). 2009. Reserves, resources and availability of energy resources 2009, Hannover, Germany. http://www.bgr.bund.de/nn_335074/EN/Themen/Energie/Downloads/annual__report__2009__en,templateId=raw,property=publicationFile.pdf/annual_report_2009_en.pdf Date accessed: 11 Sept. 2010.

Borenstein, Severin. 2008. The market value and cost of solar photovoltaic electricity production. Center for the study of energy markets. CSEM WP 176. Jan. 2008. http://www.ucei.berkeley.edu/PDF/csemwp176.pdf Date accessed: 11 Sept. 2010.

Brockmann, H., H.J. Rütten, K.A. Haas and W. Scherer. 2004. Review of the Neutron Spectrum Calculation Methods in the Computer Code System VSOP-99. Report nr. FZJ-ISR-RC-5084/2004, Issue 1. Forschungszentrum Jülich GmbH, Germany.

Bunn, M., S. Fetter, J.P. Holdren and B. van der Zwaan. 2003. The economics of reprocessing vs. direct disposal of spent nuclear fuel. – Final report. Project on Managing the Atom. Belfer Center for Science and International Affairs. Cambridge, Massachusetts.

Burnie, Shaun, Hideyuki Ban, AM Smith and Paul Leventhal. 1999. Open Letter to the Director General of the International Atomic Energy Agency, Dr Mohamed ElBaradei. April 13, 1999. http://www.nci.org/c/c41299.htm Date accessed: 6 Jan. 2007.

Caspers, L.M. 1968. Comparison between measured and calculated stationary thermal neutron spectra in heterogeneous systems. Ph.D. thesis in the technical sciences. Technische Hogeschool Delft.

Cooper, Mark. 2009. The economics of nuclear reactors: Renaissance or relapse? Institute for energy and the environment. Vermont Law School. June 2009. http://www.vermontlaw.edu/Documents/Cooper%20Report%20on%20Nuclear%20Economics%20FINAL%5B1%5D.pdf Date accessed: 12 Sept. 2010.

DOE. 2002. A Technology Roadmap for Generation IV Nuclear Energy Systems. http://www.nuclear.energy.gov/genIV/documents/gen_iv_roadmap.pdf Date accessed: 31 Jul. 2007.

DOE. 2006a. Global Nuclear Energy Partnership (GNEP). http://www.gnep.energy.gov Date accessed: 15 Jan. 2007.

DOE. 2006b. Advanced Fuel Cycle Initiative (AFCI) Comparison Report, FY 2006 Update (July 2006). http://www.ne.doe.gov/pdfFiles/fy06AfciComparisonReportToCongress.pdf Date accessed: 15 Jan. 2007.

DOE. 2007. Global Nuclear Energy Partnership Strategic Plan. GNEP-167312, Rev. 0. http://www.gnep.energy.gov/pdfs/gnepStrategicPlanJanuary2007.pdf Date accessed: 15 Jan. 2007.

EUROPEAN COMMISSION. 2003. External Costs: Research results on socio-environmental damages due to electricity and transport. Directorate-General for Research. ExternE project. EUR 20198. http://www.externe.info/externpr.pdf Date accessed: 12 Sept. 2010.

European Nuclear Society. 2010. Critical mass. http://www.euronuclear.org/info/encyclopedia/criticalmass.htm Date accessed: 1 Aug. 2010.

Ezoubtchenko, A.A., M. Saito, V.V. Artisyuk and H. Sagara. 2005. Proliferation resistance properties of U and Pu isotopes. Progress in Nuclear Energy, Vol. 47, No. 1-4: 701-707, 2005. www.sciencedirect.com Date accessed: 1 Aug. 2010.

Fen, V., M. Lebedev, V. Sarytchev and W. Scherer. 1992. Modelling of Neutron Absorbers in High Temperature Reactors by Combined Transport-Diffusion Methods. Forschungszentrum Jülich GmbH. ISR, JÜL-2573, (January 1992)

Fetter, Steve Matthew and Bun. 2006. Uranium resources for the long-term. School of Public Policy, University of Maryland and John F. Kennedy School of Government Harvard University, Cambridge, USA College Park, USA.
http://phys4.harvard.edu/~wilson/energypmp/2006_Fetter_and_Bunn.doc Date accessed: 14 Sep. 2010.

Fthenakis, Vasilis. 2009. Sustainability of photovoltaics: The case for thin-film solar cells. Renewable and Sustainable Energy Reviews 13 (2009) 2746–2750. www.sciencedirect.com Date accessed: 11 Sept. 2010.

Gerwin, H. and W. Scherer. 1979. Ein Diffusiontheoretisches Simulationsverfahren zur Beschreibung des oberen Hohlraumes im Kugelhaufen-Hochtemperaturreaktor. Forschungszentrum Jülich, JÜL - 1599, 1979.

Gintner, S.K. 2010. Thorium-based fuel cycles: Saving uranium in a 200 MWth pebble bed high temperature reactor. Nov. 2010. Masters mini-dissertation. North-West University, South Africa.

Gougar, H., W. Yoon and A. Ougouag. 2010. Multiscale Analysis of Pebble Bed Reactors. Proceedings of HTR2010: 5-th International topical Meeting on High Temperature Reactor Technology. 18-20 October 2010. Prague, Czech Republic.

Hansen, U., E. Teuchert. 1971. Influence of coated-particle structure in thermal-neutron-spectrum energy range. Nuclear Science and Design, Issue 44: 12-17, 1971.

Herring, J. Stephen, Philip E. MacDonald, Kevan D. Weaver and Craig Kullberg. 2001. Low cost, proliferation resistant, uranium–thorium dioxide fuels for light water reactors. Nuclear Engineering and Design, Vol. 203, Issue 1: 65-85, 1 Jan. 2001.
http://www.sciencedirect.com/science?_ob=MImg&_imagekey=B6V4D-424TJJ1-6-1B&_cdi=5756&_user=4050432&_orig=search&_coverDate=01%2F01%2F2001&_qd=1&_sk=997969998&view=c&wchp=dGLbVlb-

zSkWA&md5=d459ff793f009892d808f8f39032c536&ie=/sdarticle.pdf Date accessed: 19 Jan. 2007.

Hoegberg, Lars. 1998. Risk perception, safety goals and regulatory decision-making. Reliability Engineering and System Safety 59 (1998): 135-139.

Honek, H.C. 1961. THERMOS - A Thermalization Transport Theory Code for Reactor Lattice Calculation. Brookhaven National Laboratory, BNL-5826.

IAEA. 1997. Fuel performance and fission product behaviour in gas cooled reactors. IAEA-Tecdoc-978, November 1997. Vienna. Edited by K. Verfondern.
http://www.iaea.org/inis/aws/htgr/

IAEA. 2003. Potential of thorium based fuel cycles to constrain plutonium and reduce long lived waste toxicity. IAEA-TECDOC - 1349, April 2003.

IAEA. 2005. Annual Report for 2005: Annex: 6, Table A20.
http://www.iaea.org/Publications/Reports/Anrep2005/annex_tables.pdf Date accessed: 6 Jan. 2007.

IAEA. 2009. Status of Minor Actinide fuel development. IAEA Nuclear Energy Series, No. NF-T-4.6. Viena.

IAEA. 2010. RAF3007, Workshop on Uranium Data Collection & Reporting: Red Book – Uranium: Resources, Production and Demand.
http://www.iaea.org/OurWork/ST/NE/NEFW/documents/RawMaterials/RTC-Ghana-2010/5.RedBook.pdf Date accessed: 14 Sept. 2010.

INEEL. 2003. NGNP point design –Results of the initial neutronics and thermal-hydraulic assessments during FY-03. INEEL/EXT-03-00870, Revision 1. September 2003. http://www.inl.gov/technicalpublications/Documents/2699872.pdf Date accessed: 1 Feb. 2007.

International Energy Agency. 2009. World Energy Outlook 2009.
www.worldenergyoutlook.org/docs/weo2009/WEO2009_es_english.pdf Date accessed: 11 Sept. 2010.

International Panel on Fissile Materials. 2006. Global fissile material report 2006: Developing the technical basis for policy initiatives to secure and irreversibly reduce stocks of nuclear weapons and fissile materials.

http://www.fissilematerials.org/ipfm/site_down/ipfmreport06.pdf Date accessed: 12 Jan. 2007.

Jonnet, J., J.L. Kloosterman and B. Boer. 2010. Performance of TRISO particles fueled with plutonium and minor actinides in a PBMR-400 core design. Nuclear Engineering and Design 240 (2010): 1320–1331. http://www.janleenkloosterman.nl/papers/jonnet1001.pdf Date accessed: 28 Dec. 2010.

Kang, Jungmin and Frank N. von Hippel. 2001. U-232 and the Proliferation-Resistance of U-233 in Spent Fuel. Science & Global Security, Volume 9: 1-32.
http://www.informaworld.com/index/788806452.pdf Date accessed: 18 Sept. 2010.

Kazimi, M.S., Czerwinski, K.R., Driscoll, M.J., Hejzlar, P., Meyer and J.E. 1999. On the use of thorium in light water reactors. Massachusetts Institute of Technology Press. MIT-NFC-TR-016. http://www.thoriumpower.com/files/MIT%20article%20april%201999.pdf Date accessed: 4 Aug. 2009.

Kessler, G., W. Höbel, B. Goel and W. Seifritz. 2008a. Potential nuclear explosive yield of reactor-grade plutonium using the disassembly theory of early reactor safety analysis. Nuclear Engineering and Design 238 (2008): 3475–3499. http://www.sciencedirect.com Date accessed: 21 Sept. 2010.

Kessler, G., C. Broeders, W. Hoebel, B. Goel and D.Wilhelm. 2008b. A new scientific solution for preventing the misuse of reactor-grade plutonium as nuclear explosive. Nuclear Engineering and Design, 238 (2008): 3429–3444. http://www.sciencedirect.com Date accessed: 21 Sept. 2010.

Kim, Kang-Seog, Jin-Young Cho, Hyun Chul Lee, Jae Man Noh and Sung Quun Zee. 2007. Development of a physics analysis procedure for the prismatic very high temperature gas-cooled reactors. Annals of Nuclear Energy, 34 (2007): 849–860
http://www.sciencedirect.com Date accessed: 16 May 2010.

Kloosterman, J.L. and J.M. Li. 1995. Transmutation of Americium in Fission Reactors. Proc. International Conference on Evaluation of Emerging Nuclear Fuel Cycle Systems (GLOBAL'95): 1106-1113 (1995), Versailles, France.
http://www.janleenkloosterman.nl/papers/klooster9502.pdf Date accessed: 29 Dec. 2010.

Kloosterman J.L. Application of boron and gadolinium burnable poison particles in UO2 and PuO_2 fuels in HTRs. Annals of Nuclear Energy, 30 (2003): 1807–1819.

Kugeler, Kurt. 2007. Lecture notes for HTR Technology. North-West University, Potchefstroom, South Africa.

Lahoda, Edward. 2006. Personal communication to E.J. Mulder, supplying Pu isotopics for PWR fuel with 53000 MWd/T heavy metal burn-up.

Lamarsh, John R. and Anthony J. Baratta. 2001. Introduction to Nuclear Engineering. Third Edition. Prentice Hall. Upper Saddle River, New Jersey.

Lando, Ben. 2006. Analysis: Reid's Yucca and nuke waste plan. United Press International. 4 Dec. 2006. http://www.upi.com/Energy/view.php?StoryID=20061204-033735-1872r Date accessed: 19 Jan. 2007.

Lebenhaft, Julian R. 2002. MCNP4B modeling of pebble-bed reactors. Masters thesis. Massachusetts Institute of Technology, Feb. 2002.
http://dspace.mit.edu/handle/1721.1/28288 Date accessed: 15 May 2010.

Lidskog, Rolf and Ann-Catrin Andersson. 2002. The management of radioactive waste: A description of ten countries.
http://www.skb.se/upload/publications/pdf/The%20management.pdf Date accessed: 12 Sept. 2010.

MacKay, David J.C. 2007. Enhancing Electrical Supply by Pumped Storage in Tidal Lagoons. Cavendish Laboratory, University of Cambridge. March 13, 2007 – Draft 1.8.
http://www.inference.phy.cam.ac.uk/sustainable/book/tex/Lagoons.pdf Date accessed: 11 Sept. 2010.

Makhijani, Arjun and Michelle Boyd. 2009. Thorium fuel: No panacea for nuclear power. Physicians for Social Responsibility. http://www.ieer.org/fctsheet/thorium2009factsheet.pdf Date accessed: 18 Sept. 2010.

Mark, J.C. 1992. Explosive properties of reactor-grade plutonium. Science and Global Security, vol. 3: 1–13.

Mulder, Eben Johan. 1998. Pebble bed reactor with equalised core power distribution – inherently safe and simple. Ph.D. dissertation in Engineering, submitted to the Faculty of Mechanical Engineering at the University of North-Rhine Westfalia, Aachen. Promotor: Doctor rer. nat. Eberhard Teuchert.

Mulder, Eben. 2006. Modelling of the Reactivity Control and Shut-down System in VSOP-A. Unpublished lecture notes for the module *Pebble Bed Reactor Design* (NUCI886) in the Masters in Nuclear Engineering Programme at the Post Graduate School for Nuclear Science and Engineering at the North-West University, PUK Campus, South Africa.

Mulder, Eben and Eberhard Teuchert. 2006a. V.S.O.P.-A: Computer code system for reactor physics and fuel cycle simulation - Input Manual. Copyright by NTC.(Pty) Ltd.

Mulder, Eben and Eberhard Teuchert. 2006b. Characteristics of a different fuel cycle in a PBMR-400 for burning reactor-grade plutonium. Proceedings HTR2006: 3^{-rd} International topical Meeting on High Temperature Reactor Technology, Paper B00000170, 4-6 October 2006. Johannesburg, South Africa..

Mulder, Eben, Dawid Serfontein and Eberhard Teuchert. 2008. Deep Burn Strategy for Pure Reactor-Grade Plutonium in Pebble Bed High Temperature Gas-Cooled Reactors. Proceedings HTR2008: 4^{-th} International topical Meeting on High Temperature Reactor Technology. 1-4 October 2008. Washington, D.C., USA.

Mulder, Eben, Dawid Serfontein, Willem van der Merwe and Eberhard Teuchert. 2010. Thorium and uranium fuel cycle symbiosis in a Pebble Bed High Temperature Reactor. Proceedings of HTR2010: 5-th International topical Meeting on High Temperature Reactor Technology, 18-20 October 2010. Prague, Czech Republic.

Naicker, Vishnu V. 2006. Evaluation of the neutronic boundary conditions used in the diffusion analysis model of the PBMR core. Masters dissertation. North-West University, Potchefstroom, South Africa.

Oi, Noboru. 1998. Plutonium challenges: Changing dimensions of global cooperation. IAEA Bulletin, Volume 40, No. 1 (March 1998).
http://www.iaea.org/Publications/Magazines/Bulletin/Bull401/ Date accessed: 6 Jan. 2007.

Organisation for Economic Co-Operation and Development (OECD): Nuclear Energy Agency. 1995. Physics of plutonium recycling, volume III: Void reactivity effect in pressurized- water reactors: Benchmark Results Analysis.
http://www.nea.fr/html/science/wppr/plutonium-recycling-vol3.PDF Date accessed: 20 Jan. 2007.

Organisation for Economic Co-Operation and Development (OECD): Nuclear Energy Agency. 2002. Physics of plutonium recycling, volume VI: Multiple Pu recycling in advanced PWRs. http://www.nea.fr/html/science/wppr/vol-6.html Date accessed: 19 Jan. 2007.

Organisation for Economic Co-Operation and Development (OECD): Nuclear Energy Agency. 2003a. Plutonium management in the medium term: A review by the OECD/NEA Working Party on the Physics of Plutonium Fuels and Innovative Fuel Cycles (WPPR). NEA 4451. http://www.nea.fr/html/science/docs/pubs/nea4451-plutonium.pdf Date accessed: 5 Jan. 2007.

Organisation for Economic Co-Operation and Development (OECD.): Nuclear Energy Agency. 2003b. G Hosking and T D Newton. Benchmark specification for an HTR fuelled with reactor grade plutonium (or reactor grade Pu/Th and U/Th). Nuclear Science Committee proposal, NEA/NSC/DOC(2003), 22, 12 Nov. 2003. http://www.nea.fr/listsmh/mox/doc00038.doc Date accessed: 4 Jan. 2007.

Organisation for Economic Co-Operation and Development (OECD.): Nuclear Energy Agency. 2007. J G Hosking and T D Newton. Physics of plutonium recycling, volume VIII: Results of a Benchmark Considering a High-temperature Reactor (HTR) Fuelled with Reactor-grade Plutonium. Nuclear Science Committee, NEA No. 6200.

Pellaud, Bruno. 2002. Proliferation aspects of plutonium recycling. Journal of Nuclear Materials Management. Fall 2002, volume XXXI, no. 1: 30-38. Icogne, Switzerland. http://www.inmm.org/topics/contents/fall02issue/pellaud.pdf Date accessed: 15 Jan. 2007.

Plukienë, Rita. 2003. Evolution of transuranium isotopic composition in power reactors and innovative nuclear systems for transmutation. Summary of the doctoral thesis Vytautas Magnus University, Institute of physics, Kaunas, Lithuania. http://www-dapnia.cea.fr/Phocea/file.php?class=std&&file=Doc/Publications/Archives/dapnia-03-12-T.pdf Date accessed: 9 Jan. 2007.

PUMA. 2010. Plutonium and Minor Actinide Management in Thermal High-Temperature Gas-Cooled Reactors: Publishable Final Activity Report. Project of the EURATOM 6-th Framework Programme. Document no. PUMA-1006-D411g, Nov. 2010. http://www.puma-project.eu Date accessed: Jan 2011.

Reitsma, F. and D. Naidoo. 2003. Evaluating the control rod modelling approach used in the South African PBMR: comparison of VSOP calculations with ASTRA experiments. Nuclear Engineering and Design, 222 (2003): 147–159. http://www.sciencedirect.com Date accessed: 2010.

Reitsma, Frederik. 2004. The Pebble Bed Modular Reactor Layout and Neutronics Design of the Equilibrium Cycle. PHYSOR 2004. The Physics of Fuel Cycles and Advanced Nuclear

Systems: Global Developments. Chicago, Illinois, April 25-29, 2004. Available on CD ROM from the American Nuclear Society, Lagrange Park, IL. (2004), or from the author at frederik.reitsma@pbmr.co.za

Reitsma, Frederik. 2011. Personal communication: Email (7 Jan. 2011) in which the internal design target of the maximum fuel temperature during normal operation of 1130°C for the PBMR DPP-400 is described, with reference to PBMR Internal Report 025491, Rev C, 2006.

Rineiski, A., G. Kessler. 2010. Proliferation-resistant fuel options for thermal and fast reactors avoiding neptunium production. Nuclear Engineering and Design, 240 (2010): 500–510. http://www.sciencedirect.com Date accessed: 25 Sept. 2010.

Ritch, John. 2007. Nuclear Power as a Global Imperative: Presenting the Case for Public Policy. Third Annual Summer Institute of the World Nuclear University. 24 Aug. 2007.

Rodriguez, C., A. Baxter, D. McEachern, M. Fikani, F. Venneri. 2003. Deep-Burn: Making nuclear waste transmutation practical. Nuclear Engineering and Design, Vol. 222 (2003): 299–317. http://linkinghub.elsevier.com/retrieve/pii/S0029549303000347 Date accessed: May 2007.

Rütten, H. J., K. A. Haas, H. Brockmann, W. Scherer and S Sen. 2007. V. S. O. P. (99/05) (Release 2): Computer Code System for Reactor Physics and Fuel Cycle Simulation. (October 15, 2007)

Salvatores, M., R. Hill, I. Slessarev and G. Youinou. 2004. The Physics of TRU Transmutation – A Systematic Approach to the Intercomparison of Systems. Proceedings of the PHYSOR 2004 topical meeting -The Physics of Fuel Cycles and Advanced Nuclear Systems: Global Developments. Chicago, Illinois, April 25-29, 2004, on CD-ROM, American Nuclear Society, Lagrange Park, IL.

Schulz, T.L. 2006. Westinghouse AP1000 advanced passive plant. Nuclear Engineering and Design, 236 (2006): 1547–1557. www.sciencedirect.com Date accessed: Oct. 2009.

Sen, S., F. Albornos and F. Reitsma. Comparison of VSOP and MCNP results of PBMR equilibrium core models. Proceedings HTR2006: 3rd International Topical Meeting on High Temperature Reactor Technology. October 1-4, 2006, Johannesburg, South Africa.

Slabber, Johan. 2004. Pebble fuel advantages. Paper B15, 2nd International Topical Meeting on High Temperature Reactor Technology. Beijing, China, September 22-24, 2004.

Serfontein, Dawid, Eben Mulder and Eberhard Teuchert. 2008. Proposal for an international experimental pebble bed reactor. Proceedings HTR2008: 4-th International topical Meeting on High Temperature Reactor Technology. 1-4 October 2008. Washington, D.C., USA.

Somers, J. 2007. Plutonium and Minor Actinide fuels for HTR. PUMA deliverable D211 of EU FP6 project. Report. nr. JRC-ITU-TPW-2007/01.

Stacey, Weston M. 2001. Nuclear Reactor Physics. John Wiley & Sons, Inc. New York.

Strydom, Gerhard. Xenon-induced axial power oscillations in the 400MWPBMR. Nuclear Engineering and Design, 238 (2008): 2960–2975.

Taiwo, T. A., M. Fatone, G. Palmiotti and R. N. Hill. 2002. Physics Studies for a Particle-Bed Gas Cooled Fast Reactor Core Design. Reactor Analysis and Engineering Division, Argonne National Laboratory, USA. Proceedings of the Conference on High Temperature Reactors: 1-5. Petten, NL, April 22-24, 2002. http://www.iaea.org/inis/aws/htgr/fulltext/htr2002_305.pdf Date accessed: 19 Jan. 2007.

Takano, H., Y. Fujine and J. Saito. 1990. Minor actinide transmutation in fission reactors. Proceedings of the First International Information Exchange Meeting on Actinide and Fission Product Separation and Transmutation 1990, Mito, Japan. Japan Atomic Energy Research Institute. http://www.nea.fr/html/pt/docs/iem/mito90/mit-4-03.pdf Date accessed: 23 Jan. 2007.

Talamo, Alberto, Waclaw Gudowski, Jerzy Cetnar and Francesco Venneri. 2004. Key physical parameters and temperature reactivity coefficients of the deep burn modular helium reactor fueled with LWRs waste. Annals of Nuclear Energy, 31 (2004): 1913–1937. http://www.sciencedirect.com Date accessed: 3 December 2007.

Tamada, Masao, Seko Noriaki, Kasai Noboru and Shimizu Takao. 2006. Cost Estimation of Uranium Recovery from Seawater with System of Braid Type Adsorbent. Transactions of the Atomic Energy Society of Japan, **V**ol.5; no.4: 358-363 (2006). http://sciencelinks.jp/j-east/article/200704/000020070407A0057435.php Date accessed: 12 Sept. 2010.

Teuchert, E., H.J. Rütten, H. Werner, K.A. Haas and R. Schulten. 1979. Closed thorium cycles in the Pebble Bed HTR. Kernforschungsanlage Jülich GmbH, Institut für Reaktorentwickling.

Tran, H.N. and Y. Kato. 2009. An optimal loading principle of burnable poisons for an OTTO refueling scheme in pebble bed HTGR cores. Nuclear Engineering and Design, 239 (2009): 2357–2364.

Tuˇcek, Kamil, Johan Carlsson and Hartmut Wider. 2006. Comparison of sodium and lead-cooled fast reactors regarding reactor physics aspects, severe safety and economical issues. Nuclear Engineering and Design, Vol. 236 (2006): 1589–1598. http://www.sciencedirect.com Date accessed: 30 May 2010.

Tyobeka ,Bismark, Kostadin Ivanov and Andreas Pautz. Evaluation of PBMR control rod worth using full three-dimensional deterministic transport methods. Annals of Nuclear Energy, 35 (2008): 1050–1055.

Venter, J.H. 2004. Fuel: German experience summary report. PBMR (Pty.) Ltd. Proprietary report, Class 2. Document Number: 020235.

Venter, J.H. and H. Nabielek. 2006. Fuel: Performance envelope of modern HTR TRISO fuel report. Proceedings HTR2006: 3rd International Topical Meeting on High Temperature Reactor Technology. October 1-4, 2006, Johannesburg, South Africa.

Westlén, Daniel. 2007. Why Faster is Better - On Minor Actinide Transmutation in Hard Neutron Spectra. PhD Thesis. KTH School of Engineering Sciences, Stockholm, Sweden. http://www.diva-portal.org/diva/getDocument?urn_nbn_se_kth_diva-4280-2__fulltext.pdf Date accessed: 21 May 2007.

Wikipedia. 2007. Yucca Mountain. http://en.wikipedia.org/wiki/Yucca_Mountain Date Accessed: 19 Jan. 2007.

World Nuclear Association. 2005. The New Economics of Nuclear Power. WNA report. http://www.world-nuclear.com/reference/pdf/economics.pdf Date accessed: 11 Sept. 2010.

World Nuclear News. 2009. Obama dumps Yucca Mountain. 27 February 2009. http://www.world-nuclear-news.org/newsarticle.aspx?id=24743 Date Accessed: 9 March 2009.

World Nuclear News. 2010. Uranium resources for at least a century. 20 July 2010. http://www.world-nuclear-news.org/newsarticle.aspx?id=28086&terms=uranium%20resources Date accessed: 11 Sept. 2010.

World Nuclear News. 2011. Germany hastens first reactor closures. 6 June 2011. http://www.world-nuclear-news.org/newsarticle.aspx?id=30154&terms=germany Date accessed: 9 July 2011.

6 APPENDIX: Automatic translation of VSOP-A input models to VSOP 99/05

Due to the fact that a large number of VSOP-A input models for different reactors, of which many were developed by E.J. Mulder, are available, there exists a need for the translation of these models to VSOP 99/05. Therefore the author wrote a C++ code in the Microsoft Visual Studio 2005 environment that automatically scanned the VSOP 99/05 manual (Rütten *et al*, 2007) for the format of all the input cards and for the names of the variables it contains. This code then wrote Fortran WRITE statements for Compaq Visual Fortran 6 (which largely conforms to Fortran 90) for each VSOP 99/05 card to a text file. These statements were manually copied to the VSOP-A Fortran code. After having read each VSOP-A input card from the input model, the VSOP-A Fortran code then used these WRITE statements to automatically translate the contents of each VSOP-A input card to the equivalent VSOP 99/05 input card model and to then write it to a new VSOP 99/05 input model. This process was complicated by the many discrepancies between the structure of the VSOP-A and VSOP 99/05 input cards.

6.1 Discrepancies between the VSOP-A and VSOP 99/05 input models

Unfortunately VSOP 99/05 does not have backward compatibility with the input models from VSOP-A: the collection of VSOP-A input cards contain many variables that were omitted from, or never existed in, the VSOP 99/05 input cards. By the collection of input cards are not meant the specific set of input cards in a specific reactor model, but rather the full set of possible input cards, as described in the respective input manuals (Mulder and Teuchert, 2006a; Rütten *et al*, 2007) of these codes. Sometimes the specific functionality in VSOP-A was perhaps viewed as too general and was therefore omitted in VSOP 99/05. At other occasions the functionality was retained but the variable that described the functionality was either hard-wired to a specific option in VSOP 99/05 or it was integrated into an extra option of an existing variable in VSOP 99/05. The VSOP 99/05 input cards also contain many new variables. Sometimes one variable with, for instance, four options in VSOP-A was split into a variable, with the same name in VSOP 99/05, but with only two options, plus a new variable which caries the remaining two options. In some cases a VSOP-A variable retained its name in VSOP 99/05, but its function changed and in other instances the name changed, but the function remained the same.

Seeing that VSOP-A had branched off from the line of codes which produced VSOP 99/05 since 1994, their manuals do not refer to each other and therefore do not document these differences. The author thus had to discover these by means of a detailed variable by variable comparison of the two manuals. In the cases where the new variables in VSOP

99/05 were in this way derived from existing variables in VSOP-A, the translation statements, which were added to the VSOP-A Fortran code, were designed to automatically transform the old variables into the new ones. In the cases where completely new variables with new functions were introduced in VSOP 99/05, the author selected the options that corresponded the closest to the approach which was used in the VSOP-A input model and hardwired this assigned values into the translation statements in the VSOP-A code. A warning line was then written to the newly created VSOP 99/05 input file to warn the user of this hard-wiring, so that the user would know to manually change this value in the VSOP 99/05 input model, if required. Since these new variables in the translation statements in the VSOP-A Fortran code were automatically introduced by the C++ code which created these statements from the VSOP 99/05 input manual, the danger was ever present that the author would miss the fact that a new variable was introduced and that these translation statements in the VSOP-A code would then write the undefined values of these new variables to the VSOP 99/05 input file, with potentially catastrophic consequences. Therefore the error checking options of the Fortran compiler were changed in order to create a warning whenever a variable in the VSOP-A code was used without it having been initialised first. This was done within the visual development environment, by using the Fortran tab in the Project menu, Settings dialog box by checking the “Uninitialized variables” option under Compilation Diagnostics.

Table 29 describes some of the new variables in VSOP 99/05 and the way in which they were hardwired in the translation statements in the VSOP-A code.

Table 29: Important new variables in VSOP 99/05

VSOP 99/05 Card: **Variable names**	**Rationale for assigning value of variable**
R6 (Restart card from VSOP-A Card R8): **NEWCOST** **INGC24** **NOBURNUP**	R6 is a Restart card and therefore is in another subroutine than R7. Therefore the declarations and initialisations for R7 do not apply to R6 and thus these were declared and initialised here. The following 'WARNING!' was written to the VSOP 99/05 input file: VSOP99:R6: "Hardwired": 'NEWCOST=0 because the option to define new cost parameters was not available in VSOP-A. INGC24_99=0 because the possibility of resetting the anisotropic diffusion coefficients (induced through NGC24) was not available in VSOP-A. NOBURNUP=0 in order to enforce burn-up calculation, because this was the only option available in VSOP-A'
R7: NOBURNUP	Declared and initialised NOBURNUP=0, so that burn-up will have to be performed. The following 'WARNING!' was written to the VSOP-A input file: 'VSOP99:R7: "Hardwired": NOBURNUP=0 in order to enforce burn-up calculation, because this was the only option available in VSOP-A'

6.2 C++ translation code for VSOP-A models to VSOP 99/05

These translation codes were created in the following way:

The original manual for the *V.S.O.P. 99/05 (release 2) Computer Code System for Reactor Physics and Fuel Cycle Simulation* (Rütten *et al*, 2007) was supplemented with comments. An extract from this file, beginning at the description of the input card *S1*, was then saved from Word to a plain text file, using a format that writes the different columns in each Word table below each other, indicating the end of each column by a Tab character.

A C++ code were then written in Microsoft Visual Studio 2005 to automatically identify and read the properties of each VSOP 99/05 input card from this text file:

- All comment lines were read and discarded, until the heading row of the first table was encountered. This line contained the card name and Format, e.g. "Card S1 Format (A4,3I4)". This columns was then called **Column 0**. All subsequent lines in Column 0 were then read and discarded, until a

tab-character was read, which indicated that the first of the three data columns of this Table, i.e. **Column 1**, will ensue in the next line.

- The Numeric Labels for each variable was then read from Column 1, e.g. 1, 2,… Each Numeric Label demarcated the Table Row in which the variable definition for the next variable started. This starting row number was identical for Column 1, Column 2 and Column 3, except that for some cards Column 2 or Column 3 had some lines, pertaining to the definition of Variable 1, which preceded the starting row number of the Numeric Label of Variable one. This anomaly regarding Variable 1 was circumvented in the following way:
  Suppose that the Numeric Label, i.e. "1" of Variable 1 started in Row Number 3 of Column 1, the Numeric Label of Variable 2 in Row Number 7 and that of Variable 3 in Row Number 12. It was then assumed that the definition of Variable 1 in Column 2 and Column 3 started earlier than in Column 1, i.e. already in Row Number 1, instead of 3, but ended in Row Number 6, just as in Column 1. For the ensuing Variables, the standard Row Number definitions from Column 1 was applied to Columns 2 and 3. However, for the last variable in each card, a similar extension in definition scope, as for Variable 1, was assumed, but this time downwards to the end of the Column 2 and 3, as indicated by the presence of a tab-character.

  Column 2 contained the Variable Names for each Variable, which were read from the Row Numbers of the scope of each variable, as described above. However the following anomaly was found in the use of a tab-character to indicate the borders between two Columns: at the border between Column 0 and Column 1, the tab-character in the text file was followed by garbage, which probably was the remnants from the text box that surrounded Column 0 in the table in the Word document. This was then discarded and the next line in the text file was defined as Row Number 1 of Column 1. However, at the border between Column1 and Column 2, the demarcation tab-character was found in a single line, which contained no garbage. The part before the tab contained the last Row of Column 1 and the part after the tab contained the first row of Column 2. Therefore this line had to be split into these two constituting parts, while the tab-character was only interpreted as the demarcating marker and was subsequently discarded. The same procedure was followed at the border between Column 2 and 3. However, at the tab indicating the end of Column 3, and therefore the end of that table, only the part of the line before the tab was retained and defined as the lae discarded.

- The following error in this structure were discovered and corrected:
  The original "vsop99_05_rel2_pbmr_dawid_2w.doc" had the problem that most lines in the columns were explicitly truncated by an end of paragraph marker. However, some lines in Column 3, the comment column, were not truncated in this way. They consisted of long paragraphs that contained only one paragraph marker at the end of several lines, which were automatically wrapped by Word to fit the column width. However, when this Word data were exported to the text file, as described above, Word did not export this wrapping, i.e. these paragraphs were written out as single long lines of text. This meant that all the lines below, in Column 3 of each affected Card, which in Word were pushed down by the wrapping of these long paragraphs, now moved up accordingly, thereby discarding the alignment between the three columns, which define each variable. This meant that the description of e.g. variable three would now be aligned with the numeric label and name of variable 2, which caused havoc in the automatic identification and association algorithms of described above.
  The affected long lines were therefore truncated manually by inserting end of paragraph markers in the same positions where Word's automatic wrapping occurred, thereby restoring the original alignment of the Word file in this text file. Since the pushing down of subsequent variables is not relevant if the long line occurred in the description of the last variable on the card, such cases were left unaltered.

This C++ code was then programmed to automatically compose and write the Fortran 90 WRITE statements, which contained the contents of each VSOP 99/05 input card, as it has been translated from the VSOP-A input card, to a new Fortran source code file. These Fortran statements were then copied manually into a new subroutine in the existing VSOP-A Fortran source codes: After having read each VSOP-A input card from a VSOP-A input model, VSOP-A then calls this subroutine which then writes this data out to a new VSOP 99/05 input model, using the WRITE-statements in this subroutine, which were automatically composed from the VSOP 99/05 manual, by the C++ code. This procedure was complicated by the fact that in many cases, one or more variables from a given VSOP-A input card were moved to different input cards in VSOP 99/05. This meant that when a given VSOP-A input card has been read by VSOP-A, its contents could not be written to the corresponding VSOP 99/05 input card, because this VSOP 99/05 input card might have contained some variables that belonged to a subsequent VSOP-A input card, and would thus only be read at a later stage. In these cases, the whole group of related VSOP-A input cards first had to be read, where after its contents was then to written to the corresponding group of VSOP 99/05 input

cards. This significantly complicated the programming, because these differences in the input card structures had to be determined manually, and without any warning of such discrepancies in the manuals of the two codes. A further complication was that variables names that are identical in the VSOP-A and VSOP 99-05 manuals, in many cases, differed from the actual names used inside the VSOP-A Fortran code. This meant that in these cases the WRITE statements that were automatically composed from the VSOP 99/05 manual referred to variables that did not actually exist in the VSOP-A Fortran code. This problem was solved by creating an in-between step in the VSOP-A code in which the contents of the actual VSOP-A variables were first copied to the newly created variables with the names stated in the manuals. This solved the nomenclature problem, so that the WRITE statements then functioned properly.

6.3 Manual corrections to automatically translated VSOP 99/05 models

In many places VSOP 99/05 uses quite different calculation methodologies, compared to VSOP-A. Therefore many VSOP-A variables refer to concepts that have been discarded in VSOP 99/05, while many new variables in VSOP 99/05 sometimes have no direct equivalent in VSOP-A. Therefore an automatic one-to-one mapping of the VSOP-A variables onto the VSOP 99/05 variables is in many cases not possible. In such cases, the values that would reproduce as closely as possible the original calculations in VSOP-A, were assigned to the new variables in VSOP 99/05. Therefore, after automatically translating the VSOP-A input model to VSOP 99/05, the following corrections were made manually.

6.3.1 Concatenation of IN-VOLMA, IN-DA2 and IN-HL

The VSOP 99/05 Fortran project produces a single executable file, which reads a single input text file. The VSOP-A system of codes, by contrast, consists of three separate Fortran projects which produces three independent executable files, i.e. BIR_A.EXE, DAT_A.EXE and VSOP_A.EXE, which each reads a separate input text file, i.e. IN-VOLMA or IN-BIR, IN-DA2 and IN-HL, respectively. The translation statements that were inserted into these three Fortran projects thus produce as output three corresponding VSOP 99/05 input files, i.e. IN99_VOLMA.i (or IN99_BIR.i), IN99_DAT.i and IN99_VSOP.i . These three files were therefore concatenated to produce the required single VSOP 99/05 input file.

6.3.2 Translation of definitions of reactor geometry

1. In the VSOP-A model, KANAL = 7 on card BI-2, which indicates that 7 channels are to be defined in the VSOP layout of the core. On cards BI-3 these channels are

defined as five core flow channels, bracketed by respectively the inner and outer reflector channel, which are also connected to the definition of the inner and outer conusses. The nomenclature also changed in that the VSOP-A manual speaks of a “conus”, while the VSOP 99/05 manual calls it a “cone”, with the plural “cones” (Mulder and Teuchert, 2006a; Rütten *et al*, 2007). The inner VSOP-A conus is defined at the end of the inner reflector channel definition and the outer conus at the end of the outer core flow channel definition, in conjunction with the outer reflector channel definition. The conus batches are defined on cards V11.

In VSOP 99/05, however, defining the reflectors and cones as channels are not allowed any more and thus KANAL defines only the number of **core flow** channels and is declared on card BI1, while these channels are defined on cards BI2. The geometry of the cones is defined on card BI6. Where VSOP-A allowed the possibility of different geometries for the inner and outer conusses, VSOP 99/05 uses a single radial thickness (RKONUS) and height (ZKONUS) to define both cones. The batches for these cones are defined on cards V7 – V9.

This discarding of two reflector channels were done by translation statements that were manually added to the VSOP-A Fortran code, so that the relevant cards in the translated VSOP 99/05 input file were reduced from:

```
  1    0   -1    7                    BI1
 -1    0    0                         BI2
  0   24    7                         BI2
  0   18    7                         BI2
  0   18    7                         BI2
  0   18    7                         BI2
  1   24    7                         BI2
 -1    0    0                         BI2
```

to:

```
  1    0   -1    5                    BI1
  0   24    7                         BI2
  0   18    7                         BI2
  0   18    7                         BI2
  0   18    7                         BI2
  1   24    7                         BI2
```

2. VSOP-A defines the radial coarse meshes for the outer parts of the reactor, in which the VSOP-layers and CITATION-compositions are congruent, on the single card BI-6, and those inside the core on the single card BI-9.

   VSOP 99/05 combines all these on the multiple cards BI3. The concept also changed significantly:

   (1) The concept of placeholder core coarse meshes on VSOP-A card BI-6 was omitted in VSOP 99/05 card BI3 and was replaced by the real core coarse meshes from VSOP-A card BI-9. This substitution was complicated by the fact that VSOP-A does not require that the number of placeholder core coarse meshes on BI-6 must correspond to the number of actual core coarse meshes in BI-9. In the current VSOP-A model, 5 core coarse meshes on BI-6 served as placeholders for 9 real core coarse meshes on BI-9.

   (2) A new variable, IOP(I) was introduced: If IOP(I)= 0 or 1, the coarse mesh falls within CITATION's neutron diffusion calculation, but if IOP(I)=2, it falls outside the neutron diffusion area and is used for THERMIX thermal flow calculations only. Since

VSOP 99/05 cards BI5 define only the CITATION material composition identification numbers, these THERMIX only meshes were dropped from BI5:

In VSOP-A, IMAX is defined as the total number of radial coarse meshes on card BI-6, i.e. place holder coarse meshes inside the core + the real coarse meshes surrounding the core, including those that lay outside the diffusion calculation area. IMAX is subsequently used to define the number of area id.-numbers in each card BI-8, which means that the cards BI-8 map the total reactor volume, but only as depicted on BI-6, ignoring the information for the core from BI-9.

In VSOP 99/05 the total number of radial coarse meshes on BI3 increased to four more that those on VSOP-A's BI-6 because the 5 placeholder core coarse meshes in BI-6 were replaced with the 9 actual core coarse meshes from VSOP-A's BI-9. However, in VSOP 99/05 the definition of IMAX is reduced to the total number of only those radial coarse meshes that falls within the CITATION diffusion calculation area.

3. The combining of VSOP-A's axial coarse meshes on BI-7 and its core axial coarse meshes on BI-10 onto VSOP 99/05's total set of axial coarse meshes on BI4 is done exactly analogously to the radial coarse meshes. Therefore BI-7's NMAX is also redefined in VSOP 99/05 to be the total number of only the axial coarse meshes within the diffusion calculation area, as depicted on cards BI4.

4. Where VSOP-A's cards BI-8 map, in a coarser grid, all the radial and axial coarse meshes from BI-6 and BI-7 for the total reactor, the VSOP 99/05 cards BI5 map, in a finer grid, only the CITATION diffusion calculation radial and axial coarse meshes from BI3 and BI4. Since this reduction to only the diffusion area is not yet coded into the automatic translation statements, VSOP-A's cards BI-8 were simply copied to VSOP 99/05's cards BI-5 during the automatic translation and therefore had to be modified manually. The following two approaches are relevant:

    a. In the PBMR Company's official PBMR DPP-400 VSOP 99/05 input model, the core barrel and the reactor pressure vessel were excluded from the CITATION diffusion calculation area. Thus the diffusion calculation area consisted only of the inner reflector + the fuel core annulus + the 90 cm thick external reflector. In order to compensate for the absorption of neutrons in the metals of the core barrel and the reactor pressure vessel, the region outside this diffusion calculation area was defined by means of an extrapolated length at which the flux is forced to zero. This extrapolated length was determined by means of transport calculations (Naicker, 2006). In this approach, the meshes

from the VSOP-A model that fell outside the VSOP 99/05 diffusion calculation area were deleted from the VSOP 99/05 cards BI5.

b. For the present study, the followed approach were used:
In the original VSOP-A model, the neutron diffusion calculations were extended over the whole reactor volume, including the core barrel and the reactor pressure vessel. Therefore the above-mentioned distinction between the diffusion calculation area and the non-diffusion calculation area did not apply. In order to avoid calculational difficulties, due to the sharp transition in the material compositions at the junction between the external reflector and the core barrel, the metals of the core barrel and reactor pressure vessel were mixed into the graphite in the material definitions of the outermost parts of the external graphite reflector, i.e. the part further out than the inner 90 cm of the external reflector.

In translating this model to VSOP 99/05 , the author wrote translation statements into the VSOP-A codes that included all these coarse meshes outside the core in the CITATION diffusion calculation area by assigning IOP(I) and NOP(I) =1 on VSOP 99/05's cards BI3 and BI4.

VSOP 99/05's cards BI5 were composed out of VSOP-A's cards BI-8 by manually duplicating the core rows and columns in order to reflect the substitution of the placeholder radial coarse meshes on VSOP-A card BI-6 and the axial ones on BI-7 with the larger number of real radial and axial core coarse meshes from BI-9 and BI-10 respectively.
The five placeholder radial core coarse mesh columns, which are shown below with core identification numbers indicated by zeros and the core rows and columns marked in bold, were duplicated over the whole axial length of the diffusion area, in order to increase these to the nine actual radial core coarse meshes from VSOP 99/05's BI3. This was done by duplicating the column on either side of the central core column twice, in order to maintain the radial symmetry of the core. Each number on cards BI5 occupies only three spaces, compared to four on VSOP-A cards BI-8, and therefore the extent of this expansion is not immediately obvious. Similarly, the axial coarse core mesh rows were also expanded by duplicating each core row once, working from the top and bottom towards the centre. The central row was duplicated

more times until the number of core rows corresponded to the axial core coarse meshes in VSOP 99/05 card BI4, i.e. 22.

Cards BI-8 from the VSOP-A input model

```
 62  62  62  62  62  62  62  62  62  62  16  63  63  63  63  63  64  95  95 BI-8
 89   2  76   1  66  66  66  66  66  66  16  67  67  67  67  43  64  94  95 BI-8
 89   2  76   1  55  55  55  55  55  55  16  54  54  54  54  43  64  94  95 BI-8
 89   2  76   1   3   3   3   3   3  11  16  28  33  33  33  43  64  94  95 BI-8
 89   2  77   1   4   4   4   4   4  11  17  38  38  38  33  43  64  94  95 BI-8
 90  59  78  88   0   0   0   0   0  12  18  29  34  39  96  44  64  94  95 BI-8
 90  59  79  88   0   0   0   0   0  12  19  29  34  39  96  44  64  94  95 BI-8
 90  59  80  88   0   0   0   0   0  12  20  29  34  39  96  44  64  94  95 BI-8
 91  60  81  56   0   0   0   0   0  13  21  30  35  40  97  45  64  94  95 BI-8
 91  60  82  56   0   0   0   0   0  13  22  30  35  40  97  45  64  94  95 BI-8
 91  60  83  56   0   0   0   0   0  13  23  30  35  40  97  45  64  94  95 BI-8
 92  61  84  57   0   0   0   0   0  14  24  31  36  41  98  46  64  94  95 BI-8
 92  61  85  57   0   0   0   0   0  14  25  31  36  41  98  46  64  94  95 BI-8
 92  61  86  57   0   0   0   0   0  14  26  31  36  41  98  46  64  94  95 BI-8
 92  61  87  58   0   0   0   0   0  15  27  32  37  42  99  47  64  94  95 BI-8
 93  58  58  58   6  10   5  10   7  15  15  32  37  42  99  47  64  94  95 BI-8
 93  72  72  72  68  10   5  10  69  70  70  70  70  71  70  47  64  94  95 BI-8
 93  58  58  58   8  10   5  10   9  48  48  48  49  52  49  47  64  94  95 BI-8
 93  73  73  73   8  10   5  10   9  74  74  74  75  75  75  47  64  94  95 BI-8
 93  58  58  58   8  10   5  10   9  48  48  48  49  49  49  47  64  94  95 BI-8
 93  58  58  58  53  53  53  53  53  50  50  50  50  50  50  47  64  94  95 BI-8
 93  58  58  58  51  51  51  51  51  50  50  50  50  50  50  47  64  94  95 BI-8
 65  65  65  65  65  65  65  65  65  65  65  65  65  65  65  65  64  95  95 BI-8
```

Translated cards BI5 in the VSOP 99/05 input model

```
62 62 62 62 62 62 62 62 62 62 62 62 62 16 63 63 63 63 63 64 95 95      BI5
89  2 76  1 66 66 66 66 66 66 66 66 66 66 16 67 67 67 67 43 64 94 95   BI5
89  2 76  1 55 55 55 55 55 55 55 55 55 55 16 54 54 54 54 43 64 94 95   BI5
89  2 76  1  3  3  3  3  3  3  3  3  3  3 11 16 28 33 33 33 43 64 94 95 BI5
89  2 77  1  4  4  4  4  4  4  4  4  4  4 11 17 38 38 38 33 43 64 94 95 BI5
90 59 78 88  0  0  0  0  0  0  0  0  0  0 12 18 29 34 39 96 44 64 94 95 BI5
90 59 78 88  0  0  0  0  0  0  0  0  0  0 12 18 29 34 39 96 44 64 94 95 BI5
90 59 79 88  0  0  0  0  0  0  0  0  0  0 12 19 29 34 39 96 44 64 94 95 BI5
90 59 79 88  0  0  0  0  0  0  0  0  0  0 12 19 29 34 39 96 44 64 94 95 BI5
90 59 80 88  0  0  0  0  0  0  0  0  0  0 12 20 29 34 39 96 44 64 94 95 BI5
90 59 80 88  0  0  0  0  0  0  0  0  0  0 12 20 29 34 39 96 44 64 94 95 BI5
91 60 81 56  0  0  0  0  0  0  0  0  0  0 13 21 30 35 40 97 45 64 94 95 BI5
91 60 81 56  0  0  0  0  0  0  0  0  0  0 13 21 30 35 40 97 45 64 94 95 BI5
91 60 82 56  0  0  0  0  0  0  0  0  0  0 13 22 30 35 40 97 45 64 94 95 BI5
91 60 82 56  0  0  0  0  0  0  0  0  0  0 13 22 30 35 40 97 45 64 94 95 BI5
91 60 83 56  0  0  0  0  0  0  0  0  0  0 13 23 30 35 40 97 45 64 94 95 BI5
91 60 83 56  0  0  0  0  0  0  0  0  0  0 13 23 30 35 40 97 45 64 94 95 BI5
91 60 83 56  0  0  0  0  0  0  0  0  0  0 13 23 30 35 40 97 45 64 94 95 BI5
91 60 83 56  0  0  0  0  0  0  0  0  0  0 13 23 30 35 40 97 45 64 94 95 BI5
92 61 84 57  0  0  0  0  0  0  0  0  0  0 14 24 31 36 41 98 46 64 94 95 BI5
92 61 84 57  0  0  0  0  0  0  0  0  0  0 14 24 31 36 41 98 46 64 94 95 BI5
92 61 85 57  0  0  0  0  0  0  0  0  0  0 14 25 31 36 41 98 46 64 94 95 BI5
92 61 85 57  0  0  0  0  0  0  0  0  0  0 14 25 31 36 41 98 46 64 94 95 BI5
92 61 86 57  0  0  0  0  0  0  0  0  0  0 14 26 31 36 41 98 46 64 94 95 BI5
92 61 86 57  0  0  0  0  0  0  0  0  0  0 14 26 31 36 41 98 46 64 94 95 BI5
92 61 87 58  0  0  0  0  0  0  0  0  0  0 15 27 32 37 42 99 47 64 94 95 BI5
92 61 87 58  0  0  0  0  0  0  0  0  0  0 15 27 32 37 42 99 47 64 94 95 BI5
93 58 58 58  6 10 10 10  5 10 10 10  7 15 15 32 37 42 99 47 64 94 95   BI5
93 72 72 72 68 10 10 10  5 10 10 10 69 70 70 70 70 71 70 47 64 94 95   BI5
93 58 58 58  8 10 10 10  5 10 10 10  9 48 48 48 49 52 49 47 64 94 95   BI5
93 73 73 73  8 10 10 10  5 10 10 10  9 74 74 74 75 75 75 47 64 94 95   BI5
93 58 58 58  8 10 10 10  5 10 10 10  9 48 48 48 49 49 49 47 64 94 95   BI5
93 58 58 58 53 53 53 53 53 53 53 53 53 50 50 50 50 50 50 47 64 94 95   BI5
93 58 58 58 51 51 51 51 51 51 51 51 51 50 50 50 50 50 50 47 64 94 95   BI5
65 65 65 65 65 65 65 65 65 65 65 65 65 65 65 65 65 65 65 64 95 95      BI5
```

5. **VSOP 99/05: Card BI6**. In VSOP-A, BIR_A.EXE was first run with an input file, in this case called IN-VOLMA, which defines a very fine grid (IZFEIN = 24000 and JRFEIN = 9000) for the purpose of accurately calculating the volume matrix. Once this volume matrix has been stored to the hard disk, BIR_A.EXE was rerun with a new input file, IN-BIR, which is identical to IN-VOLMA, except that uses a much coarser fine grid, in order to save on calculation time. VSOP 99/05, however, uses only a single input file and therefore the fine grid can only be specified once. Therefore the very fine grid from IN-VOLMA was used.

   The new VSOP 99/05 variable, KONUS, on card BI6 was also manually set = 2, in order to indicate that both an inner and an outer cone are defined.

6. **VSOP 99/05: Card BI7**. Since the inner and outer cone/reflector channels were omitted in VSOP 99/05, the corresponding first and last cards BI7 were also automatically omitted by the translation statements that were added to VSOP-A.

6.3.3 THERMIX calculations in the VSOP 99/05 model

In the original VSOP-A models, THERMIX were run from a separate input model, which used the restart file created by the preceding VSOP-A run as input. THERMIX then calculated an estimate of the equilibrium temperature distribution for the reactor. These temperatures were then manually copied into the VSOP-A main run input model and the process was repeated in an iterative manner until the temperatures and k_{eff} converged.

For the VSOP 99/05 calculations of the present study, two different approaches were used:

Firstly the converged equilibrium VSOP-A input models were translated to the VSOP 99/05 input model, as described above. This model was then executed in VSOP 99/05, without running THERMIX, i.e. the temperature distribution calculated by THERMIX in the VSOP-A run was retained. This was used to compare the results for VSOP-A and VSOP 99/05, for identical temperature distributions

In the second approach, the first approach was extended to run THERMIX from within the standard VSOP 99/05 main run input model by iteratively calling THERMIX from within the VSOP 99/05 input model. The 57.3 cm thick top axial coarse core mesh on card BI4 was subdivided into a 20.3 cm and a 37 cm core mesh, in order to be able to define the flow channel for the cooling gas. The corresponding row on cards BI5 was expanded correspondingly.)

This was used to compare the results of VSOP-A and VSOP 99/05, for the case where each code was allowed to calculate its own equilibrium temperature distribution.

6.3.4 Translation of GAM-I- and VSOP-identification numbers

IN VSOP-A the GAM-I-identification numbers (Mulder and Teuchert, 2006a: Table III) of all relevant nuclides are specified on card D2 as the elements of IMAT(I), I = 1, KMAT, with I the VSOP Id. number of each nuclide, according to the specific sequence of nuclide types specified in Table V (Mulder and Teuchert, 2006a). The series of 13 heavy metals (^{232}Th to ^{237}Np) appears first is this sequence and is fixed, but must nonetheless be specified explicitly in the input file.

In VSOP 99/05 this set of heavy metals on card D2 is extended to 28 (^{232}Th – ^{244}Cm) and therefore occupies VSOP-Id. numbers 1 to 28. However these are now hard-wired inside the code and therefore are not allowed to be explicitly specified as elements of IMAT(I) on card D2, as was the case in VSOP-A. Therefore, while the values of I remains I = 1, KMAT, each corresponding VSOP-Id. number changed to = I + 28. The GAM-I-Id. numbers and their

sequence, and thus the VSOP-Id. numbers, are listed respectively in Table II and Table IV in the VSOP 99/05 manual (Rütten *et al*, 2007).

Several of the GAM-I Identification numbers differ between the tables listed in the manuals of VSOP-A and VSOP 99/05. While these differences were initially thought to represent a newer version of the GAM-I-library, it was discovered during the present study that these differences were due to errors in Table III in the VSOP-A manual and that the VSOP-A code actually interprets the GAM-I-Identification numbers exactly as stated in Table II of the VSOP 99/05 manual. The only exception was that GAM-I = 150 is interpreted by VSOP-A as the compound "Dummy Poison in C", as correctly stated in the VSOP-A manual, while VSOP 99/05 does not accept GAM-I=150 as a valid entry since this Dummy Poison was omitted from the VSOP 99/05 code. It was also discovered that card D2 in the VSOP-A input models from the pilot study was not contaminated by these errors in the VSOP-A manual, i.e. they were already correctly based on the VSOP 99/05 manual. Therefore, during the translation to VSOP 99/05, these GAM-I Id.-numbers were retained, except for GAM-I = 150 (Dummy Poison in C) which was translated to GAM-I =4 (^{Nat}B), as described below. However, the positions in the sequence on card D2 were changed, in order to account for the discarding of the heavy metals from this card in VSOP 99/05. The following procedure was built into the VSOP-A system of codes in order to achieve this automatic translation:

(a) The VSOP-A GAM-I Identification numbers, read from the VSOP-A input model, were assigned to the variable GAM-I-A and the translated numbers to the variable GAM-I_99/05. Every GAM-I-A value that was read by the DAT-A code from card D2 as IMAT(I), I = 1, KMAT, was tested to see whether it fell in the list of heavy metals that were omitted in VSOP 99/05. If so, it was discarded by translating it to GAM-I_99/05 = 0, and by writing a corresponding warning to the VSOP 99/05 input file which was being created. However, if GAM-I-A = 150, it was translated to GAM-I_99/05 = 4 (natural Boron). The Dummy Poison in C nuclide concentrations in the reflector regions were also transformed to the equivalent concentrations of natural Boron as described in the next section. All this transformation data, created by the DAT-A module in the code, were stored in a translation matrix and written to a text file on the hard disk as a permanent transformation map to be read during the subsequent runs of VSOP-A.EXE.

(b) Since the GAM-I-A numbers on VSOP-A's card D19 were already correct, they were retained, except for GAM-I-A = 150. Initial efforts to transform these Dummy Poison in C concentrations in these fuel types to natural Boron, according to the transformation constant derived for the reflector regions (see next section), produced significant changes in the value of k_{eff} in the start-up core. This was probably due to the fact that the equivalent concentration

in the reflector regions was derived in a well-thermalised neutron spectrum and therefore was not applicable in the more epithermal spectrum in the fuel. This problem was circumvented by removing all these neutron poisons, including Dummy Poison in C, from all the fuel types in both VSOP-A and VSOP 99/05. (See next section.)

(c) The code deduces the VSOP-Id. nrs. from the sequence of the GAM-I-Id. nrs. on card D2. Subsequently, in, for instance, the VSOP 99/05 card V8 (for which the VSOP-A equivalent is card V12), these VSOP-Id. nrs are used to refer back to these GAM-I-Id. nrs. In VSOP-A the VSOP-Id.nr. is simply = I, with I the index in IMAT(I) on card D2.
Although VSOP 99/05 omitted the heavy metals from IMAT(I), since these are now hard-wired inside the code, they were not omitted from the list of VSOP-Id. nrs. Therefore the first nuclide after the heavy metals in VSOP-A, i.e. IMAT(14), with VSOP-A-Id.nr. = 14, should now be allocated to IMAT(1) in VSOP 99/05, with

$$\text{VSOP_99/05-Id. number} = 1 + 28$$
$$= \text{VSOP-A-Id. number} - 13 + 28$$

6.3.5 Translation of ^{238}Pu definitions

The VSOP-A input models from the pilot study defined ^{238}Pu as an additional fission product on cards V4, V8 and V9, in order to force the code to calculate its concentrations in the fuel. Since ^{238}Pu is now included in the standard list of 28 heavy metals in VSOP 99/05, and therefore was also omitted from IMAT, the simple transformation described above had to be expanded. Since ^{238}Pu is already included in the standard series of heavy metals and transmutation chains of VSOP 99/05, a re-definition of ^{238}Pu as a fission product was not allowable and thus had to be removed during the translation from VSOP-A to VSOP 99/05.

6.3.5.1 Removal of ^{238}Pu definitions from LEU fuel cycles

For the simulation of the LEU fuel cycles, the intention was merely to obtain the concentrations of ^{238}Pu in the spent fuel, for the purpose radiotoxicity and proliferation resistance calculations. Due to the very low concentrations of ^{238}Pu in the LEU cycles, its inclusion did not have a significant influence on k_{eff}. Since the presence of ^{238}Pu did not have a significant effect on k_{eff} in VSOP-A LEU fuel cycles, it was opted to remove this definition of ^{238}Pu as a fission product from these VSOP-A models, so that it would not necessary to devise a special way of removing it during the translation to VSOP 99/05. Since ^{238}Pu was thus removed from VSOP-A's card D2, KMAT had consequently to be reduce on VSOP-A cards D1 and V3. On VSOP-A card V4, NO had to be reduced from 45 to 44, indicating the replacement of this definition of ^{238}Pu as a fission product with the default handling of the built in fission product chain 44. Correspondingly KETT and NLT were reduced from 1 to 0

and cards V8 and V9 were deleted. The removal of ^{238}Pu from the sequence of nuclides on Card D2 caused all the VSOP-Identification numbers above it to move one position in order to fill its place, for instance the original VSOP-Id.-number of control poison (^{10}B with GAM-I=130), reduced from 59 to 58, etc. Therefore all the higher VSOP-Id.-numbers on cards V12 were reduced correspondingly. (For input models that featured the manipulation of nuclide concentrations during burn-up, e.g. the modification of control poison concentrations, the VSOP-Id.-numbers on the relevant cards would have had to be changed as well.)

Since the number of nuclides was reduced by one, the reprocessing factor for ^{238}Pu had to be removed from VSOP-A card R1.

Since ^{238}Pu was in this case not explicitly specified on cards T9 or T9A, it was not necessary to modify these cards. Once this definition of ^{238}Pu as a fission product was removed from the VSOP-A input models, it played no further part in the translation of these models to VSOP 99/05.

6.3.5.2 Translation of ^{238}Pu in Pu fuel cycles

In the Pu(PWR) VSOP-A fuel cycle, the fraction of ^{238}Pu was significant and therefore neutron capture in this fertile nuclide caused a significant loss of neutrons, so that its inclusion in the fresh fuel caused k_{eff} to be reduced by about 0.6%. Therefore ^{238}Pu's definition as a fission product had to be retained in die VSOP-A models, in order to be able to include it in fresh fuel. Therefore the following algorithm was developed for its automatic translation to VSOP 99/05:

- Initialise the counter for the nuclides on VSOP 99/05's card D2: **I_99/05 = 1**
- Loop through the elements of VSOP-A's IMAT(I).
- **If (GAM-I_99/05 = 0)** (i.e. the nuclide is an element of the set of 28 VSOP 99/05 heavy metals omitted in VSOP 99/05):
    - The nuclide is discarded from IMAT_99/05(I) and thus is not written to the translated VSOP 99/05's card D2.
    - Therefore the counter is not incremented.

- **Else:**
    - IMAT_99/05(I_99/05) = GAM-I_99/05
    - VSOP_99/05-Id. number = I_99/05 + 28
    - Increment I_99/05.
- **Repeat the loop**.

The highest value attained by I_99/05 was used to define KMAT_99/05 and was written to VSOP 99/05 card D1 and IMAT_99/05() to card D2. The corresponding values for VSOP-A and NSOP 99/05 were also written to the transformation matrix and stored on the hard disk.

Subsequent references to the VSOP-A-Identification numbers, for instance during the translation of VSOP-A card V12 to VSOP 99/05 card V8, was transformed by locating each VSOP_A-Id. number in the said transformation matrix and replacing it by the corresponding VSOP_99/05-Id. number.

Since the translation to VSOP 99/05 automatically omitted ^{238}Pu from the sequence of nuclides on Card D2, its definition as a fission product on VSOP 99/05's cards V1, V2, V4 and V5 were removed manually, just as in the case of the LEU cycle, described above.

Since ^{238}Pu is automatically included as a heavy metal in VSOP 99/05, it was simply retained in the definition of the VSOP 99/05 fuel types.

VSOP 99/05 card R1 contains the reprocessing factors for all the nuclides (the KTOT = 28 heavy metals + the KMAT (from card D1) non-heavy metal nuclides). Since the number of nuclides increased and the sequence of the nuclides changes from VSOP-A to VSOP 99/05, translation instructions were manually added to the VSOP-A code to automatically transfer these changes to the VSOP 99/05 input model, including dropping the reprocessing factor for GAM-I=150. For all these new heavy metals in VSOP 99/05, reprocessing factors of 1.00 were allocated, which correspond to perfect recovery during reprocessing.

6.3.6 Addition of new VSOP 99/05 card R14A

A new feature in VSOP 99/05 is that the new card R14A forces one to specify whether the temperatures will be read form the sets of cards R14 and R15, or will be read form alternative sources. An appropriate translation statement was added to the VSOP-A code, in order to insert card R14A, with IOPT = 0, which corresponds to the standard practice in VSOP-A.

6.3.7 Automatic admixture of graphite ("dummy") spheres

VSOP-A offers the feature of specifying automatic admixture of dummy spheres, i.e. fuel free graphite spheres, into a fuel type by specifying INDBK = 1.0 and BK > 0.0 on card D12 and a relevant value for ROBK on card R13. However, VSOP 99/05 does not offer equivalent variables and therefore this part of the fuel specification was lost during the initial automatic translation of the VSOP-A input model to VSOP 99/05. Since the original VSOP-A model used this feature for admixing dummy spheres to the Provisional Start-up fuel (Fuel type 3, variant 01), the translated start-up fuel did not contain these dummy spheres, and therefore k_{eff} for the VSOP 99/05 start-up core differed very much from that of the VSOP-A. Since there was no obvious way to automatically translate this feature to the VSOP 99/05 input model, the author circumvented the problem by adding an instruction to VSOP-A which warns the operator that this feature will not be translated automatically to the VSOP 99/05 input file. The operator is then advised to either stop the run and remove this feature from the VSOP-A input model, or continue and then add it manually to the translated VSOP 99/05 model afterwards.

For this study, the author replaced the use of a mixture of fuel and dummy spheres as start-up fuel with 100% fuel spheres, but with a lower fissile enrichment. The Provisional Start-up fuel was modified to 9 g LEU/sphere with a 5.33% fissile atomic density enrichment, in order to have an enrichment similar to the equilibrium core.

6.4 Replacement of Dummy Poison in graphite with natural Boron

The different types of commercial nuclear graphite contain low, but different, concentrations of impurities. The macroscopic capture cross-section, Σ_γ, for a specific type of nuclear graphite is therefore calculated as Σ_γ for natural graphite + the sum of Σ_γ for all of these impurities. VSOP-A allows for the approximation of the effect of the sum of all these impurities by a suitable concentration of a single pseudo nuclide called "Poison in C dummy" which was assigned the identification number 150 in both the GAM-I and the THERMOS libraries. Since both these libraries use the same identification numbers for this nuclide, this poison will be referred to as GAM-I-150, for short, in this thesis. (This nomenclature will be used for all nuclides, in order to distinguish these GAM and THERMOS identification numbers from the VSOP identification numbers, which are variably assigned on input card D2 of both VSOP-A and VSOP 99/05, and which differs between these two codes, because the codes use different numbers of heavy metals and because the heavy metals are not explicitly included in card D2 for VSOP 99/05.)

Sine VSOP 99/05 does not allow the use of GAM-I-150, the different impurities must either be included explicitly in the definition of the graphite compositions for the reactor and fuel, or must be replaced with an equivalent concentration of a suitable absorber, like ^{10}B or natural Boron (GAM-I-4). This last strategy was initially adopted in the translation of VSOP-A to VSOP 99/05 input models, using the following procedure:

In the reference PBMR-400 VSOP-A models from the pilot study GAM-I-150 was included on cards V12 in varying concentrations in the batches of the regions of the reflectors and reflector cones. This model produced a value of k_{eff} = 0.9997. The effect of GAM-I-150 on k_{eff} was investigated by changing its homogenised atom densities (in atoms/barn.cm) in the reflector and reflector-cones. During a test run, these densities, in only a number of regions, were decreased by about a factor two in order to test the sensitivity of k_{eff} to changes in the poison concentration. However this resulted in calculational instabilities and the run aborted automatically. This suggests that VSOP-A cannot handle sharp transitions in neutron poison concentrations in the reflectors. Calculational stability was regained by reducing all these initial GAM-I-150 densities by multiplying DEN by the same factor for all batches. This was repeated for factors 0.9 to 0.09 as shown in Table 30.

Table 30: k_{eff} as a function of GAM-I-150 concentration

Factor C_{150} in C_{150} * Atom density(DEN) of GAM-I-150	**k_{eff}**
1.0	0.9997
0.9	0.9999
0.5	1.0006
0.09	Calculation aborted

The equivalent concentration of natural Boron (B-Nat: GAM-I-4) to replace the GAM-I-150 was determined by replacing GAM-I-150 with GAM-I-4 on this same set of cards. Since B-Nat is a much stronger neutron poison than GAM-I-150, the original atom densities had to be reduced sharply. The original value of k_{eff} = 0.9997 was regained by varying these B-Nat concentrations, as shown in Table 31. The factor 5.9E-7was subsequently used to replace all GAM-I-150 concentrations in the reflector regions in the VSOP 99/05 input model with the equivalent ^{Nat}B.

Translation statements were also manually added to the VSOP-A code to remove all remaining references to GAM-I-150 from the translated VSOP 99/05 input model, such as the removing the corresponding card from the series of cards T10.

Table 31: k_{eff} as a function of B-Nat concentration

Factor C in C * Atom density(DEN) of GAM-I-4	k_{eff}
1.0E-7	1.0013
2.0E-7	1.0009
4.5E-7	1.0001
5.9E-7	0.9997

After die GAM-I-150 concentrations in the reflector regions were successfully converted to their equivalent ^{Nat}B-values, the same was attempted for the GAM-I-150 in the fuel elements, as specified on cards D19:

In the latest VSOP-A reference case model by E.J. Mulder ("RF06-OCT; 24/18...; 2D;400-MW;WITH SS316;4GR;7%BYPASS SIMUL;NORMAL FUEL") the impurities in the equilibrium fuel type (101), as originally specified for the PBMR-400 by the SGL Company, are mimicked by a combination of 1.51147E-08 nuclides/barn.cm ^{Nat}B and 0.343 E-10 nuclides/barn.cm of ^{135}Xe (GAM-I-87). In the other VSOP-A fuel types, a GAM-I-150 concentration of 0.317, relative to the graphite density, were used instead of this concentration of ^{Nat}B, except for the dummy fuel, which used a lower concentration of GAM-I-150. The only of these fuels relevant to this study was the Provisional Start-up fuel type (301). When this concentration of GAM-I-150 was transformed to ^{Nat}B, according to the conversion factor for the reflector regions, a ^{Nat}B concentration of only 0.97962E-08 nuclides/barn.cm was obtained. This underestimation is probably due to the fact that the conversion factor for the reflectors was determined in a strongly moderated neutron spectrum, while the spectrum in the fuel is much more epithermal. Since the composition of GAM-I-150 is quite different from Nat-B, it is to be expected that the energy dependence of its radiative capture cross-sections will differ. A possible solution to this problem is to replace these GAM-I-150 concentrations in these fuel types in Mulder's VSOP-A model by the ^{Nat}B concentration which he used in the equilibrium fuel, which means that no automatic conversion will have to be done by the code. However it was eventually decided to circumvent these problems by removing all these neutrons poisons from all the fuel types in

the VSOP-A input models, and consequently from the translated VSOP 99/05 input model. These poisons are deemed as not relevant in the equilibrium fuel, since they will in reality, to a large extent, have been burnt away by the time that equilibrium is reached. While they are in principle relevant to the start-up fuel, the start-up fuel was deemed as not important for the present study, since a detailed simulation of the start-up core falls outside the scope of this study. Therefore it was deemed acceptable to use start-up fuel which produced a start-up core for which k_{eff} fluctuated strongly during the initial burn-in phase, typically between 1.15 and 0.97. The perturbations in the burn-up pattern, produced by these unrealistic start-up conditions, were eliminated from the calculation of the last part of the burn-in sequence towards the equilibrium core by increasing the total number of operating cycles in the burn-in sequence from Mulder's standard 342 cycles to 522 cycles.

6.5 Corrections to the VSOP-A input model

After the manual corrections to the VSOP 99/05 input model were made, the VSOP 99/05 code was run and the output compared to that of the original VSOP-A model. Further discrepancies between the codes were then discovered. Modifications were then made to the VSOP-A input model, as described below, in order to compensate for these discrepancies. This modified VSOP-A model was then again translated to VSOP 99/05 and used for subsequent simulations.

6.5.1 Fission spectrum

In the original VSOP-A input model of the pilot study for the Pu(PWR) fuel cycle, the ^{235}U energy spectrum was selected for the fission source neutrons (i.e. MSTU = 5 on card G1). For the present study the ^{239}Pu spectrum was selected (MSTU = 11). This caused the equilibrium value for k_{eff} to decrease very slightly from 1.00478 to 1.00410.

6.5.2 Specification of x and y in Pu-O_x-C_y in VSOP-A

In the VSOP-A input manual card D10 is described as containing variables x and y as its 5-th and 6-th data entries, for the plutonium oxide/carbide (Pu-O_x-C_y) case, i.e. for INDBS = 7 on card D8. In order to accurately simulate experimentally measured atomic compositions of plutonium dioxide fuel, the input model from the pilot study used these entries to specify the Pu(PWR) mixture as $PuO_{2.05359}C_0$. However, upon inspection of the Fortran code it was discovered that these x and y entries on card D10 are in fact ignored by the code and that therefore these entries in the VSOP-A manual (Mulder and Teuchert, 2006a) are erroneous and should be removed. Therefore, in reality, cards D8 and D10 are identical in VSOP-A and VSOP 99/05, as is correctly depicted in the VSOP 99/05 manual (Rütten *et al*, 2007). The

option INDBS = 7 on card D8 selects PuO_2, and card D10 only contains the first four entries, which specifies the Pu isotopic fractions, i.e. ^{239}Pu, ^{240}Pu, ^{241}Pu and ^{242}Pu.

The superfluous x and y entries were removed from the VSOP-A input models for the present study, without any effect on the results. Since x and y do not appear in the VSOP 99/05 manual, they also were absent from the automatic translation code, and therefore no correction to this code was required.

6.5.3 Specification of the fissile enrichment for Pu

The VSOP-A manual (Mulder and Teuchert, 2006a) requires the specification of the fissile enrichment (ANR on card D7), irrespective of the fuel type, while the VSOP 99/05 manual (Rütten *et al*, 2007) specifies that ANR should be set to zero for the PuO_2 case, i.e. INDBS = 7 on card D8 (since the fractions of ^{239}Pu, ^{240}Pu, ^{241}Pu and ^{242}Pu are explicitly specified on card D10).

Through experimentation it was discovered that the value of ANR is irrelevant to VSOP-A's fuel composition calculations for the PuO_2 case, as is suggested by the VSOP 99/05 manual. Since explicitly specifying the enrichment, while the code in fact ignores it, could lead to erroneous human interpretations of the input models, ANR was reset to ANR = 0. in the VSOP-A model for the present study.

6.5.4 Specification of FUTYP on card T6

A potential pitfall regarding automated passing on of the fuel type parameters from DAT_A.EXE to the modules THERMOS, GAM and VSOP was discovered. On VSOP-A card T6 the parameter FUTYP can be used to specify the fuel type to be used in the geometry of THERMOS. The geometry of this fuel type, including the packing fraction of the coated particles, will then be read automatically by THERMOS from the data files written by DAT_A.EXE to the hard disk, instead of being respecified explicitly on card T7. However, in creating this FUTYP the last two digits of the full fuel element identification number, NFUTYP from card D6, are discarded: the fuel type identification numbers for two variants of the same main fuel type, for instance NFUTP = 601 and NFUTP = 602 will thus both be reduced to FUTYP = 6.0. Since only one identification number is used to pass the geometries of these two variants of fuel type 6, the differences between these, e.g. specification of a fixed heavy metal density, vs. specification of a fixed coated particle packing fraction, are necessarily lost in this automatic passing of data to THERMOS. (The same problem occurs when the fuel type geometries are passed automatically to ZUT on VSOP-A card Z3.) Therefore, in this study, the practice of specifying slightly varying fuel types as variants of a main fuel typed

was discontinued, in order to remove any ambiguity during the automatic passing of fuel type parameters to THERMOS.

6.5.5 Discrepancies between the interpretation of the heavy metal densities between VSOP-A and VSOP 99/05

In IN-DA2, the input model for DAT_A.FOR in the VSOP-A system of codes, for the Pu(PWR) case of the pilot study, option 1 in the VSOP-A manual (Mulder and Teuchert, 2006a: Table I) was originally used for the specification of the fuel spheres:

For the PuO_2, fuel type 601, the inner radius of the shell-type fuel zone (SRO = 1.8 cm on card D13) and the outer radius of the fuel zone (R1 = 2.5 cm) and the outer radius of the fuel sphere (R2 = 3 cm) was specified on card D12 and the homogenised heavy metal mass density in the fuel zone (ROSM = 0.073140 atoms/(barn.cm)) on card D13. From these parameters and from the radius (RK = 0.012 cm) and the mass density (ROBR1 = 10.129 g/cm^3) of the fuel in the fuel kernel on card D9 and from the thicknesses (cards D8 and D11) of the coatings of the TRISO coated particles (CPs), the code then calculated the coated particle packing fraction of the coated particles in the fuel zone and wrote these parameters to the output file (OU-DA2).

6.5.5.1 Differences in coated particle packing fraction and homogenised heavy metal density

From the specified heavy metal density, VSOP-A calculated the coated particle packing fraction = 0.17971.
When these input cards were automatically translated to the VSOP 99/05 input model, VSOP 99/05, however, calculated the packing fraction = 0.18452.
VSOP-A thus calculated the packing fraction 2.607% lower than VSOP 99/05.

Similarly, for its transfer of data to the VSOP_A module, DAT_A calculated the homogenised atom densities of the Pu isotopes lower, for instance ^{239}Pu was 2.608% lower, with the exception of ^{238}Pu for which it calculated exactly the same value as VSOP 99/05.

VSOP 99/05 calculated the total mass of heavy metals (HM) almost identical to the designed nominal value of 3 g heavy metal/fuel sphere at 3.0003 g heavy metal/sphere, of which 2.0630 g was fissile, yielding a fissile enrichment of 68.760%.
Again VSOP-A calculated the heavy metal content lower as 2.9220 g/sphere, of which 2.0092 g was fissile, corresponding to an enrichment of 68.761%.
It is thus clear that, while VSOP-A calculated the heavy metal content lower by 2.610%, the enrichments were virtually identical.

6.5.5.2 Analysis

These differences in the calculation and interpretation of the heavy metal content may be due to the fact that VSOP 99/05 includes ^{238}Pu in its list of heavy metals, while in VSOP-A it was defined as a fission product. Because of its more complete definition of the list of heavy metals, VSOP 99/05 will be used as the standard to which VSOP-A's interpretation of the heavy metals will be compared:

The homogenised heavy metal mass density in the fuel zone of the fuel sphere (ROSM on card D12) and the mass density of the fuel in the fuel kernel (ROBR1) were identically specified in both the VSOP-A and VSOP 99/05 models. While the VSOP-A manual does not clearly state what is included in these definitions, the difference between their calculated packing fractions suggests that the two codes interpret these densities differently.

In this case the 2.609 weight% ^{238}Pu was defined as a fission product in the VSOP-A model and its homogenised atom density in the fuel zone was specified on card D19. This 2.609% is almost exactly the magnitude of the differences in results between VSOP 99/05 and VSOP-A, listed above. It thus seems clear that differences in the way that ^{238}Pu is handled, are responsible for the differences in results. VSOP-A did not include ^{238}Pu in its output list of heavy metals when e.g. the fractional neutron absorptions were listed in the output file of the VSOP-module, OU-HL. Its contribution was therefore presumably included in the lumped absorptions of the unspecified fission products. From this it would seem logical that VSOP-A would not include this ^{238}Pu in its interpretation of the specified input homogenised heavy metal mass density in the fuel zone.

6.5.5.2.1 Correction to the VSOP-A packing fraction calculations

These discrepancies in the interpretation of the heavy metal density was circumvented by replacing option 1 for the fuel specification with option 2 in the VSOP-A manual (Mulder and Teuchert, 2006a: Table I), i.e. the explicit specification of the homogenised MH mass density in the fuel zone was replaced by explicit specification of the packing fraction of the coated particles in the fuel zone (FF1 on card D12), from which the code then calculates the homogenised heavy metal mass density. The packing fraction from VSOP 99/05's was therefore inserted into the VSOP-A model, i.e. FF1= 0.18452.

6.5.5.2.2 Results

VSOP-A now over estimated the homogenised heavy metal mass density in the fuel zone by 2.678%. However, all the other parameters were calculated correctly, including the individual homogenised atom densities and the total mass of heavy metals/fuel sphere. Since it is

clearly better to have correct nuclide densities, although their interpretation by the code as being either heavy metals or fission products may be incorrect, rather than the original case where the individual nuclide densities were incorrect, this method of fuel specification was used for all subsequent simulations in the present study.

6.5.5.3 Discrepancies between the interpretations of input and burn-up heavy metal densities in VSOP 99/05

6.5.5.3.1 Input heavy metal densities

VSOP 99/05's interpretation of the heavy metals in the fuel spheres was investigated further:

The input data for the VSOP-module, i.e. the output data of the DATA-2 module that were automatically saved on the hard disk and thus passed as input to the VSOP-module, for the 3 g/sphere Pu(PWR) case were analysed.
From the input-specifications for the fuel spheres, DATA-2 calculated the heavy metal content per fuel sphere = 3.0002 g.

The interpretation of thus value was then checked by reconstructing the contents of one fuel sphere from the homogenised atom densities reported in this DATA-2 output. Since the homogenisation calculations mix the void surrounding the average fuel sphere into the nuclide densities contained in that fuel sphere, the total volume of a single fuel sphere + the void surrounding it was obtained by calculating the physical volume of the fuel sphere from its radius and by dividing this volume by the fuel sphere filling fraction of 0.61. The masses of all the Pu isotopes in this fuel sphere were calculated from by multiplying this total volume with the associated nuclide densities. When these masses were added, a total heavy metal content of 3.0844 g was obtained, compared to 2.9992 g when ^{238}Pu was excluded from this summation. It is clear that the 0.0851 g ^{238}Pu which this sphere contained was responsible for this discrepancy. From this analysis it was further clear that the DATA-2 module in VSOP 99/05 excludes ^{238}Pu from its summation of the heavy metal content of a fuel sphere type.

6.5.5.3.2 Heavy metal densities in burn-up results

VSOP 99/05's interpretation of the masses in the output of its VSOP-module and specifically its burn-up results for the equilibrium core, was investigated:

Under the heading "PERFORMANCE DATA OF CYCLE", the data under the sub-heading "FUEL SUPPLY - DISCHARGE (KG/GWD(TH))" was investigated. All the heavy metal masses, supplied/GWD(TH) were added. The reciprocal of this sum is by definition the burn-up in GWD(TH)/kg_{HM} supplied. After conversion to MWD/T_{HM} this was compared and found to be only 0.07% larger than the burn-up listed under the same "PERFORMANCE DATA OF

CYCLE" heading as "AVG. BURNUP". This small difference is probably due to round-off errors. It is in any case clear that for the calculation of the burn-up, the VSOP-module includes ^{238}Pu in its summation of heavy metal masses. When this check was repeated for the Pu(PWR)+MA case, it was found that even the MA are included in this summation.

6.5.5.4 Conclusion on heavy metal nomenclature

From the above it is clear that VSOP 99/05 excludes ^{238}Pu and the MA from its summation of the heavy metal masses when the DATA-2-module calculates the input data for the VSOP-module, while the VSOP-module includes these when it sums the heavy metal masses for the calculation of the burn-up. In order to retain congruence between the data analysis in this thesis and the direct output of the code, this convention was retained in this study. In order to avoid ambiguity, this Pu heavy metal content, which excludes ^{238}Pu, was called Pu_{HM}, according to the following nomenclature for heavy metal:

In the bookkeeping for the mass of heavy metals for the specification of the heavy metal content of fresh fuel spheres, VSOP 99/05 include only those heavy metals that are specified on the input cards that describe the contents of the fuel kernels, i.e. cards D7 to D12. The heavy metals specified as homogenised atom densities on VSOP 99/05 Card D17 are thus excluded, for instance ^{237}Np, ^{238}Pu and all MA. The loadings of these MA are therefore also not affected by adjustment of the packing fraction of the coated fuel particles (FF1) or the homogenised heavy metal density in the fuel zone (ROSM) on card D12. The DATA-2-module thus treat these heavy metals as if they are impurities in the matrix graphite, although their distribution, i.e. in the fuel kernels, matrix graphite etc. can be specified for THERMOS on card T10. The output of the DATA-2-module consequently always underestimates the heavy metal content of the fuel sphere types. This becomes highly significant when significant quantities of other heavy metals are included in fresh fuel, as happened in the present Pu(PWR)+MA mixture. In this study this exclusive heavy metal definition was retained for the specification of fresh fuel types, i.e. Pu_{HM} refers to Pu excluding ^{238}Pu, as opposed to "Total Pu", which will refer to Pu_{HM} + ^{238}Pu and "Total HM", which will include all heavy metals.

However, when burn-ups are reported, the VSOP-module includes ^{238}Pu and the MA in its summation of the heavy metal mass supplied to the reactor.

6.5.6 Modifications to SUBROUTINE ZUT for the PuO_2-case

SUBROUTINE ZUT divides by DZERO, which has to do with the ^{238}U concentration and is therefore = 0.0 for the PuO_2-case. This causes a floating point error. Therefore the original DAT_A.FOR in the VSOP-A system of codes did not call SUBROUTINE ZUT for the PuO_2-case (i.e. if INDBS = 7). Since ZUT processes the double heterogeneity data and writes

these data to the output file (OU-DA2) and to the data files on the hard disk that is later read by VSOP_A.FOR, not calling it meant that several parameters, including the radius of the fuel kernel were not initialised and were thus stored as 0.0. Since this could potentially have had serious consequences, the author tried to correct this: Mr. Frederik Reitsma confirmed that the VSOP 99/05 code does indeed call ZUT for the PuO_2 case. Therefore DAT_A.FOR was modified for the present study to do likewise. The division by zero error was circumvented by means of an IF statement that only executes this division by DZERO if DZERO > 0.0.

Comparisons of the output files before and after this modification confirmed that this change did solve the problem of incomplete output without changing the calculated results. It is thus clear that the results of the original version were not negatively affected by not calling ZUT.

6.5.7 Differences in treatment of ^{234}U

VSOP-A card D1 has an option (IU4) for including or excluding the small contribution of ^{234}U from fresh fuel (Mulder and Teuchert, 2006a). VSOP 99/05 has no such option and the treatment of ^{234}U is not discussed in its manual (Rütten *et al*, 2007). The Pu-fuel used in this study contained no ^{234}U. However comparison of the VSOP output files revealed that VSOP 99/05 listed very small atomic densities for ^{234}U (in the order of 1E-13 nuclides/(barn.cm^2)) and still lower densities for the other uranium isotopes above it in the core. This is in contrast with VSOP-A which listed these nuclide densities as zero, in spite of the fact that the option for the inclusion of ^{234}U in the fresh fuel was switched on. It is thus clear that VSOP 99/05 is hardwired to calculate the contribution of ^{234}U in more detail than VSOP-A. Since the fresh Pu-fuel contains no ^{234}U, it probably came from $\alpha-$ decay of ^{238}Pu. The higher U-isotopes then probably come from radiative capture of neutrons by this ^{234}U etc. Since these concentrations were so small, the fact that VSOP-A discarded them was deemed as insignificant and was therefore ignored.

6.5.8 Batch and storage box volume fluctuations during fuel shuffling

6.5.8.1 Method

At the first glance, the definitions of the fuel shuffling procedure on VSOP-A cards R24 (or VSOP 99/05 cards R21) seem straight forward. However, the author discovered that these definitions are complex and un-transparent and that they do not define the volumes of the fuel batches in the core flow channel layers and of the storage boxes constantly throughout the fuel cycle:

For the modified three-pass fuel cycle used in the pilot study, the fuel shuffling from the Fresh Fuel Store (FFS) into the fuel Batches in the top Layer of each Flow Channel (Ch), the downward flow to the next Layer with each fuel shuffling, emptying of the bottom Layer into the Storage Boxes (STB) and recirculation to the top of the reactor in the modified 3-pass fuel cycle was defined by the following VSOP-A cards:

```
    1 1.453616E+6  -601          1.                                R5: FFS(1)
```

and

```
   1                    1   1                  0.066668           R24: Ch(1)
   210001                                      0.066668           R24
   310002                                      0.066668           R24
   4                    1   1                  1.0                R24
  93   89                                                         R24
  94   90                                                         R24
  95   91                                                         R24
  96   92                                                         R24
  97                   1   1                  0.266665           R24: Ch(2)
  9810001                                     0.266665           R24
  9910002                                     0.266665           R24
 100                   1   1                   1.                R24
 165  161 1                                                      R24
 166  162 2                                                      R24
 167  163                                                        R24
 168  164 1                                                      R24
 169                   1   1                  0.266665           R24: Ch(3)
 17010001                                    0.266665           R24
 17110002                                    0.266665           R24
 172                   1   1                   1.                R24
 237  233 1                                                      R24
 238  234 2                                                      R24
 239  235                                                        R24
 240  236 1                                                      R24
 241                   1   1                  0.266665           R24: Ch(4)
 24210001                                    0.266665           R24
 24310002                                    0.266665           R24
 244                   1   1                   1.                R24
 309  305 1                                                      R24
 310  306 2                                                      R24
 311  307                                                        R24
 312  308 1                                                      R24
 313                   1   1                  0.133336           R24: Ch(5)
 31410001                                    0.133336           R24
 31510002                                    0.133336           R24
 316                   1   1                   1.                R24
 405  401 2                                                      R24
 406  402                                                        R24
 407  403                                                        R24
-408  404 2                                                      R24
```

A representation of the fuel shuffling defined in these cards for the central flow channels (Ch(2), Ch(3) and Ch(4)) are displayed in Table 32.

Table 32: Shuffling of fresh fuel into the batches of the central flow channels (Ch(2), Ch(3) and Ch(4)), flowing down into the storage boxes (STB()) and recirculation to top of channels, for a standard 3-pass fuel cycle.

1-st Batch	**2-nd Batch**	**3-rd Batch**	**4-th Batch**
0.266665 * FFS	**0.266665 * STB(1)**	**0.266665 * STB(2)**	**1.0 * FFS**
STB(1)	**STB(2)**	**Spent Fuel Tank**	**STB(1)**

The key to the interpretation of these cards R24 is:

In the actual input model for VSOP-A, several fresh fuel stores were defined, for potential use in fuel cycles where more than one fuel type would be mixed. However, in this fuel cycle only one Fresh Fuel Store, i.e. FFS(1) was used. Therefore, for the sake of brevity, FFS(1) was, form this point onwards, replaced by FFS.

For this standard 3-pass fuel cycle, the volume of FFS was defined as:

FFS = (Sum of the volumes of the first Layer in each of the 5 Flow Channels) / 3

It should, however, be noted that the volumes of the different flow channels are not identical, i.e. each of the three central Flow Channels have the same volume:

Ch(2) = Ch(3) = Ch(5) = 0.266665 * Volume of the fuel core.

For the smaller internal and external Flow Channels:

CH(1) = 0.066667 * Fuel core volume

CH(5) = 0.133333 * Fuel core volume

Since there are four fuel Batches/Layer and since Ch(1), the inner flow channel next to the central reflector, and Ch(5), the outer flow channel next to the external reflector, contains 24 layers each and the central flow channels (Ch(2), Ch(3) and Ch(4)) only 18 Layers each, the numbering of the Batches are as follows:

Ch(1), 1-st Layer = Layer(1): 1-st Batch = Batch(1),…, 4-th Batch = Batch(4),…,

24-th Layer = Layer(24): 1-st Batch = Batch(137),…, 4-th Batch = Batch(140).

Ch(2): 1-st Layer = Layer(25): 1-st Batch = Batch(97), …, 4-th Batch = Batch(100),…

18-th Layer = Layer(42): 1-st Batch = Batch(165),…, 4-th Batch = Batch(168).

.

.

Ch(5): 1-st Layer = Layer(79): 1-st Batch = Batch(313), …, 4-th Batch = Batch(316),…

24-th Layer = Layer(102): 1-st Batch = Batch(417),…, 4-th Batch = Batch(420).

The flow patterns for the 1-st Batch for all three central flow channels are identical, and also for the 2-nd to 4-th Batches. However, the fact that, for instance the 1-st Batch, in Ch(2) is numbered differently from the 1-st Batches in Ch(3) and Ch(4) obscures this symmetry in cards R24. Therefore the real batch numbers was replaced with 1-st Batch, 2-nd Batch etc. in the schematic representation in the table above.

The code treats the volume of FFS as infinite, i.e. not depletable, and therefore FFS serves only as a unit of measurement for the definition of the volumes to be loaded into the different Batches. The volume of each Layer is fixed and is uniquely defined by the definition of the core geometry in BIRGIT. However the volume of each of the four Batches in each Layer is variable and is only constrained by the fact that the sum of the volumes of all four batches must be equal to the fixed volume of the Layer. The volume of only the 1-st Batch in each Layer is constant and uniquely determined on cards R24 as a fixed fraction of the fixed volume of FFS.

The volumes of the 2-nd and 3-rd Batches depend on the volumes of STB(1) and STB(2) respectively. However the volume of any STB at the beginning of every fuel shuffling is variable and is redefined during every fuel shuffling as the total volume of fuel that was loaded into it from all the flow channels during the preceding fuel shuffling. Therefore, in order to know the volume of any STB for a given fuel shuffling, the complete volume history of all the preceding fuel shufflings of all channels must to be known. Once the volume of the STB is defined, the code will treat it as depletable during the following reload, after which it

will be redefined.

While the volume of the 2-nd and 3-rde Batches are fixed fractions of the variable STB volumes, the volume of the 4-th Batch is a variable fraction of the fixed FFS. This fraction is recursively defined by the constraint:

Volume of the 4-th Batch = Fixed Volume of the Layer

- **the variable volumes of (1-st Batch + 2-nd Batch + 3-rd Batch)**

The volumes of the 2-nd and 3-rd Batches are in some cases difficult to assess intuitively, since full prior knowledge of the pre-history of all Batch volumes are required and therefore the volume of the 4-th Batch then defies all intuitive assessment:

In a simple 3-pass fuel shuffling, the volumes of the first three batches in a Layer would typically be defined to be just smaller that a third of the fixed Layer volume and therefore the 4-th batch would then be tiny and would be used only to compensate for any round off errors in the calculation of the these first three batches. In such a simple model $STB(1) \approx STB(2) \approx FFS(1)$ and therefore these cards become easy to interpret intuitively.

In the Pu-case of the pilot study, however, the fuel shuffling was complicated by the fact that the burn-up proceeded faster in Ch(5), due to very large thermal fission cross-sections of ^{239}Pu and ^{241}Pu and the influx of thermal neutrons from the external reflector and even faster in Ch(1) next to the central reflector. Therefore the 1-st pass, 2-nd pass and 3-rd pass fuel Batches all reached their target burn-up during the a single pass through Ch(1) and was therefore directed to the spent fuel tank upon exiting from the bottom of this Channel. In Ch(2) only Pass(2) and Pass(3) were similarly directed to the spent fuel, while Pass(1), i.e. the 1-st Batch + the 4-th Batch is directed to STB(2), instead of to the usual STB(1). Therefore STB(1) is deprived of all input from CH(1) and Ch(2) and therefore STB(1) < FFS.

Therefore the 2-nd Batch in every Channel < 1-st Batch.

Due to similarly losses STB(2) < STB(1) and thus the 3-rd Batch < 2-nd Batch.

All these losses of volume is then compensated by a significant automatic increase in the volume of the 4-th Batch, due to the constraint that the sum of the volumes of the four Batches must equal the fixed volume of very Layer.

All of this is complicated every time the fuel shuffling is redefined (on a new set of cards R24) within a sequence of operating cycles. In this case this applies to the transition from the 1–st

static core that was defined via cards V11 to the first fuel shuffling defined on the 1-st set of cards R24:

On cards V11 all four Batches in every Layer was defined equally, i.e. it contained a quarter of the Layer volumes. As mentioned above, the intended volumes for the 1-st, 2-nd and 3-rd Batches in each Layer, in the simple 3-pass fuel shuffling, is simply a third of that Layer, with the 4-th Batch volume negligible. When reshuffling started, these 1-st core Batch volumes, which differed from the intended volumes, then distorted the volumes of the STB's. The 1-st + 4-th Batches, of each Flow Channel, which were directed to STB(1), then contained half of each respective Layer, instead of the intended third. Since STB(1) was thus defined too large, the 2-nd Batches at the top of the Channels were also defined to large. However STB(2) were initially filled with only a quarter of each Layer, instead of a the intended third, and were thus defined too small. Therefore the 3-rd batches of all five Flow Channels were loaded too small, which recursively affected the 4-th batch etc. However, the 1-st Batches of each Flow Channel were not affected by these unintended variations in volume, and were thus defined to a third of the Layer volume, as intended. As these 1-st Batches eventually exited the Flow Channels and got loaded into STB(1), the volume of STB(1) was gradually reduced to the intended volume, which then began to corrected the volumes of 2-nd Batches, etc. The magnitudes of the initial errors were thus gradually diluted. These recursive errors affected the ratio of fresh fuel to older fuel in the core and thus distorted k_{eff} and the shape of the neutron flux and therefore the burn-up pattern and thus the spectrum calculation, which probably perpetuated this error, even after all the Layers of the 1-st core have been removed from the core and all the volumes have been restored to their equilibrium values. The author indeed noted that small distortions in the volumes of the Batches persisted even up to the equilibrium core (Operating Cycle 342) of the standard 6-pass fuel shuffling for VSOP-A simulation of the LEU core in the PBMR-400. However, these did not affect k_{eff} close to the equilibrium cycles significantly and the author indeed observed perfect convergence of k_{eff} when the number op operating cycles were increased to 458. (The PBMR Company did not use this recursive definition for the last batch in their VSOP 99/05 model for the PBMR DPP-400. Therefore their equilibrium batch volumes are defined identical to the volumes of the first core and therefore do not suffer from this problem.) However, due to the extra distortions derived from the fuel losses due to the faster burn-up in Ch(1) and Ch(5), the volume fluctuations were much larger for this Pu-cycle and indeed caused small, but significant, fluctuations in k_{eff} up to the equilibrium core, as will be shown below.

The author solved this problem by deriving and solving a set of equations that uniquely satisfies the recursive definitions of the Batch volumes on the cards R24 above. An extra 81

fuel shufflings were then inserted before these cards R24. These churned the problematically defined first core Layers, with their deviant Batch volumes, out of the core and filled all batches with fresh fuel with the calculated equilibrium volumes and performed the spectrum and diffusion calculations. When the normal cards R24 started, all STB's were therefore filled with their intended equilibrium volumes and thus none of the above mentioned distortions occurred.

The fuel shufflings for Ch(1) and Ch(2) are summarised in Table 33 and Table 34 respectively.

Table 33: Shuffling of fresh fuel into the batches of the inner flow channel next to the central reflector, Ch(1), flowing down and out into the spent fuel tank, for the modified 3-pass Pu-fuel cycle.

1-st Batch	**2-nd Batch**	**3-rd Batch**	**4-th Batch**
0.066668 * FFS	0.066668 * STB(1)	0.066668 * STB(2)	1.0 * FFS
Spent Fuel Tank	Spent Fuel Tank	Spent Fuel Tank	Spent Fuel Tank

Table 34: Shuffling of fresh fuel into the batches of the flow channel next to the external reflector, Ch(5), flowing down into the spent fuel tank and into the STB(2), with recirculation to top of channels, for the modified 3-pass Pu-fuel cycle.

1-st Batch	**2-nd Batch**	**3-rd Batch**	**4-th Batch**
0.133336 * FFS	0.133336 * STB(1)	0.133336 * STB(2)	1.0 * FFS
STB(2)	**Spent Fuel Tank**	**Spent Fuel Tank**	**STB(2)**

From these three tables, the following set of equations for the recursive definition of the Batch volumes was derived:

Definitions

For a simple 3-pass cycle, for which FFS was originally defined, each pass fills a third of the volume of the 1-st Layer, summed over all five Flow Channels:

FFS = [$\sum_{i=1}^{5} First\ Layer(Ch(i))$] / 3

1-st Batch Sum = $\sum_{i=1}^{5} First\ Batch\ in\ First\ Layer(Ch(i))$

For the modified 3-pass fuel cycle described in the three tables above, the volumes of the Batch sums, which is the volumes for the standard 3-pass fuel cycle minus reduction by early exit to the spent fuel tank, can be added over all five Flow Channels from the three tables above. Since in the simple 3-pass fuel cycle, the volume of the 4-th Batch is negligible during the equilibrium cycles, it will initially be ignored here. The reduced volumes then become:

1-st Batch Sum = 1.0 * FFS

2-nd Batch Sum = STB(1) = 3 * 0.266665 * FFS = 0.799995 * 1-st Batch Sum

= 0.799995 * FFS

3-rd Batch Sum = STB(2) = 3 * 0.266665 * STB(1) + 0.133336 * FFS

= 0.639992 * FFS + 0.133336 * FFS

= 0.773328 FFS

This can now be summed over the top Layers of all the Flow Channels:

$\sum_{i=1}^{5} First\ Layer(Ch(i))$ = 1-st Batch Sum + 2-nd Batch Sum + 3-rd Batch Sum

= 2.573323 * FFS

But, since in order to fill the fixed volumes of these Layers,

$\sum_{i=1}^{5} First\ Layer(Ch(i))$ should = 3.0 * FFS, the 4-th Batch in every Layer of the modified 3-pass fuel cycle will then automatically increase in volume in order to fill these Layers. This will then create the unwanted oscillations in Batch volumes described above. The author,

however, circumvented this problem by defining a volume correct ion factor that would enable the first three Batches to fill all these Layers:

Volcor = 3.0 / $\sum_{i=1}^{5} First\ Layer(Ch(i))$ = 3.0 / 2.573323 = 1.1658078

The true volumes of the Batches in the modified 3-pass Pu fuel cycle is thus obtained by applying this volume correction to the set of reduced volume equations above, in order to yield:

1-st Batch Sum = 1.0 * FFS * Volcor

= 1.1658078 *FFS

2-nd Batch Sum = STB(1) = 3 * 0.266665 * FFS * Volcor = 0.799995 * 1.1658078

= 0.9326404 * FFS

3-rd Batch Sum = STB(2) = 0.773328 FFS * Volcor

= 0.9015518 * FFS

These corrections were applied in the following way in VSOP-A:

The start-up core, which was formed with each of the four Batches in each Layer containing a quarter of the volume of each Layer, were churned out into the spent fuel tank by loading all four Batches in the top Layer of every Flow Channel from the FFS with the corrected Batch volumes. On the Cards R24, the volume fractions from Table 32 to Table 34 were modified in the following way: all STBs were replaced with FFS and the corrections from the equations above for the 1-st, 2-nd and 3-rd Batches were applied, to yield the volume fractions in Table 35 to Table 36.

Table 35: Shuffling of fresh fuel into the batches of the central flow channels (Ch(2), Ch(3) and Ch(4)), flowing down into the storage boxes (STB()) and recirculation to top of channels, for a the replacement of the start-up fuel core in the modified 3-pass Pu fuel cycle.

1-st Batch	**2-nd Batch**	**3-rd Batch**	**4-th Batch**
0.266665 * 1.1658078 *FFS	0.266665 * 0.9326404 * FFS	0.266665 * 0.9015518 * FFS	1.0 * FFS
Spent Fuel Tank	Spent Fuel Tank	Spent Fuel Tank	Spent Fuel Tank

Table 36: Shuffling of fresh fuel into the batches of the inner flow channel next to the central reflector, Ch(1), flowing down and out into the spent fuel tank, for a the replacement of the start-up fuel core in the **modified** 3-pass Pu fuel cycle.

1-st Batch	**2-nd Batch**	**3-rd Batch**	**4-th Batch**
0.066668 * 1.1658078 *FFS	0.066668 * 0.9326404 * FFS	0.066668 * 0.9015518 * FFS	1.0 * FFS
Spent Fuel Tank	Spent Fuel Tank	Spent Fuel Tank	Spent Fuel Tank

Table 37: Shuffling of fresh fuel into the batches of the flow channel next to the external reflector, Ch(5), flowing down into the spent fuel tank and into the STB(2), with recirculation to top of channels, for a the replacement of the start-up fuel core in the modified 3-pass Pu fuel cycle.

1-st Batch	**2-nd Batch**	**3-rd Batch**	**4-th Batch**
0.133336 * 1.1658078 *FFS	0.133336 * 0.9326404 * FFS	0.133336 * 0.9015518 * FFS	1.0 * FFS
Spent Fuel Tank	Spent Fuel Tank	Spent Fuel Tank	Spent Fuel Tank

Since these corrected volumes for the 1-st to 3-rd Batches filled the whole volume of each Layer, the 4t-th Batches shrunk back to insignificant volumes, representing only the round-off errors in the Batch volume calculations, as was its original purpose.

After this fuel cycle was set up, a sufficient number of fuel shufflings were performed in order to send the whole start-up core to the spent fuel tank. A new fuel cycle was then defined, in order to load the Storage Boxes with the correct equilibrium volumes. For this fuel cycle the

volume fractions of Table 35 to Table 37 were retained, but the STBs of Table 32 to Table 35 were reinstated. One fuel shuffling was used to fill the STBs with these corrected volumes.

Lastly the equilibrium cycle was defined:

For the 1-st Batches the corrected volume fractions from Table 35 to Table 37 were retained. For the 2-nd and 3-rd Batches the filling pattern from the STBs from Table 32 to Table 35 were restored. Since the volumes of these STBs were already corrected by the above procedure, no further corrections were needed and thus the original volume fractions from Table 32 to Table 35 were restored. From this point onwards the burn-in procedure commenced in order to produce the correct burn-ups for the equilibrium cycle.

The efficiency of these volume corrections was checked by monitoring the volumes of the different Batches under the heading “BATCH VOLUME” in the “global neutronic balance” in the VSOP-A output file, which was produced by setting the output option IPRIN(3)=-1 on Card R9.

Corrections for the 6-pass fuel cycle were deduced in similar manner.

6.5.8.2 Results

These corrections solved the problem. This was indicated by the fact that the first correction procedure stabilised the volumes of the 1-st to 3-rd Batches to their equilibrium values, where they remained up to the equilibrium cycle. This was confirmed by the fact that first correction restored the volumes of the 4-th Batches to insignificant values, where they remained.

Before these volume corrections were applied, k_{eff} over the last 176 burn-up cycles would not converge perfectly, but rather repeatedly oscillated between the same values with an amplitude of 0.00011. However when the volumes were corrected, k_{eff} converged perfectly.

6.5.8.3 Conclusion

A small, but significant oscillation persisted up to the equilibrium core, but this disappeared completely once the volumes of the batches and STB’s were corrected.

7 Appendix: Miscellaneous methods and data

The following methods and data do not form part of the original contribution of this study, and are therefore not intended for examination with regards to the determination of whether this study made an original contribution. These methods and data were inherited and were used "as is" and therefore does not form part of the student's own contribution. However, they are included for the sake of clarity as to the methods that were used to produce some of the results shown in the main document and because they may form the basis of future studies.

7.1 Discussion of the differences between VSOP-A and VSOP 99/05 LEU results.

At the beginning of the study, an attempt was made to reconcile the LEU results for the VSOP-A and VSOP 99/05 codes. A long list of differences between both the two codes was then discovered, as spelled out in the Appendix. A key reason for many of these differences is that many of the generalities in VSOP-A, which are deemed desirable for research purposes, were removed from VSOP 99/05 in order to "hardwire" the code towards easier modelling of PBRs for the purpose of facilitating the design and licensing of the PBMR DPP reactor. VSOP-A, for instance, allows the specification of some parameters and options that are appropriate for other reactor types, but would not be appropriate for the PBRs. This freedom in VSOP-A implies that the user of the code needs to have specialist knowledge of the appropriate values and options, in order to be able to accurately model PBRs. In the hands of less experienced users, the risk of introducing significant errors in VSOP-A models is thus large. By "hardwiring" many of these parameters to only the values and options appropriate to PBRs, the risk of such errors has thus been reduced significantly.

It soon became clear that, for the reasons explained in the Appendix, that reconciling these differences would be very complicated at best, and impossible at worst. The goal for the verification of the present input models was therefore not to reconcile these differences, in order to get identical results, but rather to serve as a quality control procedure in the verification of the translation of Mulder's input models from VSOP-A to VSOP 99/05.

Due to these inherent differences, the assumption from the outset was that the translation of the LEU models would lead to small, but significant, changes in the results, and the differences that were indeed found are therefore not viewed as a matter of concern. On the contrary, these differences can be viewed as welcome evidence of significant independence between Mulder's VSOP-A code and the VSOP 99/05 code, which would be necessary if the one code were to be used by the National Nuclear Regulator (NNR) to review results obtained with the other.

Apart from the differences in the codes, a large number of small, but significant, differences between the values and options used in E.J. Mulder's PBMR-400 VSOP-A input model, and the PBMR (Pty.) Ltd's official PBMR DPP-400 model for VSOP 99/05, were also discovered. At the beginning of the study, an attempt was made to reconcile these differences. It was, however, soon discovered that verifying the effects of all of these differences would comprise a large study on its own, which would not contribute strongly to the goals of the present study. Therefore the reconciliation of these models was excluded in the demarcation section of the present study. In stead it was decided to use only Mulder's PBMR-400 models for VSOP-A, as well as its translations to VSOP 99/05.

PBMR (Pty.) Ltd's PBMR DPP-400 VSOP 99/05 model was only used to compare the final burn-up and temperatures, as was reported in the previous sections. The differences between these models are therefore not relevant to the results of the present study.

However, the PBMR (Pty.) Ltd's PBMR DPP-400 VSOP 99/05 model was used throughout as a reference source, in order to better understand the options and values used in Mulder's VSOP-A model. In the many instances where the input required by the VSOP-A and VSOP 99/05 codes were incompatible and a direct and equivalent translation from the VSOP-A model to VSOP 99/05 was thus not possible, the PBMR (Pty.) Ltd's PBMR DPP-400 VSOP 99/05 model was used as a guideline for appropriate ways to replace these untranslatable portions of data. Understanding the differences between these two models was therefore important for the present study and may again become important for follow-up studies. Therefore, in spite of the fact that the PBMR (Pty.) Ltd's PBMR DPP-400 VSOP 99/05 model was used to produce the results of the present study a list of the most important differences between these models are now discussed. Except for the list of small conceptual differences between the codes, which have been described in the Appendix, but which will probably not affect calculation results significantly, the following differences can be expected to possibly affect results in future studies significantly:

- E.J. Mulder informed the present author in private discussions that he had developed a version of the THERMIX code for VSOP-A, which differs significantly from THERMIX in VSOP 99/05.

- THERMIX in VSOP 99/05 differentiates between the heat conductivity of the fuel spheres of each fuel pass.

- VSOP 99/05 was the result of a series of versions, that each included significant differences, compared to the previous version. Calibrations of different input options

and new additions to the code for VSOP 99/3 to VSOP 99/4 are described by Brockmann *et al* (2004: Table 4). The most important change was replacing B^2 for the leakage term with DB^2, which increased k_{eff} by 1.3 Nile, which would increase the average burn-up by about 5 MWd/kg heavy metal. It is thus clear that there are larger differences between the results within the VSOP 99/3 to VSOP 99/4 series, than were found between VSOP-A and VSOP 99/05 in the present study. Since the evolution of VSOP 99 was not synchronised with developments within VSOP-A, it would be difficult to establish which version of VSOP 99 is the most similar to VSOP-A, except that it is clear that VSOP-A uses B^2 for the leakage term, instead of DB^2 which was implemented in VSOP 99, since version VSOP 99/4.

- Although the Pu + MA content in the LEU fuel cycle is low, the fact that VSOP 99/05 does include the MA in its neutronic calculations and do use resonance integrals for the calculation of the epithermal self-shielding factors for ^{240}Pu en ^{242}Pu, can be expected to cause significant differences, as will also be shown below.

Mulder's PBMR-400 input models and PBMR (Pty.) Ltd's PBMR DPP-400 input model also contained the following significant differences:

- PBMR DPP-400 used thinner axial flow channels next to the internal and external reflectors, and consequently thicker ones for the three central flow channels. In the main results section of the present study it will be shown that the increased power/fuel sphere, directly adjacent to the reflectors, falls off with distance from the reflector much quicker for Pu(PWR) than for LEU. Therefore, for Pu(PWR) Spectrum Zones adjacent to the reflectors, the part of the Spectrum Zone closest to the reflector will experience much higher burn-up than its opposite end. However, the burn-up calculations smeared the burn-up out over the entire Spectrum Zone and thus assigned the much lower average burn-up, and consequently the lower average depletion rate, to the whole Spectrum Zone. The thinner these outer Spectrum Zones are, the smaller the differences between their maximum and average power and depletion will be and thus the smaller the potential errors that they might introduce.

- The relative flow speeds between the flow channels also differed between the two models. In the PBMR-400 model the two outer fuel flow channels, adjacent to the reflectors, are subdivided into 24 Layers, compared to 18 Layers for the three inner flow channels. This means that the inner channels flow at 1.333 times the speed of the outer channels. However, in the PBMR DPP-400 model, the outer channels were divided into 20 Layers, compared to 13 in the inner channels and thus the inner

channels flowed at 1.538 times the speed of the outer channels, which is 15.4% faster than in the PBMR-400 model. Viewed from the perspective of the outer channels, the outer channels flow significantly slower in the PBMR DPP-400. Especially in Pu(PWR) fuel cycles, where the depletion during the first pass in these channels adjacent to the reflectors is much higher than for LEU cycles, this may mean that the fuel at the bottom of the outer fuel channels in the PBMR DPP-400 model may become depleted to such an extent that the simulated power might drop off sharply at the bottom. This may increase the simulated power peaking, which may increase both the simulated maximum power/sphere and the maximum fuel temperature. This means that the PBMR DPP-400 model will produce more conservative results, compared to the PBMR-400 model which will produce more optimistic results.

These differences in flow speed were probably caused by the differences in channel thickness. In real reactors, the decreased fuel flow speed in the outer channels are caused by the friction between the fuel spheres and the reflectors. Therefore this effect decreases with distance from the reflectors. In the simulations average fuel flow speeds were calculated across each flow channel. The thinner outer channels of the PBMR DPP-400 model would thus include less of the faster flowing inner fuel in this averaging, which explains its lower average flow speeds. Since the fuel channel flow rates for both models were based on the results of the PFC3D calculational pebble flow experiments (private communication from E.J. Mulder, 30 May 2011 and F. Reitsma, 6 July 2011), these can be used with confidence.

- PBMR-400 used the traditional lower energy cut-offs for the three epithermal energy groups in the four group approach on VSOP-A card G5 and VSOP 99/05 card G6, i.e. 100000 eV, 29 eV and 1.860 eV. However, PBMR DPP-400 used five energy groups with the lower limits of the first four: 100,000 eV, 10,000 eV, 130 eV and 1.86 eV. Widening the lowest epithermal group from 29 eV – 1.86 eV to 130 eV – 1.86 eV was based on simulations by Brockmann *et al* (2004) that showed that iteration stability improves if all the significant epithermal capture resonances are included in the lowest epithermal group.
  In the present study the first mentioned traditional four group energy window structure was retained for the following reasons:

  - Brockmann's changing of the energy windows was related to the change from B^2 to DB^2 for the leakage term. Since VSOP-A uses B^2, changing to

Brockmann's new energy windows might not necessarily produce similar improvements in convergence. If these windows were to be changed, this step would have to be accompanied by a detailed optimisation study.

- All optimisation of the VSOP-A models and code was explicitly excluded in the demarcation section of the present study.

- For the neutronics core model, Mulder's PMR-400 model addressed the problem of the abrupt discontinuity between the atom densities at the junction of the external graphite reflector and the steel core barrel by mixing the atom densities of these differing regions, in the areas around this junction. However, the PBMR DPP-400 model used an updated extrapolation length on the outer boundary of the external reflector to simulate in this way the contribution of the metals of the core barrel and RPV. The extrapolation length on this boundary was determined by means of transport calculations (Naicker, 2006).

- Similarly the two THERMIX models were developed independently and thus contained differences. An attempt to translate Mulder's VSOP-A PBMR-400 THERMIX input model to VSOP 99/05 revealed significant differences between the structures of the THERMIX input cards of these two codes. Rather than trying to reconcile these differences, the author opted to copy and paste the THERMIX input model of the PBMR DPP-400 into the translated VSOP 99/05 version of the PBMR-400 model.

  The final VSOP 99/05 PBMR DPP-400 input model for the LEU fuel cycle in the present study thus consisted of the neutronic part of Mulder's VSOP-A PBMR-400 model, translated to VSOP 99/05, combined with the VSOP 99/05 THERMIX model, developed by the PBMR (Pty.) Ltd.

- Therefore it should be expected that the results of the present VSOP 99/05 model may not be fully compatible with either of the two original models.

- In view of these differences, it should be understandable that the main aim of the present study was not comparison of the VSOP-A and VSOP 99/05 results, but rather comparison of different fuel cycles, simulated with VSOP 99/05 only.

7.2 Simulation of control rods

7.2.1 Introduction

Description of the reactor geometry and fuel cycles are given in the main document. The distribution of neutrons in a reactor is theoretically described by the transport equation. Since fully realistic numerical solutions to this set of equations are very calculation intensive, the diffusion approximation (Lamarsh and Baratta, 2001: 237) is normally applied and solved, as is the case in VSOP. However, the diffusion approximation is not valid in the following cases (Lamarsh and Baratta, 2001: 235):

- When a medium strongly absorbs neutrons.
- Within about three mean paths of a neutron source or the edge of a medium.
- When the scattering of neutrons is strongly anisotropic.

- Therefore diffusion calculations are not valid in or near control rods (CRs). Various methods to correct diffusion calculations of control rod worths have been developed. Reitsma and Naidoo (2003) and Sen *et al* (2006) implemented both the Method of Equivalence Cross-Sections (MECS) of Fen *et al* (1992) and the method of Equivalent Boron Concentrations (EBC), which in this study will be called the MEB (Method of Equivalent Boronation). Reitsma and Naidoo (2003) simulated these methods for a 3-D VSOP 94 model for LEU fuel in the ASTRA experimental facility and Sen *et al* (2006) for the PBMR DPP-400 reactor. They compared these results to measured control rod worths from the ASTRA and found that both methods gave satisfactory results. They warned, however, that these correction methods did not conserve either the neutron flux distributions or the neutron reaction rates throughout the reactor and should therefore be used with caution.

They implemented the simulation technique for the MECS by first simulating the neutron flux in a single control rod and its surrounding environment by means of a 1-D cylindrical unit cell transport calculation. Diffusion parameters and reaction cross sections were then derived from the results of the transport calculations in such a manner that the reaction rates for the transport and diffusion methods, in the absorber region and its surroundings, would be the same. This was done by relating the leakage rates in the two methods. These diffusion parameters and cross-sections were then entered as input data for a 3-D diffusion calculation of the ASTRA facility in VSOP. The control rod worths calculated with VSOP were then compared to those experimentally measured in the ASTRA facility.

In spite of the acceptable results obtained, Reitsma and Naidoo warned of several implementation challenges that they experienced with the MECS, limiting its practicality. It should further be noted that the fact that their method requires 3-D VSOP calculations of a representative slice of the full reactor geometry, presents a significant challenge because 3-D reactor simulations are calculation intensive, especially when thermal hydraulic effects are included in the simulations.

The MEB is a much simpler method in which the boron concentration in the control rod regions in VSOP is varied until the calculated control rod worths equal the experimentally measured values, or in cases where experimental worths are not available, they equal worths obtained from more sophisticated simulation technique, i.e. the MECS in this case.

7.2.2 Method

The following version, developed by E.J. Mulder, of this MECS + MEB method was used in this study:

Mulder added a 3-D MEB to the 3-D MECS, i.e. 24 3-D control rods was simulated in VSOP-A by varying the ^{10}B atom density in the control rod meshes in a 1/24 slice of the core until the calculated control rod worth equalled the value obtained with the 3-D MECS. Mulder then used this 3-D MEB to do temperature-coupled diffusion calculations for the core with the control rods inserted to various depths. This was done to simulate the adjustment of the control rods in order to counter the ^{135}Xe poisoning following the power variations during the 100%/ 40%/ 100% load following. While the equivalent ^{10}B concentrations, used for providing xenon-override during load following, from these simulations were inherited in the standard input models, these simulations were not repeated in the present study.

For the present study control rod simulations were limited to the calculation of the shut-down margins. Therefore only the 2-D MEB was combined with the 3-D MECS (Mulder, 2006). This 2-D equivalent boron concentration in VSOP-A was then transferred to the 2-D VSOP 99/05 equilibrium core models.

7.2.2.1 3-D MECS simulations in VSOP-A

For the 3-D MECS, diffusion simulations of 12 full length inserted control rods were simulated by performing these calculations for a single control rod in VSOP-A for a pie-slice comprising 1/12 of the core of the PBMR-400 reactor. By defining reflective boundaries for the surfaces where this slice was cut, results that are equivalent to a full reactor core with 12 control rods were obtained, based upon the assumption of azimuthal symmetry between the control rod slices. This 12 control rod simulation represents the situation where 12 of the PBMR DPP-

400's 24 half-length control rods were lowered into the bottom half of the core and 12 into the top half of the core, which is the equivalent to 12 full length control rods fully inserted over the whole length of the core. These simulations were implemented as follows for both the LEU and Pu(PWR) fuel cycles:

1. Fuel compositions:

    a. The 3-D MECS VSOP-A start-up core for the LEU case, with the control rod fully withdrawn from the reactor, was filled with the standard fresh 9 g heavy metal /fuel sphere LEU(9.71 a/o%) equilibrium fuel spheres, with the standard LEU fuel sphere geometry. However, a significant concentration of 3.0 E-6 atoms/(barn.cm) of natural boron was added, in order to reduce k_{eff}. This was also done in the TOTMOS driver fuel.

    b. For the LEU equilibrium VSOP-A core (see below), the same fuel as for the start-up core was used, except that the natural boron was removed and that the core was then burnt in to equilibrium.

    c. For the Pu(PWR) case, the standard shell-ball fuel with 2.92 g heavy metal/sphere and an atomic fuel composition of ^{239}Pu = 55.45%; ^{240}Pu = 24.26%; ^{241}Pu = 13.41%; ^{242}Pu = 6.88% was used. Since this was used to create an equilibrium core, no neutron poisons were added.

2. These core simulations were then developed in the following ways:

    a. The phenomenon encountered in the pilot study, namely that VSOP-A calculated the start-up core as being only marginally critical when filled with fresh equilibrium Pu(PWR) fuel spheres, proved to be more problematic here. Natural boron was now added to this fresh fuel, in order to match the composition of the driver fuel in VSOP. This reduced k_{eff} below 1.0 and caused it to be unstable, i.e. when the spectrum and diffusion calculations were repeated consecutively for this zero burn-up core, k_{eff} rapidly decreased even further. In the pilot study, this problem was overcome by gradually adding the Pu fuel spheres to an equilibrium LEU core and in the burn-in sequence of the equilibrium core of the present study, by first doing a significant number of burn-up cycles, before trying to perform reliable spectrum and diffusion calculations.

    However, this restriction precluded the calculation of the MECS and the MEB

for the start-up core of the present study. Therefore, the Pu(PWR) core was first burnt-in to equilibrium, using fresh equilibrium fuel, without natural boron. Thereafter the MECS and MEB calculations were performed. In order to save calculation time for the 3-D case, a shortened burn-in sequence was developed in which the convergence of k_{eff} was accelerated by increasing the core power for the start-up core and then rapidly tapering it off towards the standard 400 MW_{th} as the core started to approach equilibrium.

k_{eff} was then noted with the control rod fully withdrawn, as well as with the control rod fully inserted, by means of restart runs, as described below. Since the TOTMOS transport calculations did not take ^{135}Xe poisoning into account, ^{135}Xe-posoning was eliminated in VSOP-A as well by first reducing the power to virtually zero and allowing four days of ^{135}Xe decay. The worth of the 12 control rods in the full core was defined as the difference in k_{eff} for the case where this one control rod was fully inserted into and the case where it was fully withdrawn from the 1/12 slice of the 3-D core, for the respective fuel cycles.

b. For the LEU case, the NSOP-A calculations were first performed for the start-up core: The core power was set to virtually zero. A constant temperature of 1000 K, i.e. 727°C, was set throughout the reactor, in order to correspond to the temperature of the control rod transport calculations in TOTMOS. Operating cycles were repeated until k_{eff} had stabilised. k_{eff} was then noted with the control rod fully withdrawn, as well as with the control rod fully inserted, as described below.

c. In order to investigate the sensitivity of the MECS and MEB to burn-up and more realistic temperatures, these VSOP-A calculations were repeated for an equilibrium core: The start-up core was burnt in to equilibrium, including the iterative calculation of the equilibrium temperatures by means of the THERMIX code. The control rod-worth calculations were repeated, again at virtually zero power and after ^{135}Xe decay.

3. Since the worth of a control rod increases with thermal neutron flux in the volume into which the control rod is to be inserted, the maximum thermal neutron flux in the external reflector, with the control rods fully withdrawn, was reported for all the 2-D control rod studies below. In order to be able to compare these fluxes at different power levels on an equal basis, fluxes were normalised to the thermal power output of the reactors.

4. When the control rod was withdrawn, the effect of the empty control rod channel was simulated by inserting the set of cross sections and diffusion constants for the diffusion method for voids (Gerwin and Scherer, 1979), which is a standard feature in VSOP, into the control rod meshes.

   When the control rod was inserted, the set of cross sections and diffusion constants, pre-calculated with TOTMOS according to the MECS (Fen *et al*, 1992), was inserted into the control rod meshes via VSOP-A cards C7-1 to C7-6. These constants and cross-sections were automatically produced by the TOTMOS transport code, which was used to perform the 1-D cylindrical cell calculations for a control rod embedded in an annulus of graphite moderator and an outer annulus of fuel and graphite mixture, which served as driver fuel for the neutron reactions, as will be described in more detail below. This was repeated for LEU and Pu(PWR) driver fuel respectively. Since these cross-sections and constants fully represented the simulated effects of all the materials in the control rod, no control poison nuclide concentrations were inserted into the control rod channels for the 3-D MECS VSOP-A simulations.

7.2.2.2 2-D MEB simulations in VSOP-A.

The 3-D worth of the 12 control rods of the MECS was then translated to the 2-D MEB in VSOP-A. VSOP-A, rather than VSOP 99/05, was used for the 2-D case, because the author only had access to the 3-D models in VSOP-A. Due to the significant differences in the calculation algorithms between VSOP-A and VSOP 99/05, as far as Pu fuel cycles are concerned, VSOP-A had to be used for the 2-D simulation too, in order to preserve equivalence of the calculation algorithms. The same fuel cycles of the 3-D cases, were also run in the 2-D cases and with the equivalent core geometry. The 3-D approach of simulating the control rods by inserting equivalent cross-sections into the control rod regions, was replaced by inserting an equivalent ^{10}B concentration in the 2-D control rod regions. This ^{10}B atom density was then varied to yield the same control rod worth, as was obtained for the 3-D MECS. A problem was, however, encountered when the ^{10}B atom density was increased to 2.3 E-6 atoms/(barn.cm) for the Pu(PWR) case: the abrupt increase in neutron captures, from the case with the control rods fully out to fully in, perturbed the neutron flux to the extent that the iteration convergence limits were violated, causing the code to abort the calculation. This problem was circumvented by first inserting the control rods fully at a lower density of 1.6 E-6 atoms/(barn.cm). Once the flux converged significantly at this density, the atom density was then increased to the desired level, where after the k_{eff} converged without a problem.

This 2-D method was thus the 2-D MEB appended to the 3-D MECS.

This equivalent ^{10}B concentration, for each 2-D MEB in VSOP-A, was subsequently transferred to the 2-D VSOP 99/05 equilibrium core for calculation of the shut-down balances for the control rods. As an additional check on the validity of the MEB, the worth of the 12 control rods in the VSOP 99/05 core was calculated for the fully inserted vs. fully withdrawn cases. Since VSOP 99/05 yielded significantly different results, compared to VSOP-A, in most of the calculations in this study, a significant difference in the control rod worth was also expected.

7.2.2.3 2-D control rod xenon transient override margin calculations in VSOP 99/05

Before the shut-down margins, with the 12 control rods fully inserted, could be calculated, the ability of the current insertion depths of the control rods into the equilibrium cores to provide the required xenon poisoning override, had to be evaluated. These should be inserted deep enough to provide sufficient insertion of positive reactivity to override xenon poisoning by withdrawing these control rods during the standard required 100% / 40% / 100% load following for the PBMR DPP-400 reactor.

In the 2-D VSOP-A input models for both the LEU and Pu(PWR) fuel cycles, inherited from the pilot study and then translated to VSOP 99/05, the equivalent ^{10}B atom density for all 24 control rods in the external reflector, i.e. 6.75 E-6 ^{10}B atoms/(barn.cm) in the 2-D control poison annulus, was inserted to a depth of 195.1 cm below the top reflector for the equilibrium core. This depth consisted of the 78.5 cm depth of the void between the bottom of the top reflector and the top of the fuel core + 116.6 cm fuel core depth. This ^{10}B concentration was based on unpublished VSOP-A MEB calculations by E.J. Mulder for the partial insertion of all 24 control rods into the PBMR-400 LEU (U/Pu) equilibrium core for the purpose of providing xenon-override.

The standard operating procedures of the PBMR DPP-400 includes the restriction that the control rods may not be withdrawn to above the bottom of the top reflector. This procedure was thus adhered to in this simulation. It is also for this reason that only the insertion depth below the top reflector is reported.

In the pilot study was reported that both the positive reactivity insertion required to override the xenon transient and the ability of the control rods to provide this positive reactivity insertion were less in the Pu(PWR) core, due to the lower thermal neutron flux, caused by the higher thermal absorption cross-section of ^{239}Pu and ^{239}Pu, compared to the ^{235}U in LEU. In the present study these VSOP-A results were tested in VSOP 99/05 in the following way:

The decrease in k_{eff}, due to the build-up of ^{135}Xe, during the reduction in power from 100% to 40%, was simulated in VSOP 99/05 in the following way:

1. Restart files were prepared from both the LEU and Pu(PWR) VSOP 99/05 equilibrium cores. During the subsequent restart runs, the fuel shuffling was stopped, while the core power was maintained at 400 MW_{th} and k_{eff} was maintained at criticality. This standard procedure was performed by reducing the operating cycle duration to half of a normal cycle, i.e. the number of large burn-up time steps per operating cycle was reduced from two to one on a card R9 + R14, where after fuel shuffling was stopped (NKEEP = 002) on the next card R9. The reason for this was :

   During the normal operating cycles, two large burn-up time steps were used, where after the fuel shuffling was performed. Since k_{eff} decreases continuously during these two burn-up time steps, the value of k_{eff} in the middle of the cycle, i.e. after the first large burn-up time step, was taken as representative of the average over the whole burn-up cycle. All the fuel cycles were fine tuned to yield average equilibrium values of k_{eff} as close as possible to 1.00000. This means that at the beginning of the first time step, k_{eff} would be significantly greater than 1.00000 and at the end of the second time step significantly less than 1.00000. k_{eff} would then be restored to significantly greater than 1.00000 by the fuel shuffling at the end of this operating cycle. This means that if the fuel shuffling did not take place at the end of such a normal burn-up cycle, k_{eff} would be “frozen” at significantly less than 1.00000. By reducing the duration of this first operating cycle, at the end of which the fuel shuffling would not take place, to one large time step, this problem was overcome, i.e. k_{eff} at the end of this static operating cycle, was maintained at close to 1.00000.

   (Some of the parameters given on any card R9(N) applies to Operating Cycle(N), while others will only apply from Operating Cycle(N+1) onwards. The burn-up parameters in particular, such as the number of large burn-up steps, the time duration of these steps and the core power are applied only during the fuel shuffling at the end of Operating Cycle(N), and will thus only affect the burn-up performance from Operating Cycle(N+1). On the contrary, the instruction to stop the fuel shuffling on any card R9(N), already becomes effective for Operating Cycle(N). Therefore, in order to decrease the number of large burn-up steps and stop the fuel shuffling during the same Operating Cycle(N+1), the reduction in the number of burn-up steps had to already be specified on card R9(N) and the ceasing of the fuel shuffling only on card R9(N+1).)

2. The time length/large burn-up time step was then reduced to virtually zero, in order to "freeze" this critical static equilibrium core, where after five operating cycles were performed to stabilise k_{eff}, which was then noted. The equilibrium temperature distribution was also retained.

3. The core power was now reduced from 100% to 40% (= 160 MW_{th}), in order to initiate the ^{135}Xe poisoning transient, caused by load following. The time length per large burn-up step (DELDAY) was then reduced to half an hour and 20 burn-up cycles were performed, with Spectrum and Diffusion calculations at each cycle. This covered ten hours of the transient, which included the minimum in k_{eff}.

   Once the time of minimum in k_{eff} was established, the procedure was rerun. Right after the burn-up cycle with the minimum k_{eff}, the length of the large burn-up time steps was reduced to virtually zero, in order to "freeze in" the maximum xenon-poisoning. Five cycles were used to stabilise k_{eff}, after which k_{eff} was noted.
   The decrease in k_{eff} was defined as the effect of the ^{135}Xe poisoning that had to be overridden by the withdrawal of the 24 control rods.

4. The equivalent ^{10}B concentration of all 24 control rods was then withdrawn to the bottom of the top reflector and k_{eff} was again stabilised. The difference between this increase in k_{eff}, supplied by withdrawing the control rods, and the positive reactivity insertion required to override the xenon poisoning was then reported as the xenon override margin.

   Each time such a significant and abrupt modification was made to the reactivity of the core, five operating cycles for the 2-D cases and ten for the 3-D cases, which included Spectrum and Diffusion calculations, were performed in order to stabilise k_{eff}, before k_{eff} was noted.

7.2.2.4 2-D control rod shut-down balance in VSOP 99/05

Once the 2-D MEB was calculated in VSOP-A, this ^{10}B atom density was transferred to the 2-D VSOP 99/05 model for the PBMR DPP-400 equilibrium core, for each fuel cycle. These were the equilibrium cores for the 9 g LEU and the 3 g Pu(PWR) fuel cycles respectively, with the equilibrium temperature profiles, described in Par. 3.3. This was then used to calculate both the hot and cold shut-down balances for the control rods in the following way:

1. The fuel shuffling in the equilibrium core was stopped, as described above, in order to "freeze" the equilibrium core.

2. The core power was simultaneously reduced to virtually zero, in order to initiate the ^{135}Xe poisoning shut-down transient. Burn-up cycles were then introduced for a total of four days, in order to reach the maximum reactivity of the shut-down reactor core, due to the decay of ^{135}Xe and other isotopes.
   Δk_{eff} defined the contribution of nuclide decay to the shut-down balance.

   After four days, the burn-up cycle length was reduced to virtually zero, in order to retain that level of isotope decay.
   k_{eff} was stabilised and noted, together with the maximum thermal neutron flux in the external reflector.

3. Temperatures:

   a. For the calculation of the hot shut-down margin, the equilibrium temperature distribution was retained.

   b. For the cold shut-down balance, the temperature throughout the core was reduced to 50°C, which was considered the long term cold shut-down temperature. k_{eff} was stabilised and noted, together with the maximum thermal neutron flux in the external reflector. Temperatures were reduced in the following sequence, and the contribution of each to the cold shut-down requirement was noted:

      i. Resonance absorbers in the fuel, i.e. Doppler effect for ^{238}U in LEU and for ^{240}Pu and ^{242}Pu in Pu(PWR).

      ii. Moderators in the fuel spheres, i.e. carbon and oxygen.

      iii. Graphite reflectors.

4. The contribution of the insertion of the control rods to the shut-down balance was subsequently calculated by fully inserting the MEB ^{10}B concentrations from, VSOP-A for the 12 control rods, into the 2-D VSOP 99/05 core. The partial insertion of the higher MEB concentration for all of the 24 control rods was thus replaced with the full insertion of the lower concentration for the 12 control rods. For the LEU equilibrium VSOP 99/05 core, the ^{10}B MEB concentrations from respectively the VSOP-A start-up and equilibrium cores were inserted, in order to investigate the sensitivity of the VSOP 99/05 shut-down balance to the nuclide composition of the VSOP-A core that was used for the MEB.

Where the initial concentrations for the main run were inserted into Batches 16 to 19 with VSOP 99/05 cards V7 and V8 only, all the control rod batches were modified via HNUC on card R9, followed by the atom density on card R19A and the numbers of the individual batches on card R19B. It is, however, important to note the difference in batch number definitions:

a. The variables KD18 on Cards V7 use the batch number definitions of cards BI5, in this case Batch Id. = 16 - 27 for the 12 batches of the full length of the control rod channel, from the top of the diffusion area to the floor of the fuel core.
   This includes 199.3 cm of channel above the bottom of the top reflector, 78.5 cm next to the void below this reflector and 1162.5 cm next to the fuel core. The total insertion depth below the bottom of the top reflector thus equals 1241.0 cm.

b. However, IBAE on card R19B uses the "FINAL ID. NUMBERS OF VSOP-BATCHES", listed in a diagram under this same heading in the BIRGIT output. The numbers for the same 12 batches for the control rod channel thus changed to 732 – 743.

5. Δk_{eff} for each of these steps was noted and constituted the components of the shut-down balance.

6. The control rods were then totally withdrawn from the reactor, in order to compare the full length worth of the 12 control rods in the 2-D VSOP 99/05 core to that of VSOP-A.

7.2.3 Results for control rod calculations

7.2.3.1 Simulation of diffusion coefficients with TOTMOS

The input data for the 1-D cylindrical cell transport simulation of the control rod in TOTMOS are shown in **Table 38**. The control rod was simulated as a number of annuli, starting with a void in the centre (Zone(1)). The B_4C in Zone(3) was sandwiched between an inner (Zone(2) and an outer (Zone(4)) iron pipe. Zone(5) is a void which simulated the gap between the outer edge of the control rod and the inner edge of the hole in the reflector. Zones (6) to (10) simulated the graphite reflector, while Zone(11) simulated the fuel zone in which the LEU and Pu(PWR) driver fuel and the graphite of the fuel spheres are respectively homogenised. The surface on the outside of the outer fuel zone was an albedo with a reflection factor of 1.0. All materials were simulated at a temperature of 1000 K.

Table 38: Input data for the 1-D cylindrical cell transport simulation of the control rod in TOTMOS.

Zone	Description	Thickness of annulus (cm)	Atom density (atoms/(barn.cm))	
1	Void in centre	4.10 (= Radius of central cylinder)	0.0	
2	Inner iron pipe	0.10	8.4E-2 Fe-Nat	
3	B_4C	0.80	1.05E-1 B-Nat	
			2.62E-2 ^{12}C	
4	Outer iron pipe	0.25	8.4E-2 Fe-Nat	
5	Void	1.25	0.0	
6	Reflector	2.5	8.5E-2 ^{12}C	
7	Reflector	1.0	8.5E-2 ^{12}C	
8	Reflector	1.0	8.5E-2 ^{12}C	
9	Reflector	1.53	8.5E-2 ^{12}C	
10	Reflector	2.47	8.5E-2 ^{12}C	
			Driver fuel:	
			LEU	**Pu(PWR)**
11	Fuel zone	30.0	0.11936E-4 ^{235}U	0.21941E-4 ^{239}Pu
			0.11086E-3 ^{238}U	0.95998E-5 ^{240}Pu
				0.53052E-5 ^{241}Pu
			0.52335E-1 ^{12}C	0.52606E-1 ^{12}C
			0.300000-5 B-Nat	0.30000E-5 B-Nat

The fine group neutron fluxes were solved and then collapsed to a few group structure for the four groups, with the energy boundaries as close as possible to the VSOP case, as is shown in **Table 39**.

Table 39: Energy groups for TOTMOS simulation

Group	Energy limits* (eV)
1	1.0E+07 to 6.3928E+05
2	6.3928E+05 to 29.023
3	29.023 to 1.9
4	1.9 to 2.5E-03

Note: *: The boundaries of the small energy groups that are available in TOTMOS differ slightly from those in VSOP and therefore the boundaries of the broad energy groups also had to be chosen slightly differently than in VSOP. For instance, the upper cut-off energy of 2.04 eV for the thermal group (Group 4) in VSOP had to be approximated by 1.9 eV in TOTMOS. Since these differences are small, it was assumed that they did not significantly influence the results.

TOTMOS produced the following diffusion constants, and cross-sections for the LEU driver fuel:

GRP.	ROD-KONST.	DIFF.-KONST.	SIGMA-REMOV.	SIGMA-ABS.	NUESIGF.
1	7.61140E-03	1.09604E+00	1.29150E-03	1.47216E-03	1.35823E-20
2	8.17437E-02	4.11151E+00	4.80442E-05	3.21578E-02	7.56760E-20
3	2.52500E-01	2.97685E+00	1.31931E-04	1.69451E-01	7.09226E-19
4	2.66935E-01	2.97006E+00	1.79274E-06	1.89331E-01	4.29761E-18

TOTMOS produced the following diffusion constants, and cross-sections for the Pu(PWR) driver fuel:

GRP.	ROD-KONST.	DIFF.-KONST.	SIGMA-REMOV.	SIGMA-ABS.	NUESIGF.
1	7.58824E-03	1.04530E+00	1.28821E-03	1.47209E-03	5.54713E-20
2	8.11451E-02	4.16948E+00	4.73216E-05	3.18432E-02	2.19198E-19
3	2.50604E-01	2.92999E+00	1.34209E-04	1.69627E-01	4.74655E-18
4	3.17852E-01	4.37185E+00	5.47602E-06	1.84548E-01	2.51330E-17

The macroscopic absorption cross-sections for all energy groups were inserted into the 3-D VSOP-A input models into card C7-3, the macroscopic removal cross-sections into card C7-4 and the radial thickness into card C7-5. The diffusion constants were then normalised to that of group four and were inserted as input for the control rod mesh for the 3-D VSOP-A diffusion calculation, via VSOP-A card C7-6, as shown in **Table 40**. (**Warning: It was later discovered that some other studies did not use this normalisation**, but rather worked with the constants as is. This issue will be resolved in a follow-up study. In the mean time the **data produced here should be used with caution**.)

Table 40: Diffusion constants produced by 1-D transport calculations in TOTMOS for VSOP-A card C7-6.

Group	LEU		PU(PWR)	
	Diffusion constant from TOTMOS	Normalised for VSOP-A card C7-6	Diffusion constant from TOTMOS	Normalised for VSOP-A card C7-6
1	1.09604E+00	0.36903	1.04530E+00	0.23910
2	4.11151E+00	1.38432	4.16948E+00	0.95371
3	2.97685E+00	1.00229	2.92999E+00	0.67020
4	2.97006E+00	1.00000	4.37185E+00	1.00000

7.2.3.2 3-D MECS control rod worths and 2-D MEB in VSOP-A

After entering these parameters into the control rod meshes and loading the fuels, as described above, the control rod worths were calculated for the 3-D VSOP-A case.

Thereafter the 2-D MEB was calculated in VSOP-A for Pu(PWR), as shown in **Table 41**. The equivalent ^{10}B atom density was varied until the difference between the control rod worth was < 1E-4.

Table 41: 3-D MECS control rod worths and 2-D MEB in VSOP-A, based upon the start-up or equilibrium cores, without control rods and after ^{135}Xe decay.

Fuel Core	**k_{eff} (3-D MECS: 12 CRs out)**	**k_{eff} (3-D MECS: 12 CRs in)**	**3-D MECS CR worth** (Δk_{eff})	**k_{eff} (2-D MEB: 12 CRs out)**	**Maximum thermal neutron flux in external reflector** (10^3 neutrons/ cm^2/s /W_{th})	**k_{eff} (2-D MEB: 12 CRs in)**	**2-D MEB: Equivalent ^{10}B atom density** (10^{-6} atoms / (barn.cm))
LEU (Start-up)	1.02652	0.95097	**-0.0756**	1.04176	231.5	0.96618	**2.396**
LEU (Equi-librium)	1.02119	0.93476	**-0.0864**	1.02940	423.8	0.94297	**1.704**
Pu (PWR) (Equi-librium)	1.01471	0.96358	**-0.0511**	1.01642	154.5	0.96528	**2.292**

After transferring the 2-D equivalent ^{10}B MEB atom density from VSOP-A to the equilibrium cores of VSOP 99/05, the 12CR worths were recalculated, as shown in **Table 42**.

Table 42: 2-D control rod worths in VSOP 99/05 equilibrium cores, with equilibrium temperatures, after ^{135}Xe decay and for 12 CRs completely out versus completely in.

VSOP 99/05 equilibrium core	**Equivalent ^{10}B atom density from VSOP-A MEB: Source and density** (10^{-6} atoms / (barn.cm))	**k_{eff} (12 CRs out)**	**Maximum thermal neutron flux in external reflector** (10^3 n^{**} / $cm^2/s/W_{th}$)	**k_{eff} (12 CRs in)**	**2-D 12 CR worth** (Δk_{eff})
LEU	**LEU** (Start-up) = **2.396**	1.04556	467.5	0.93693	-0.0918
	LEU (Eq*) = **1.704**			0.95251	-0.0763
Pu(PWR)	**Pu(PWR)** (Eq*) = **2.292**	1.03267	170.7	0.96151	-0.0547
	LEU (Eq*) = **1.704**			0.97077	-0.0454

Acronyms: *: Eq =Equilibrium core; **: n = neutrons.

7.2.3.3 2-D control rod xenon transient override margin calculations in VSOP 99/05

The results for the xenon override margin calculations are shown in **Table 43**.

Table 43: 2-D control rod xenon override margins in VSOP 99/05 for partial insertion of 24 control rods into equilibrium cores.

Fuel Core	**k_{eff}** (Eq. with 24 CRs in 195.1 cm below top reflector)	**k_{eff} -Min** at Max ^{135}Xe	**Δk_{eff}** (^{135}Xe tran-sient to be over-ridden)	**Time** of k_{eff} – Min (h)	**k_{eff}** (CRs out to bottom of top reflec-tor)	**Max thermal neutron flux in external reflector** (10^3 n** / cm^2/s/W_{th})	**Δk_{eff}** (over-ride ability of CRs)	**Over-ride margin** (Δk_{eff})
LEU	1.00008	0.98455	**-0.0155**	5.0	0.99870	445.3	**+0.0142**	**-0.0013** (Not sufficient)
Pu (PWR)	1.00005	0.99903	**-0.0010**	4.5	1.01463	206.7	**+0.0156**	**+0.0146**

Notes: *: Eq. stands for equilibrium core; **: n stands for neutrons.

In order to further investigate this much smaller xenon override requirement for the Pu(PWR) core, the ^{135}Xe concentrations for the two cores are compared in **Table 44**.

Table 44: ^{135}Xe atom density variations responsible for override requirement.

Fuel Core	**^{135}Xe atom density** (**Eq.** at **100%** power) (10^{-10} atoms/ (barn.cm))	**^{135}Xe atom density** (at **k_{eff} –Min,** i.e. at Max ^{135}Xe after reducing power to **40%**) (10^{-10} atoms/ (barn.cm))	**Increase (%)**
LEU	0.9139	1.252	**37.0**
Pu (PWR)	3.069	3.218	**4.9**

Discussion

It is clear from these results that inserting the 24 control rods to the same depth for both the LEU and Pu(PWR) fuel cycles, is sub-optimal from the perspective of supplying the minimum required ^{135}Xe-poisoning override:

The override abilities of the control rods are similar in the two cores, i.e. only slightly higher for the Pu(PWR) core (Table 14). However, the override required by the increased ^{135}Xe poisoning is 15.5 times smaller for the Pu(PWR) core. Therefore, while this insertion depth provides only 91.7% of the required xenon override ability for the LEU equilibrium fuel cycle, it provides 1560% of the requirement for the Pu(PWR) core.

The cause of this much smaller override requirement for the Pu(PWR) core was revealed by the comparison of the increase in ^{135}Xe concentrations, during the power reduction from 100% to 40% (Table 15):

It should firstly be noted that the total negative reactivity inserted by ^{135}Xe poisoning (i.e. the negative of the positive reactivity inserted by four days of ^{135}Xe decay from Table 16) of -0.0287 for the equilibrium LEU core is about double the -0.0161 for the Pu(PWR) core. However, this larger reactivity effect in the LEU core is caused by a ^{135}Xe concentration of only 0.9139 x 10^{-10} atoms/ (barn.cm), compared to the more than three times larger 3.069 x 10^{-10} atoms/ (barn.cm) of the PU(PWR) core (Table 15). This larger reactivity effect, paradoxically caused by a lower ^{135}Xe concentration, is explained in part by the maximum thermal neutron flux in the external reflector for the LEU core, which is about double the value of the Pu(PWR) core (Table 14) and which is used here as a proxy for the thermal neutron flux in the core. It is further explained by the well known fact that the thermal neutron spectrum is much harder for Pu than for LEU, which sharply reduces the thermal neutron capture, due to the fact that the thermal microscopic capture cross-section of ^{135}Xe decreases sharply with increasing energy. The 15.6 times smaller xenon override requirement for Pu thus stands in sharp contrast to the total xenon poisoning effect which is smaller by only a factor two. The additional factor 7.8 can be explained in the following way:

Because of the lower and harder thermal neutron flux in the Pu core, much less ^{135}Xe nuclides capture neutrons and thus the removal rate of ^{135}Xe through capture is much smaller than in the LEU core. Since the ^{135}I production rates, i.e. the fission product yields (Lamarsh and Baratta, 2001: Table 7.7), are similar from the fissioning of ^{239}Pu and ^{235}U, the production rates of ^{135}Xe, through decay of ^{135}I, would also be similar for the two cores. Therefore the reduced ^{135}Xe removal rate is what caused the equilibrium ^{135}Xe concentration

in the Pu core to build up to more than three times that of the LEU core. This means that the decay rate of ^{135}Xe in the Pu core is also more than three times that in the LEU core. If the power of both cores were to be shut down completely, the evolution of the ^{135}Xe concentrations would be determined solely by the production rates from ^{135}I decay, which would be similar for both cores, and the decay rates of ^{135}Xe, which would be three times higher in the Pu core. In both cases the production rates would be higher than the decay rates and thus ^{135}Xe would build up. However, because of the much larger decay rate in the Pu core, the difference between the production and decay rates would be much smaller, and thus the build up of ^{135}Xe would occur much slower and peak at a much lower value in the Pu core. The dynamics of the power reduction from 100% to 40% are similar to those of a total shut-down, and thus the much smaller ^{135}Xe override requirement of the Pu core can similarly be explained by its higher ^{135}Xe decay rate.

This large excess reactivity, due to the deep insertion of the control rods, means that if the control rods were to be accidentally withdrawn during equilibrium operation of the Pu(PWR) core, a large+0.0156 Δk_{eff} reactivity will be inserted into the core. The factor 15.5 smaller xenon override requirement of the Pu(PWR) core provides the opportunity to strongly reduce this excess reactivity, which will then virtually eliminate the safety risk associated with accidental withdrawal of the control rods. Such a reduced insertion of the control rods into the equilibrium core will also improve the shut-down margins correspondingly by providing a larger reserve length of control rod insertion that could be added by fully inserting the control rods during shut-down.

However, a preliminary pilot study showed that the withdrawal of the 24 control rods to only 25% into the void above the fuel core, after which the core was again burnt to its new equilibrium state, actually affected the burn-up performance negatively. The axial power peak near the top of the core increased significantly and moved even closer to the top of the core. This increased the maximum power/fuel sphere to even more unacceptable levels. The increased peaking significantly increased the maximum power produced per fuel sphere. It also increased the axial buckling, which increased the leakage into the top reflector. Since the void above the top of the core causes leakage in the top reflector to be higher than it would otherwise have been, the void amplified this increased leakage in the top reflector. Therefore the total core leakage increased slightly, which caused the conversion ratio, and therefore the average burn-up, to decrease slightly. It is thus clear that a significant withdrawal of the control rods from the equilibrium core will only be beneficial if this is combined with a re-optimisation of the fuel composition and core lay-out, in order to decrease the peaking near the top of the core and thus the leakage in the top reflector. Since

such an optimisation falls outside the scope of the present study, it is referred to the redesign of the core proposed for the follow-up study.

The much smaller ^{135}Xe-override requirement of the Pu(PWR) core also introduces the opportunity to design a Pu-based reactor that can produce peak following, i.e. much more aggressive load following than the current 100% / 40% / 100% for the LEU-fuelled PBMR DPP-400. This is also referred to the follow-up study.

7.2.3.4 2-D 12 control rod shut-down balance in VSOP 99/05

The 2-D zero power, hot as well as cold, shut-down balances, after four days of ^{135}Xe decay, for both the LEU and Pu(PWR) equilibrium VSOP 99/05 cores are shown in **Table 45**. The shut-down balances were calculated for the different equivalent ^{10}B atom densities, obtained from the 2-D VSOP-A MEB, described above.

Table 45 2-D 12 control rod shut-down balance in VSOP 99/05.

		VSOP 99/05 equilibrium core		
Parameter	**Unit**	**LEU (High ^{10}B)**	**LEU (Low ^{10}B)**	**Pu(PWR)**
k_{eff} (Eq. with 24 CRs in 195.1 cm below top reflector)		1.00008		1.00005
Hot shut-down capability: 12 CRs fully in after 4 Days ^{135}Xe decay (see below)	Δk_{eff}	-0.092	-0.076	-0.055
Hot shut-down margin	Δk_{eff}	**-0.063**	**-0.048**	**-0.039**
Max. thermal neutron flux in external reflector before hot shut-down	10^3 n^{**}/cm^2 $/s/W_{th}$	467.5		170.7
Contributions to cold shut-down requirement:				
4 Days of ^{135}Xe decay (= **Hot shut-down requirement**)	Δk_{eff}	+0.0287		+0.0161
Reduction of eq. temperatures to 50°C:				
Resonance absorbers in fuel (Doppler)	Δk_{eff}	+0.0362		+0.0033
Moderators (C + O) in fuel	Δk_{eff}	+0.0324		+0.0140
Graphite in reflectors	Δk_{eff}	-0.0325		-0.0220
Total (= Cold Shut-down requirement)	Δk_{eff}	**+0.0648**		**+0.0115**
Max. thermal neutron flux in external reflector before insertion of CRs	10^3 n^{**}/cm^2 $/s/W_{th}$	362.2		195.7
Cold shut-down capability of 12 CRs:				
Equivalent ^{10}B atom density for 12 CRs from VSOP-A MEB: (**Source + density**)	10^{-6} Atoms / (barn.cm)	**LEU(Start-up) = 2.396**	**LEU(Eq*) = 1.704**	**Pu(PWR)(Eq*) = 2.319**
Full insertion of 12 CRs	Δk_{eff}	**-0.0955**	**-0.0825**	**-0.0604**
Cold shut-down margin	Δk_{eff}	**-0.031**	**-0.018**	**-0.049**

Notes: *: Eq stands for equilibrium core; **: n stands for neutrons.

7.2.4 Discussion of the control rod performance

7.2.4.1 Uncertainties in the results

The equivalent ^{10}B concentration for the 2-D MEB for the LEU equilibrium core was 40.6% higher than for the LEU start-up core (Table 12). This indicates that these concentrations are sensitive to the nuclide composition in the core. By the same reasoning, it would then also be sensitive to the temperatures in the core and to differences in the calculation algorithms, i.e. the significant differences between the reactivity results for the Pu(PWR) core that were obtained between VSOP-A and VSOP 99/05 in the results in the next chapters.

Therefore the following discrepancies between the 1-D transport calculations and TOTMOS, the 3-D diffusion calculations and the 2-D MEB calculations in VSOP-A and the final shut-down calculations in VSOP 99/05 can be expected to have introduced significant uncertainties or errors in the results:

1. The TOTMOS calculations were performed at a constant temperature of 1000 K, while the hot shut-down calculations in VSOP 99/05 were performed at the full range of equilibrium temperatures and the cold shut-down calculations were performed at a constant temperature of 50°C.

2. The nuclide composition of the fresh start-up LEU and Pu fuels in TOTMOS differed significantly from the equilibrium fuel compositions in VSOP.

3. The neutron spectrum for a 2-D poison annulus can be expected to be harder than for 3-D control rods, as is argued in more detail in the following section.

4. The reactivity of the start-up cores was significantly higher than for the critical equilibrium cores.

Measures to mitigate these uncertainties will be proposed below for a follow-up study.

7.2.4.2 Safety analysis

The effects of these uncertainties in the ^{10}B concentrations were mitigated by the fact that these annuli were significantly “black” i.e. the poison concentrations were so high that significant self-shielding occurred in these. Therefore relatively large variations in ^{10}B concentrations produced smaller variations in the control rod worths (Table 16):

- The 40.6% increase in ^{10}B concentration from the low to the high LEU MEB cases, caused only a 21% increase in the hot shut-down capability for the LEU equilibrium core in VSOP 99/05 and

- only a 15.8% increase in the cold shut-down capability.

The largest uncertainty pertains to the shut-down margins for the Pu(PWR) core:

Since it was not possible to stabilise the reactivity calculations for the VSOP-A Pu(PWR) start-up core, the MECS and MEB was calculated for the equilibrium cores only, for which the nuclide composition and the reactivity differed significantly from the start-up Pu fuel used in TOTMOS. However, from Table 12 it is clear that in the LEU case, replacing the start-up core with the equilibrium core in the MECS and MEB, strongly decreased the resulting equivalent ^{10}B concentration. Assuming that the same applies for the Pu(PWR) case, it can then be assumed that the equivalent ^{10}B concentration from the equilibrium Pu(PWR) MEB underestimated the value that would have been obtained for the more correct start-up case. Therefore the shut-down margins calculated with this lower poison concentration should also be conservative and can thus be assumed to have no negative consequences for the safety case.

It is important to note that, in spite of the too low ^{10}B concentrations used:

- All the cores could be safely shut down under all the simulated conditions.
- The cold shut-down margin for the Pu(PWR) core (Table 16) was better than for the LEU core.
- Although the hot shut-down margin, with the high ^{10}B concentration, of the LEU core was better than for the Pu(PWR) core, the Pu margin was still adequate.
- As was pointed out in the discussion of the xenon override margins (Table 14), the Pu core has an override margin of +0.0146 k_{eff}. If the excess reactivity were to be reduced accordingly by inserting the control rod less deeply into the core, the shut-down margins could be improved by a similar amount. This would make the Pu hot shut-down margin similar to that of the LEU core and will improve the lead of the Pu(PWR) cold shut-down margin even further.
- As a conservative measure the lowest equivalent ^{10}B concentration that was obtained in this study, i.e. 1.704 ^{10}B atoms/(barn.cm) for the MEB obtained with the LEU equilibrium core, was inserted for the VSOP 99/05 equilibrium core. Although the shut-down margins were significantly reduced to a hot shut-down margin of only -

0.029 and -0.041 for the cold core, the core could still be shut down comfortably under this conservative assumption.

7.2.5 Verification and validation of control rod calculations

It is clear from the results presented by Reitsma and Naidoo (2003), Sen *et al* (2006) and Mulder (2006) that in their 3-D VSOP simulations, both the MECS and MEB gave acceptable results. Their verification process included comparison to MCNP simulations.

When the 2-D MEB is added onto the 3-D MECS, as was done in the present study, the MEB will, by definition reproduce the results of the MECS, for the calibration core. It is, however, to be expected that the 2-D MEB will be more sensitive to variations in the core composition, compared to the 3-D MECS:

In the 3-D MECS, the only significant non-physical assumption is the diffusion approximation, which was compensated for by correcting the diffusion parameters and reaction cross-sections via the transport results. However, apart from any calculational errors this might introduce, replacing the individual 3-D control rods with a smeared out control poison annulus should significantly alter the neutron reactions in physical reality:

For 3-D control rods the spaces between the control rods are much larger than the thickness of the control rods. Therefore a significant fraction of the neutrons in the external reflector may diffuse back to the fuel core, without having passed through one of the control rods. The energy spectrum of a significant fraction of the neutrons that do diffuse back to the fuel will thus be unaffected by the presence of the control rods. Therefore the interactions between these neutrons and the fuel will not be affected by the presence of the control rods, for instance their capture-to-fission ratios will not be affected. However, when the control rods are replaced with a control poison annulus, which in the case of the PBMR DPP-400 is very close to the fuel core, almost all thermal neutrons that return from the external reflector to the fuel core, will have passed through this poison annulus. Since σ_γ for ^{10}B is very high at the lower end of the thermal energy range and then decreases rapidly with increasing energy, the lower part of the thermal neutron spectrum will be reduced sharply upon passing through this annulus, while higher energy neutrons will be much less affected. The annulus will act as a high pass neutron filter and the spectrum of the neutrons that diffused back to the fuel will thus be significantly harder, compared to the case for the control rods. Since LEU fuel is not very sensitive to changes in the neutron spectrum, this hardening of the spectrum should not significantly alter the core physics for the LEU case. However, as will be shown in

the burn-up calculations below, Pu(PWR) is very sensitive to changes in the neutron spectrum:

Both ^{241}Pu and ^{239}Pu have a very high thermal fission resonance. Since this resonance of ^{241}Pu peaks at a lower energy than ^{239}Pu, a hardening of the spectrum will reduce the number of ^{241}Pu fissions more than the ^{239}Pu fissions. However, the physics characteristics of these nuclides differ significantly, for instance ^{241}Pu gives a positive Uniform Temperature Reactivity Coefficient (UTC) below 500°C (see Par. 3.4.1 above), while ^{239}Pu gives negative uniform temperature reactivity coefficient at all relevant temperatures. Therefore, replacing the 3-D control rods with a 2-D ^{10}B-annulus will create a reduction in the magnitude of the positive uniform temperature reactivity coefficient of the core at low temperatures, and will thus affect the shut-down margins. By similar logic, it may affect other core parameters, such as the radial power profile during normal operation, with the control rods partially inserted for reactivity control.

The 2-D MEB method should therefore be used with more caution for Pu cores, compared to the LEU for which the verification studies, mentioned above, were performed. Pu verification studies should thus be repeated with MCNP simulations. However, a detailed verification programme would cause too much of a diversion from the main focus of the present study and was therefore excluded by the demarcation of this study and is thus left for a follow-up study.

As far as the present results are concerned, in addition to the uncertainties pointed out above, the following matter of concern was identified:

The 3-D VSOP-A iterations for k_{eff}, both for the LEU and Pu(PWR) cases, did not converge properly. While k_{eff} for the 2-D core normally converged well within five operating cycles, after, for instance, the control rods have been inserted, the values for the 3-D core took at least 100 operating cycles to converge reasonably. More concerning was the fact that the 2-D and 3-D calculations converged to significantly differing values. While differences were to be expected when the control rods were inserted, this problem also occurred when the control rods were not present: For instance the 3-D LEU start-up core, with the control rods fully withdrawn, converged to k_{eff} = 1.02652, while the 2-D case converged to 1.04176 (Table 12). Since only the differences between k_{eff} for the control rods in vs. out have been used for the MECS calculation, these differences in the absolute values of k_{eff} might be less problematic than they seem. However, they still suggest that there are significant uncertainties/errors in the 3-D models or codes.

Checks confirmed that the fuel loading, temperatures etc. were specified identically for the 2-D and 3-D models. The core volume and fuel flow channel volumes are also identical. However, the calculation meshes differed significantly in the R- and Z-directions, and of course, the 3-D case had a unique set of azimuthal meshes, which might have contributed to these convergence problems. Since no other 3-D model was available, it was not possible to identify the source of these errors by means of comparison to a reference model.

It has been pointed out above that the transfer of results for Pu calculations from VSOP-A to VSOP 99/05 probably introduces significant changes in the results. It was therefore deemed better to develop a 3-D VSOP 99/05 Pu model, rather than to try and solve the problems in the current 3-D VSOP-A model. This view is supported by the fact that several modifications have been introduced in VSOP 99 for the specific purpose of improving its convergence. As has been pointed out, the development of such a model will present a significant challenge, and was thus referred to the follow-up study.

7.2.6 Proposal for control rod follow-up study

It is expected that the uncertainties, introduced by the methods used in the present study, as discussed above, could be mitigated by the following methods in a follow-up study:

1. The differences between the start-up fuel compositions in TOTMOS and the equilibrium fuel in the final 2-D VSOP cores can be eliminated by extracting the most important equilibrium atom densities from the VSOP equilibrium cores and transferring these to TOTMOS.

2. Differences in temperatures can be eliminated by performing separate TOTMOS, MECS and MEB calculations for the hot and cold cores and then using the appropriate ^{10}B concentrations in the various final cases.

3. The differences between the PU reactivity results for VSOP-A and VSOP 99/05 can be eliminated by developing a 3-D VSOP 99/05 simulation core, so that VSOP-A can be completely removed from the Pu calculations. However, this step will pose significant challenges:

    a. The VSOP 99/05 manual (Rütten *et al*, 2007) currently does not describe a method for specifying the fuel flow channels for the 3-D case. In order to proceed with the development of a 3-D model, the manual will thus first have to be updated. However, this will require access to the VSOP 99/05 source code, which was not available for the present study.

b. Even if the 3-D flow channels can be specified, VSOP if the 3-D flow channels can be specified, the cone at the bottom cannot be modelled and fuel will move through the core all at the same speed.

c. Due to these and other challenges, the PBMR (Pty.) Ltd did not develop a full 3-D VSOP 99 input model, but rather transferred the atom densities from a 2-D equilibrium core to a stand-alone 3-D CITATION diffusion calculation for a static core.

d. A similar effect can probably be obtained by defining a static 3-D model in VSOP 99/05, which would eliminate the need to specify the fuel flow channels. Atom densities from an equilibrium 2-D VSOP 99/05 core can then be transferred to individual Regions in the 3-D model. This will still pose a significant amount of work.

e. The differences between core physics for the individual 3-D control rods and a 2-D control poison annulus can be eliminated by transferring all the relevant data to such a 3-D core thereby eliminating all 2-D control rod calculations.

Transferring all adapted data for all cores to a 3-D model will probably be too labour intensive to be of much practical use. A better method will probably be to execute sensitivity studies on all these effects and to then determine conservative assumptions, under which the 2-D MEB will always underestimate the 3-D control rod shut-down margins. These assumptions can be checked by Monté Carlo calculations. Once such a set of conservative assumptions has been deduced for all relevant core types, the 2-D MEB can then be used with confidence, in spite of the knowledge that it contains significant inaccuracies.

7.2.7 Conclusions

1. It was shown from the literature that the MECS + MEB simulation techniques for the control rod shut-down margins have been verified sufficiently for LEU fuel cycles.

2. However, significant uncertainties/errors have been pointed out in the present results for the Pu(PWR) fuel cycle. In spite of these uncertainties, it was shown that under conservative assumptions all simulated cores could be safely shut down under all simulated core conditions. Therefore it is concluded that shut-down margins for the Pu(PWR) fuel cycle are not an issue of significant concern.

3. Correction techniques for the uncertainties/errors in the present results have been referred to a follow-up study.

4. Since the technique for the simulation of the control rods has explicitly been excluded, in the demarcation section, from the list of original contributions claimed for this study, any shortcomings in these calculations should not affect the validity of the claims for original contributions by the present study.